5-2019

Mountain-Block Recharge to the Cache Valley Principal Aquifer and Geochemical Controls on Groundwater Movement in Alpine Karst

Skyler J. Sorsby
Utah State University

MOUNTAIN-BLOCK RECHARGE TO THE CACHE VALLEY PRINCIPAL AQUIFER AND GEOCHEMICAL CONTROLS ON GROUNDWATER MOVEMENT IN ALPINE KARST

by

Skyler J. Sorsby

A thesis submitted in partial fulfillment
of the requirements for the degree

of

MASTER OF SCIENCE

in

Geology

Approved:

_____	_____
Thomas E. Lachmar, Ph.D.	Dennis Newell, Ph.D.
Major Professor	Committee Member
_____	_____
Robert Q. Oaks, Jr., Ph.D.	Richard S. Inouye, Ph.D.
Committee Member	Vice Provost for Graduate Studies

UTAH STATE UNIVERSITY
Logan, Utah

2019

ABSTRACT

Mountain-block recharge to the Cache Valley principal aquifer and geochemical controls on groundwater movement in alpine karst

by

Skyler J. Sorsby, Master of Science

Utah State University, 2019

Major Professor: Dr. Thomas E. Lachmar
Department: Geology

Alpine karst aquifers govern the behavior of multiple hydrologic resources, yet associated solution enhancement precludes traditional modeling endeavors. The Bear River Range alpine karst system directly supplies a spring-fed municipal water resource, sustains local surface water for much of the year, and likely contributes mountain-block recharge to an adjacent valley-fill aquifer. Incremental discharge measurements of the Logan River constrain a possible volume of approximately 2.32×10^6 m^3/y (1.88×10^3 af/y) that could seep through alpine karst as mountain-block recharge. Time-series analysis of Logan River discharge fits a recession-curve model of rapid karst drainage, a large vertical hydraulic gradient, and minimal long-term aquifer storage. Hydrograph data for all gauged years suggest that the saturated zone drains to as low as 50% of its storage

capacity during high-recharge years and 20% during droughts, and that this variability can occur over the span of several years.

Oxygen and hydrogen stable isotopes adhere closely to the Utah Local Meteoric Water Line. Oxygen isotope values of snow vary systematically with altitude (-0.28 ± 0.12 ‰ per 100 m) and in conjunction with dye traces are useful for qualitative assessment of spring recharge areas. Carbon stable-isotope values are intermediate to atmospheric (-7.3 ‰), bedrock (-2.2 to +0.6 ‰), and soil-gas CO_2 (-23.3 ‰), and likely result from open-system water-rock interactions along groundwater flowpaths.

Major-ion analysis shows that all spring waters are undersaturated to saturated with respect to calcite and mostly saturated to supersaturated with respect to stoichiometric dolomite. Likely, this reflects dissolution of calcian dolomite or high-magnesium calcite along all flowpaths. Due to increased solubility of dolomite over calcite at low temperatures, carbonate-mineral dissolution in alpine karst likely proceeds incongruently, and complicates geochemical interpretation of flowpaths.

Chlorofluorocarbon (CFC) and tritium analyses suggest that spring waters are a binary mixture of sub-annual and older recharge. However, the oldest likely end-member age is on the order of 33-70 years for CFCs and 60-65 years for tritium. Although this finding suggests that the stored volume might be greater than the amount accommodated solely by caverns, it still reflects the inability of the alpine karst aquifer to store large amounts of water over long time spans.

(238 pages)

PUBLIC ABSTRACT

Mountain-block recharge to the Cache Valley principal aquifer and geochemical controls on groundwater movement in alpine karst

Skyler Sorsby

Groundwater is documented to flow through solution-widened fractures and bedding planes in limestone and dolostone units in low-relief topography. This enhancement, or karstification, is much harder to study in alpine environments like the Bear River Range of northern Utah. This is problematic, due to the fact that the Bear River Range karst aquifer system supplies the City of Logan with a large quantity of water at Dewitt Spring. Furthermore, the karst aquifer sustains the Logan River for much of the year, and may allow groundwater to flow directly in the subsurface to the Cache Valley principal aquifer system.

Flow measurements along the Logan River constrain a minimum volume of 2.32×10^6 m^3/y (1.88×10^3 af/y) that could recharge the Cache Valley principal aquifer. Hydraulic characteristics of alpine karst were estimated by analysis of major ions, stable isotopes, and dissolved gases in spring waters. These data reflect quick groundwater flow through caverns, with no evidence for "diffuse" flow anticipated by some to occupy interstitial space. In fact, the oldest reasonable estimated recharge age for groundwater is 70 years. Young recharge, fast flow, and low storage capability indicate that alpine karst aquifers are very sensitive to droughts and that related water resources are vulnerable to longer-term changes in climate.

ACKNOWLEDGMENTS

Many peers and mentors in the USU Geology Department offered indispensable insight and feedback. Dr. Tom Lachmar taught me to think like a hydrogeologist, and spent many hours with me in both the field and classroom to prepare me for success. Dr. Dennis Newell helped me to build a strong foundation in aqueous geochemistry, and to recognize its utility in hydrology. Dr. Bob Oaks taught me to think stratigraphically. Several undergraduate students assisted with field and labwork, and contributed to the success of the project: Zac Bybee, Nathan Gunnell, and Jordan Parkinson. Andrew Lonero, the USU Geochemistry Lab manager, also gave critical help.

I would like to thank my wife, Darcie, for her dedication to my success. She accompanied me on midnight runs up Logan Canyon to collect samples, helped measure flow in cold weather, and was patient throughout the research process. I would like to thank my parents, who taught me to work hard, and my sister, who helped me to write well. Thanks also my roommates for all of their support.

Special thanks to Larry Spangler and John Solder at the USGS Utah Water Science Center for sharing their insight into Bear River Range hydrogeology and environmental tracers. This research was funded in part by the Utah State University Department of Geology, the Geological Society of America, and the American Association of Petroleum Geology. Thanks to them, I was able to perform all of the work I had hoped to do.

Skyler J. Sorsby

CONTENTS

LIST OF TABLES

LIST OF FIGURES

INTRODUCTION

Problem statement

Alpine carbonate aquifer hydraulics control the availability and longevity of multiple water resources, yet are often complicated by solution-enhanced bedrock permeability (karstification). Karstification occurs as carbonate minerals dissolve along geologically favorable flowpaths (Van der Land et al., 2013) and introduces significant anisotropy that precludes traditional porous-media flow modeling (White, 2003; Teutsch and Sauter, 1991). This, in turn, cripples the ability to predict long-term hydrologic responses to climate variability.

Recent efforts to characterize karst aquifers resulted in a variety of new methods, including novel quantification of groundwater and surface-water interactions, application of geophysical surveys, and numerical modeling (Hartmann et al., 2014). However, recharge areas in alpine settings are typically devoid of wells and infeasible for surface geophysical surveys due to rugged terrain. High (100+ m) vertical hydraulic gradients and deep flowpaths in alpine karst (Filippini et al., 2018) further hinder the utility of these approaches. Dye traces (Taylor and Greene, 2001), hydrograph decomposition (Padilla et al., 1994), and environmental tracers (Delbart et al., 2014) are used to delineate groundwater basins, qualitatively assess hydraulic behavior, and place bounds on residence time in lowland settings. However, these tools each have shortcomings and are often used independently, resulting in an incomplete or inaccurate aquifer conceptual model (Eisenlohr et al., 1997; Kovacs and Perrochet, 2008).

The Bear River Range of northern Utah (Fig. 1) contains an alpine karst aquifer system that may provide mountain-block recharge (MBR) to Cache Valley (Lachmar et al., 2004), supplies a spring-fed municipal water resource (Spangler, 2001), and sustains the baseflow of the Logan River (Gooseff et al., 2005). Here, surface-water flow monitoring and geochemical modeling are used to characterize the alpine karst aquifer and its effect on related hydrologic resources by testing the following hypotheses:

- Considerable flow is lost from the Logan River to the Bear River Range subsurface and balances existing estimates of MBR to Cache Valley.
- Discharge magnitude of springs in the Bear River Range is inversely proportional to mean residence time in the alpine karst aquifer.
- The alpine karst aquifer contains three types of flowpaths: fast flow in well-developed karst, slower flow in less-developed karst, and very slow flow through enhanced bedrock pore space.

The eastern margin of Cache Valley is adjacent to the Bear River Range and hosts a highly productive aquifer system (Bjorklund and McGreevy, 1971), later termed the principal aquifer by Robinson (1999). Calibration of the most recent groundwater numerical model for the principal aquifer required subsurface recharge from the Bear River Range in order for computed hydraulic heads to match observations (Myers, 2003). That model superseded an older version that assumed the mountain-front fault to act as an impermeable boundary condition (Kariya et al., 1994) and one that permitted subsurface recharge (Clyde et al., 1994). As simulated pumping within the principal aquifer

produced greatly different impacts on surface water in the Myers (2003) and Kariya et al. (1994) models, a need exists for field estimation of MBR.

Mountain-block recharge cannot be measured directly, and therefore is typically estimated by solute mass-balance (Aishlin and McNamara, 2011), water-balance calculations (Wilson and Guan, 2004), or with noble-gas tracers (Manning and Solomon, 2004). Incremental monitoring of river discharge also allows direct estimation of possible upland contributions to an aquifer (Kalbus et al., 2006).

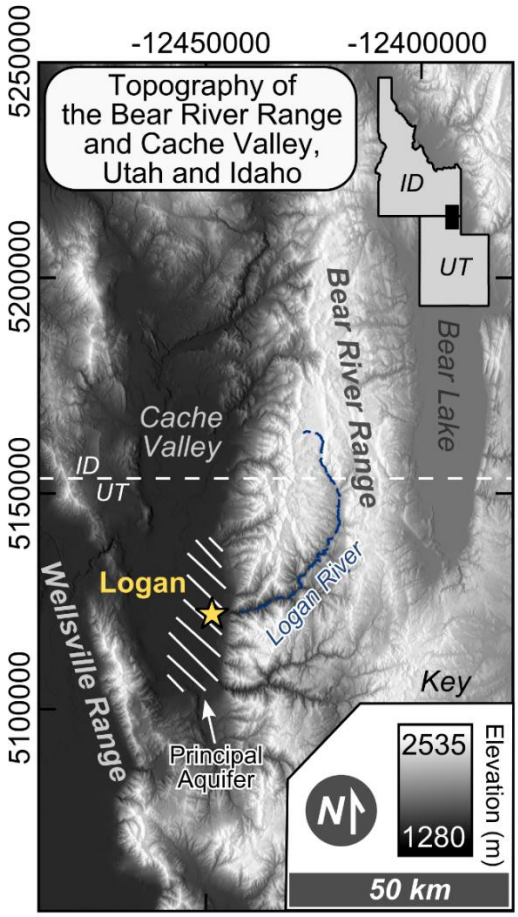

Figure 1. Topography of Cache Valley and the Bear River Range in northern Utah and southern Idaho. The principal aquifer is shown in dashed white. The coordinate system is UTM Zone 12 N.

Gathro et al. (2016) documented losses to the subsurface from the upper Logan River in June 2015 via the incremental streamflow method. In July and August 2015, they documented increasing contributions to the river from groundwater as total in-channel discharge decreased. They inferred that high-stage conditions in the Logan River force losses to the alpine karst aquifer system that in turn may flow downgradient into the Cache Valley principal aquifer. If this is true, integrated losses from the Logan River are a minimum estimate of mountain-block recharge. Neilson et al. (2018) also used the incremental streamflow method over a larger spatial scale to identify simultaneous gains from and losses to groundwater in different reaches of the Logan River, confirming the complexity of the problem.

Myers' (2003) numerical model simply assigned mountain-block recharge to occur uniformly across the mountain front. This simplification does not account for spatial heterogeneity of mountain-front geology and structure (Lowe and Galloway, 1993; Dover, 1995; Evans et al., 1996), which may restrict subsurface recharge to certain areas. If so, groundwater geochemistry should vary in valley-marginal wells. If Myers' (2003) simplification is correct, geochemistry should be relatively invariant in most valley-marginal wells and change with distance away from the mountain front.

The shape of a spring hydrograph relates to the hydraulic structure of a contributing karst groundwater basin (Ford and Williams, 2007). Recession-curve models are often used to assess these properties, but it is unclear at present whether they record the piecewise response of flowpaths with different permeabilities (Doctor and Alexander, 2005) or simply distinguish vadose- from saturated-zone drainage (Mangin, 1975).

A number of cold springs drain into the Logan River, with discharges ranging from 0.03 to 0.71 cubic meters per second (m^3/s) or 1 to 25 cubic feet per second (cfs; Mundorff, 1971; Spangler, 2001). It is unknown if discharge magnitude is a function of permeability in alpine karst, although this is likely the case in lowland karst aquifers (White, 2002).

Kolesar et al. (2005) identified an order-of-magnitude difference in groundwater saturation indices between Dewitt and Spring Hollow Springs. They inferred that the higher degrees of saturation observed in Spring Hollow Spring implied a longer aquifer residence time and lower karst development despite ubiquitously high discharge. However, no subsequent age dating was performed on either spring, and it is unclear if mineral saturation truly relates to residence time or instead to flowpath environmental controls. Correct understanding of this phenomenon bears implications for residence time in alpine karst, and may possibly aid in identifying less permeable upland groundwater basins.

Water-rock interactions within alpine karst impart unique geochemical signatures pertaining to flowpath hydrogeology and the presence or lack of air in the subsurface, which corresponds to dissolution in an open- or closed-system, respectively (Deines et al., 1974). If air were available during most of the dissolution process, it would indicate a high degree of permeability associated with fast, conduit-controlled flow. Dissolved gas and isotopic tracers also place constraints on residence time and aid in understanding aquifer hydraulics (Delbart et al., 2014; Yager et al., 2013).

Stable isotopes of oxygen and hydrogen may locally undergo temperature-controlled fractionation at high altitudes (Bright, 2009), although it is commonly assumed that this effect is negligible in both alpine snow and continental interiors (Coplen et al., 2000). Identification of topographic controls on snowpack isotopic composition would be an important first step towards understanding the isotope hydrology of recharge in alpine karst.

Purpose and objectives

The purpose of this study is to test the previously stated hypotheses by quantifying groundwater-surface water exchanges, water-rock interactions, and residence times in the Bear River Range alpine karst system. This endeavor will increase understanding of hydrologic resources linked to the alpine karst aquifer, and will take place by completing the following objectives:

Groundwater-surface-water interactions

1) Measuring discharge of the Logan River and its tributaries on a monthly basis should determine if and when water is lost to the alpine karst aquifer system. Quantification of net losses will help to estimate the volume of subsurface recharge to the principal aquifer, which can be compared to values predicted by the Myers (2003) model and estimated from tritium data of Robinson (1999) by Oaks (2004).

2) Analyzing hydrograph recession of the Logan River to determine if it adheres to a piecewise Maillet (1905) model of groundwater drainage from both

secondary- and primary-porosity features in alpine karst or simply describes drainage of the vadose and saturated zones (e.g., Mangin, 1975).

3) Comparison of groundwater-solute concentrations and CO_2 partial pressures in mountain-block wells and springs with those installed in the Cache Valley aquifer system to identify where mountain-block recharge might occur. If concentrations and partial pressures are uniform along the mountain front, Myers' (2003) spatial simplification of subsurface recharge might sufficiently describe reality.

Water-rock interactions

1) Analyzing stable isotopes of oxygen and hydrogen in snow to determine if they vary systematically with topographic variables in the Bear River Range and possibly serve as suitable tracers for recharge.

2) Analyzing spring solute concentrations to determine if those in low-discharge springs correspond to closed-system dissolution of dolomite and calcite and if those in high-discharge springs correspond to open-system dissolution in air-filled caverns.

3) Using the major-ion chemistry of each spring to determine if unique signatures exist that relate to whole-rock chemistry of specific hydrogeologic flowpaths. Springs traced with dye from recharge to discharge within the Garden City Limestone should contain very little magnesium, and springs recharged within and discharging from overlying dolostone units should have calcium to magnesium (Ca/Mg) ratios that reflect varying levels of groundwater interaction with dolomite.

Groundwater residence times

1) Measuring chlorofluorocarbon (CFC) and tritium concentrations in springs to assess whether or not they drain groundwater in equilibrium with contemporary atmospheric values reflective of short (weeks to months) residence times. Low concentrations in springs would indicate longer (decadal or older) residence times.

2) Comparing calcite and dolomite saturation indices with CFC and tritium data to assess whether they reflect residence time, as inferred by Kolesar et al. (2005), or simply differences in water-rock interactions.

The objectives stated above were tested by fieldwork and modeling endeavors in this study that included the following tasks:

1) Monitoring flow of the Logan River and its tributary streams and springs on a monthly basis to assess interactions of the Logan River with alpine karst.

2) Compiling Logan River hydrographs from 1922-2017 and applying mechanistic curve-fitting procedures to identify possible recession models that describe hydraulics of the alpine karst aquifer.

3) Measuring spring major-ion concentrations and carbon stable-isotope ratios for seasonally high- and low-flow conditions and comparing them with water-rock reaction-path models.

4) Measuring oxygen- and hydrogen-isotope ratios in springs, streams, and the alpine snowpack to assess topographic variability.

5) Measuring chlorofluorocarbon and tritium concentrations in two high-flow and two low-flow springs for comparison with lumped-parameter models of recharge age (Jurgens et al., 2012).

Location

The Bear River Range is a north-south trending topographic high in northern Utah and southern Idaho, bounded to the east by Bear Lake Valley and the west by Cache Valley (Fig. 1). The range is about 100 km from north to south and 30 km from east to west, and spans a geographic area greater than 4,000 km^2. Altitude ranges from 1,360 to 3,040 m above sea level (asl), with an average of 2,170 m (USGS NED, 2016).

Climate is semi-arid in the Bear River Range, which is geographically classified as undifferentiated highlands (Pope and Brough, 1996). Vegetation transitions from steppe-land grasses and shrubs at lower altitudes to evergreen forest and eventually tundra at highest altitudes (DeGraff, 1976). Snowmelt is the primary source of groundwater recharge within the Bear River Range (Spangler, 2001). Annual accumulated precipitation ranges from an average liquid equivalent of 122 cm at high altitudes (Tony Grove Lake SNOTEL site; USDA, 2018) to 64 cm at lower altitudes (Tony Grove Ranger Station SNOTEL site; USDA, 2018).

The Logan River is the largest stream in the Bear River Range (Bjorklund and McGreevy, 1971), where it loses flow to groundwater for at least part of the year (Gathro et al., 2016). Blacksmith Fork and the Little Bear River also drain the western flank of the Bear River Range, and numerous streams drain the eastern flank. As these streams do not spatially relate to the principal aquifer, they are not addressed in this study.

BACKGROUND

Geologic setting

Bear River Range stratigraphy comprises a nearly 7,600 m-thick sequence of Paleozoic marine limestones, dolostones, and interbedded siliciclastic deposits (Williams, 1948, 1958; Francis, 1972). Karstic dissolution along bedding planes and fractures in carbonate bedrock greatly increases permeability and permits rapid groundwater flow (Spangler, 2012; Bahr, 2016). Quartzites and shales separate thick carbonate aquifer units and likely act as aquicludes (Spangler, 2001; Dover, 1995; Fig. 2, Fig. 3).

Stratigraphy

Precambrian-Cambrian

Precambrian units are limited in outcrop extent within Logan Canyon, yet may spatially control recharge to the alpine aquifer along the mountain front (Fig. 3). The Precambrian Mutual (Zm), Brown's Hole (Zb), and Geertsen Canyon (Brigham Group; Cgl, Cgu, Cg) Formations comprise a thick (1,676+ m) sequence of quartzites, volcaniclastics, and minor shales (Fig. 4; Dover, 1995). Fault offsets are negligible compared to stratigraphic thickness, causing these units to likely serve as the effective base of the alpine aquifer system. The Brigham Group conformably underlies a thick sequence of Cambrian carbonate and minor shale and arkosic sandstone units, including the Langston (Cl), Ute (Cu), Blacksmith (Cbl), Bloomington (Cb), Nounan (Cn, OCsn), Worm Creek (Csw), and St. Charles (OCs) Formations.

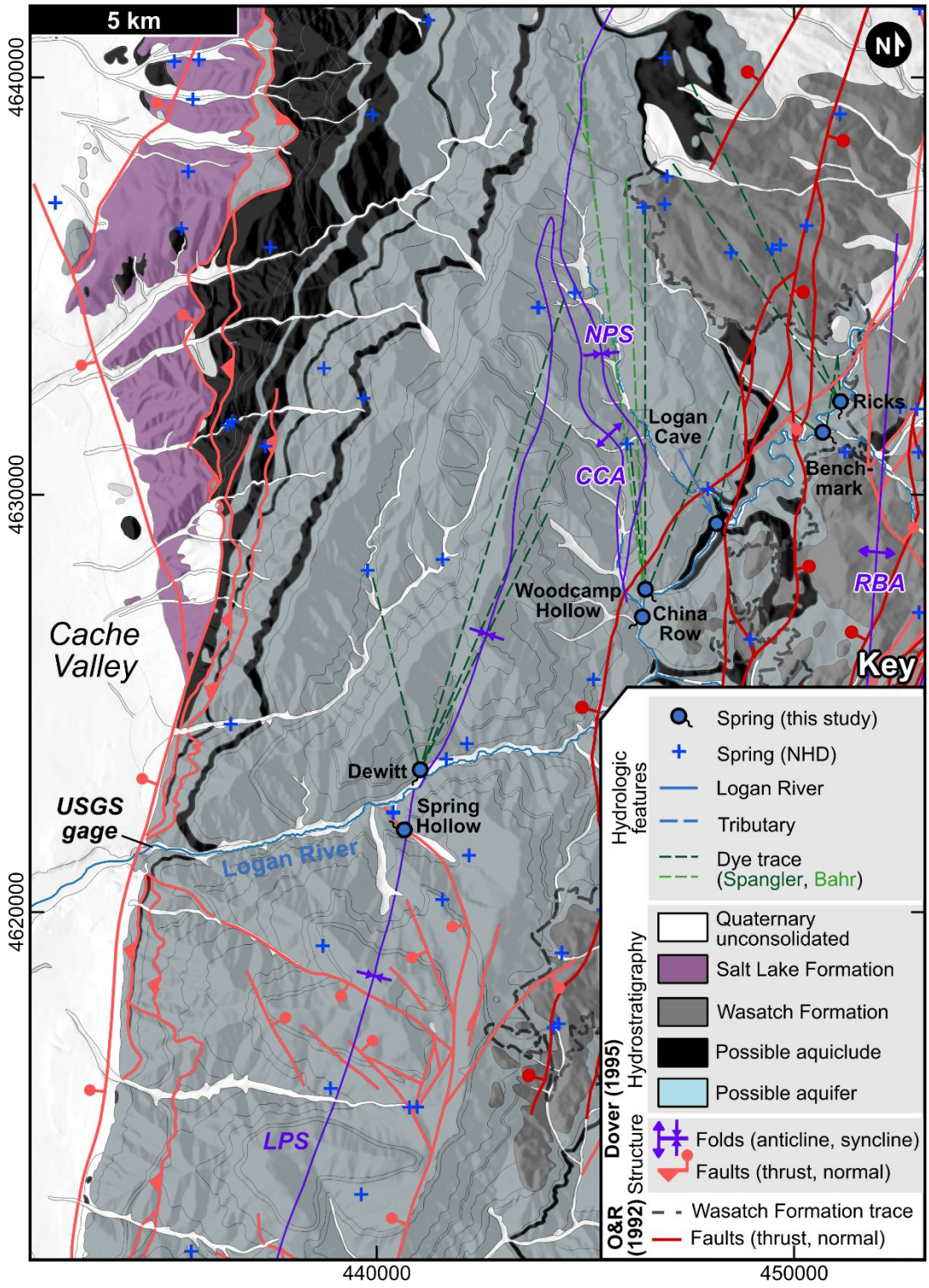

Figure 2. Hydrogeology, major structures, springs, and dye-traced recharge areas in the Bear River Range (Dover, 1995; Bahr, 2016; Oaks and Runnells, 1992; Spangler, 2001).

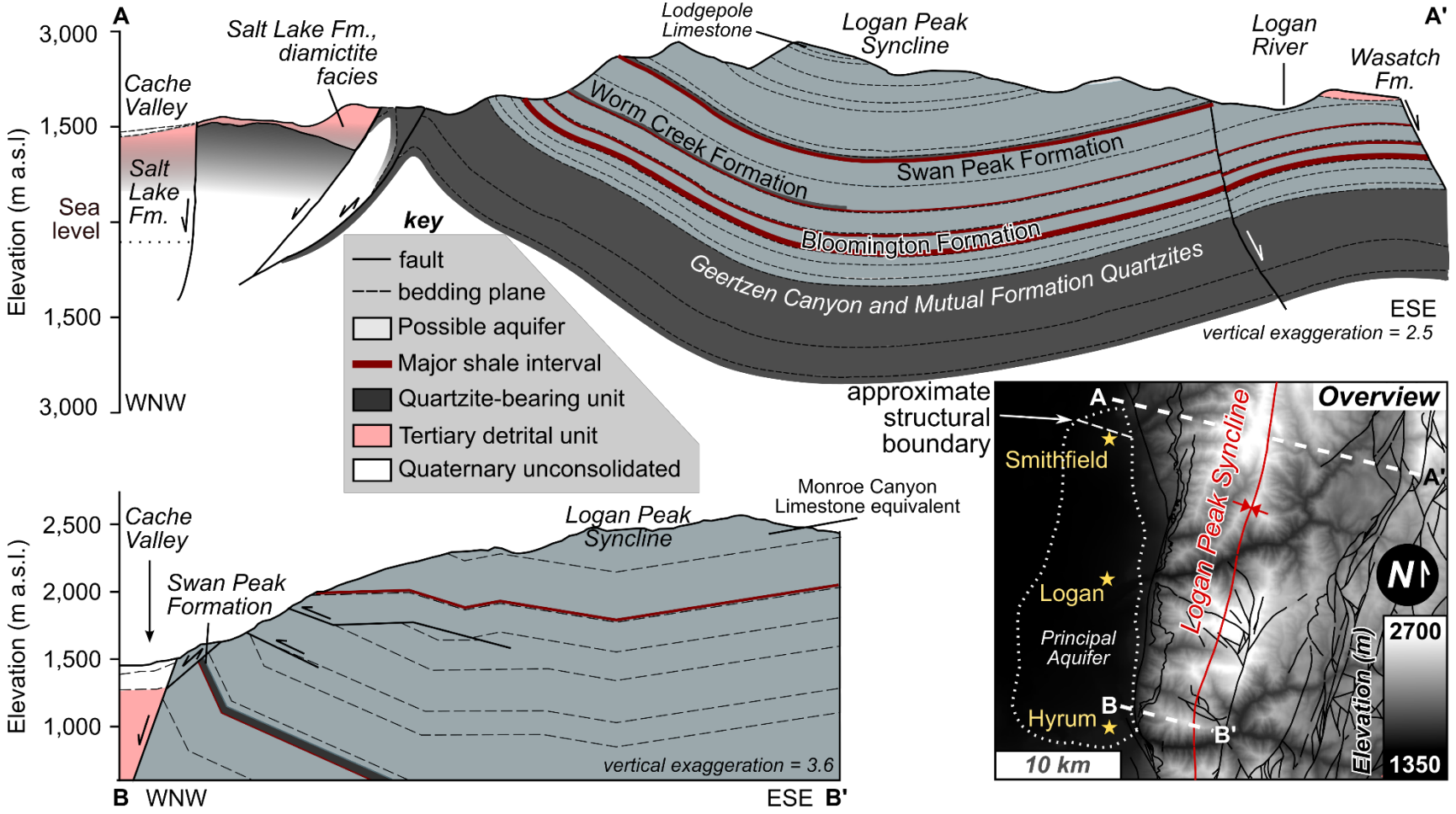

Figure 3. Hydrogeologic cross sections of the western Bear River Range from Smithfield, UT to Temple Fork (A-A') and Hyrum, UT into the range front (B-B'). Cross sections and structural features are modified from Dover (1995) and Evans and Oaks (1996).

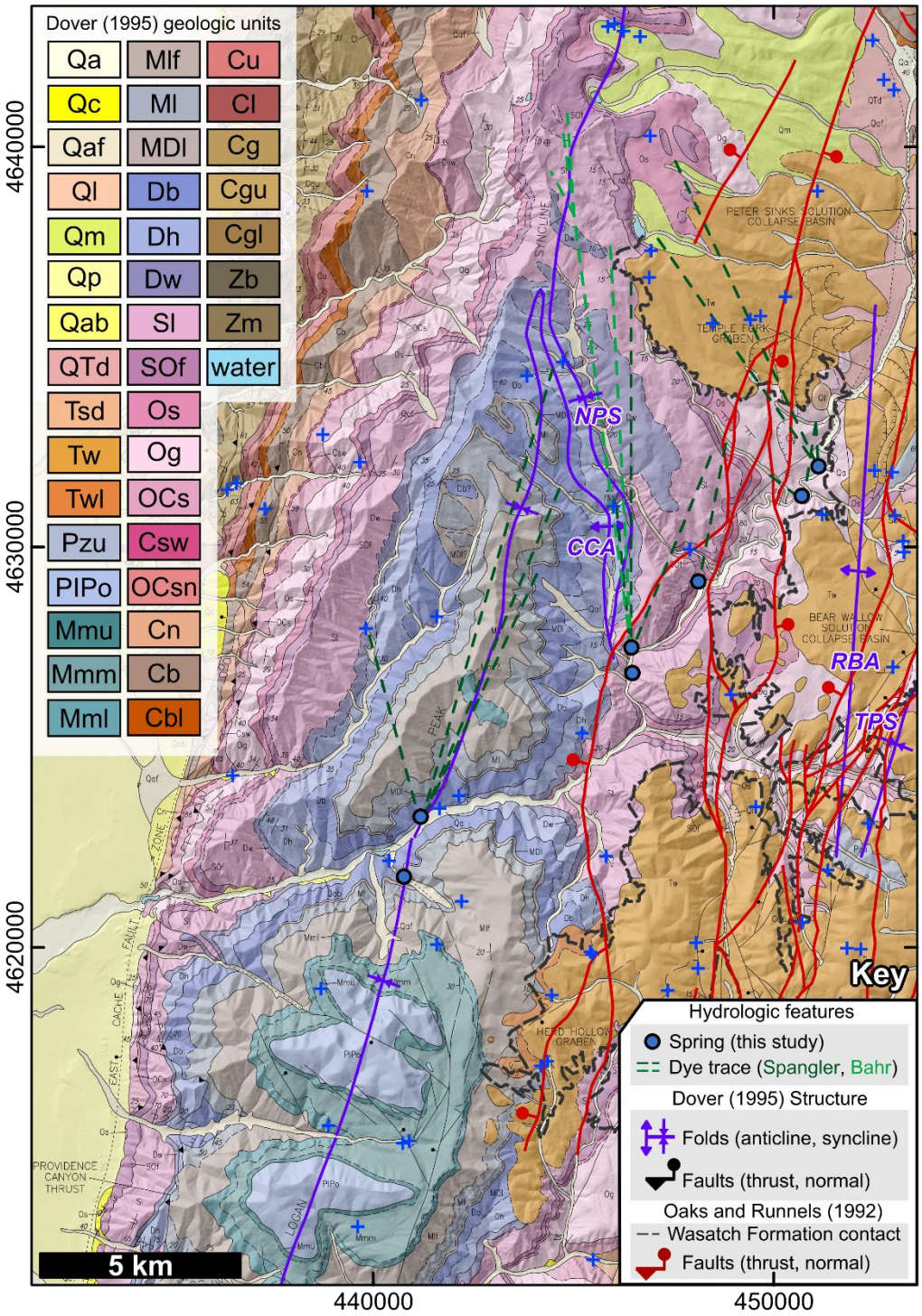

Figure 4. Dover (1995) geologic map with updated structures from Oaks (1993; TPS = Temple Peak syncline, RBA = Red Banks anticline, Bahr (2016) and Oaks and Runnells (1992); CCA = Cottonwood Creek anticline, NPS = Naomi Peak syncline), and dye traces from Spangler (2001) and Bahr (2016).

The basal Hodges Shale Member (~92 m thick) and an upper shale member (~ 46 m thick; Williams, 1948) of the Bloomington Formation (Chappelle, 1975) are likely impermeable barriers to vertical groundwater flow (Fig. 3), as are the shale beds of the two underlying formations. Shale, dolostone, and arkose in the Worm Creek Formation (Csw), between the Cambrian Nounan (Cn) and Cambrian-Ordovician St. Charles Formations (OCs), may likewise restrict vertical groundwater flow.

Ordovician - Silurian

The mainly dolostone St. Charles Formation (OCs) contains fewer shale interbeds than underlying formations and may have similar hydrologic characteristics to the overlying Garden City Limestone (Og). The ~37 m-thick basal shale of the overlying Swan Peak Formation (Os) likely acts as an effective aquiclude, partitioning groundwater from the overlying Fish Haven (SOf) and Laketown (Sl) Dolomites (Spangler, 2012), which are also primary aquifer units (Bahr, 2016).

Devonian-Pennsylvanian

The remaining Paleozoic stratigraphy above the Laketown Dolomite comprises the following potential carbonate aquifer units (Fig. 4): the Water Canyon Formation (Dw), Hyrum Dolomite (Dh), Beirdneau Formation (Db), Leatham Formation (MDl), Lodgepole Limestone (Ml) Monroe Canyon Limestone (Mml, Mmm, Mmu), Oquirrh Formation (PlPo), and other undivided Paleozoic units (Pzu; Dover, 1995). A phosphatic shale ~61 m thick in the Little Flat Formation (Mlf) may partition aquifer units to the south of the Logan River, where it underlies younger Paleozoic carbonates.

Tertiary - Quaternary

Higher altitudes in the Bear River Range are capped unconformably by a veneer of the Tertiary Wasatch Formation (Tw, Twl), a poorly-sorted unit composed of gravelly muds with minor gravels and abrupt facies changes (Figs. 2-4; Williams, 1948; Oaks and Runnells, 1992). Alpine basins are mantled with Pleistocene deposits from the Bull Lake and Pinedale (and perhaps older) glaciations (Qm), landslides, (Ql), alluvial fans (Qaf), and colluvium (Qc) that obscure structural geologic relations and karst features (DeGraff, 1976; Wilson, 1976; Dover, 1995). Numerous small springs and marshy areas emerge along the downhill basal contacts of the Wasatch Formation (Oaks and Runnells, 1992), indicating its ability to partition the hydrologic system in places.

Topographic relief caused by Basin-and-Range extension governed deposition of the Tertiary Salt Lake Formation (Tsd) in Cache Valley, comprising a sequence of conglomerate, tuff, and sandstone members (Williams, 1962; Goessel et al., 1999; Oaks et al., 1999). Subsequent inundation by Lake Bonneville and at least three older lakes during the Pleistocene resulted in deposition of multiple lacustrine sequences (Qab, Qp; Dover, 1995; Oaks et al., 2014, 2018). Thick clay beds comprise near-surface stratigraphy in the valley center, while deltaic gravels (Qa) and conglomerates intercalate near canyon mouths on the eastern margin (Robinson, 1999). The spatial distribution and thickness of near-surface lacustrine and deltaic deposits controls the geometry of the Cache Valley principal aquifer and its recharge areas (Bjorklund and McGreevy, 1971; Robinson, 1999; Thomas et al., 2011). Previous hydrogeologic studies in Cache Valley and the Bear River Range are presented in detail in the PREVIOUS WORK chapter.

Structure

Basin-and-Range normal faulting that cuts the NNE-trending, south-dipping, Sevier-age Logan Peak syncline (LPS) controls range-front relief (Fig. 4; Williams, 1948; McCalpin, 1989, 1994; Evans and Oaks, 1996, Evans et al., 1996). The western limb of the syncline is steeper in the vicinity of Naomi Peak, and funnels groundwater flow southeast to discharge at springs in Logan Canyon (Spangler, 2001).

Impermeable quartzite and shale units within a fault-bounded bedrock block (Fig. 3; Dover, 1995) divide units in the LPS from Cache Valley deposits and may act as a barrier to mountain-block recharge. Locally numerous joints (Oaks, written communication), however, may permit some amount of flow across the quartzite units. Geologic mapping by Williams (1948) and Dover (1995) documented extensive aerial exposure of the Geertsen Canyon Quartzite in the vicinity of Smithfield, UT, and ESE dip of carbonate bedrock units in the LPS (33-66º).

Eastward dip generally decreases to the south, reaching 20-40º in the vicinity of Logan, UT (Dover, 1995; Evans et al., 1996). The Garden City Limestone, a known aquifer unit, also enters the subsurface at this latitude due to the southward plunge of the LPS, and introduces the possibility for direct mountain-block recharge along bedding planes. Complicated structure in the mountain-front fault zone predicted by Dover (1995), Evans et al. (1996), and Oaks (2004) would require groundwater to flow along a fracture network generally perpendicular to the mountain front in order to traverse quartzite and near-vertical shale units. This is likely to occur, as several producing wells

adjacent to the mountain front are isolated from seepage due to continuous deepwater lake deposits that extend to the East Cache fault (Oaks, written communication).

Eastward bedrock dip decreases farther to the south, such that minor anticlinal folding reverses dip direction to the west (Section C-C' in Evans et al., 1996). Just north of Hyrum, UT, mountain-front geometry possibly simplifies, such that the Garden City Limestone directly contacts Cache Valley sediments and only a small fault-bounded carbonate bedrock wedge possibly separates the Laketown Dolomite from these deposits. If the alpine karst aquifer system is isolated or partially restricted from Cache Valley between Logan and Millville Canyon, high pressure-head from distal recharge at higher altitudes could drive deep groundwater flow upward into the principal aquifer.

Folds and high-angle normal faults that vary from east- to west-dipping deform the interior of the Bear River Range (Dover, 1995). The Red Banks anticline (Oaks, unpublished map) may partition the aquifer system along the southeast flank of the Logan River, by forcing groundwater to flow along the Temple Peak syncline into the Temple Fork surface catchment. North of Hyde Park Canyon along the western range front, several thrusts and the Bannock detachment fault (Oriel and Platt, 1979, 1980; Lowe and Galloway, 1993) complicate westward subsurface flow.

Conceptual karst hydrologic models

Parameterization of alpine karst aquifers is critical to determining the behavior of related water resources, yet lies beyond the scope of traditional porous-media flow models (Teutsch and Sauter, 1991). Dissolution of carbonate minerals can enhance permeability of fractures, bedding planes, and pore space (White, 2003). Flowpath

architecture associated with this enhancement may adhere to several conceptual models (Fig. 5). A single-porosity karst flow model assumes that all groundwater moves through solution-enhanced conduits on the order of days to weeks (flowpath a). A double-porosity model adds a flow component of intermediate velocity (years to decades) that moves through a less-developed karst network (flowpath b). A triple-porosity model adds a third flow component of slow velocity (hundreds to thousands of years) that moves through solution-enhanced pore space in bedrock according to Darcy's law (flowpath c). Most flow typically occurs in conduits and along less-enhanced fractures. Most storage occurs interstitially if enhanced pore space is present (White, 1993), which may not be the case in the Bear River Range. Documentation of the presence or lack of each component is clearly necessary for accurate numerical modeling (Taylor and Greene, 2001).

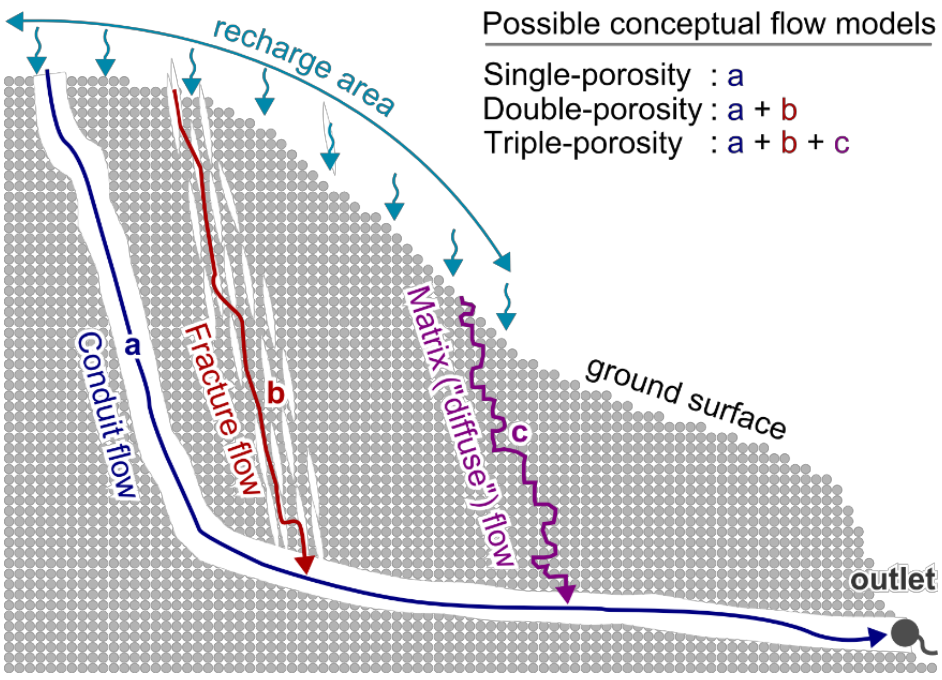

Figure 5. Schematic of single, double, and triple porosity conceptual models (after White, 2003). Subsurface white areas are void space.

Assessing groundwater and surface-water interactions

Incremental streamflow

The most mechanistically rigorous methods for quantifying groundwater and surface-water interactions involve piezometers or wells, which are often infeasible to install in rugged alpine bedrock environments (Kalbus et al., 2006). Seepage meters and temperature measurements are more commonly used to determine riverine groundwater exchange rates in such settings (Becker et al., 2004). In a structurally complicated, large-scale fluvial system, losses to groundwater likely occur at discrete locations difficult to identify or access. It is also likely that stream temperature is controlled more by atmospheric contact and cold spring and tributary inflows than by upward seepage of groundwater. Use of Na and Cl (conservative, assuming minimal ion exchange with clays) as flux tracers is also problematic due to the use of salt to de-ice proximal alpine roads. In this case, incremental streamflow measurements are the most suitable method for estimating gains from or losses to groundwater (Kalbus et al., 2006).

The incremental streamflow method involves measuring discharge at the upstream and downstream ends of a reach, as well as at confluences with all tributaries. Tributary inputs are added to upstream discharge, the sum of which is compared to the actual downstream discharge. If tributary inputs sum to a larger amount than the downstream value, leakage to groundwater occurred within the reach. In rivers that traverse unconsolidated sediments, such losses may simply move at a slower pace through unconsolidated substrate as hyporheic flow and re-enter the channel downstream

(Winter et al., 1998). However, losses through a bedrock channel are more likely to flow along structures (e.g., fractures or bedding planes) to lower-altitude discharge zones.

Geochemical facies analysis

Groundwater geochemistry in valley-fill aquifers is influenced by the spatial distribution and solute load of recharge, which may be assessed with systematic facies analysis. In practice, this involves comparing major-ion concentrations and other geochemical parameters across an aquifer (Back and Hanshaw, 1965). Stiff (1951) diagrams are a compact way of comparing relative changes in the charge amount of aqueous species in milliequivelants per liter (meq/L). Total dissolved solids (TDS) in groundwater accumulate as reactions with aquifer materials progress. Hence, increases in TDS westward from the mountain front may also aid in identifying recharge zones.

Stream leakage through valley-margin sediments, also known as mountain-front recharge, is another mechanism of replenishing valley-fill aquifers (Wilson and Guan, 2004). Surface water in equilibrium with the atmosphere has a CO_2 partial pressure (pCO_2) of approximately $10^{-3.39}$ atmospheres (Scripps, 2018). Groundwater pCO_2 is higher, due to addition of CO_2 in soil, as well as reactions with aquifer materials or contaminants (Deines et al., 1974; Choi et al., 1998). As groundwater emerges at Earth's surface, degassing occurs and lowers pCO_2 toward atmospheric equilibrium. Accordingly, near-atmospheric pCO_2 in a valley-fill aquifer indicates recharge from surface water and may aid in distinguishing between mountain-block (high pCO_2) and mountain-front (low pCO_2) recharge.

Analysis of master-recession curves

Stream hydrographs are divisible into three basic components: a rising limb, a peak, and a recession limb (Fig 6). As runoff dwindles following a recharge event (e.g., storms or snowmelt), the recession limb undergoes inflection and is afterwards dominated by groundwater drainage. This concave-up recession portion of the hydrograph may further divide into one or several piecewise curves depending on the permeability and geometry of the contributing aquifer (Kovacs and Perrochet, 2008). Fitting mechanistic models to adjacent concave-up segments parameterizes subsurface hydraulic characteristics. However, it is rare for a hydrograph to recede without interruption by one or several storm events. This difficulty is usually circumvented by creation of a master recession curve (MRC).

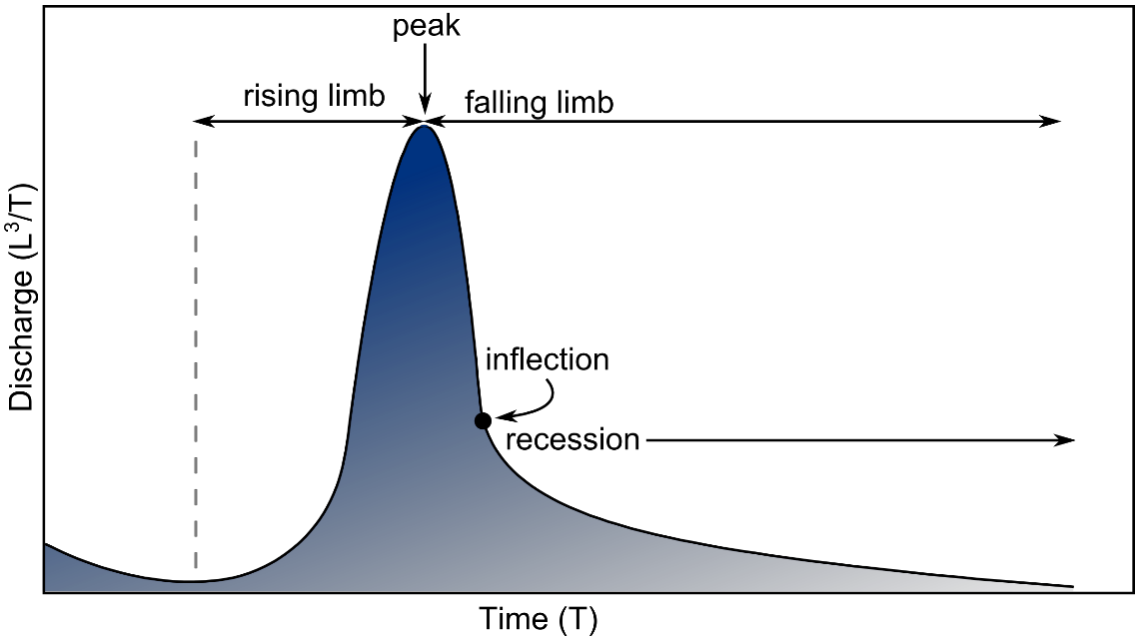

Figure 6. Schematic diagram of a typical hydrograph following a recharge event.

Aquifer parameters govern groundwater discharge to a stream following recharge events, and pristine segments from many hydrographs for that stream translate laterally to form a unified, "master" recession curve. The shape of this curve is related to hydraulic parameters of the contributing aquifer. Although MRCs were traditionally arranged by hand, Gregor and Malik (2012) developed an algorithm using strongly hybridized genetics and artificial-immune networks to optimize the process. As with pumping or slug tests in wells, a strong conceptual understanding of the local hydrogeology is required in order to select and fit the appropriate model to an MRC.

The oldest and most commonly used model was proposed by Maillet (1905) to describe baseflow drainage of a homogeneous, porous-media reservoir to a stream:

$$Q(t) = q_o e^{-\propto t} \tag{1}$$

In this model $Q(t)$ is the hydrograph discharge (L^3/T) at time t during recession, q_o is the initial discharge (L^3/T), and $\propto$ is the recession coefficient, which is physically linked to multiple aquifer parameters by the following formula (Rorabaugh, 1964):

$$\propto = \frac{\pi^2 kb}{4SL^2} \tag{2}$$

In this expression, k is the mean hydraulic conductivity of the dominant flowpath, b is the saturated thickness of the aquifer above the measurement point, S is aquifer storativity, and L is the one-dimensional length of the flowpath (Kovacs and Perrochet, 2008). Doctor and Alexander (2005) fitted the Maillet (1905) model in a piecewise fasion to an MRC in an attempt to identify three flowpaths with different $\propto$-values, and hence possibly different hydraulic conductivities (Fig. 7). However, numerical modeling shows that this approach incorrectly attributes several flowpath permeability types to

simpler systems that may have only one (Kovacs and Perochet, 2008). Mangin (1975) constructed a piecewise model for karst hydrographs that attributed the steep onset of recession to groundwater drainage from the unsaturated zone into the saturated zone (flood recession), rather than to a higher-permeability flowpath.

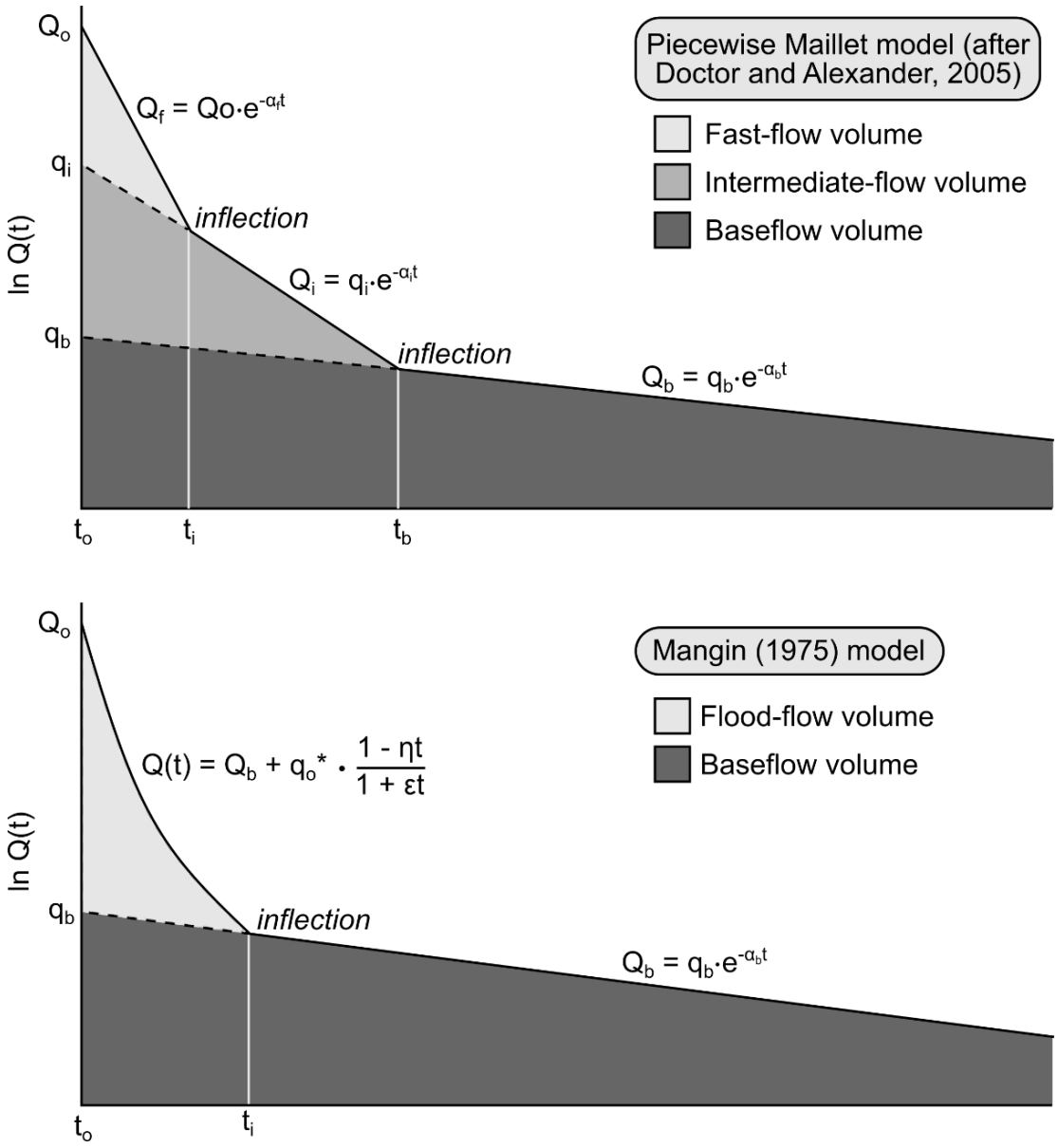

Figure 7. Competing hydraulic models for karst hydrograph recession.

Flood recession is described by the following nonlinear equation:

$$\psi(t) = q_o^* \left(\frac{1-\eta t}{1+\varepsilon t}\right) + Q_b \quad (3)$$

In this expression, q_o^* is the difference between total discharge and the baseflow component at time t, ε is an empirical parameter that relates to flow velocity, Q_b is the extrapolation of Maillet's formula to $t = 0$, and η relates to mean transit time through the unsaturated zone by:

$$\eta = \frac{1}{t_i} \quad (4)$$

In this expression, t_i is the duration of flood recession in days. Total discharge at any point is described by Mangin (1975) as the following piecewise relationship:

$$Q(t) = \psi_t + \phi_t \quad (5)$$

In this expression, ψ_t becomes zero at t_i and ϕ_t is simply Maillet's formula. Integration of ϕ_t yields an estimate for the total amount of water temporarily stored in caves, or dynamic storage, above the measurement gauging point (Ford and Williams, 2007):

$$V_o^b = \int_0^\infty q_o^b e^{-\propto t} dt = \frac{q_o^b}{\propto} \quad (6)$$

Major-ion analysis of water-rock interactions

Water-rock interactions in an aquifer impart a distinct major-ion fingerprint (Langmuir, 1997). Infiltrated precipitation reacts with soil carbon to produce an elevated pCO_2 value that remains essentially fixed along aquifer flowpaths (Deines et al., 1974). Groundwater flowpaths align more with open-system conditions (abundant CO_2 gas) or closed-system conditions (no CO_2 replenishment). Available CO_2 gas in open systems, in

turn, replenishes the dissolved CO_2 load and permits greater dissolution of carbonate minerals into groundwater.

Groundwater composition in a karst aquifer should reflect interaction with calcian (cd) or stoichiometric (d) dolomite and pure (c) or magnesian (mc) calcite end-members (Szramek et al., 2007), depending on the dominant mineralogy. These reactions obey the following equations and thermodynamic equilibrium constants, from Langmuir (1971), Wigley (1972), Plummer et al. (1978), and Plummer and Mckenzie (1974):

$$Ca_{0.54}Mg_{0.46}CO_3(s) = 0.54Ca(aq) + 0.46Mg(aq) + CO_3(aq) \quad (7)$$

$K_{cd\ 4\%} = 10^{-16.49}\ at\ 25^0\ C$

$$Ca_{0.5}Mg_{0.5}CO_3(s) = 0.5Ca(aq) + 0.5Mg(aq) + CO_3(aq) \quad (8)$$

$K_d = 10^{-17.00}\ at\ 25^0\ C$

$$CaCO_3(s) = Ca^+(aq) + CO_3^-(aq) \quad (9)$$

$K_c = 10^{+8.56}\ at\ 25^0\ C$

$$Ca_{0.97}Mg_{0.03}CO_3 = 0.97Ca^{2+} + 0.03Mg^{2+} + CO3^{2-} \quad (10)$$

$K_{mc\ 3\%} = 10^{-8.6}\ at\ 25^0\ C$

$$Ca_{0.81}Mg_{0.19}CO_3 = 0.81Ca^{2+} + 0.19Mg^{2+} + CO3^{2-} \quad (11)$$

$K_{mc\ 19\%} = 10^{-7.4}\ at\ 25^0\ C$

Congruent mineral dissolution according to these reactions in either open or closed systems should result in calcium to magnesium (Ca/Mg) ratios greater than or equal to 1, possibly representative of the degree of interaction with and stoichiometry of different carbonate minerals (e.g., Bright, 2009). However, Langmuir (1971) documented Ca/Mg ratios less than one in a carbonate aquifer in central Pennsylvania, and cited

incongruent mineral dissolution as the mechanism. Once reached, calcite saturation in a solution is maintained via precipitation to the solid phase as dissolution of dolomite continues to occur. This results in non-stoichiometric evolution of the Ca/Mg ratio according to the following equilibrium expression (Langmuir, 1971):

$$\frac{K_c^2}{K_d} = \frac{[Ca^{2+}]}{[Mg^{2+}]} \tag{12}$$

The constants for calcite (K_c) and dolomite (K_d) equilibria are temperature dependent, with higher values of K_d than K_c at lower temperatures (Williams et al., 2007). Hence, increasingly cold temperatures may enhance incongruent mineral dissolution and drive the equilibrium molar Ca/Mg ratio to values less than one.

Saturation indices describe groundwater equilibrium with respect to specific aquifer minerals and aid understanding of water-rock interactions (Langmuir, 1997). Groundwater may exhibit higher saturation indices with increasing residence time (Jacobson and Langmuir, 1974). In this case, saturation indices may be used as a proxy for recharge age, and aid in identifying less-karstified areas of an aquifer.

Caution must be taken when interpreting these data, as subsurface conditions may naturally alter groundwater saturation prior to discharge. For example, CO_2 outgassing or biological activity may induce supersaturation and are unrelated to residence time (Moral et al., 2008; Herman and Lorah, 1987). Equilibrium modeling also assumes that dissolution reactions are in steady state. Differences in kinetic reactions during short residence times or at certain groundwater temperatures may also produce supersaturated conditions (White, 1997).

Stable isotopes in precipitation and groundwater

Water molecules contain two dominant stable-isotope pairs of oxygen and hydrogen: $^{18}O/^{16}O$ and $^{2}H/^{1}H$. In practice, these ratios are reported using delta notion as $\delta^{18}O$ and $\delta^{2}H$ in per mil (Gat and Gonfiontini, 1981) via the following expression:

$$\delta = \left(\frac{R_{sample}}{R_{standard}} - 1\right) * 1000 \quad (13)$$

In this expression, R_{sample} is the isotopic ratio of the sample, and $R_{standard}$ is the ratio of an International lab standard. The lab standard is calibrated to the International standards, available from the International Atomic Energy Agency (IAEA), such as Vienna Standard Mean Ocean Water, for reporting hydrogen and oxygen stable isotopes (VSMOW; Groning et al., 2007). VSMOW (now depleted) and VSMOW2 (the newest version) are carefully mixed batches of distilled ocean water that are isotopically identical to the original SMOW standard (Lin et al., 2010). VSMOW is defined as 0 ‰ for $\delta^{18}O$ and $\delta^{2}H$.

Ordinary least-squares regression of a global dataset of meteoric $\delta^{18}O$ and $\delta^{2}H$ values yields a strong linear relationship known as the global meteoric water line (GMWL; Craig, 1961), defined by the equation:

$$\delta^{2}H = 8 * \delta^{18}O + 10 \quad (14)$$

On a regional scale, stable isotopes of oxygen and hydrogen in precipitation deviate from the GMWL along a local meteoric water line (LMWL; Kendall and Doctor, 2003). Kinetic fractionation also results in systematic offsets from the LMWL that reflect particular hydrologic processes, like evaporation (Rozenski et al., 2001).

Temperature-controlled fractionation of oxygen and hydrogen isotopes occurs between liquid and vapor as air masses release precipitation at higher altitudes in alpine systems (Gat et al., 2001). As infiltration occurs, stable isotopes conservatively maintain recharge signatures along flowpaths with no mixing (Poage and Chamberlain, 2001). Isotope values from precipitation at different altitudes are often used to create a linear model, known as an "altitude gradient" (‰ per 100 m; e.g., James et al., 2000) that explains topographic controls on fractionation in fallen precipitation. Altitude-dominated fractionation effects leeward of mountain crests or in continental interiors are thought inferior to rainout and other effects (Clark and Fritz, 1997). However, several studies document the presence of reasonable altitude gradients (-0.18 to -0.26 ‰ per 100 m) in these settings (James et al., 2000; Hynek et al., 2004). Although altitude gradients do not represent the signatures of infiltrated recharge, they may aid interpretation of recharge areas if compared qualitatively with topographic and geologic data (Blasch and Bryson, 2007), and help build understanding of precipitation dynamics.

Carbon 13 stable-isotope ratios ($\delta^{13}C$) are reported with respect to the Vienna Pee-Dee Belemnite (VPDB; Chang and Li, 1990), and are non-conservative in groundwater due to interactions with carbon-bearing Earth materials and gases (Kendall and Doctor, 2003). Current globally averaged atmospheric CO_2 has a $\delta^{13}C$ value near -8 ‰ (Gat et al., 2001). Plant-respired soil CO_2 values are near -25 ‰ in forested, temperate (C3) vegetation zones (Deines, 1980). Paleozoic carbonate minerals generally contain a signature close to 0 ‰ (Kendall and Doctor, 2003). The idealized equilibrium reaction of soil-derived carbonic acid with carbonate aquifer materials produces a $\delta^{13}C$ value of

dissolved inorganic carbon (DIC) intermediate between these two sources and the different carbon species in solution.

Groundwater exposure to cavern air permits mass transfer with a large gaseous CO_2 reservoir (an open system) of fixed $\delta^{13}C$ that drives dissolution and raises TDIC beyond closed-system equilibrium (Doctor et al., 2008). Geochemical modeling after Frondini et al. (2014) permits a direct comparison of groundwater TDIC and $\delta^{13}C$ of DIC with expected values from dissolution of carbonate minerals in open- or closed systems along flowpaths with different, fixed CO_2 partial pressures (Fig. 8).

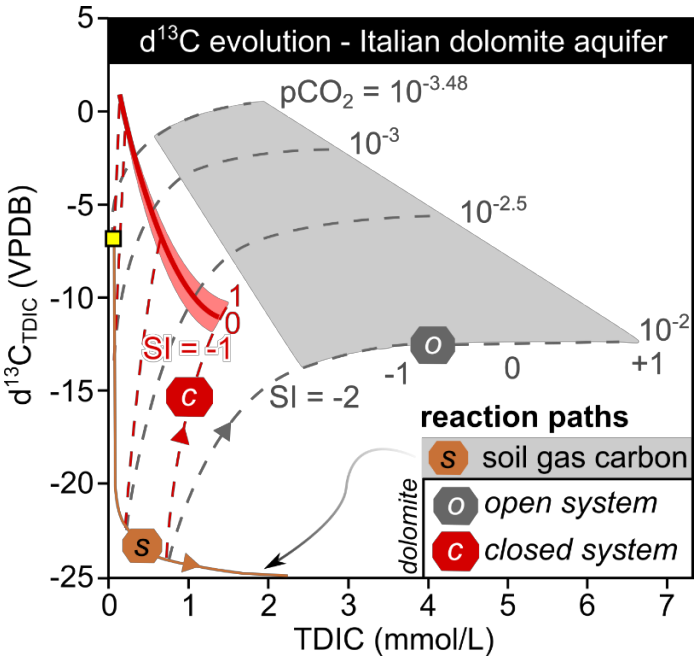

Figure 8. $\delta^{13}C$ evolution curves with congruent dolomite dissolution in open (gray lines) and closed (red lines) conditions in an Italian karst aquifer (Frondini et al., 2014)

Evolution of carbon stable isotopes should adhere to the finite-difference solution to the following mass-balance equation from Wigley et al. (1978):

$$\delta^{13}C_{TDIC} + \Delta(\delta^{13}C_{TDIC}) = \frac{(\delta^{13}C_{TDIC}+1000)(TDIC-\sum_{i=1}^{M} a_{i-1}\Delta O_i)}{TDIC+\Delta(TDIC)} + \frac{(\sum_{i=1}^{N}(\delta^{13}C_i^*+1000)\Delta I_i)}{TDIC+\Delta(TDIC)} - 1000 \quad (15)$$

The left side of the equation is the total-carbon-isotopic composition at the end of each reaction step, $\delta^{13}C_{TDIC}$ is the groundwater-isotopic composition at the beginning of each step, total dissolved inorganic carbon (TDIC) is related to the carbon in the dominant aqueous species by the following relationship:

$$TDIC = mH_2CO_3 + mHCO_3^- + mCO_3^{2-} \quad (16)$$

a is the fractionation factor between aqueous carbon species and precipitated carbonate minerals, O_i is the amount of carbon precipitated in the step, I_i is the amount of carbon dissolved in the step (from cavern atmosphere or carbonate minerals), and *M* and *N* are the total number of dissolving and precipitating carbon phases, respectively. Carbonic acid (H_2CO_3) and bicarbonate (HCO_3^-) likely constitute the bulk of the dissolved carbon in Bear River Range groundwater, as carbonate-ion (CO_3^{2-}) concentrations are negligible at pH values less than eight (Deines et al., 1974). The mass-balance equation for evolving cave atmosphere-isotopic composition then simplifies to:

$$\delta^{13}C_{atm} = \frac{mH_2CO_3*\delta^{13}C_{H_2CO_3}+mHCO_3^-*\delta^{13}C_{HCO_3}^-}{TDIC} \quad (17)$$

The $\delta^{13}C$ of added primary aqueous species are related to a fixed cave-air $\delta^{13}C$ of CO_2 for each flowpath:

$$\delta^{13}C_{H_2CO_3} = K_0\delta^{13}C_{CO_2} + (K_0 - 1) * 10^3 \quad (18)$$

$$\delta^{13}C_{HCO_3^-} = K_1\delta^{13}C_{CO_2} + (K_1 - 1) * 10^3 \quad (19)$$

K_0 and K_1 as fractionation factors, equivalent to α, are temperature dependent:

$$1000 * \ln(K_0) = -0.91 + 0.0063 * \frac{10^6}{T^3} \quad (20)$$

$$1000 * \ln(K_1) = -4.54 + 1.099 * \frac{10^6}{T^2} \quad (21)$$

and T is in Kelvin. In a system where little or no mineral precipitation occurs, O_i is approximately zero, and the formula for evolution of aqueous TDIC becomes:

$$\delta^{13}C_{TDIC} + \Delta(\delta^{13}C_{TDIC}) = \frac{(\delta^{13}C_{TDIC}+1000)(TDIC)}{TDIC+\Delta(TDIC)} + \frac{(\delta^{13}C_{atm}+1000)(m_{C_{atm}})}{TDIC+\Delta(TDIC)} +$$

$$\frac{(\delta^{13}C_{mineral}+1000)(m_{C_{mineral}})}{TDIC+\Delta(TDIC)} - 1000 \quad (22)$$

Multi-tracer analysis of groundwater age

Environmental tracers are commonly employed in groundwater studies to estimate aquifer residence times on the order of tens to thousands of years, yet are difficult to use in karst environments. Dissolution of inorganic carbon (e.g., from carbonate rocks) biases ^{14}C ages to anomalously old apparent values and requires geochemical corrections rife with uncertainty (Plummer and Glynn, 2013). Dissolved gases, like ^{3}He or chlorofluorocarbons (CFCs) remain at essentially fixed concentrations in closed-system conditions, yet will exchange with subterranean air in open systems (Busenberg et al., 2006; Solomon et al., 2006). However, open-system exchange of CFCs (e.g., in caverns) is poorly understood, and they are occasionally used for dating groundwater in lowland karst (Land and Huff, 2010; Ozyurt, 2008; Delbart et al., 2014). Further, these complications only exist in the unsaturated zone. Groundwater ages may accordingly reflect transit time in the saturated zone fairly well (Darling et al., 2012), and together with an estimate of transit time through the unsaturated zone, may yield a cumulative estimate of subsurface residence time.

The radioactive isotope tritium (^3H) comprises part of the molecular structure of water and is relatively conservative when exposed to the atmosphere. Nuclear testing in the 1950s and 1960s drastically increased atmospheric content, which raised levels in the northern hemisphere three orders of magnitude from about 1 Tritium Unit (TU) to higher than 7,000 TU in the northern United States (Michel, 1989). In the years following cessation of above-ground nuclear testing, recharge was inferred as "pre-bomb" (pre-testing) or "recent" (post-testing) based on exceedance of tritium concentration above historical atmospheric levels. With a half-life of 12.32 years (Gat et al., 2001), radioactive decay and isotopic rainout effects have lowered modern atmospheric tritium concentrations nearly to former background levels. Tritium concentrations were monitored in precipitation in Salt Lake City, UT, from 1963 to 1984, and ranged from 12.5 to 8,230 TU (IAEA GNIP, 2014). Correlation with other monitoring stations (usually Ottawa, Canada) is a common technique used to extend local records (Michel, 1989), as performed previously by Manning and Solomon (2004) to aid interpretation of the Salt Lake Valley aquifer system prior to the year 2000. The record may also be forecasted by the decay equation (Jurgens et al., 2012). Correlation and prediction through the year 2018 is performed in the METHODS section to estimate historical and modern tritium inputs to northern Utah groundwater.

Determination of groundwater age from environmental tracer data is more involved than simply matching aqueous concentrations to adjusted air curves (assumes all molecules are the same age). Current practice involves comparison of multiple tracer concentrations against "black box" age models that correspond to different hydrogeologic

flowpath types and groundwater age distributions. The model of best fit is then used to constrain a mean recharge age (e.g., Solder et al., 2016). Maloszewski and Zuber (1985, 1993) first developed these lumped-parameter models (LPM) for determining residence time in both porous-media and fractured-bedrock aquifers. The TracerLPM algorithm is a well-known LPM designed and maintained by the USGS, and has become a standard for interpretation of tracer data (Jurgens et al., 2012).

Although most models are conceptually based on flow through granular porous media, they may be abstracted for use in karst systems. Data from aquifer systems without well-understood flowpaths are first assessed in terms of either a simple piston-flow or exponential-mixing model (Fig. 9). A piston-flow model (PFM) assumes that recharge occurs through a finite area at the beginning of the flowpath, and does not mix with water of other ages as it moves through the aquifer (same age for all molecules). This model describes a confined granular aquifer with a small recharge area or an unconfined granular aquifer sampled at shallow depths along a single groundwater flowline. An exponential mixing model (EMM) permits recharge to occur uniformly along the flowpath (e.g., an unconfined granular aquifer), such that age increases with depth as well as lateral distance. In karst aquifers, a piston-flow model would align with a cavern-dominated flow regime that permits rapid infiltration, relatively little groundwater mixing, and quick transit to spring outlets. An exponential-mixing model would correspond to “diffuse” recharge along a flowpath, which would in turn imply large amounts of storage.

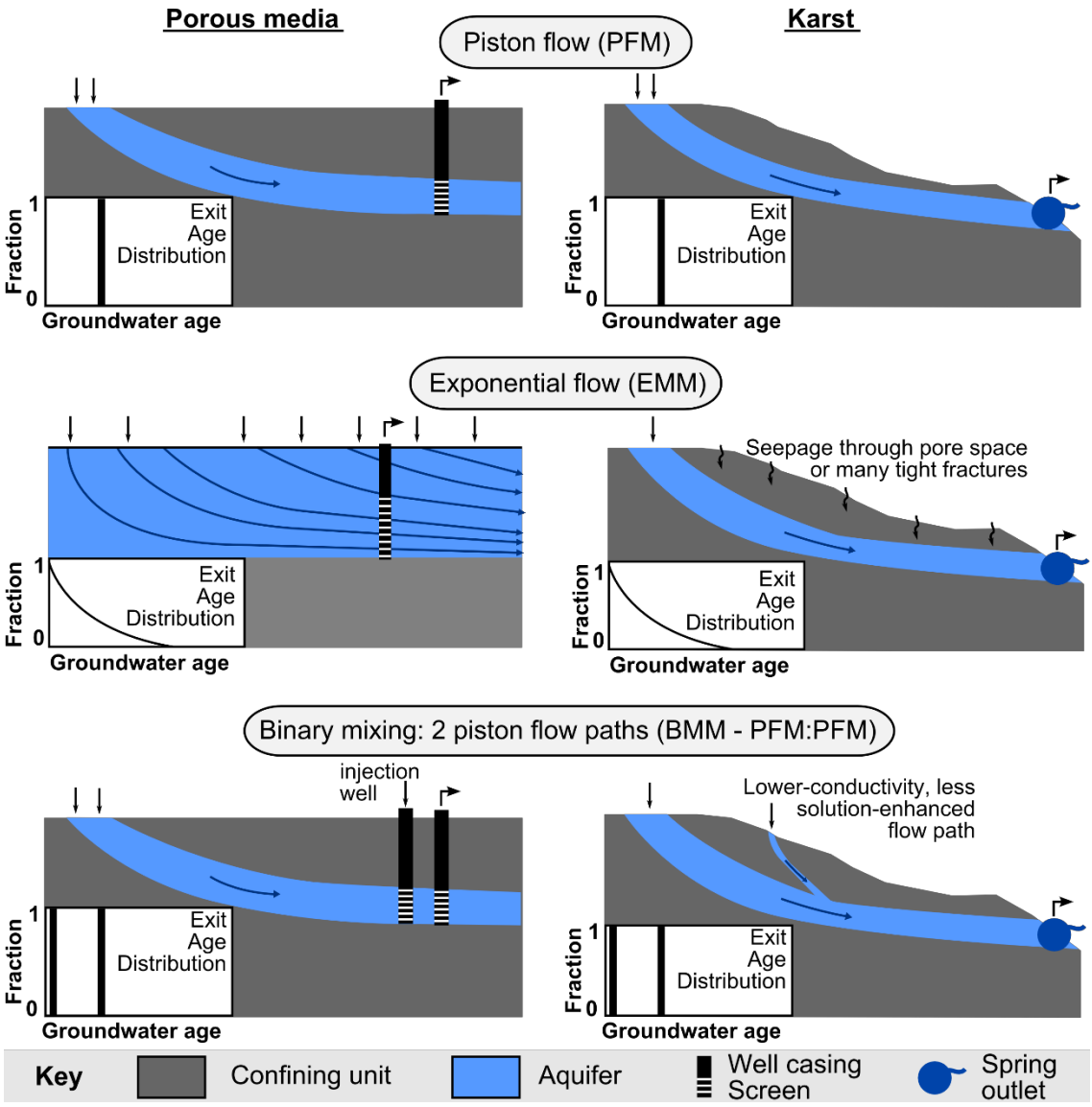

Figure 9. Schematics of lumped-parameter models that could describe groundwater flowpaths and residence times for Bear River Range springs.

Lumped-parameter tracer models consist of a cross-plot of two atmospheric tracer time-series, corrected to represent either PFM or EMM concentrations in groundwater (Fig. 10; Jurgens et al., 2012). If field data fall along or very close to the curve, the curve serves as a direct input function for age. However, data that fall along a straight line

connecting two locations on the curve likely represent a binary mixture of two groundwater components with different mean ages. Position on the line reflects the relative contribution from each groundwater component. Meaningful placement of the binary mixing line requires knowledge of one mean age. One end is usually fixed at zero concentration to infer a recharge contribution older than documented by historical air curves. Known sub-annual residence times would conversely fix the line at zero age.

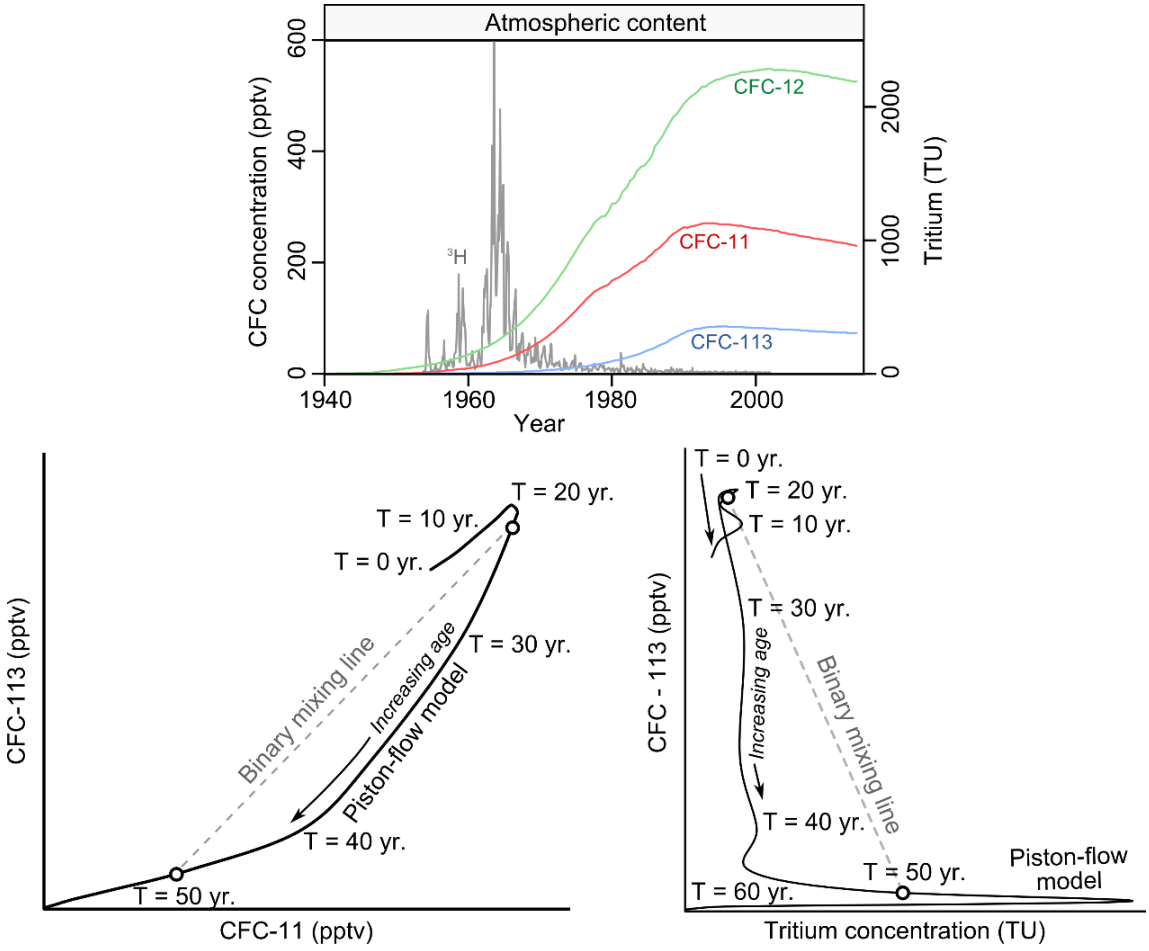

Figure 10. Air concentration curves (Jurgens et al., 2012) and example lumped-parameter models.

PREVIOUS WORK

Groundwater in Cache Valley

Bjorklund and McGreevy (1971) identified a deep, confined aquifer in the Utah portion of eastern Cache Valley, between Smithfield, Hyrum, and Wellsville, and asserted its capability to support industrial growth. Analysis of driller's logs delineated an overlying, laterally continuous clay layer totaling 31 to 37 m thick that decoupled the deep, confined aquifer from a shallow unconfined aquifer (Fig. 11).

Later numerical modeling performed for Cache Valley, by Kariya, Roark, and Hansen (KRH; 1994) of the United States Geological Survey (USGS), represented the clay layers as discontinuous and permitted flow between the shallow and deep aquifers (Fig. 11). To facilitate calculations in their model, KRH assumed that no subsurface recharge occurs from the mountain block into Cache Valley. However, the basis for these interpretations did not involve analysis of new well logs, as evidenced by three other studies (Clyde et al., 1994; Robinson, 1999; Thomas et al., 2011), and instead adhered closely to the preexisting conceptual model for the Salt Lake Valley aquifer system (Anderson et al., 1994; Inkenbrandt, 2010). KRH selected specific wells east of US Highway 89/91 that showed gaps in the clays, and ignored those farther west for which confining layers were recorded. They also excluded several deep oil wells and two other deep-water wells in mid-valley that belonged to the Bear River Water Conservancy District. The KRH model predicted that increased pumping in the principal aquifer would reduce spring and stream discharges due to hydraulic connection and infringe upon surface water rights, which resulted in a moratorium on well permits.

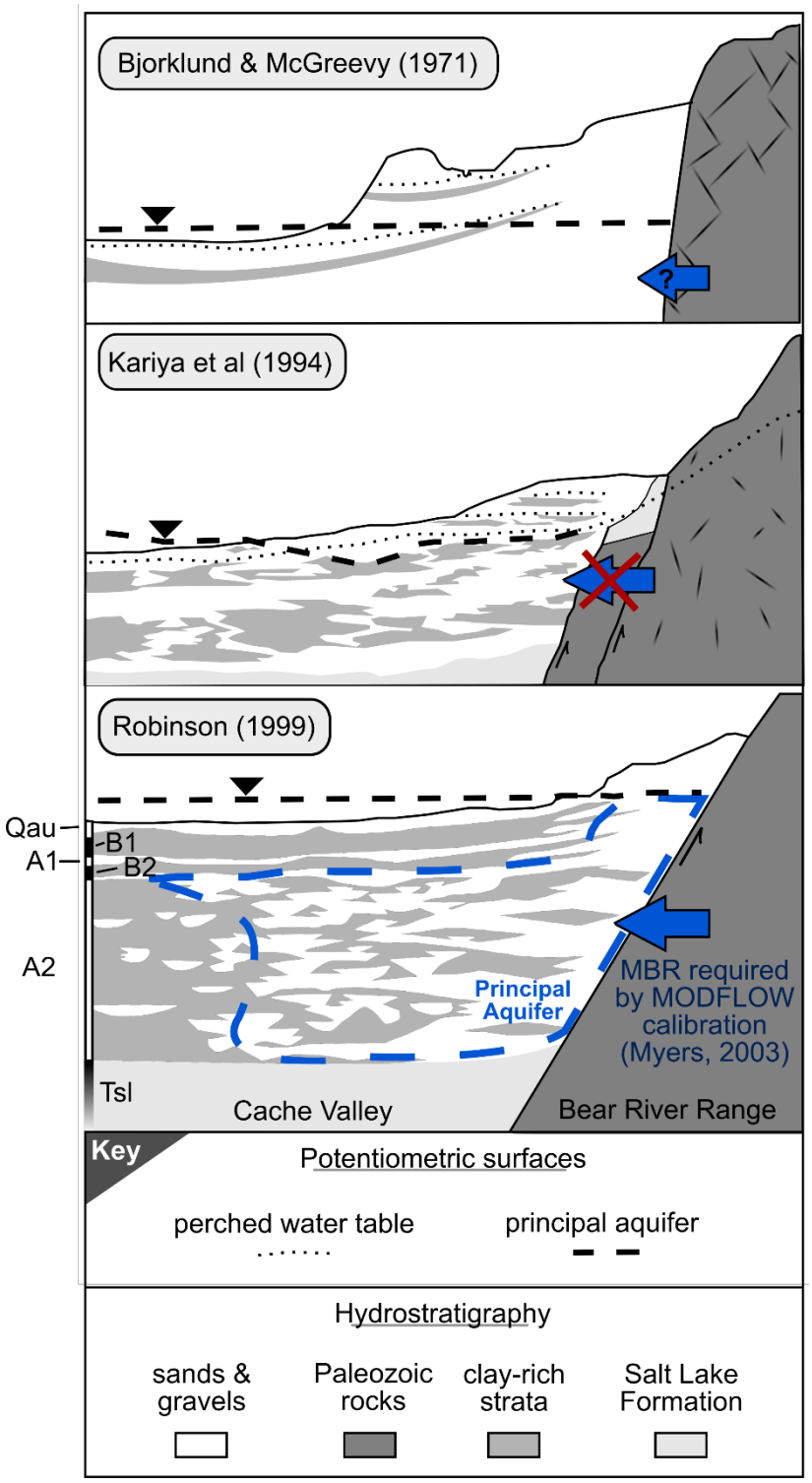

Figure 11. Conceptual hydrostratigraphic models for the principal aquifer system in Cache Valley, UT with varying requirements for mountain-block recharge.

Robinson (1999) revised Cache Valley hydrostratigraphy from analysis of over 200 driller's logs of deep-water wells. In doing so, he identified two continuous clay-confining layers with sediment oxidation-reduction patterns that likely correspond to deposition in four to five deepwater lakes (Oaks et al., 2014, 2018). These clay-confining layers clearly separate the principal aquifer from the overlying shallow, unconfined aquifer (Fig. 11). Robinson (1999) also applied multiple lines of geochemical evidence to demonstrate the presence of old groundwater in the principal aquifer and decoupling from shallow unconfined groundwater and surface water in Cache Valley. He also reviewed water-level records that superseded KRH (1994) and showed relatively constant long-term hydraulic heads that were independent of changes in pumping.

The detailed hydrostratigraphic sections and evidence for complete confinement of the principal aquifer from Robinson's study were used to create a new MODFLOW groundwater numerical model that produced significantly different results (Myers, 2003). Mountain-block recharge from the Bear River Range and Wellsville Mountains (1.8 m^3/s, or 63 cfs) was assessed during model calibration and produced hydraulic heads that matched observations better than the KRH model. This particular recharge contribution was postulated by Bjorklund and McGreevy (1971), with the caveat that underflow from the range would be difficult or impossible to measure by conventional methods.

Myers (2003) then used his calibrated model to predict the response of the principal aquifer to long-term stresses and identify effects on surface water and shallow groundwater. A transient simulation with normal precipitation levels and 20 new wells completed in the principal aquifer produced little effect on the shallow, unconfined

aquifer throughout 30 years. However, a 30-year period of decreased precipitation and no change in withdrawals from the principal aquifer clearly reduced discharge from the unconfined aquifer to surface-water features. If this newer model is correct, then the purpose of the pumping moratorium emplaced to protect surface water rights in Cache Valley incorrectly attributed truly important climatic stresses to anthropogenic causes.

Olsen (2007) performed a subsequent study to assess the seasonal behavior of springs in Cache Valley, and showed that variation in spring discharge did not correlate with the timing of pumping in the principal aquifer. Stable-isotope analysis revealed a strong similarity between shallow groundwater and canal water, but not to water of the principal aquifer. These data together support the Robinson (1999) conceptual model and the conclusions made by Myers (2003) in which the principal aquifer is isolated from the shallow unconfined aquifer.

To date, no research has attempted to quantify an annual volume of mountain-block recharge to the Cache Valley principal aquifer. King (2004) estimated underflow from the Powder Mountain area north into Cache Valley through the Davenport drainage area as 7.11×10^6 m^3/y (5.76×10^3 af/y). Oaks (2004) used the tritium data of Robinson (1999) to estimate underflow of 1.73×10^7 to 3.45×10^7 m^3/y (1.40×10^4 to 2.80×10^4 af/y) into the principal aquifer from the vicinity of Blacksmith Fork Canyon toward College Ward.

Incremental flow measurements along the Logan River and canals near the mountain front revealed that losses to groundwater were minimal in August and

November of 1990 (Roark and Hansen, 1992). However, seepage from the Logan River may occur during other seasons, as the aquifer system is locally unconfined.

Although calibration of the Myers (2003) MODFLOW groundwater model yielded an estimate of steady-state recharge from the mountain block to Cache Valley, a specific areal distribution was not determined. Instead, MBR was set to occur along the entire eastern margin of the principal aquifer. As limestone and dolostone have very low hydraulic conductivities (Van der Land et. al., 2013), flow likely emanates from bedding planes and fractures truncated at the mountain front. Mountain-front structure and quartzite-bearing stratigraphy documented by Dover (1995) and Evans et al. (1996) are likely hindrances to recharge across the northern portion of the East Cache fault, although fracture-dominated flow may occur.

If recharge enters the southern end of the principal aquifer directly from the mountain block, groundwater in that vicinity should have total dissolved solids concentrations (~250 mg/L) and pCO_2 ($10^{-2.1}$ atm) comparable to that measured in the mountain-block well in Blacksmith Fork Canyon (UT4900223 Well #4). Infiltration of surface water through unconfined sediments at the valley margins would also impart a distinct geochemical signature. Water in equilibrium with atmospheric CO_2 has a pCO_2 value near $10^{-3.39}$ atm. A low value on this order could indicate a substantial recharge contribution from surface water. Patterns in TDS and other geochemical parameters, along with spatial assessment of Stiff diagrams, may aid spatial assessment of recharge to the principal aquifer.

Groundwater and surface water in the Bear River Range

Surface water

The Logan River is the largest stream in the Bear River Range (Bjorklund and McGreevy, 1971), parallels, then crosses the LPS, and traverses a number of dipping geologic units (Figs. 4, 12; Spangler, 2012; Dover, 1995). Gathro et al. (2016) performed pilot discharge measurements and noted considerable losses to groundwater from the reach of the Logan River between Ricks Spring and Right Hand Fork during high-flow conditions. They also noted smaller losses from the Logan River between Right Hand Fork and Third Dam during mid-to-late summer.

Neilson et al. (2018) measured discharge of the Logan River and its tributary springs and streams over a wider geographic range than selected for this study, but did not partition reaches according to geologic substrate changes (e.g., the contact between the Garden City and Swan Peak Formations). They used chemical and physical flow data to infer simultaneous exchanges with the bedrock aquifer system in discrete reaches of the Logan River and documented seasonal variations in groundwater-surface water fluxes. These data together indicate both spatial and temporal complexity in the Logan River's interaction with the alpine karst system. As the locations of these interations are likely stratigraphically controlled, realignment of reach boundaries may yield additional information regarding the quantity and fate of water lost to the subsurface. These observations set a compelling basis for geologically informed discharge monitoring of the Logan River system for the purpose of estimating a minimum volume that could enter Cache Valley from the mountain block.

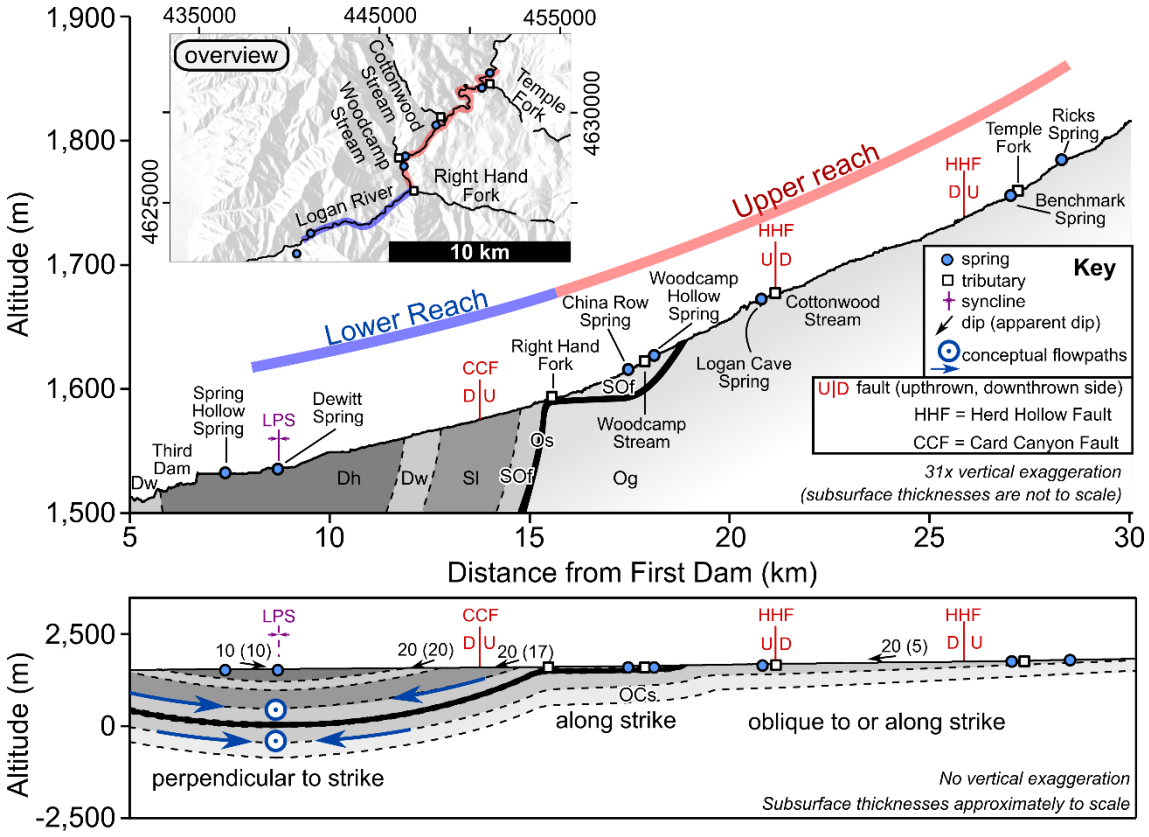

Figure 12. Geologic substrates of the Logan River between Ricks Spring and Third Dam in Logan Canyon (Dover, 1995) and possible hydrogeologic flowpaths.

Springs and their recharge areas

Seven primary springs drain dolostone- and limestone-aquifer units adjacent to the Logan River (Table 1, Fig. 13; Spangler, 2001). From northeast to southwest, they are Ricks, Benchmark, Logan Cave, Woodcamp Hollow, China Row, Dewitt, and Spring Hollow Springs. Together, they sustain the Logan River's baseflow (Gooseff et al., 2005). Dye traces indicate that some portion of recharge can travel across topographic divides and drop up to 300 m in a highly intricate conduit system to discharge at springs, spending as little as 2-4 weeks in the subsurface (Spangler, 2004).

Table 1. Sites surveyed for discharge and chemical sampling by Gathro et al. (2016) and in this study, in the NAD83 UTM Zone 12N coordinate system.

Site name	Easting *Meters*	Northing *Meters*	Altitude *Meters*	Description
Upper Logan River	451,163.0	4,631,930.1	1,783.9	A meander in the Logan River slightly upstream of Ricks Spring, across Highway 89 to the east, downstream of the fault diversion
Ricks Spring	451,094.0	4,631,957.1	1,792.9	Outlet lies in an alcove west of Highway 89 adjacent to a well-marked pullout.
Temple Fork	450,859.0	4,631,302.1	1,758.9	Adjacent to the Temple Fork parking area,.
Benchmark Spring	450,716.0	4,631,145.1	1,761.9	Outlet lies on a hillside west of Highway 89 at the base of Blind Hollow.
Cottonwood Creek	448,405.1	4,629,093.2	1,679.9	Adjacent to the Highway 89 bridge over Cottonwood Creek.
Logan Cave Spring	448,105.2	4,629,066.3	1,701.9	Several hundred feet west along Highway 89 from the Cottonwood Creek bridge.
Woodcamp Hollow Spring	446,412.2	4,627,348.3	1,627.9	East across the Logan River from the Woodcamp Hollow Campground.
Woodcamp Hollow Creek	446,292.2	4,627,129.4	1,619.9	West of the Logan River and southwest of the road leading to the Woodcamp Hollow trailhead.
China Row Spring	446,329.2	4,626,790.4	1,619.9	East of Highway 89 at an unmarked pullout and culvert that permits flow from the spring to the Logan River.
Middle Logan River	446,702.2	4,625,732.4	1,597.9	At the bridge over the Logan River immediately upstream of the confluence with Right Hand Fork.
Right Hand Fork	446,835.2	4,625,435.4	1,602.9	Adjacent to an unmarked picinic area south of the road.
Dewitt Spring	441,161.5	4,623,078.5	1,536.9	The overflow trough of the City of Logan's Dewitt Spring facility.
Lower Logan River	440,978.5	4,622,767.6	1,533.9	The Logan River adjacent to the Dewitt Picnic Area turnoff from Highway 89.
Spring Hollow Spring	440,605.5	4,621,755.6	1,622.9	Outlet is southwest of Crimson Trail, nearly 1 km from Highway 89.

Logan Cave, Benchmark, and Ricks Springs discharge from the upper Garden City Limestone, which is the lowest exposed aquifer unit contacting the selected reaches of the Logan River in this study (Spangler, 2012). Wood Camp Hollow and China Row Springs discharge from the overlying Laketown Dolomite on opposite sides of the Logan

River. Spring Hollow and Dewitt Springs discharge up-section from the Beirdneau (Db) and Water Canyon (Dw) Formations along the axis of the Logan Peak syncline.

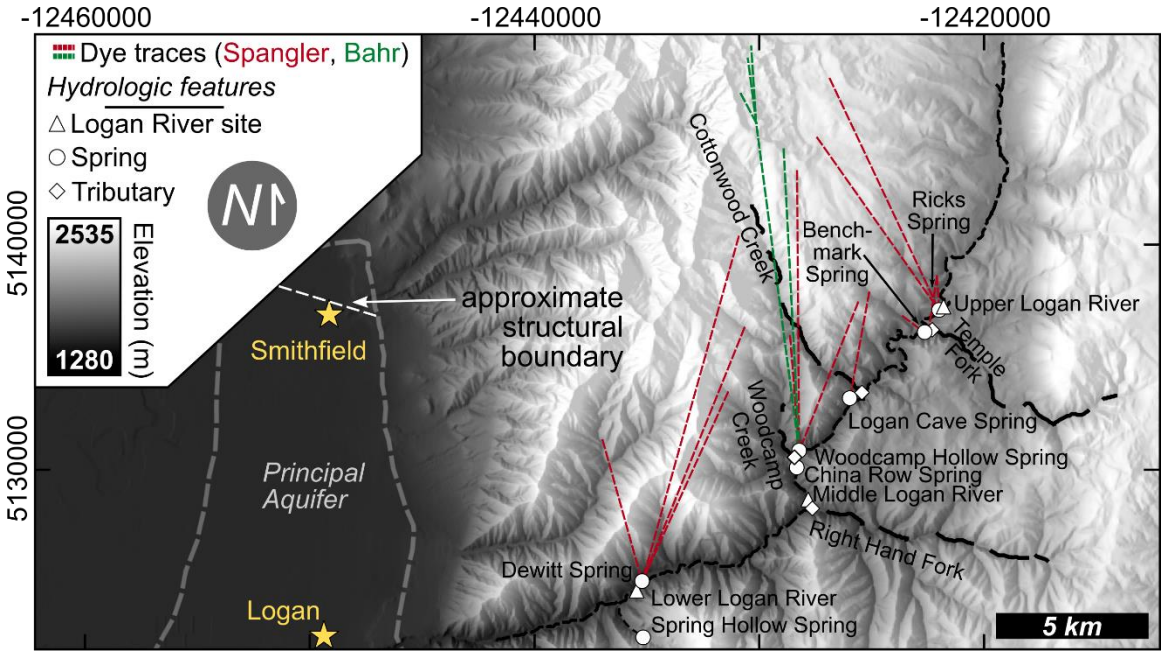

Figure 13. Springs, streams, and dye traces in Logan Canyon, Bear River Range (Spangler, 2001; Bahr, 2016), and a structural boundary to the principal aquifer (Oaks et al., 1999).

New dye-tracing data (Bahr, 2016) support the hypothesis that the Cottonwood Creek anticline (Oaks and Runnells, 1992) acts as a hydrologic partition between the Dewitt and Wood Camp Hollow Spring groundwater basins. Faults cut across the recharge areas of at least Ricks, Benchmark, Logan Cave, Woodcamp Hollow, and Spring Hollow Springs and contribute to the complexity of flowpath geometries.

The outlet of Ricks Spring lies between the Tony Grove Ranger Station and the confluence of Temple Fork with the Logan River in central Logan Canyon. Dye traces not only link Ricks Spring to recharge from altitudes at least 70-800 m higher and a

transit time of 28 days but also to a nearby diversion of the Logan River (Spangler, 2001). Ricks Spring accordingly represents a boundary to the study area, as water lost upstream on the Logan River contributes an unknown amount to the spring that does not migrate into the mountain block.

Benchmark Spring discharges from the junction of Blind Hollow and Logan Canyon. Dye traces established a link between the spring and fast-moving (17-20 days), low-altitude recharge (73-122 m above the outlet) within the Bear and Blind Hollow surface catchments (Spangler, 2001). Benchmark Spring's discharge remains below 0.03 m^3/s across seasons (Gathro et al., unpublished data), which could indicate that it drains a less karstified zone of the aquifer.

Flow to the spring at Logan Cave sources from Cottonwood Canyon and Blind Hollow from at least 35 to 390 m higher, and has a maximum quick-flow residence time of 23-28 days (Spangler, 2001). Logan Cave Spring discharges from a talus slope below the cave during late summer and fall. High-flow conditions following spring snowmelt raise the water table to the cave mouth. Seasonal flow variations in Logan Cave Spring are thought to be small and range around 0.03 m^3/s (Gathro et al., unpublished data).

Woodcamp Hollow Spring emerges from a hillside across the Logan River from the Woodcamp Hollow campground. The spring draws its highly variable flow (Gathro et al., unpublished data) from about 335 to as high as 963 m higher in the north (Spangler, 2001). Dye-trace data support the notion of a conduit-controlled flow regime that transmits groundwater from recharge areas on the order of 20-28 days.

China Row Spring is on the southeast side of the Logan River between Woodcamp Hollow and the confluence of Right Hand Fork with the Logan River. Like Benchmark Spring, China Row Spring has low (<0.03 m^3/s) discharge (Gathro et al., unpublished data). No dye-trace data exist to delineate a minimum catchment size or document the possibility of conduit flow.

Dewitt Spring sources at least 390-878 m higher to the north, around the axis of the Naomi Peak syncline (Spangler, 2002). Dye-trace data indicate a travel time of 8-31 days yet cannot describe any diffuse, slower moving component (Spangler, 2001). Dewitt Spring has several outlets, which are capped and diverted for municipal use by the City of Logan prior to release of excess flow to the Logan River. Hence, only the overflow of Dewitt Spring was measured in this study. Diverted flow of the spring is continuously gauged (UDWR, 2018), and documents drainage of large amounts of water from the alpine karst system that likely represents conduit-dominated flow.

Spring Hollow Spring discharges from an outlet nearly one kilometer up the Spring Hollow catchment from Highway 89, and flows into the Logan River from the south. While its discharge varies considerably across the seasons (Gathro et al., unpublished data), it may drain large quantities of older water (Kolesar et al., 2005). No dye-trace data exist to determine a minimum recharge altitude or catchment size, or to document the presence of quick-flowing groundwater.

Water-rock interactions and residence times

Only a few studies have attempted to assess water-rock interactions or residence times in the Bear River Range alpine karst aquifer. Gooseff et al. (2005) identified

moderate seasonal variation in major ions and stable isotopes in Spring Hollow and Dewitt Springs that may describe snowmelt dilution of a longer residing baseflow component. The possibility for decadal-scale residence time is supported by qualitative tritium analysis of eastern Bear River Range springs (Bright, 2009).

Kolesar et al. (2005) also identified order-of-magnitude differences in saturation (dolomite, quartz) between Spring Hollow and Dewitt Springs despite ubiquitously high flows, and suggested that groundwater south of the Logan River has a longer residence time. Recent radiogenic-isotope and dissolved-gas analysis in the Colorado River Basin supports this inference, and shows that high-flow springs can drain old groundwater (Solder et al., 2016). Rice (1987) and Rice and Spangler (1999) further used dolomite and calcite-saturation indices in conjunction with tritium data to infer a correlation between larger saturation indices and older ages. Hence, traditional karst hydrologic interpretations based only on flow variability may prove inaccurate in alpine settings.

Bright (2009) qualitatively assessed tritium data to infer decadal residence times for some springs in the eastern Bear River Range. This supports the likelihood that residence times for springs in Logan Canyon lie within the scope of tritium- and chlorofluorocarbon dating. Dye traces (Spangler, 2001; Bahr, 2016) support the existence of sub-annual residence times in all surveyed springs in Logan Canyon. This potentially bimodal age distribution aligns with previous work in a low-relief karst aquifer in Florida that documented a binary mixture of modern (0-7 years) and decade-scale (>60 year) residence times (Katz et al., 2009). Binary-mixing lumped-parameter models (BMM) may likewise represent residence times in the Bear River Range alpine-karst system.

Neilson et al. (2018) predicted the presence of diffuse flow in the alpine karst aquifer based upon solute mass-balance calculations for the Logan River. However, they assumed a composition for the diffuse-flow endmember, and checked it against the composition from a local bedrock well that they also assumed to represent diffuse recharge. However, it is highly unlikely that a bedrock well would produce water unless completed in a fracture or otherwise solution-enhanced zone that would better represent conduit flow. Further, only Na and Cl were selected for the mass-balance calculations of groundwater exchanges with the Logan River, despite the fact that the proximal Highway 89 receives copious amounts of road salt in the winter. Despite this clear anthropogenic source for both Na and Cl, it was never referenced in their analysis. Due to the confounding nature of anthropogenic sources for conserative solutes (Na, Cl) in the Logan River, this study will approach the possibility of long-residing diffuse flow within the alpine karst aquifer from a non river-centric perspective.

Bright (2009) noted a qualitative relationship of $\delta^{18}O$ and $\delta^{2}H$ with sampling latitude and possibly altitude for streams in the eastern Bear River Range. However, streams represent an integrated mixture of surface runoff and groundwater, and do not relate directly to precipitation fractionation effects (Brooks et al., 2012).

Major-ion concentrations vary among springs on the eastern flank of the Bear River Range, and may indicate stratigraphic partitioning of the karst-aquifer system (Bright, 2009). Ca/Mg molar ratios of different lithologic units in the eastern Bear River Range (Kaliser, 1972) may act as specific mixing end-member values for groundwater composition (Sperber et al., 1984). Stoichiometric dolostones (Ca/Mg = 1.0) such as the

Laketown Dolomite are rare. More commonly, Ca/Mg ratios vary from 1.1 to 1.7, toward calcian composition. Limestones are composed of relatively pure calcite and are rarely magnesian, with ratios varying from 12.8 to 94.0. However, highly variable Ca/Mg ratios are documented in Swan Creek Spring on the eastern flank of the Bear River Range, and suggest strong seasonal controls on groundwater chemistry. As the Wasatch Formation is not a major aquifer unit, it is unlikely to contribute significantly to solute concentrations.

Springs draining the eastern Bear River Range have uniformly high pCO_2 ($10^{-1.8}$ atm), which suggests that groundwater flowpaths are isolated from atmospheric conditions ($10^{-3.39}$ atm; Table 2). High discharges likely reflect transmissive, cavern-dominated flowpaths for each spring.

Table 2. CO_2 partial pressures and mean discharge for local springs (Bright, 2009).

Name	$\log_{10}(pCO_2)$ (atm)	Maximum observed discharge (m^3/s)
Paris Spring	-1.75	5.0
Swan Creek Spring	-1.78	9.1
Big Spring	-1.77	1.9

Carbon-isotope evolution paths for dissolution in open and closed systems may be calculated if total dissolved inorganic carbon (TDIC), masses of individual carbon species, and $\delta^{13}C$ values for different carbon reservoirs are known (Chiodini et al., 2000). Carbon-isotope values of calcite and dolomite in the Garden City vary between -2.2 and +0.6 ‰, with a mean of -0.95 ‰ VPDB (Davis, 2017), and likely represent local aquifer mineral $\delta^{13}C$.

Recent atmospheric $\delta^{13}C$ varies around -8.5 ‰ near Wendover, UT (NOAA ESRL, 2018), the closest station in current operation, with older (pre-industrial) values

near -7 ‰. Vogel et al. (1970) determined the following temperature-dependent per mil fractionation factor between gaseous and aqueous CO_2 in a dilute solution:

$$\varepsilon = 0.0041 * t - 1.18 \quad (23)$$

where *t* is in ºC. Between 0 ºC (snowmelt) and 10 ºC (warmest measured stream), this fractionation factor is approximately -1.2 ‰, which produces a calculated $\delta^{13}C$ value of -7.3 ‰ for post-industrial precipitation. Soil-CO_2 $\delta^{13}C$ is -23.3 ‰ in the proximal Wasatch Mountains (Cerling et al., 1991) and represents the approximate isotopic signature of the local soil-carbon reservoir. Geochemical speciation modeling in PHREEQC calculates TDIC, carbonic acid, and bicarbonate concentrations via simulated groundwater dissolution of calcite or dolomite. Flowpath $\delta^{13}C$ values should evolve according to equations 17-22 presented in the BACKGROUND chapter (Wigley et al., 1978).

METHODS

Water balance

Discharge measurements

Incremental stream-flow measurements were collected in two adjacent reaches of the Logan River (Fig. 14) whose division corresponds to changes in bedrock substrate: 1) Upstream of the confluence with Right Hand Fork (approximate lower contact of the Swan Peak Formation) to upstream of Ricks Spring, such that the fault-controlled Logan River diversion to Ricks Spring does not enter into water-balance calculations. This reach runs sub-parallel to the Logan Peak syncline and is primarily underlain by faulted Garden City Limestone. 2) From the lower boundary of the upper reach to a site adjacent to the Dewitt picnic area. In this reach, the Logan River runs nearly perpendicular to the Logan Peak syncline axis, and substrate lithologies are entirely up-section of the Garden City Limestone.

Discharge was measured for tributary streams and springs in each reach to quantify the total surface-water input. Flow velocity was measured in cross section with a Marsh McBirney Flo-Mate 2000 current meter and wading rod at 2-ft (0.61 m, upper Logan) to 3-ft (0.91 m middle and lower Logan) increments for each Logan River site and at 1-ft (0.30 m) increments for each spring and tributary stream. Discharge was calculated according to the following equation:

$$Q = \sum_i^f A_n * V_n \quad (24)$$

where Q is discharge in m^3/s (or cfs), V is velocity in meters (or feet) per second, A is the incremental cross-section area in square meters or square feet), i is the first increment measured, and f is the total number of cross-section increments (Templin et al., 1980).

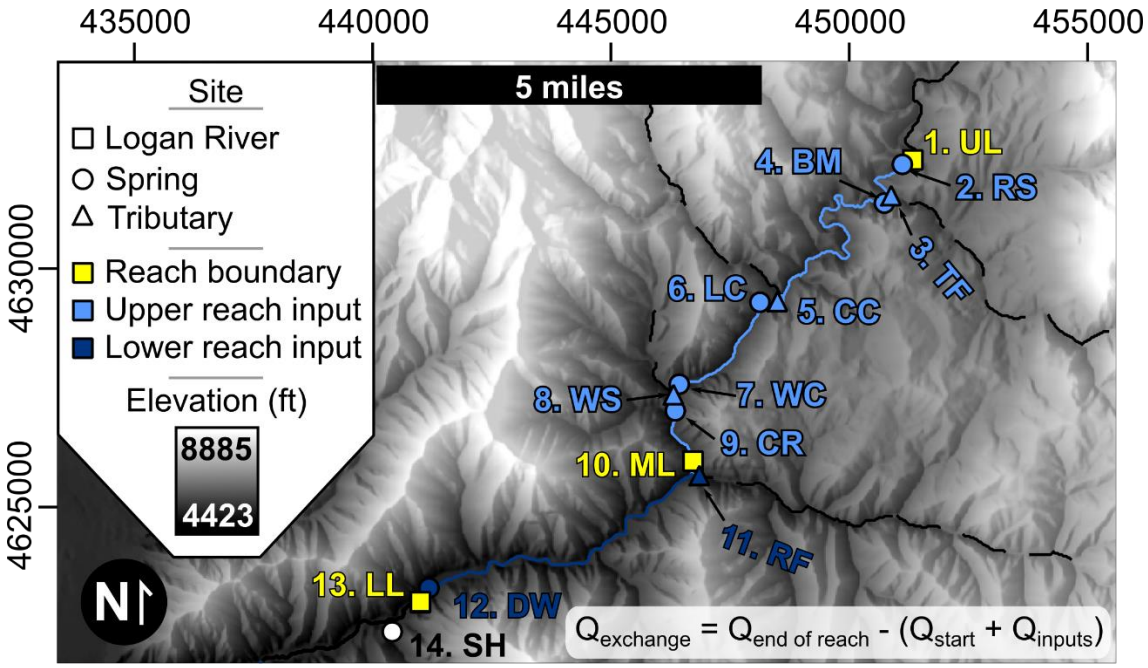

Figure 14. Upper (UL-ML) and lower reaches (ML-LL) of the Logan River surveyed in this study, along with all tributary-stream and spring inputs: RS = Ricks Spring. TF= Temple Fork, BM = Benchmark Spring, CC = Cottonwood Creek, LC = Logan Cave Spring, WC = Woodcamp Hollow Spring, WS = Woodcamp Hollow Creek, CR = China Row Spring, RF = Right Hand Fork, DW = Dewitt Spring, SH = Spring Hollow Spring.

For Benchmark, Logan Cave, and China Row Springs, it was easier to measure some or all discharge in a downstream culvert. When this was the case, the equations for flow through a partially sediment-filled pipe (Crowe et al., 2001) were used to calculate discharge. Water and sediment depth (Y_w and Y_s) and culvert radius (R) were used to find β, the central angle (in radians):

$$\beta = \operatorname{acos}\left(1 - \frac{Y}{R}\right) \quad (25)$$

The central angle was then used to find the sediment- and water-filled cross-section areas within the culvert by the following equation:

$$A = R^2 * (\beta - \cos(\beta) * \sin(\beta)) \quad (26)$$

The water-filled area was then multiplied by flow velocity, which was measured with the same Marsh McBirney Flo-Mate 2000 current meter and wading rod used at other sites.

Discharge of each tributary stream and spring were added to the initial discharge for a given reach of the Logan River, the sum of which was subtracted from the discharge at the end of the reach. This number would be approximately zero in a system without groundwater exchange, while a positive value would indicate a gain from groundwater and a negative number would indicate a loss to groundwater. These measurements were performed monthly in the pilot study from June through August 2015, and monthly as safety permitted from August 2016 through November 2017 during this study. The net volume lost to groundwater was estimated from integration of serially connected losses.

Linear regression

In order to estimate a volume lost to groundwater by the upper reach of the Logan River, data from both this and the pilot study were correlated with daily median discharges observed at the USGS gage above First Dam, near the canyon mouth. The rationale stemmed from the continuous availability of field-checked data at the USGS gage. As high-flow conditions proved too hazardous for measurement of Logan River discharge in 2017, this correlation does not span the full range of observed flows, and

thus only permits conjecture with respect to groundwater-surface water interactions. However, data collected in 2015 (a normal water year) do span the range of observed flows and are usable for correlation.

To accomplish this correlation, discharge magnitudes lost to or gained from groundwater were incorporated into a linear regression model that was used to interpolate losses for time-series integration. As an empirical model, the sole purpose is to "fill in the gaps" of missing data by correlating with a continuous data source, and does not imply a causal mechanism (Berthouex and Brown, 2002). Goodness-of-fit was assessed by standard regression statistics: p-values, parameter significance, standard errors, and r^2 values (Berthoux and Brown, 2002). Error propagation through subsequent volume estimations was accomplished via 95% confidence intervals on the mean response.

Creation of the master recession curve

A master recession curve was created from hydrograph falling limbs of the Logan River for each completely gauged year (1922-2017; USGS NWIS, 2018). Hydrographs for some years were interrupted by late-season rainfall. Accordingly, only the pristine recession portion from a given year was selected. Recession-curve fragments were broken into segments that showed a serial trend and then automatically adjusted via strongly hybridized genetic algorithms and artificial-immune networks after Gregor and Malik (2012). Nonlinear modeling was performed in the R statistical environment to fit and assess possible mechanistic models to the master recession curve.

Field chemical parameters

Chemical parameters (pH, temperature, electrical conductivity, dissolved oxygen, and alkalinity) were measured in the field at each spring, tributary stream, and site along the Logan River for each chemical sampling excursion (March, May, and November 2017). A YSI-30 salinity, conductivity, and temperature meter was used during the March and May 2017 excursions, but was replaced by a YSI EcoSense EC 300A salinity, conductivity, and temperature meter for the November excursion. A Hanna HI 9142 portable, waterproof dissolved-oxygen meter, an Orion 2013A pH meter, and a Hach model AL-AP MG-L alkalinity test kit were used to measure the remaining field chemical parameters during all field excursions. As the accuracy of the Hach test kit yields alkalinity to ± 20 mg/L, higher-precision (± 0.05 mg/L) concentrations for most samples were measured via lab titration with sulfuric acid and Bromo Blue indicator.

Major-ion analysis

Samples for major-ion analysis were collected from springs and streams during low-flow (March 2017) and high-flow (May 2017) conditions. Samples were collected at a third date (November 2017) at only Benchmark, China Row, Spring Hollow, and Dewitt Springs, concomitant to sampling for chlorofluorocarbons and tritium. Chemically clean polyethylene bottles were pre-rinsed at each site, filled with filtered sample water, and acidified with 1:1 trace-metal grade nitric acid to a pH less than 2 (Wilde, 2008). Samples for anion analysis were collected in glass bottles without acidification or filtering, as chloride and sulfate are relatively conservative and were the only intended analytes.

All samples were housed in a cooler, then a laboratory refrigerator prior to analysis. Cation and anion analyses were performed at the Utah State University Geochemistry and Water Labs via a Thermo X Series 2 Quadrupole Inductively-Coupled Plasma mass spectrometer (ICP-MS) and a Dionex Ion Chromatograph (IC) to ± 0.1 to 1.1 mg/L accuracy, respectively. The unacidified, unfiltered samples were also titrated for alkalinity as bicarbonate with 0.02 Normal sulfuric acid and Bromo Blue indicator to ± 0.05 mg/L accuracy.

Analysis of stable isotopes

Springs, tributaries, and Logan River sites were sampled for $\delta^{18}O$ and $\delta^{2}H$ stable isotopes at the same times and locations as low-flow (March 2017) and high-flow (May 2017) major-ion samples. Water for $\delta^{18}O$ and $\delta^{2}H$ stable-isotope analyses was collected at each site as grab samples in chemically clean clear or amber glass bottles, then housed in a field cooler until transferred to a laboratory refrigerator.

Snow samples for $\delta^{18}O$ and $\delta^{2}H$ stable isotope analyses were collected with a custom 10-ft (3.05 m) PVC toothed snow-coring tool in March 2017. The coring tool was driven through the snowpack until the upper soil layer was reached to ensure capture of the total snow column. The core was then cleaned of soil and ejected into a plastic 1-gallon freezer bag until total melting, at which point a chemically clean glass bottle was filled and refrigerated until analysis. Cores were collected over a range of altitudes in Logan Canyon (1,543-2,393 m asl, Fig. 15) where the snow pack was pristine and unaltered by remobilization via wind or anthropogenic activity.

Samples for carbon stable-isotope analysis were collected from springs, as only the carbon of directly discharged groundwater accurately represents water-rock interactions within the alpine-karst aquifer. These samples were collected at the same time and in the same manner as $\delta^{18}O$ and $\delta^{2}H$ samples, but in amber glass bottles to minimize aquatic biological-fractionation effects due to ongoing microbial activity (Mook, 2001). Analyses for $\delta^{18}O$, $\delta^{2}H$, and $\delta^{13}C$ were performed with a ThermoFisher Scientific Delta V Advantage isotope-ratio mass spectrometer (IRMS) with a Gasbench II peripheral, in the USU Geochemistry Lab.

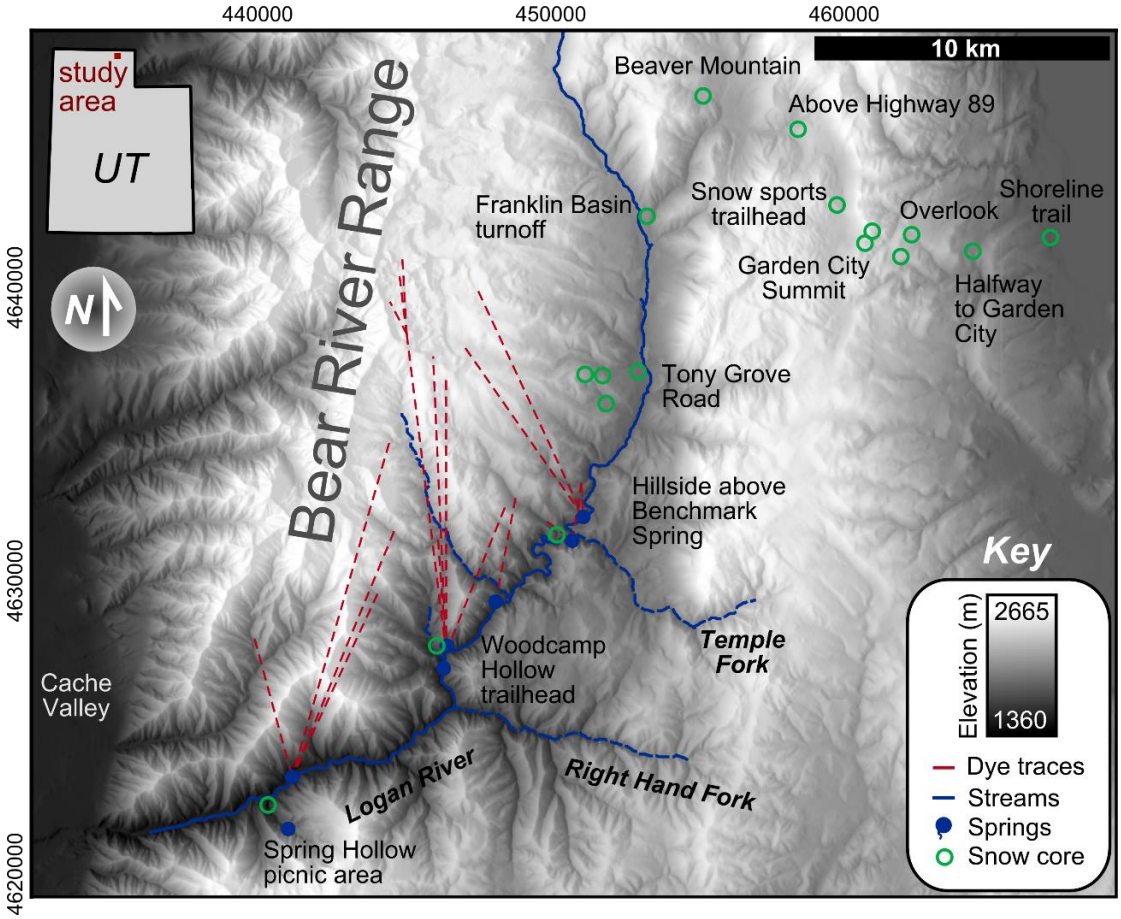

Figure 15. Locations sampled for snow $\delta^{18}O$ and $\delta^{2}H$ in early March, 2017.

Samples for hydrogen-isotope analysis were pipetted into vials, given reducing agents, capped, flushed with H_2 and He gases, and allowed to equilibrate prior to IRMS (Revesz and Coplen, 2008a). Samples for oxygen-isotope analysis were pipetted into vials, capped, flushed with CO_2 and He gases, and allowed to equilibrate prior to IRMS analysis (Revesz and Coplen, 2008b). Carbon-isotope analysis required samples to be pipetted into vials after injection with 103% phosphoric acid, whichthen were capped, flushed with CO_2 gas, and allowed to equilibrate prior to IRMS analysis. Following this, stable-isotope values were corrected for temporal drift and linearity effects and calibrated to international standards. To identify a statistical relationship of $\delta^{18}O$ and $\delta^{2}H$ to longitude (rainout distance) and altitude, bulk-snowpack stable-isotope values were assessed with analysis-of-variance. Linear regression was then used to estimate a local altitude gradient, in ‰ VSMOW per 100 m, after James et al. (2000). Precision for a data-dense altitude gradient is on the order of ± 0.5 ‰ (Brooks et al., 2012).

Geochemical modeling

Reaction paths for water-chemistry evolution were created with the PHREEQC geochemical model (Parkhurst and Appelo, 2013; after Langmuir, 1971) for the equilibrium reactions listed in the BACKGROUND chapter (equations 7-11). The enthalpy of reaction for dissolution of magnesian calcite was selected from Bischoff (1998). Enthalpies of reaction for dissolution of stoichiometric calcite and stoichiometric dolomite were obtained from the PHREEQC *llnl* database. The enthalpy of reaction for calcian dolomite was set to a default value of zero, which is standard in the absence of a thermodynamic estimate.

These models simulate simple end-member conditions for equilibrium water-rock interactions in open-system (excess gaseous CO_2) or closed-system (no CO_2 replenishment) conditions. Equilibrium speciation, saturation indices, and pCO_2 were calculated for equilibration with dolomite or calcite to assess similarity of the models to field data. Carbon mass-balance modeling was performed after Frondini et al. (2014) to incorporate $\delta^{13}C$ as a response variable that more readily distinguishes open-system and closed-system dissolution.

Chlorofluorocarbon and tritium sampling

Two high-discharge springs (Dewitt, Spring Hollow) and two low-discharge springs (Benchmark, China Row) on either side of the Logan River were sampled for chlorofluorocarbons and tritium in November 2017. A peristaltic pump with inert (Viton™ and copper) tubing was used to prevent contamination. To ensure that sampled water was subaqueous and had not yet contacted atmosphere, site conditions were assessed and modified a week prior to sampling, as follows.

The two lowest flow springs (Benchmark, China Row) seep from low-relief hillsides in central Logan Canyon. Local soil and rock were built into small retaining dams such that seepage zones were fully submerged. Dewitt Spring seeps upward through the bed of its channel, but at a much higher rate that results in a natural overlying water column of several feet. As some of the spring's water is designated for the City of Logan, and as seepage zones lie upstream of treatment, access was restricted to a hatch approximately 1.5 m above the water surface. Pre-chlorinated copper tubing extended from the pump to the vicinity of the channel bed. Spring Hollow Spring discharges

directly from a fracture that extends at least several feet below ground, sufficient for subaqueous sampling.

Chlorofluorocarbon sampling followed standard practices (USGS GDL, 2017), with copper tubing extended to the base of a 4-ounce Boston-type glass bottle within a 1-gallon stainless-steel container. The container was allowed to overflow such that a minimum of one gallon of sample water flushed through the sample bottle, which was then capped (foil-lined) underwater, with no visible air bubbles. Samples at each spring were collected in triplicate, then secured with a counter-clockwise wrap of electrical tape to prevent caps from loosening during transport. They were then inverted and stored at room temperature until delivery to the University of Utah Noble Gas Lab on the following day, where they were analyzed to a precision of ± 5% and a detection limit of 1 pg/kg for CFC-113 and 0.5 pg/kg for CFC-11 and CFC-12.

Tritium sampling at each spring was simpler, as ^{3}H is a direct constituent of water molecules and does not rapidly equilibrate with the atmosphere. Duplicate grab samples were collected in chemically clean 1-liter Nalgene © bottles, after Solomon (2017), after pre-rinsing with spring water, such that no bubbles remained. Bottles were capped underwater, then dried and secured with a counter-clockwise wrap of electrical tape to prevent loosening during overnight transport to the Brigham Young University Tritium Lab. Samples were analyzed to a precision of ± 0.1 TU and a detection limit of 0.3 TU for tritium via a Quantulus ultra-low-level liquid-scintillation counter after electrolytic enrichment (Nelson, written communication, 2017).

Lumped parameter modeling

Groundwater-age interpretation of natural tracers such as chlorofluorocarbons (CFCs) and ^{3}H is commonly accomplished with lumped-parameter modeling (Solder et al., 2016). The standard suite of lumped-parameter models, TracerLPM, is maintained by the U.S. Geological Survey (USGS). Choosing the right model requires a conceptual understanding of the flowpath and input functions for atmospheric concentrations of each tracer. Chlorofluorocarbon atmospheric concentrations are documented historically, and currently monitored at the Niwot Ridge facility in Colorado (Niwot Ridge LTER, 2018). That facility provides a direct air-curve input.

Tritium atmospheric concentrations were monitored at the IAEA Ottawa, Canada station until 2012 (IAEA, 2014), at which point records were extended with the established decay rate. As the most complete atmospheric record in North America, it is commonly correlated with incomplete records at other locations to estimate the local atmospheric history (Michel, 1989). The tritium record for Ottawa was correlated with the incomplete record from Salt Lake City (1963-1984) to produce a local estimate of atmospheric concentrations of ^{3}H through time.

RESULTS

Field measurement of streams, springs, and the Logan River

This section summarizes pilot discharge data of streams, springs, and the Logan River (Gathro et al., unpublished data; Table 3), and presents the results of monitoring from August 2016 through November 2017 (Table 4; Appendix A). Groundwater exchanges with the Logan River are calculated, complicating factors are identified, and possible solutions are also presented, as well as the results of the master recession-curve analysis.

Pilot discharge data (2015)

The discharge of all springs and tributaries to the Logan River were measured four times during June, July, and August 2015 (Table 3), aside from Woodcamp Hollow and Cottonwood Creeks, which ceased to flow in July. Logan River discharge proved more difficult to measure, as high-flow conditions at the upper and middle sites nearly exceeded the capacity of the wading rod and inhibited accuracy of flow-velocity measurements. Hence, values at these two sites from the June 2015 field excursion are only approximations. Finally, the lower Logan River site proved impossible to measure until late August 2015 due to high-flow conditions. During June 2015, the upper reach of the Logan River lost approximately 2.4 m^3/s (84 cfs). Calculations from subsequent July and August field excursions show that the upper reach gained increasing amounts from groundwater as total in-channel discharge decreased. Accordingly, it may be possible that elevation-head controls interaction of the Logan River with groundwater, such that losses

to the mountain block require high-flow conditions. Discharge at the lower Logan River site proved hazardous to measure until flow reached sufficiently low levels in late August 2015. At that point, the lower Logan River reach lost nearly 0.51 m^3/s (18 cfs). Gathro et al. (2016) conjectured that, if proportional to stage within the channel, losses in the lower reach were likely greater during high-flow conditions.

Table 3. Discharge (m^3/s) at streams, springs, and Logan River sites in 2015. Values in bold are approximations due to high flow conditions.

Site	6/6/2015	7/3/2015	8/1/2015	8/29/2015
Upper Logan River	**4.8**	3.0	1.8	1.1
Ricks Spring	1.8	0.37	0.18	0.10
Temple Fork	0.79	0.54	0.40	0.37
Benchmark Spring	0.0042	0.0059	0.0028	0.0034
Cottonwood Creek	0.25	0.00	0.00	0.00
Logan Cave Spring	0.031	0.028	0.031	0.025
Woodcamp Hollow Spring	1.4	0.71	0.45	0.28
Woodcamp Hollow Creek	0.03	0.00	0.00	0.00
China Row Spring	0.0020	0.0042	0.0045	0.0017
Middle Logan River	**6.8**	5.1	3.7	2.8
Right Hand Fork	0.37	0.37	0.28	0.24
Dewitt Spring	0.68	0.57	0.48	0.34
Lower Logan River	-	-	-	2.9
Spring Hollow Spring	-	0.45	0.31	0.18
Upper Logan gain/loss (cfs)	-2.4	0.45	0.82	0.91
Lower Logan gain/loss (cfs)	-	-	-	-0.51

Stream and spring hydrographs (August 2016 - November 2017)

Of the four tributary streams monitored in this study, only Temple Fork and Right Hand Fork are perennial (Table 4). Temple Fork stream discharge ranged from 0.28 m^3/s in October 2016 to 2.2 m^3/s in May 2017. Right Hand Fork stream discharge ranged from 0.14 m^3/s in November 2016 to 1.5 m^3/s in April 2017.

Table 4. Monthly discharge measurements (m^3/s) at each stream and spring site monitored in this study. **Bold numbers** are estimates via correlation with the USGS Logan River hydrograph. UL = Upper Logan River, RS = Ricks Spring, TF = Temple Fork, BM = Benchmark Spring, CC = Cottonwood Creek, LC = Logan Cave, WC = Woodcamp Hollow, WS = Woodcamp Hollow Creek, CR = China Row, ML = Middle Logan River, RF = Right Hand Fork, DW = Dewitt Spring overflow, LL = Lower Logan River, SH = Spring Hollow Spring, USGS = United States Geological Survey Logan River gage above First Dam.

Date	UL	RS	TF	BM	CC	LC	WC	WS	CR	ML	RF	DW	LL	SH	Gain/loss (upper reach)	Gain/loss (lower reach)	USGS gage
8/27/2016	1.5	0.15	0.45	0.0028	0.00	0.023	0.37	0.00	0.0063	3.6	0.25	0.16	3.9	0.22	1.1	-0.11	4.3
10/4/2016	0.58	0.063	0.28	0.0055	0.00	0.017	0.22	0.00	0.0085	1.9	0.15	0.28	2.0	0.11	0.73	-0.33	3.5
11/5/2016	0.75	0.048	0.31	0.0028	0.00	0.034	0.25	0.00	0.0063	2.1	0.14	0.099	2.4	0.12	0.70	0.061	4.2
3/3/2017	1.6	0.061	0.43	0.0022	0.00	0.063	0.33	0.00	0.010	3.0	0.49	0.17	4.2	0.14	0.50	0.54	5.8
4/7/2017	4.1	0.40	1.2	0.0031	0.14	0.27	0.50	0.11	0.013	-	1.5	0.36	-	0.29	-	-	13
5/11/2017	-	2.5	2.2	0.0049	0.98	0.42	2.2	1.3	0.0069	-	1.3	0.49	-	1.2	-	-	31
6/10/2017	-	**3.1**	1.8	0.018	0.95	0.27	**2.6**	1.0	0.0099	-	0.43	1.8	-	1.9	-	-	40
7/8/2017	-	1.2	1.3	0.0042	0.12	0.068	1.2	0.14	0.013	-	0.30	0.88	-	1.1	-	-	17
8/13/2017	3.0	0.42	0.93	0.0035	0.00	0.061	0.81	0.089	0.0076	5.7	0.37	0.28	7.4	0.58	0.38	1.1	8.8
9/9/2017	1.8	0.27	0.72	0.0020	0.00	0.040	0.46	0.013	0.0059	4.4	0.31	0.31	5.3	0.31	1.1	0.28	7.0
10/7/2017	1.7	0.20	0.67	0.0034	0.00	0.024	0.49	0.00	0.0077	3.3	0.21	0.19	4.6	0.19	0.20	0.90	6.0
11/18/2017	1.4	0.11	0.57	0.0029	0.00	0.044	0.39	0.00	0.0093	3.3	0.25	0.25	3.9	0.13	0.67	0.10	5.2
Minimum	0.58	0.048	0.28	0.0020	0.00	0.017	0.22	0.00	0.0059	1.9	0.14	0.10	2.0	0.11	-	-	3.5
Maximum	-	**3.1**	2.2	0.018	0.98	0.42	**2.6**	1.3	0.013	-	1.5	1.8	-	1.9	-	-	40

The two ephemeral streams in Cottonwood Canyon and Woodcamp Hollow were first documented to flow in April of 2017, with discharge values of 0.14 and 0.11 m^3/s, respectively. Although both streams reached their maximum discharges in May 2017 (0.98 and 1.3 m^3/s), Cottonwood Creek had ceased to flow in August 2017, approximately three months prior to Woodcamp Hollow Creek, which persisted until November 2017.

Maximum discharges were observed in Ricks, Woodcamp Hollow, Dewitt, and Spring Hollow Springs in June 2017 (Table 4), at which point discharge in Dewitt and Spring Hollow Springs reached 1.8 and 1.9 m^3/s respectively. Conditions were too dangerous to permit measurement of flow in Woodcamp Hollow and Ricks Springs at that time. Discharge values for both were estimated by correlation with the daily median discharge at the Logan River USGS gage via linear regression to be approximately 2.6 and 3.1 m^3/s, respectively. The linear relationship and goodness-of-fit statistics are shown in Figure 16.

Contrary to pilot data, Logan Cave Spring discharge was extremely variable, and increased to a highest observed value of 0.42 m^3/s (Table 4) in May 2017, nearly a month prior to all other springs and coincident with highest observed flow in proximal Cottonwood and Woodcamp Hollow Creeks. Possibly, this suggests that the spring at Logan Cave is recharged rapidly by surface water in nearby catchments. Benchmark and China Row Springs reached their maximum discharges in June 2017 at 0.018 and 0.023 m^3/s, respectively. China Row Spring exhibited peaks of 0.013 m^3/s in May and July.

Higher-resolution time-series data would be necessary to confirm a bimodal recharge signature.

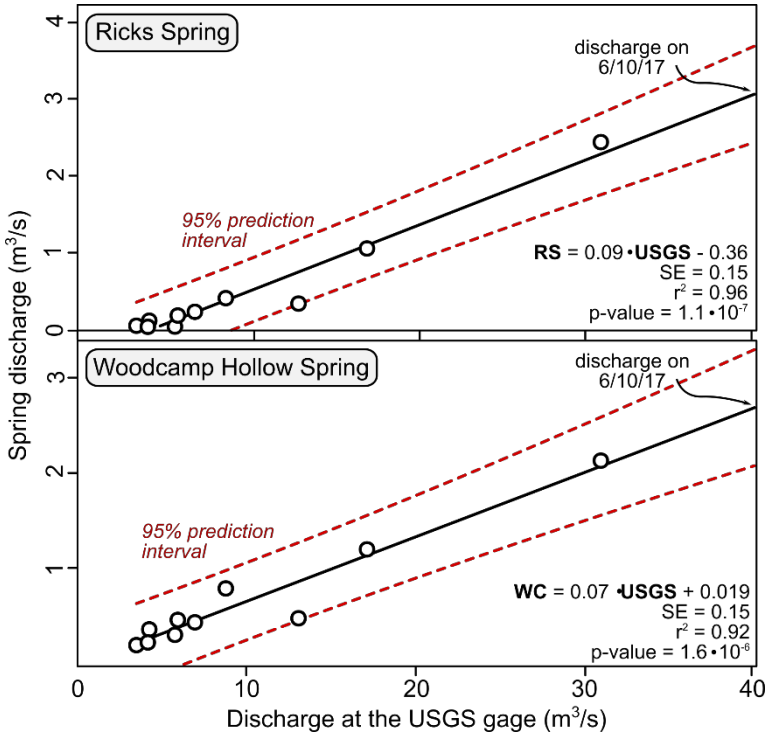

Figure 16. Discharge estimates for Woodcamp Hollow and Ricks Springs on June 10, 2017, by linear regression, with daily median discharge at the USGS Logan River gage above First Dam as the independent variable.

Difficulties

Seasonal difficulties were encountered while monitoring discharge within the study area. Temperatures dropped below the operating requirement of the flow meter and eliminated the possibility of sampling from December 2016 to the beginning of March 2017 (a total of three months). However, these data gaps are only nominally important to the study, as Logan River flow was low from November through March.

An anomalously large snowpack accumulated during the winter of 2016-2017 and

exceeded 150% of average conditions, resulting in a peak discharge nearly twice the size of that documented during the pilot study (USDA, 2018; USGS NWIS, 2018). While moderately hazardous conditions permitted measurements of Logan River flow in 2015, conditions were posed too great a hazard between April and July of 2017. However, most springs and tributaries were monitored during those months.

The abnormally high amount of snowmelt runoff activated many dry stream channels that typically do not flow. While great lengths were taken to identify each new stream, it would have been impossible for even a much larger task force to find, access, and monitor them all. Together, these anomalies obstructed water-balance calculations during spring months when the highest losses were predicted to occur.

Direct estimations via incremental streamflow of gains from, or losses to, groundwater through the Logan River channel were only possible during low-flow conditions. During this time (August-December 2016, March 2017, and August-November 2017), the upper reach of the Logan River gained from 0.20 to 1.1 m^3/s, whereas the lower reach gained from 0.061 to 1.1 m^3/s (Table 4). Notably, between 0.11 and 0.33 m^3/s were lost from the lower Logan site in late August and early October 2016, with no apparent trend.

Master recession curve

A master recession curve for the Logan River with data spanning the years 1922-2017 was assembled after Gregor and Malik (2012) in the HydroOffice RC software package. This technique uses a strongly hybridized genetic algorithm and artificial

immune network to arrange many pristine recession segments such that data dispersion is minimized. Mechanistic curve fitting tested common recession models (Fig. 17). Residual trends indicate that the piecewise-fitted Maillet (1905) model (purple envelope) does not adequately parameterize drainage from the alpine karst aquifer.

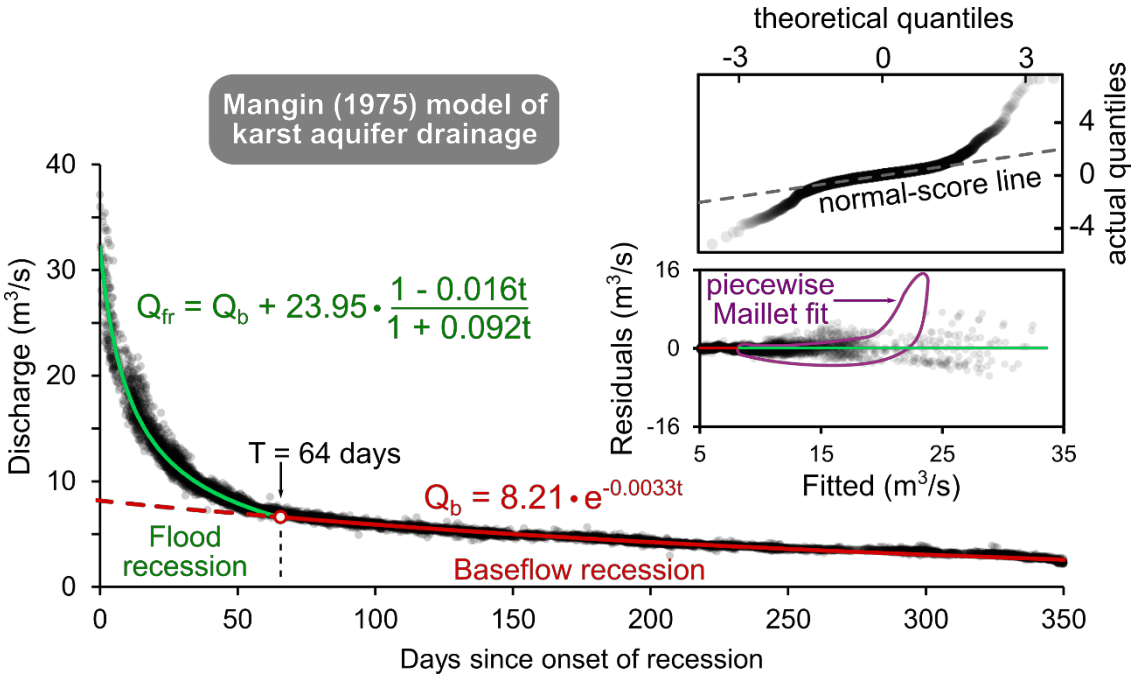

Figure 17. Master recession curve for the Logan River at the USGS gage (above First Dam) with fitted Mangin (1975) parameters and goodness-of-fit plots. Residuals from the fitted piecewise Maillet (1905) equation (purple) display a clearly deviant trend.

Further complications arise from the fact that the Maillet model is an approximate solution to the diffusion equation, designed to describe flow through homogeneous porous media, which does not capture the extreme heterogeneity and anisotropy of karst aquifers. As two piecewise curves of the MRC are readily apparent in semi-log space, it is also unlikely that a 'continuous' model (e.g., Cotagne, 1968) is applicable. A good

empirical fit with the Mangin (1975) piecewise model supports its use for interpretation of alpine karst drainage, and is described by the following two expressions:

$$Q_{fr} = Q_b + 23.95 * \frac{1-0.016*t}{1+0.092*t} \quad (27)$$

$$Q_b = 8.21 * e^{-0.0033*t} \quad (28)$$

Residuals for the Mangin model are essentially trendless, centered about zero, and normally distributed, all of which are necessary to satisfy the requirements of linear regression.

As the recession portion of the Logan River hydrograph is controlled by groundwater drainage, parameters from the fitted Mangin (1975) model likely describe hydraulic properties of the alpine-karst aquifer. These parameters are summarized in Table 5, and displayed with 95% joint-confidence regions (scatter plots of simulated variance of two parameters) in Figure 18. Joint-confidence regions are more appropriate for assessing parameter uncertainty than confidence intervals, as the latter describe a rectangle in parameter space instead of the oblong shape controlled by the degree of correlation (Berthoux and Brown, 2002). These regions are constructed via hypercube resampling according to Beale's Criterion (Beale, 1960).

Table 5. Fitted Mangin (1975) model parameters for Logan River recession.

Parameter	Value	95% confidence interval
q_o	8.21	± 0.02
$\propto$	0.00330	± 0.00002
q_o^*	23.95	± 0.34
η	0.01551	± 0.0002
t_o	64	± 2
ε	0.09196	± 0.003

Joint-confidence regions for q_o and $\propto$, as well as q_o^* and ε parameters are oblong with a positive trend, suggestive of moderate correlation. The q_o^*/η and ε/η parameters follow a weak negative trend that suggests low correlation. The regions are small, which indicates that parameters describe the data well.

Fitted parameters suggest that the unsaturated zone of the alpine-aquifer system takes approximately 64 days (η^{-1}) to drain (Table 5). The α-parameter links the concavity of the exponential portion of the recession curve to aquifer hydraulic properties (Kovacs and Perrochet, 2008). The low $\propto$ value (0.0033) could indicate high storage, long flowpaths, low conductivity, or a thin saturated zone. If the power-law portion of the Mangin (1975) model accurately describes rapid drainage of the unsaturated zone, it is likely that the saturated zone has a much lower hydraulic gradient, further addressed in the DISCUSSION chapter. The likewise rapid decrease in discharge through time from the saturated zone supports the notions that storage is minimal and that hydraulic conductivity is high. Hence, it is likely that the low $\propto$ parameter value simply describes drainage of a thin saturated zone.

Field chemical parameters

Field chemical parameters (pH, temperature, electrical conductivity, dissolved oxygen, and alkalinity) for each sampling excursion are summarized in this section and listed in Table 6. All springs are near neutral, with pH values ranging from 7.1 to 7.8. Tributary streams and the Logan River are slightly alkaline, with pH values ranging from 8.1 to 9.0. Spring temperatures are more variant than pH, with coldest groundwater

emerging from Dewitt and Spring Hollow Springs (6.4 ºC) in May and March, respectively, and warmest groundwater emerging from Benchmark Spring (11.0 ºC) in May. Surface water ranges from 4.8 ºC at the lower Logan River site in March to 10.5 ºC at Temple Fork in May.

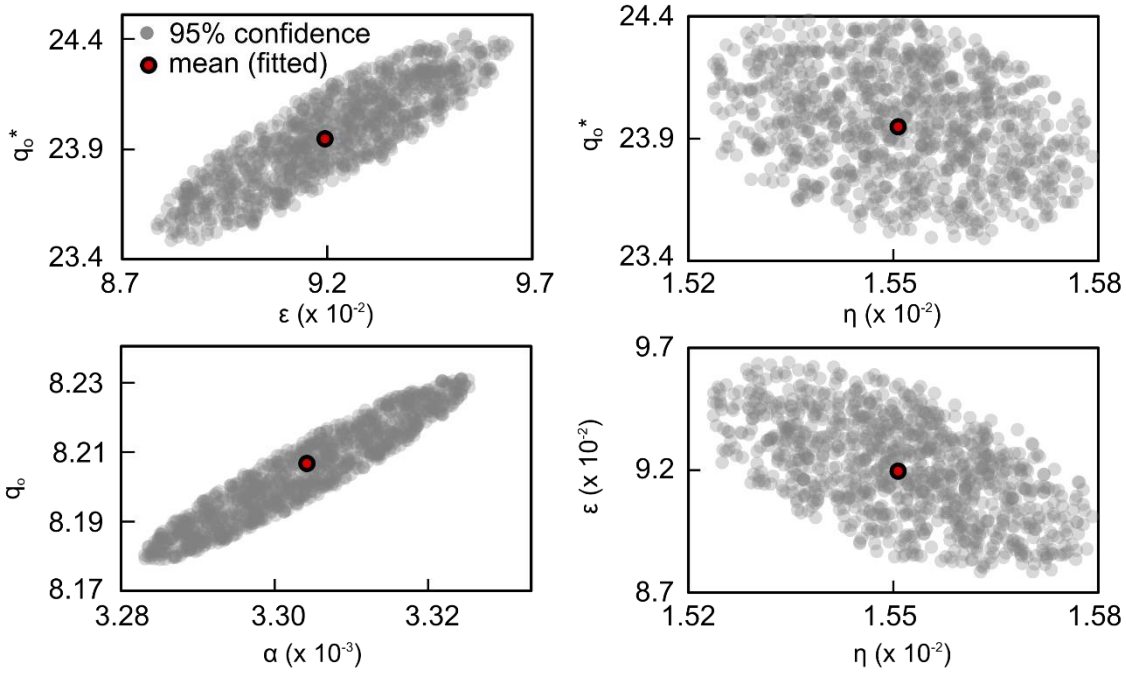

Figure 18. 95% joint-confidence regions of fitted Mangin (1975) model parameters, simulated after Beale (1960). Ellipticity relates to parameter correlation. Red circles represent mean values.

Electrical conductivity varied from site to site and across seasons. Spring values range from 193 µS at Woodcamp Hollow Spring in March to 446 µS at China Row Spring in November. Electrical conductivities of the Logan River and its tributaries are similar, ranging from 186 µS at the upper Logan River and Temple Fork in March to 378 µS at Temple Fork in May.

Table 6. Field chemical parameters from all chemical sampling excursions in Logan Canyon. NM = Not Measured.

Date	Site	pH	Temperature	Electrical Conductivity	Dissolved Oxygen	Alkalinity (Field)
		pH units	*^{o}C*	*micro-Siemens (μS)*	*mg/L*	*mg/L*
3/4/2017	Upper Logan River	9.0	5.7	186	12.5	140
3/4/2017	Ricks Spring	7.4	7.3	203	11.3	160
3/4/2017	Temple Fork	8.4	6.1	186	11.5	180
3/4/2017	Benchmark Spring	7.7	9.6	221	8.8	180
3/4/2017	Logan Cave Spring	7.3	7.3	195	11.1	180
3/4/2017	Woodcamp Hollow Spring	7.8	7.1	193	11.3	180
3/4/2017	China Row Spring	7.4	7.0	240	8.3	200
3/4/2017	Middle Logan River	8.9	6.6	198	11.8	160
3/4/2017	Right Hand Fork	8.4	7.3	216	11.5	180
3/4/2017	Dewitt Spring	7.5	7.5	198	11.0	160
3/4/2017	Lower Logan River	8.1	4.8	195	12.5	180
3/4/2017	Spring Hollow Spring	7.1	6.4	220	10.6	180
5/31/2017	Upper Logan River	8.2	10.1	214	10.0	160
5/31/2017	Ricks Spring	7.5	8.1	265	11.6	200
5/31/2017	Temple Fork	8.9	10.5	378	9.9	180
5/31/2017	Benchmark Spring	7.5	11.0	321	6.4	200
5/31/2017	Logan Cave Spring	7.5	9.1	NM	10.3	180
5/31/2017	Woodcamp Hollow Spring	7.6	9.3	NM	10.8	160
5/31/2017	China Row Spring	7.4	7.9	379	6.8	260
5/31/2017	Middle Logan River	8.3	10.0	NM	11.7	160
5/31/2017	Right Hand Fork	8.5	10.1	336	10.8	240
5/31/2017	Dewitt Spring	7.6	6.4	265	11.6	160
5/31/2017	Lower Logan River	8.5	8.5	265	10.6	120
5/31/2017	Spring Hollow Spring	7.5	6.7	277	11.5	160
11/2/2017	Benchmark Spring	7.5	9.4	270	6.8	200
11/2/2017	China Row Spring	7.5	8.8	446	5.4	220
11/3/2017	Dewitt Spring	7.6	6.8	218	NM	180
11/2/2017	Spring Hollow Spring	7.6	5.9	356	NM	180

Dissolved-oxygen concentrations are relatively invariant across space and time, although concentrations in streams (9.9-12.5 mg/L) and large springs (10.3-11.6 mg/L) exceed concentrations in Benchmark and China Row Springs (5.4-8.8 mg/L; Table 6). Overall, concentrations are near 10 mg/L, which are normal and acceptable for most fish (Behar et al., 1996).

Alkalinity via field titration ranges from 120 to 260 mg/L and varies between streams and springs in Logan Canyon (Table 6). However, the ± 20 mg/L precision of the method is undesirable for geochemical calculations, so spring samples from each excursion and surface-water samples from high-flow sampling were also analyzed via lab titration. The range of alkalinity values then shifted between 195 mg/L and 305 mg/L (Table 7). A far better precision of 0.1 mg/L was also achieved. Hence, lab-titrated values are used for all geochemical calculations involving alkalinity except for surface-water samples collected during low-flow conditions, when only field measurements were collected.

Analysis-of-variance was performed to assess the effects of changing flow conditions on field chemical parameters (Table 8). As noted above, pH varies between springs (near neutral) and streams (slightly alkaline). This may reflect the different effects of higher-pressure cavern air and lower-pressure atmosphere on dissolution, or lithological differences in water-rock interactions. Dissolved oxygen differs between springs and streams, which is likely due to low concentrations in Benchmark and China Row Springs, but not in other springs. Temperature and electrical conductivity do not vary between springs and streams, although they do increase in May, when air

Table 7. Major ions in springs, tributaries, and the Logan River from all chemical sampling events.

Site	Date	Na^+	Mg^{2+}	Al^{3+}	K^+	Ca^{2+}	HCO_3^-	SO_4^{2-}	Cl^-	Si	Charge balance
		mg/L	*mg/L*	*mg/L*	*mg/L*	*mg/L*	*mg/L*	*mg/L*	*mg/L*	*mg/L*	Percent
Upper Logan River	3/4/2017	9.5	18.4		1.6	34.5	140	2.3	18.2	3.2	**+11**
Ricks Spring	3/4/2017	5.6	19.8	0.01	1.5	37.8	234	2.2	18.2	3.3	-3
Temple Fork	3/4/2017	3.5	17.6	-	1.5	38.0	180	4.0	4.0	4.2	**+6**
Benchmark Spring	3/4/2017	5.0	22.4	0.04	1.8	38.4	250	3.0	7.3	4.7	-2
Logan Cave Spring	3/4/2017	2.1	22.2	-	1.6	33.9	238	3.1	7.3	3.7	-1
Woodcamp Spring	3/4/2017	1.3	26.8	0.01	1.1	32.4	242	2.1	1.4	2.4	0
China Row Spring	3/4/2017	30.7	28.6	-	1.6	44.0	283	4.8	55.2	3.7	+1
Middle Logan River	3/4/2017	8.2	21.2	-	1.6	36.1	160	2.9	13.3	3.2	**+9**
Right Hand Fork	3/4/2017	6.2	19.1	-	2.5	45.3	180	-	-	5.4	-
Dewitt Spring	3/4/2017	3.4	22.7	-	1.6	36.2	256	7.4	3.9	2.8	-3
Spring Hollow Spring	3/4/2017	3.5	19.6	0.01	1.6	38.1	224	14.8	2.0	3.1	+5
Lower Logan River	3/4/2017	8.9	22.1	-	1.9	41.1	180	6.1	20.5	3.4	**+9**
Upper Logan River	5/31/2017	2.6	13.2	-	1.9	29.6	195	1.5	2.3	2.8	**-10**
Ricks Spring	5/31/2017	1.6	17.0	0.02	1.7	37.8	238	1.2	1.3	2.7	-3
Temple Fork	5/31/2017	2.4	15.5	-	1.2	40.6	238	2.8	2.4	3.7	**-12**
Benchmark Spring	5/31/2017	3.9	16.6	-	1.7	28.3	262	2.2	1.8	4.8	**-16**
Logan Cave Spring	5/31/2017	1.6	19.5	-	1.5	32.0	226	3.2	6.5	2.7	-4
Woodcamp Spring	5/31/2017	0.6	23.3	0.01	0.3	26.6	226	0.8	0.6	1.8	-3
China Row Spring	5/31/2017	23.8	26.8	-	0.5	39.6	305	4.7	31.7	3.9	-3
Middle Logan River	5/31/2017	2.1	15.8	-	1.3	30.5	238	2.8	2.4	3.7	**-12**
Right Hand Fork	5/31/2017	5.7	16.9	-	2.0	46.9	287	5.3	5.6	5.5	**-12**
Dewitt Spring	5/31/2017	1.3	12.9	-	1.3	33.8	208	3.0	1.2	2.1	**-8**
Spring Hollow Spring	5/31/2017	1.8	12.6	-	1.8	40.8	232	3.9	1.8	2.9	**-7**
Lower Logan River	5/31/2017	2.7	15.6	0.01	1.7	31.5	214	1.7	4.1	2.7	**-11**
Benchmark Spring	11/2/2017	4.3	16.8	0.01	0.7	49.4	250	3.2	6.7	4.0	+1
China Row Spring	11/2/2017	7.4	19.6	0.01	0.9	55.6	287	4.0	7.3	3.4	+1
Dewitt Spring	11/3/2017	1.3	15.2	0.03	0.8	44.3	232	7.8	1.2	2.2	-3
Spring Hollow Spring	11/2/2017	2.2	15.0	0.03	2.5	50.9	232	16.3	2.2	2.8	0

temperatures became considerably warmer. The relatively high (446 μS) electrical conductivity value measured at China Row Spring does not seem to have a ready explanation.

Table 8. Analysis-of-variance for field chemical parameters between springs and streams during low- or high-flow conditions. Shading highlights significant factors.

	High vs. low flow		Spring vs. stream	
Parameter	Sum-of-squares	Significance	Sum-of-squares	Significance
pH	0.0	<90%	6.7	>99.9%
Dissolved Oxygen	0.0	<90%	6.7	>99.9%
Temperature	26.1	>99%	0.1	<90%
Electrical Conductivity	64090	>99.9%	3625	<90%

Major ions

Major-ion concentrations of springs, streams, and the Logan River during high- and low-flow conditions are summarized in Table 7. Sulfate and chloride concentrations for Right Hand Fork in March 2017 were not reported, due to freezing and breakage of the sample bottle in storage.

The quality of a major-ion analysis is assessed by balancing the charge contribution of each cation and anion (meq/L) in a water sample (Langmuir, 1997). Accurate lab methods will produce a charge balance near 0%, with discrepancies less than 5% typically considered sufficient. Charge balances for spring waters from this study ranged from 0 to 16%. Of these samples, only three exceed the 5% limit (high-flow samples from Dewitt, Spring Hollow, and Benchmark Springs). Surface water samples from low-flow conditions all exceed a charge balance of 5% due to a lack of lab-measured alkalinity, yet are included in this study for completeness.

Major ions for all water chemistries are dominated by Ca^{2+}, Mg^{2+}, and HCO_3^- across seasons. Relative cation percentages of samples from high- and low-flow conditions cluster tightly on a trilinear plot (Piper diagram) for all springs except Woodcamp Hollow and China Row (Fig. 19; Piper, 1944). The relative percentage of Mg^{2+} is highest in Woodcamp Hollow Spring, which may reflect a greater influence of dolomite in water-rock interactions in the source area.

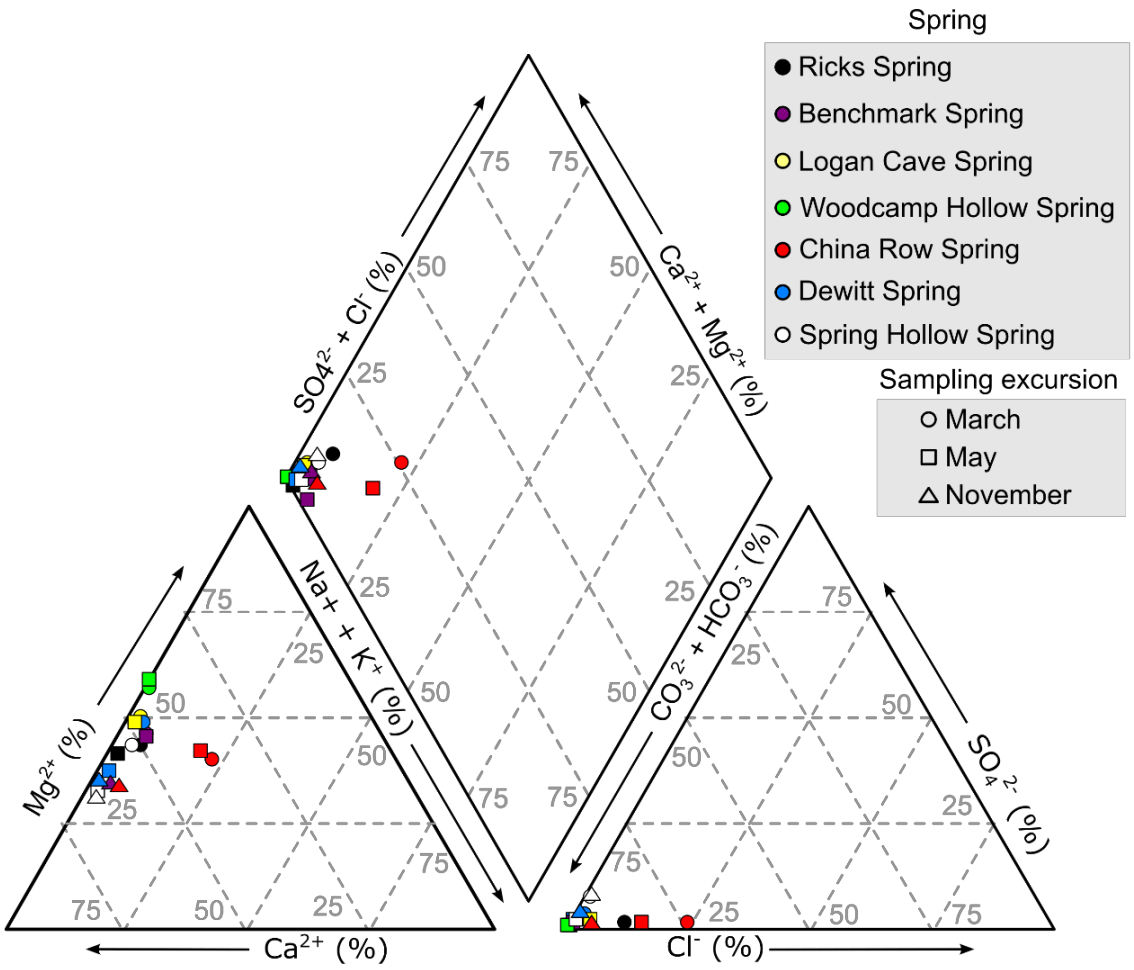

Figure 19. Piper (1994) diagram of major-ion chemistries of springs in Logan Canyon.

Increased levels of Na^+ and Cl^- are present in China Row Spring. However, late-recession resampling (November) of China Row Spring at an upslope outlet farther from Highway 89 resulted in a water chemistry with far lower chloride concentrations. Water samples collected from Ricks Spring during low-flow conditions also contain elevated sodium and chloride concentrations that are not present during high-flow conditions, and may stem from interaction with road salt and upstream interactions with the Logan River. China Row Spring's ion percentages did not change much between high- and low-flow conditions yet approached those of other springs when resampled in November.

Accordingly, concentrations in the original two samples may also relate to contamination via road salt. Relative percentages of cations and anions are similar for all surface-water samples (Fig. 20). However, the amount of chloride in the Logan River increases during low-flow conditions. This anomaly does not occur in Temple Fork, the only tributary stream monitored across seasons. As the dirt road paralleling Temple Fork is neither cleared nor salted in winter, this observation reinforces the conclusion that anomalous chloride in China Row and Ricks Springs results from an influx of road salt.

Saturation index and pCO_2 calculations in PHREEQC

CO_2 partial pressures (pCO_2) were calculated in PHREEQC for all springs, Logan River sites, and Temple Fork (Table 9). The value for Right Hand Fork was not calculated due to freezing and breakage of the sample bottle in storage. Log-transformed values are invariant across seasons for any spring or the lower Logan River (Fig. 21). Logan Cave and China Row Springs exhibit highest the pressures ($\log pCO_2 = -2.1$ atm), and Benchmark and Woodcamp Hollow Springs exhibit the lowest (both -2.5 atm).

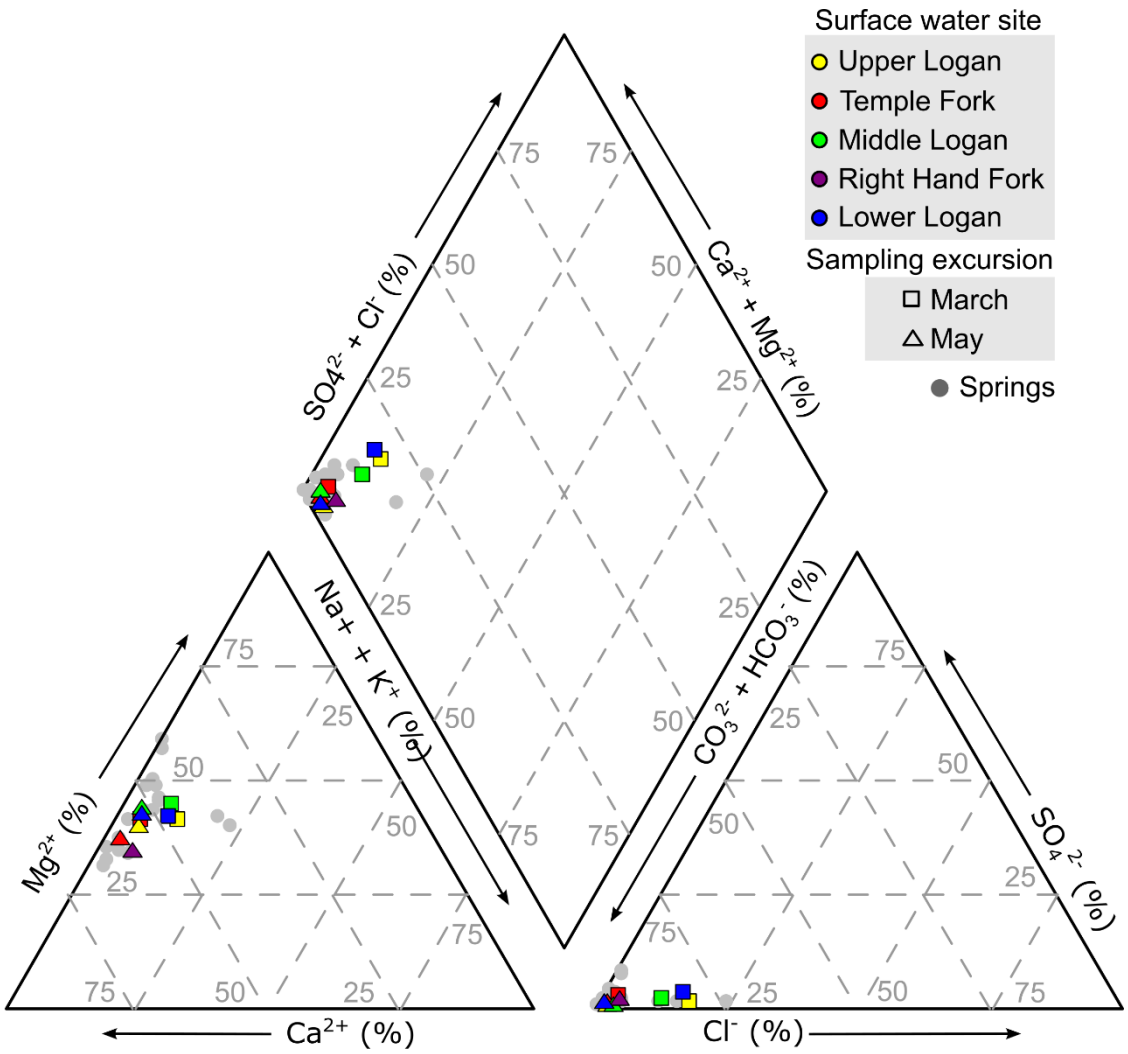

Figure 20. Piper (1944) diagram of major-ion chemistries of streams in Logan Canyon.

Log pCO_2 was calculated for surface-water samples, and is near atmospheric for most streams. Logan River sites range from -2.8 atm during high-flow conditions to -3.0 atm during low flow (Table 9). This is possibly due to large flow contributions from springs at upstream locations. The overall difference between surface water and springs highlights that outgassing of CO_2 may occur rapidly as groundwater emerges and turbulent conditions are encountered (Doctor et al., 2008).

Table 9. Calculated log pCO_2 and saturation indices with respect to possible aquifer minerals.

Site	Sampling Date	Log_{10} of pCO_2	*Saturation indices* Stoichiometric Calcite	Stoichiometric Dolomite	Quartz	Calcian Dolomite
Upper Logan	3/4/2017	-4.0	0.9	2.8	0.2	1.8
Ricks Spring	3/4/2017	-2.2	-0.4	0.2	0.2	-0.9
Temple Fork	3/4/2017	-3.3	0.6	2.1	0.3	1.1
Benchmark Spring	3/4/2017	-2.5	0.0	1.2	0.3	0.1
Logan Cave Spring	3/4/2017	-2.1	-0.5	0.1	0.2	-0.9
Woodcamp Hollow Spring	3/4/2017	-2.5	0.0	1.2	0.0	0.1
China Row Spring	3/4/2017	-2.1	-0.3	0.5	0.2	-0.5
Middle Logan	3/4/2017	-3.8	0.8	2.8	0.1	1.8
Dewitt Spring	3/4/2017	-2.3	-0.2	0.6	0.1	-0.5
Lower Logan	3/4/2017	-3.0	0.3	1.5	0.2	0.5
Spring Hollow Spring	3/4/2017	-2.0	-0.7	-0.5	0.2	-1.5
Upper Logan	5/31/2017	-3.0	0.3	1.6	0.0	0.5
Ricks Spring	5/31/2017	-2.2	-0.3	0.4	0.1	-0.7
Temple Fork	5/31/2017	-3.7	1.2	3.4	0.1	2.3
Benchmark Spring	5/31/2017	-2.2	-0.2	0.6	0.2	-0.5
Logan Cave Spring	5/31/2017	-2.3	-0.4	0.4	0.0	-0.7
Woodcamp Hollow Spring	5/31/2017	-2.4	-0.3	0.6	-0.1	-0.5
Right Hand Fork	5/31/2017	-3.2	1.0	2.8	0.4	1.7
Middle Logan	5/31/2017	-3.0	0.4	1.9	0.0	0.8
China Row Spring	5/31/2017	-2.1	-0.2	0.7	0.2	-0.4
Dewitt Spring	5/31/2017	-2.4	-0.2	0.4	0.0	-0.6
Lower Logan	5/31/2017	-2.8	0.2	1.4	0.1	0.3
Spring Hollow Spring	5/31/2017	-2.3	-0.2	0.3	0.1	-0.7
Benchmark Spring	11/2/2017	-2.2	-0.1	0.6	0.2	-0.5
China Row Spring	11/2/2017	-2.2	0.0	0.8	0.1	-0.3
Dewitt Spring	11/3/2017	-2.4	-0.1	0.6	0.0	-0.4
Spring Hollow Spring	11/2/2017	-2.4	-0.1	0.6	0.1	-0.4

Possibly, the increase in CO_2 partial pressure of the Logan River during high-flow conditions reflects increased contributions from springs such that river water at the sample sites is not yet in equilibrium with atmospheric pressure. A lower pCO_2 value for Temple Fork during high-flow conditions may indicate that springs contribute less and runoff contributes more to upland streams in its catchment.

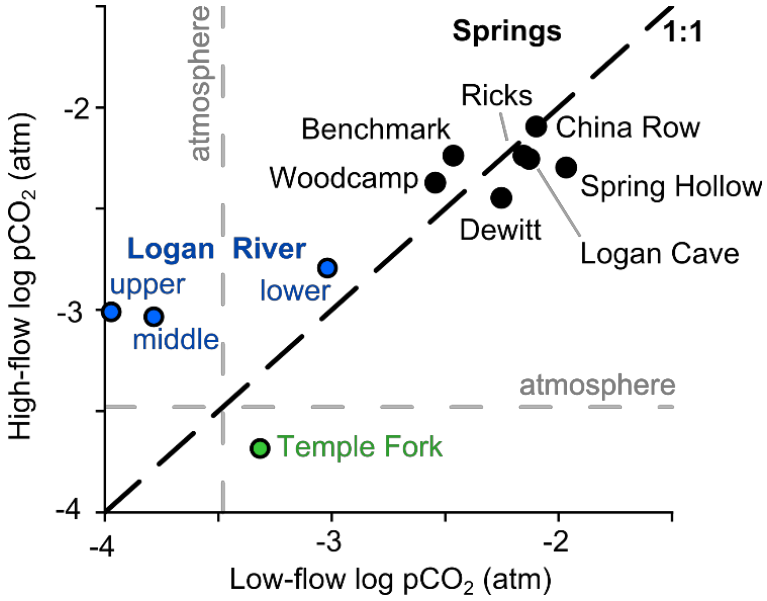

Figure 21. Seasonal variation of log pCO2 changes in springs and streams.

Saturation indices with respect to dolomite and calcite were calculated in PHREEQC from the ion-activity product (IAP) and solubility product (Ksp) via the following equation (Langmuir, 1997):

$$SI = \log\left(\frac{IAP}{K_{sp}}\right) \tag{29}$$

Saturation indices are shown in Table 9 and Figure 22. Samples collected during high-flow and low-flow conditions generally range from undersaturated to saturated with respect to calcite and saturated to supersaturated with respect to stoichiometric dolomite. However, Spring Hollow Spring was undersaturated with respect to both calcite and stoichiometric dolomite during low-flow conditions.

Saturation indices with respect to calcite and dolomite from this sampling event follow a linear trend. However, values from all sites cluster near slight calcite undersaturation and slight dolomite supersaturation in samples from later high-flow and

late-recession field excursions. Although equilibrium with respect to dolomite and calcite was estimated to be ± 0.1 SI units by Langmuir (1971), propagation of error in this study (pH = ± 0.1, Ca and Mg concentrations = ± 1 mg/L) indicates that a value on the order of ± 0.3 would be a more appropriate range for equilibrium.

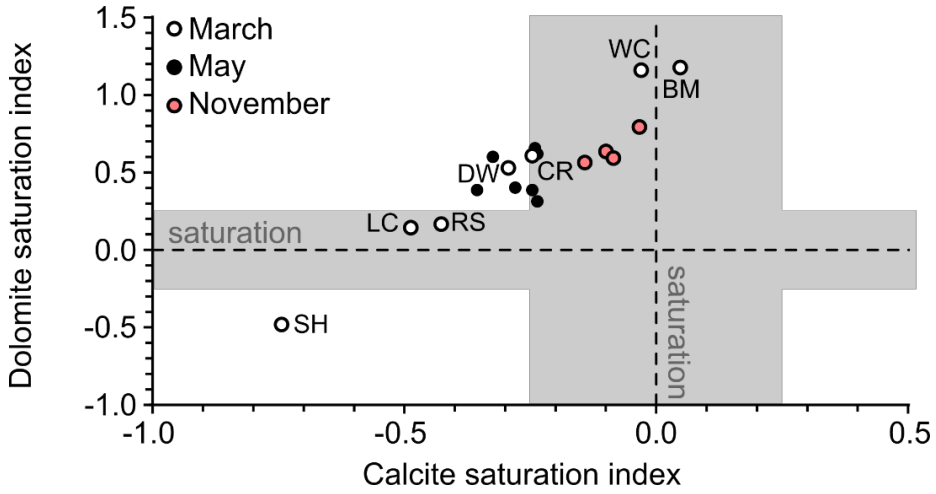

Figure 22. Seasonal changes of saturation indices with respect to dolomite and calcite for springs in Logan Canyon.

Oxygen and hydrogen stable isotope ratios

Oxygen and hydrogen stable-isotope values for springs and streams, and for the alpine snowpack at different altitudes are reported in Tables 10 and Table 11, respectively. Oxygen stable-isotope values for springs in 2017 range from -16.5 ‰ during low-flow conditions down to -18.2 ‰ during high-flow conditions. However, the compositions of high flows likely represent a mixture of new snowmelt with preexisting groundwater. To correct to the most likely recharge signature, a simple balance equation was applied using volumes and delta values from high and low flow, after Kendall and Doctor (2003). This correction shifts the high-flow range to -18.3 ‰ to -17.4 ‰.

Table 10. Oxygen (‰ VSMOW), hydrogen (‰VSMOW), and carbon (‰VPDB) stable isotopes in springs and streams.

	March 2017			May 2017						November 2017
Site	$\delta^{18}O$	$\delta^{2}H$	$\delta^{13}C$	Unadjusted $\delta^{18}O$	Adjusted $\delta^{18}O$	Unadjusted $\delta^{2}H$	Adjusted $\delta^{2}H$	Unadjusted $\delta^{13}C$	Adjusted $\delta^{13}C$	$\delta^{13}C$
Ricks Spring	-17.0	-124	-9.9	-17.4	-17.4	-127	-127	-12.3	-12.3	-
Benchmark Spring	-17.6	-137	-10.2	-18.2	-18.3	-135	-135	-10.6	-10.5	-11.6
Logan Cave Spring	-16.6	-129	-11.6	-17.6	-17.7	-132	-133	-11.8	-11.8	-
Woodcamp Hollow Spring	-16.9	-132	-11.3	-17.8	-18.0	-131	-131	-8.8	-8.4	-
China Row Spring	-16.5	-129	-11.8	-17.1	-17.9	-128	-127	-11.7	-11.9	-12.5
Dewitt Spring	-16.9	-128	-11.0	-17.6	-17.7	-125	-124	-9.1	-8.9	-12.1
Spring Hollow Spring	-17.0	-125	-10.0	-17.5	-17.5	-124	-124	-8.5	-8.4	-11.5
Upper Logan River	-16.9	-126	-	-17.2	-	-127	-	-	-	-
Temple Fork	-17.3	-129	-	-17.7	-	-127	-	-	-	-
Middle Logan River	-16.9	-131	-	-17.7	-	-130	-	-	-	-
Lower Logan River	-15.9	-121	-	-17.6	-	-127	-	-	-	-

Table 11. Locations and stable-isotope values (‰VSMOW) of snow cores collected at different altitudes in the Bear River Range.

Site description	Easting (m)	Northing (m)	$\delta^{2}H$ (‰)	$\delta^{18}O$ (‰)	Altitude (ft)
Wooded area near the intersection of Tony Grove Road and Highway 89	452,983.0	4,637,132.2	-139	-17.9	1,916.0
Wooded north-facing slope off of Tony Grove Road	451,772.1	4,637,002.1	-141	-18.0	2,076.0
Wooded false summit south of Tony Grove Road	451,175.5	4,637,043.2	-135	-17.6	2,208.0
Stand of trees south of Tony Grove road across a field	451,894.7	4,636,045.2	-140	-18.3	2,000.1
Spring Hollow picnic area	440,376.2	4,622,543.2	-132	-16.9	1,542.9
Woodcamp Hollow trailhead	446,226.5	4,627,493.1	-125	-16.0	1,649.9
Adjacent to the bridge to Woodcamp Hollow	446,341.0	4,627,372.2	-129	-16.6	1,630.1
Wooded hill above Benchmark Spring	450,639.3	4,631,504.2	-131	-17.0	1,795.0
Wooded hill above Franklin Basin turnoff	453,289.8	4,642,435.1	-143	-18.6	2,044.0
Wooded area near Beaver Mountain Resort	455,201.9	4,646,541.2	-145	-18.9	2,208.0
Wooded slope above Highway 89	458,440.6	4,645,404.2	-144	-18.9	2,279.0
Wooded slope south of snow sports trailhead	459,770.4	4,642,821.1	-141	-18.3	2,350.9
Wooded slope south of the Garden City summit	460,723.5	4,641,518.1	-142	-18.8	2,393.0
Wooded area south of Bear Lake Overlook	461,946.3	4,641,061.2	-139	-18.4	2,310.1
Wooded area, half way down Highway 89 to Garden City	462,316.6	4,641,808.2	-142	-18.9	2,265.9
Wooded area near cabins on Highway 89	464,407.3	4,641,242.1	-126	-16.7	2,023.0
Bear Lake Scenic Trail, south of Garden City	467,051.4	4,641,714.2	-134	-17.9	1,812.0

Hydrogen stable-isotope values for springs ranged from -124 ‰ during low-flow conditions down to -135 ‰ during high-flow conditions. As the same mixing principle applies to δ^2H values, the same volume-balance correction was applied, although change was only up to 1 ‰ (less than possible analytical error).

Carbon stable isotopes

Values of carbon stable isotopes of DIC for springs from all sampling excursions are listed in Table 10. Values are highly similar during low-flow conditions, with a range of -9.9 ‰ (Ricks Spring) to -11.8 ‰ (China Row Spring). Values of carbon stable isotopes increased slightly during high-flow conditions, with a range from -8.5 ‰ in Spring Hollow Spring to -12.3 ‰ in Ricks Spring. As with other stable-isotope values, $\delta^{13}C$ during high-flow conditions were corrected. As with the δ^2H values, there was no change in the maximum value and only a decrease of 0.1 ‰ in the new minimum value. All carbon stable-isotope values lie between the mean regional values for soil CO_2 (-23.3 ‰; Cerling et al., 1991) and carbonate rock (-0.95 ‰; Davis, 2017).

Dissolved gases and tritium in springs

Groundwater chlorofluorocarbon-11, -12, and -113 concentrations in pico-moles per kilogram (pmoles/kg) and tritium concentrations in tritium units (TU) are summarized in Table 12. In order to estimate the probable equivalent atmospheric concentration at the time of recharge in parts-per-thousand by volume (pptv), a correction factor involving recharge temperature and altitude was applied (Plummer et al., 2006). Air temperature in a thick unsaturated zone is typically close to the mean annual

temperature (Busenberg and Plummer, 1992). In Logan Canyon, the mean annual air temperature at SNOTEL sites from multiple altitudes is approximately 4.5 ºC (Fig. 23; USDA, 2018). A sensitivity analysis is presented in the DISCUSSION chapter to assess possible error introduced by this approximation in the event that it is invalid for the distant past. Recharge altitudes were estimated from highest-altitude dye-traced source locations (Spangler, 2001) for Benchmark and Dewitt Springs. China Row and Spring Hollow Springs were not dye traced. For the latter two, recharge altitudes were estimated from the $\delta^{18}O$-altitude gradient determined in this study, and are presented in the DISCUSSION chapter.

Table 12. Chlorofluorocarbon (± 5 %) and tritium (± 1 TU) concentrations in select springs, with an estimated recharge temperature of 4.5 degrees Celsius.

Spring	Recharge altitude	CFC-11		CFC-12		CFC-113		Tritium
	m	*pmoles/kg*	*pptv*	*pmoles/kg*	*pptv*	*pmoles/kg*	*pptv*	*TU*
Benchmark	2,133.0	2.40	108.11	1.36	244.84	0.16	23.18	1.9
China Row	2,026.0	4.74	210.97	3.04	539.34	0.36	50.51	3.5
Dewitt	1,980.9	3.50	154.74	2.22	390.98	0.21	29.43	4.2
Spring Hollow	1,947.1	1.03	45.37	1.17	205.79	0.11	15.75	4.1

The CFC-12 concentration in China Row Spring is high enough to indicate some form of contamination (University of Utah Noble Gas Lab, written communication, 2018). The CFC-11 concentration in China Row Spring, if taken alone, is high enough to confound whether the recharge is contemporary or stems from the 1980s. However, the CFC-113 concentration is low enough to unambiguously attribute a pre-1990 recharge age. Values for all other springs are low enough to reasonably infer recharge ages.

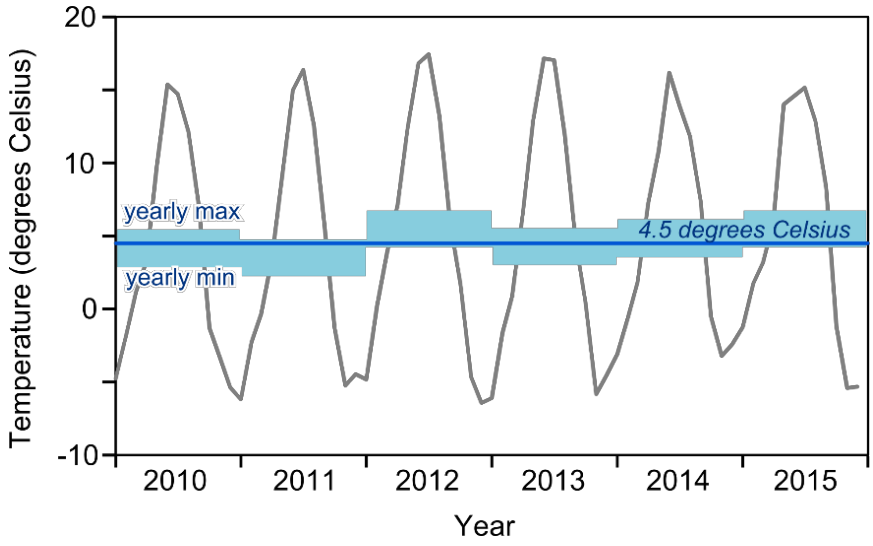

Figure 23. Time-series of monthly mean temperature of all SNOTEL sites in the central Bear River Range (USDA, 2018). Blue shaded regions represent the range of annual means from all stations.

A local record of tritium atmospheric concentrations was estimated by correlation of existing records from the Salt Lake City, Utah, station (1963-1984) with records from the Ottawa, Canada, station (1953-2012; Fig. 24). Estimation took place by the linear regression procedure established in Michel (1989), and produced the relationship:

$$SL = 1.2 * OT - 9.0 \quad (30)$$

In this linear equation, *SL* is the atmospheric tritium concentration (in TU) at the Salt Lake City station, and *OT* is the concentration (in TU) at the Ottawa station, whose record was extended to the modern day via the decay equation and included in the TracerLPM database. All spring concentrations lie within the range of estimated atmospheric values for Salt Lake City, and hence may be assessed via lumped-parameter models. Tritium concentrations in springs range from 1.9 to 4.2 TU (Table 12). These values could indicate modern, or a mixture of modern and decadal, recharge ages.

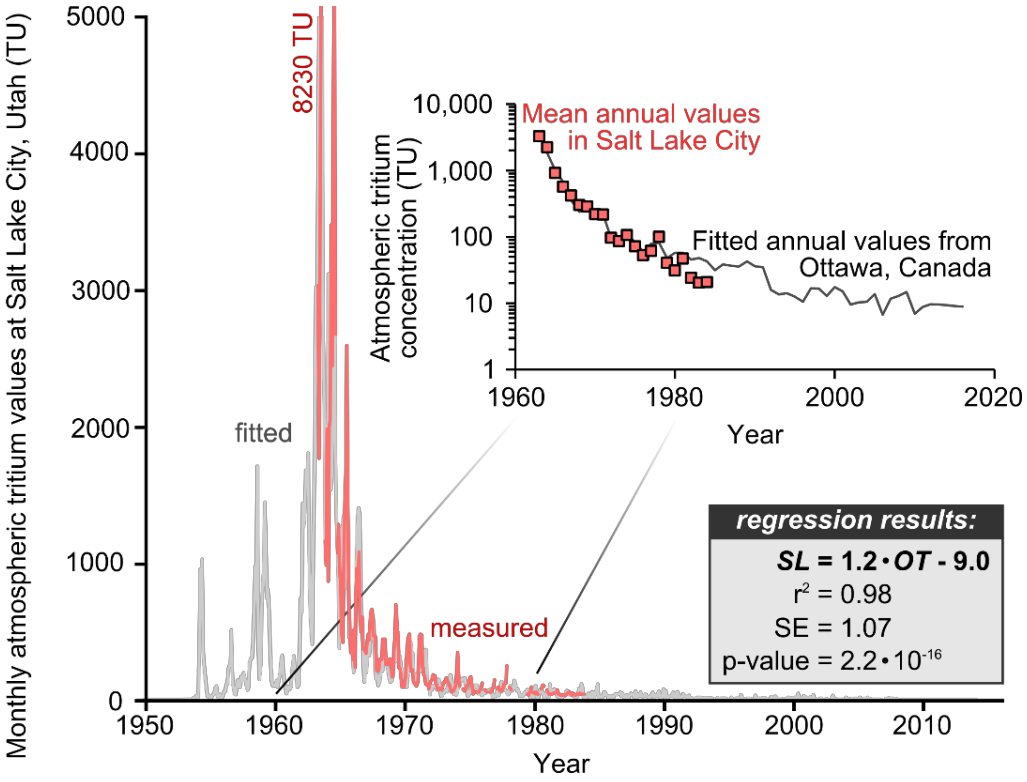

Figure 24. Estimated time-series of atmospheric tritium concentrations (USGS GDL, accessed 2017) based on correlation with the Ottawa, Ontario IAEA station.

DISCUSSION

Groundwater and surface-water interactions

Several approaches were taken to estimate net losses to groundwater from the Logan River. The most successful approach involved comparison of exchanges between the Logan River and the aquifer system with total discharge of the Logan River measured at the USGS gage. The results suggest that $2.32x10^6$ $-5.53x10^5/+6.01x10^5$ m^3 ($1.88x10^3$ $-0.45x10^3/+0.49x10^3$ af) of water is lost to the subsurface in a normal water year. Other approaches, although unsuccessful, were attempted and are included for completeness.

Empirical relationship of losses to groundwater with in-channel discharge

A qualitative relationship between decreasing in-channel discharge and increasing gains from groundwater was noted by Gathro et al. (2016). Hence, losses from the Logan River to the mountain block (and subsequently to the Cache Valley subsurface) likely require high stage. To test this, measured gains from or losses to groundwater were compared to the daily median discharge at the USGS gage above First Dam in regression analysis (Fig. 25). Median daily discharge at the USGS gage spanned flow magnitudes observed in 2015 (1.8-16 m^3/s). This resulted in the following linear relationship:

$$I = -0.0145 * Q^2 + 1.15 \quad (31)$$

Goodness-of-fit indicators (r^2, p-value, standard error, 95% confidence intervals) indicate that conceptual discharge-driven losses to groundwater are statistically feasible (Fig. 25). Data that plot in a straight line on a quantile-quantile graph and a low averaged error ($-7.93x10^{-19}$ m^3/s) indicate that residuals are normally distributed. However, the

effects of data scarcity are evident in a residual plot of model fits, where it is difficult to tell whether the empirical regression equation lacks additional variables (Berthoux and Brown, 2002).

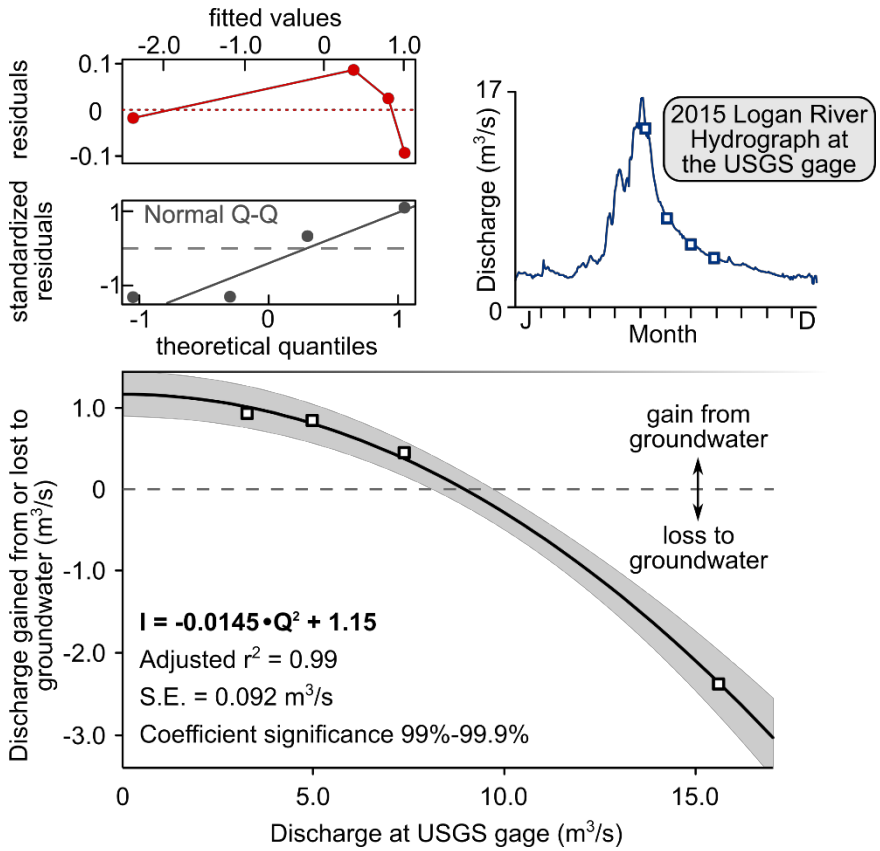

Figure 25. Empirical relationship of groundwater gains or losses in the upper reach of the Logan River with discharge at the USGS gage. White squares are field data, the black line is the best-fit curve, and the shaded region is the 95% confidence interval.

Parameters changed slightly when data from 2016 and 2017 were incorporated:

$$I = -0.0139 * Q^2 + 1.13 \quad (32)$$

The additional data still adhere to a straight line in a quantile-quantile plot, which strengthens the notion that the shape of the curve empirically fits the data (Fig. 26).

Finally, model residuals do not display any apparent trend, which suggests that additional predictor variables are not missing.

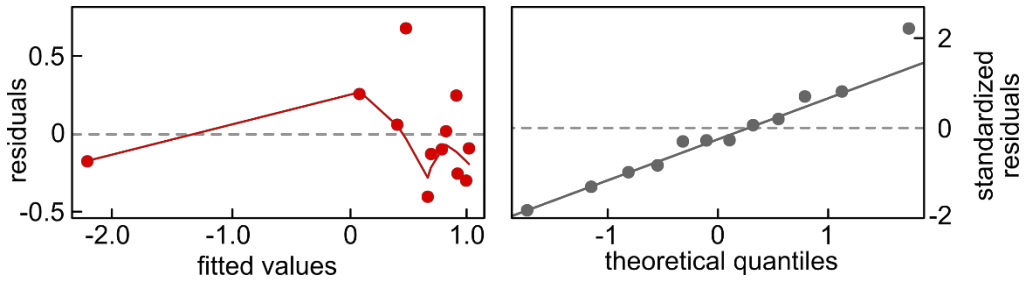

Figure 26. Residual plots for the expanded linear model that includes groundwater gains and losses in the upper Logan River reach observed in 2016 and 2017.

Estimated volume lost from the upper reach of the Logan River

This section uses the regression of the 2015 data to estimate the volume lost to groundwater in a normal water year. Daily losses to groundwater (in m^3/s) were multiplied by the appropriate conversion factor (seconds per day) to estimate the daily incremental volume lost to groundwater. Serially connected losses were summed to produce a cumulative volume contribution to groundwater during high-flow (and hence high-stage) conditions.

Uncertainty from the regression analysis was propagated through the integration via 95% confidence intervals. This resulted in a mean volume of 2.32×10^6 -5.53×10^5 / $+6.01 \times 10^5$ m^3/y (1.88×10^3 -0.45×10^3 / $+0.49 \times 10^3$ af/y) that the upper reach of the Logan River could lose to groundwater in a normal water year (Fig. 27). The volume is small in comparison to the amount budgeted by Bjorklund and McGreevy (1971) and Myers (2003), generally on the order of 1.2×10^7 to 1.2×10^8 m^3 (10^4-10^5 af). If MBR of this order

does yield groundwater to Cache Valley, it may be possible that the Logan River is not the primary source.

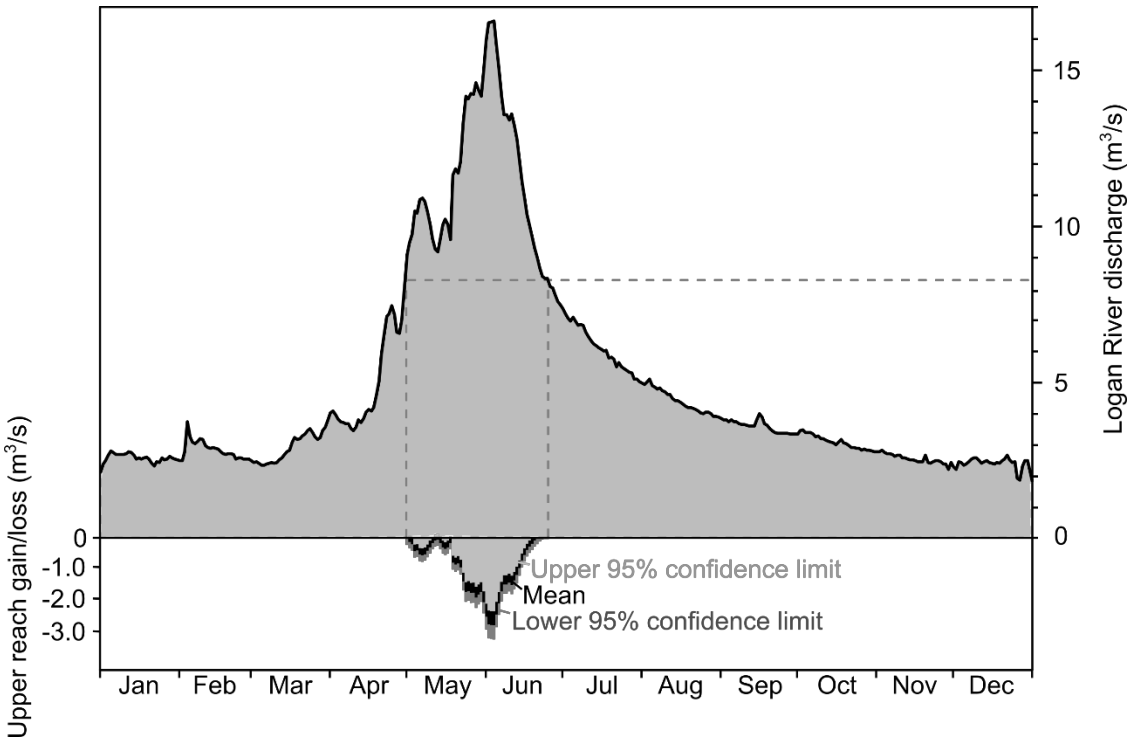

Figure 27. Time-series estimation of losses to groundwater from the upper reach of the Logan River in 2015 and an associated volume estimate.

Unsuccessful attempts to estimate losses to or gains from groundwater

Baseflow recession was applied to hydrographs (August through November 2017) of each Logan River site in order to estimate the missing discharge values between April and August 2017 (Fig. 28). The basis for this technique stems from the fact that the falling limbs of many stream hydrographs adhere to an exponential function, which forms a straight line in semi-log space (Fetter, 2001). The 2017 Logan River hydrograph clearly does not recede along a straight line in semi-log space, invalidating this approach.

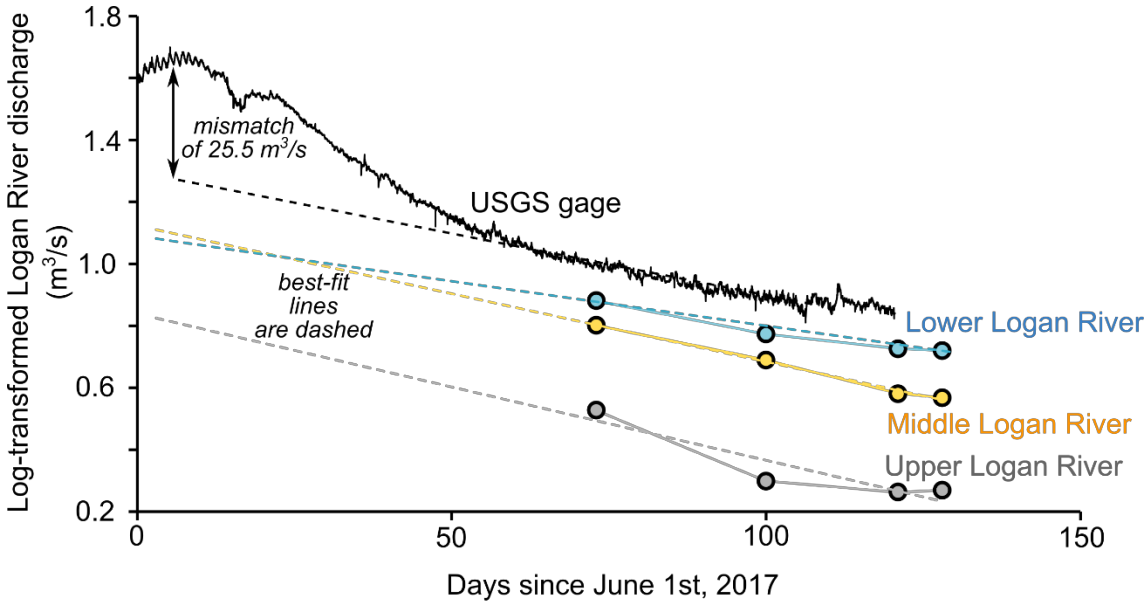

Figure 28. Semi-log plot of the 2017 Logan River hydrograph falling limb.

Several "rating curves" for monitored points along the Logan River were constructed by comparison of sparse field data with discharge at the USGS gage above First Dam. A logarithmic function appeared to describe the relationship between the gauged downstream location and the ungauged upstream locations (Fig. 29). However, use of these functions to predict flow in 2017 implicitly requires extrapolation to much higher discharge values. Hence, this approach was also discarded.

Master recession-curve analysis

The area under the baseflow portion of the fitted Mangin (1975) model represents dynamic storage in the saturated zone of the alpine-karst aquifer (Ford and Williams, 2007). This volume is determined via integration of the master recession curve:

$$V_{dynamic} = \int_0^\infty q_o e^{-\alpha t} dt \quad (33)$$

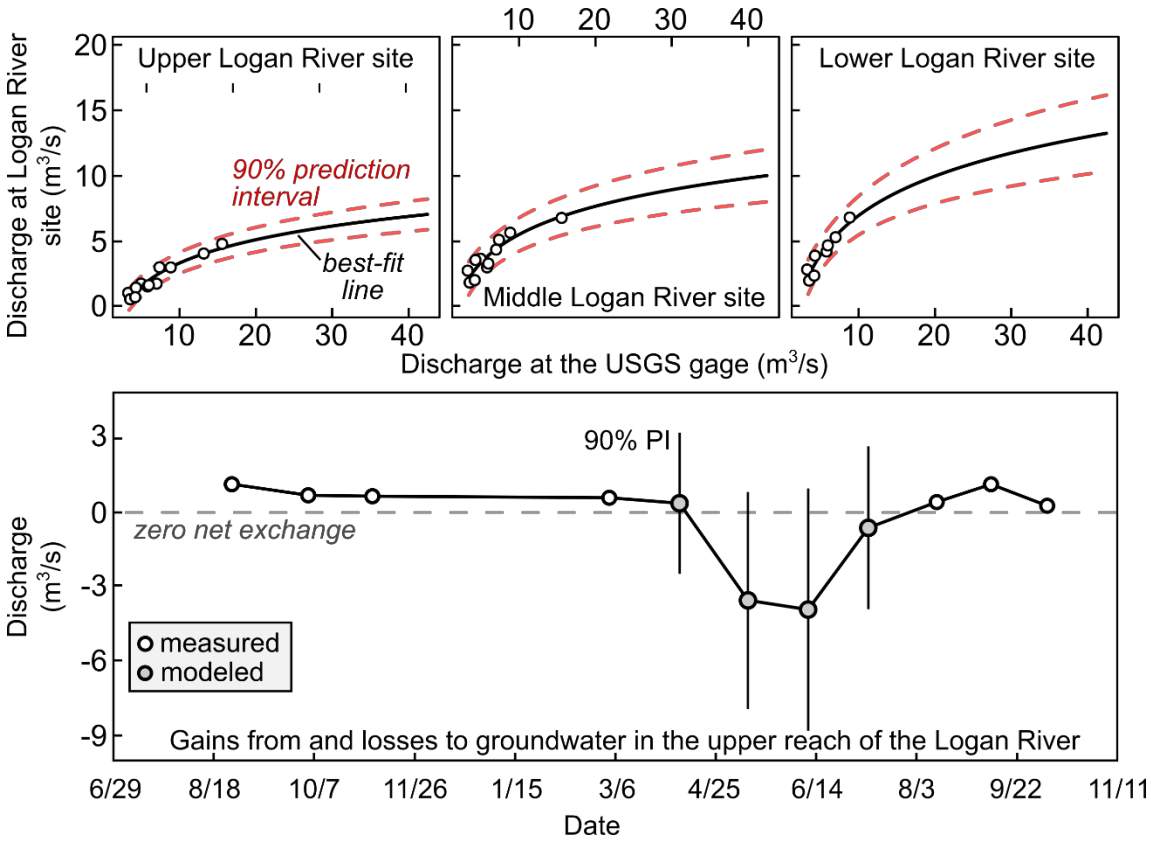

Figure 29. Rating curves for discharge at each Logan River site with respect to the USGS gage above First Dam and estimates of groundwater gains and losses in the upper reach, 2016-2017.

This value is approximately 2.09×10^8 m^3/y (1.70×10^5 af/y), or 88% of total groundwater in dynamic storage (2.37×10^8 m^3/y or 1.92×10^5 af/y), and leaves 2.80×10^7 m^3/y (2.27×10^4 af/y), or 12%, to drain from the higher caverns (the vadose zone) to the saturated zone in an average year. Extrapolation of the model to even lower values of Logan River discharge suggests that near-total drainage of the aquifer system may occur in approximately five years in the absence of any recharge events (Fig. 30a).

This kind of extrapolation, however, rests on the premise that all groundwater flowpaths have approximately the same permeability (e.g., act as conduits) and are well-

described by the exponential portion of the fitted Mangin (1975) model. If flowpaths with lower average permeability exist (e.g., less-enhanced fractures or interstitial flow), the alpine karst aquifer may adhere to a different hydraulic function during low-flow conditions. If this is the case, MRC predictions of groundwater residence time and storage are likely underestimates.

Historical annual end-of-baseflow discharge minima of the Logan River in conjunction with the fitted Mangin (1975) model produce an instantaneous glimpse of the lower bound of the master recession curve in a given year. Integration of the model from these lowest observed discharge values therefore estimates the concurrent amount of water remaining in dynamic storage. The results of this iterative integration process are presented as points along the baseflow recession model in Figure 30a, shaded to show overlapping values from different years.

Integration of the recession model was also performed at one-day increments from a discharge of q_o to a discharge of approximately zero to produce a rating curve of discharge at the USGS gage versus dynamic storage (Fig. 30b). Comparison with annual end-of-baseflow-discharge values suggests that the aquifer drains at least 50% of its dynamically stored volume in a given year and up to 80% annually during droughts (Fig. 30b). Despite this apparently high degree of responsiveness, annual discharge minima at the USGS gage never drop below 1.5 m^3/s (54 cfs), or 20% of the estimated average dynamic storage.

Time-series of the annual end-of-baseflow discharge recorded at the USGS gage (USGS NWIS, 2018), as well as annual accumulated snowfall at the nearby Salt Lake

City climate monitoring station (NOAA NWSF, 2018) are presented in Figure 31. High-frequency (year-to-year) variance of Logan River baseflow may stem in part from similarly high-frequency variability of the northern Utah snowpack (and hence, available recharge). However, consistent baseflow minima (1.5 m^3/s, 54 cfs) may indicate that even low amounts of recharge can maintain a low amount of storage in the alpine karst aquifer. This hypothesis also does not preclude the possibly important role of lower-permeability flowpaths in controlling baseflow.

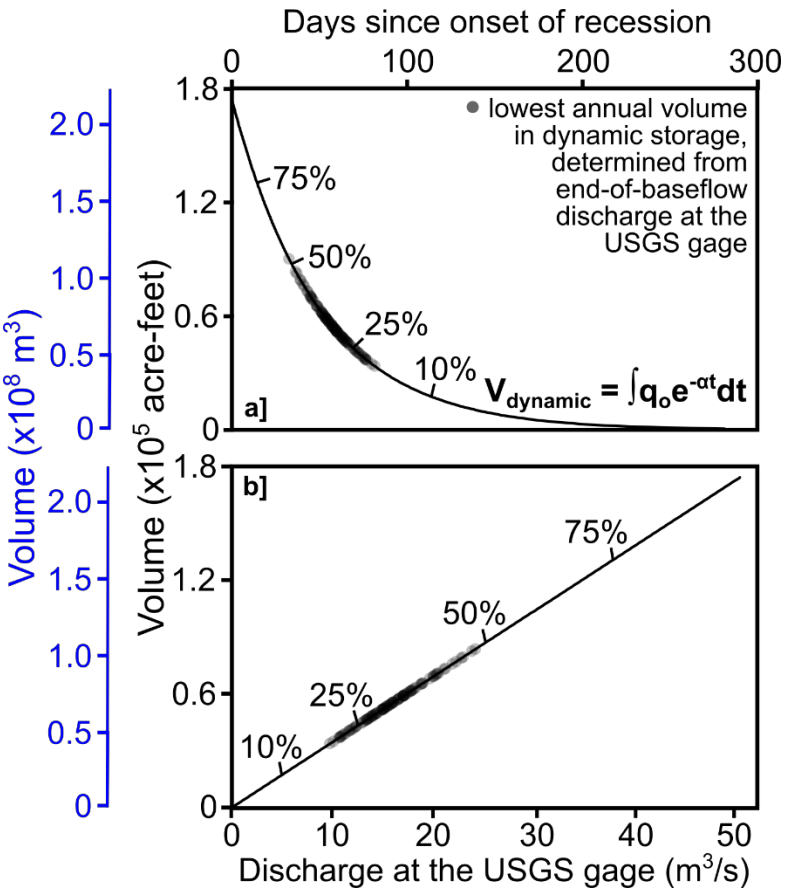

Figure 30. Predicted drainage of the alpine karst aquifer from discharge-volume relationships of the fitted Mangin (1975) model for the Logan River.

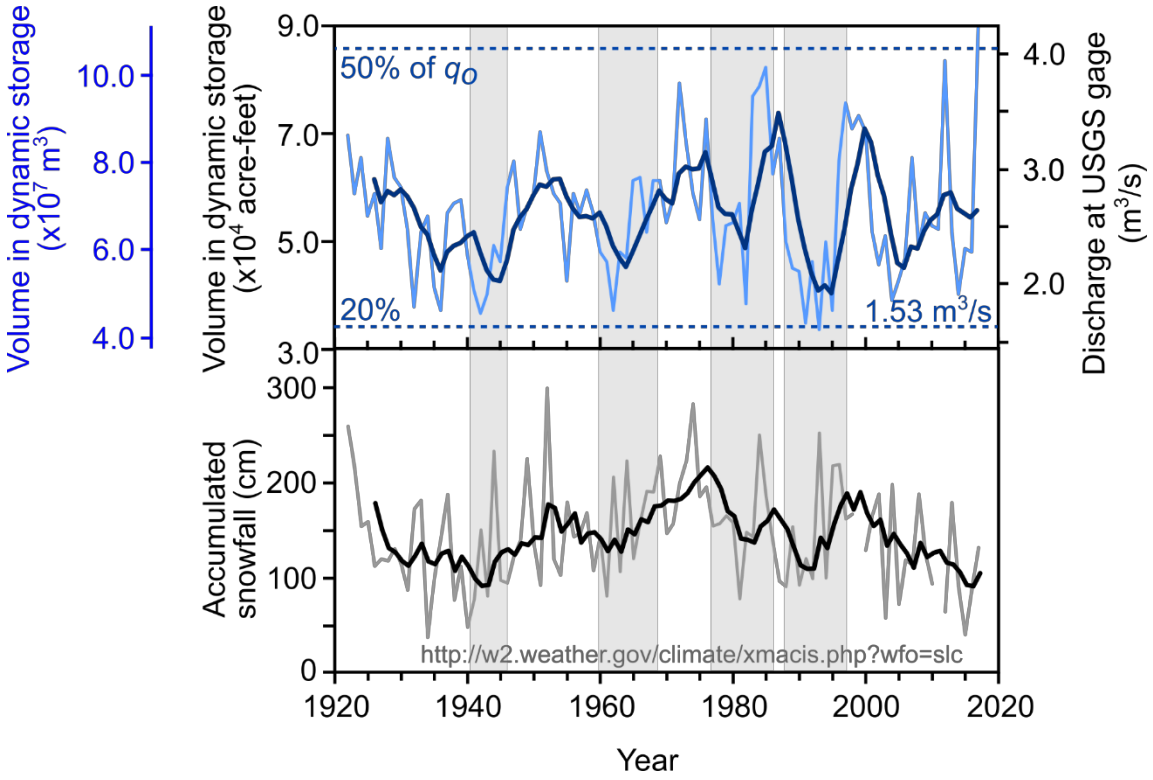

Figure 31. Historical annual variation of baseflow in the Bear River Range alpine karst system and snowfall amounts recorded in northern Utah (Salt Lake City station). Bold lines represent 5-year moving averages.

Spring-flow variability

High seasonal flow variation at each spring (Fig. 32) suggests that all springs drain some amount of quickly transmitted groundwater, as documented by Spangler (2001, 2012). As Benchmark and China Row Springs appear to reach peak flow synchronously with springs that have high recharge altitudes, and not with the proximal Logan Cave Spring, they may likewise receive recharge from higher altitudes. Conversely, it is possible that lower-altitude snowmelt enters the subsurface earlier but is inhibited from traveling as quickly by lesser karst development. This is likely the case for China Row Spring, which does not have access to a higher-altitude recharge zone.

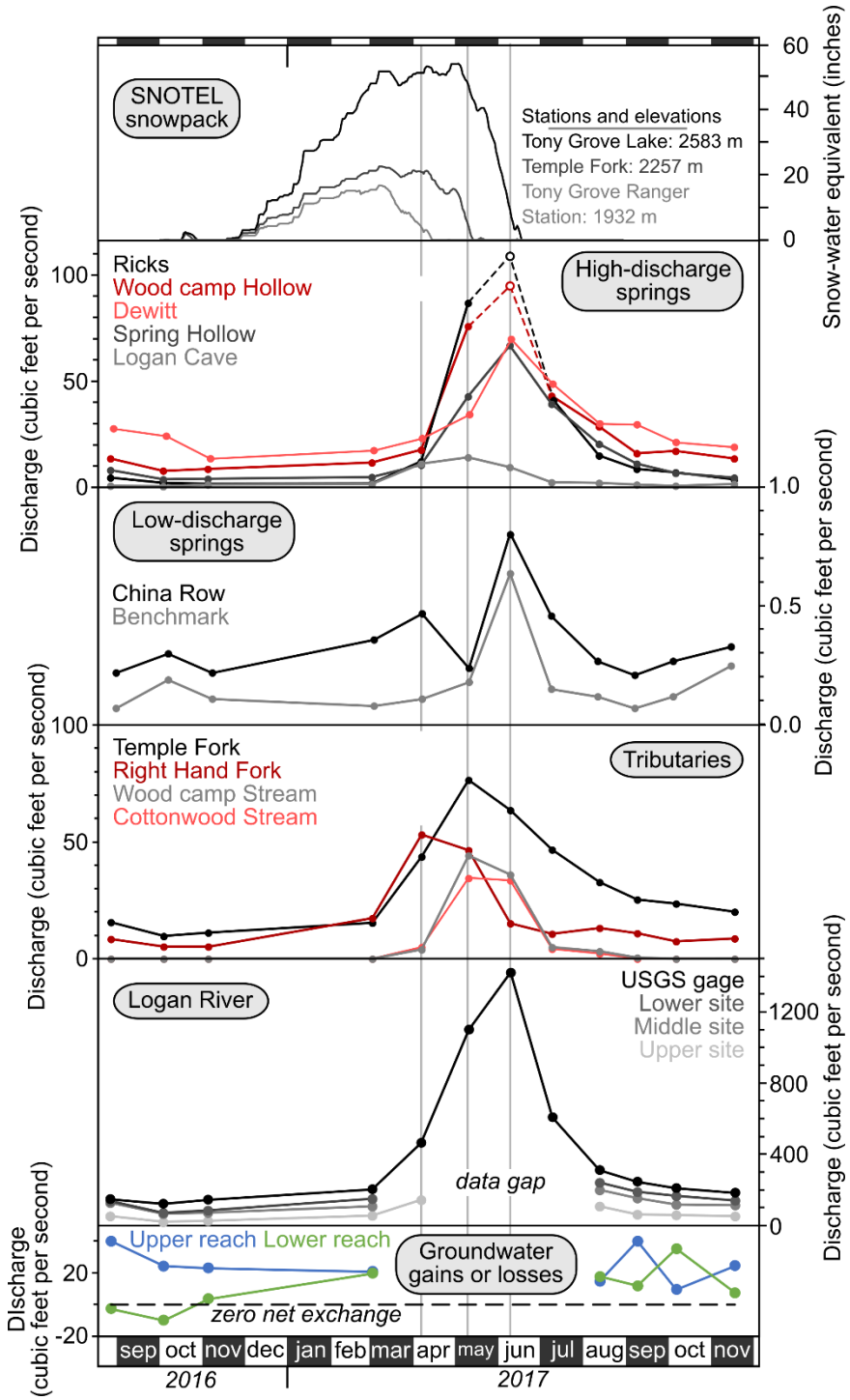

Figure 32. SNOTEL snow-water equivalent at representative altitudes in Logan Canyon (USDA, 2018), discharge data for springs and streams, and groundwater gains and losses of the upper and lower Logan River reaches (USGS NWIS, 2018).

Hydrograph separation in this study has a resolution of about one month due to sampling frequency, yet reveals several interesting temporal phenomena. Highest flows in all springs except Logan Cave and China Row Springs were observed on June 10, 2017. This event follows the onset of snowmelt at low altitudes (Tony Grove Ranger Station and Temple Fork, both March 12, 2017; USDA, 2018) by 90 days, and at higher altitudes (Tony Grove Lake, May 5, 2017; USDA, 2018) by only 36 days.

The China Row Spring hydrograph potentially has two peaks: one on May 11, and another on July 8, 2017, which postdates the onset of snowpack melting at low altitudes (e.g., those within the recharge area) by 59 and 119 days, respectively. While some snowmelt may flow more quickly through conduits, some flow may take twice as long to move through a lower-permeability flowpath. Testing of this hypothesis would require a higher resolution hydrograph and a targeted dye-trace campaign.

Logan Cave Spring reached highest observed flow earlier than other springs (May 11, 2017), coincident with highest flows of the proximal Cottonwood and Woodcamp Hollow Creeks. Due to hydrograph synchronism, it is likely that a well-developed conduit system lies upgradient of Logan Cave Spring, and that it receives recharge from ephemeral streams.

High flow variability was observed in each spring, which updates the conceptual flow model of the pilot study (Gathro et al., unpublished data) in which Logan Cave, China Row, and Benchmark Springs did not respond rapidly to recharge. As a high degree of responsiveness was observed in this study, it is unlikely that these springs drain less-karstified zones of the alpine karst aquifer.

Groundwater geochemistry in Cache Valley

Geochemical similarities between the Cache Valley principal aquifer and various recharge mechanisms are assessed in this section. Stiff (1951) diagrams were created from publicly available USGS National Water Information System water-quality data (USGS NWIS, 2018) for each well (Appendix B), and are displayed with calculated pCO_2 and TDS in Figure 33. Stiff diagrams are narrower (less dissolved solids) for wells proximal to the mouth of Logan Canyon than for wells completed in mountain-front bedrock. Together with near-atmospheric groundwater pCO_2 values in this area, it is likely that recharge occurs by direction infiltration of the Logan River through locally unconfined deltaic sediments. This inference is supported by the fact that pCO_2 values increase and Stiff diagrams widen with distance from the mouth of Logan Canyon, which implies greater interaction of groundwater with aquifer materials.

Stiff diagrams, pCO_2 values, and TDS concentrations in bedrock and valley-marginal wells near Blacksmith Fork and Green Canyons are similar to each other, possibly supporting the notion that subsurface recharge from the mountain block occurs in those locations. However, as noted in the BACKGROUND chapter, mountain-front structure and stratigraphy north of Millville, Utah likely serve as a hydrogeologic partition. Hence, it is possible that the area west of Green Canyon reflects the natural evolution of northward-migrating Logan River water that infiltrated near First Dam.

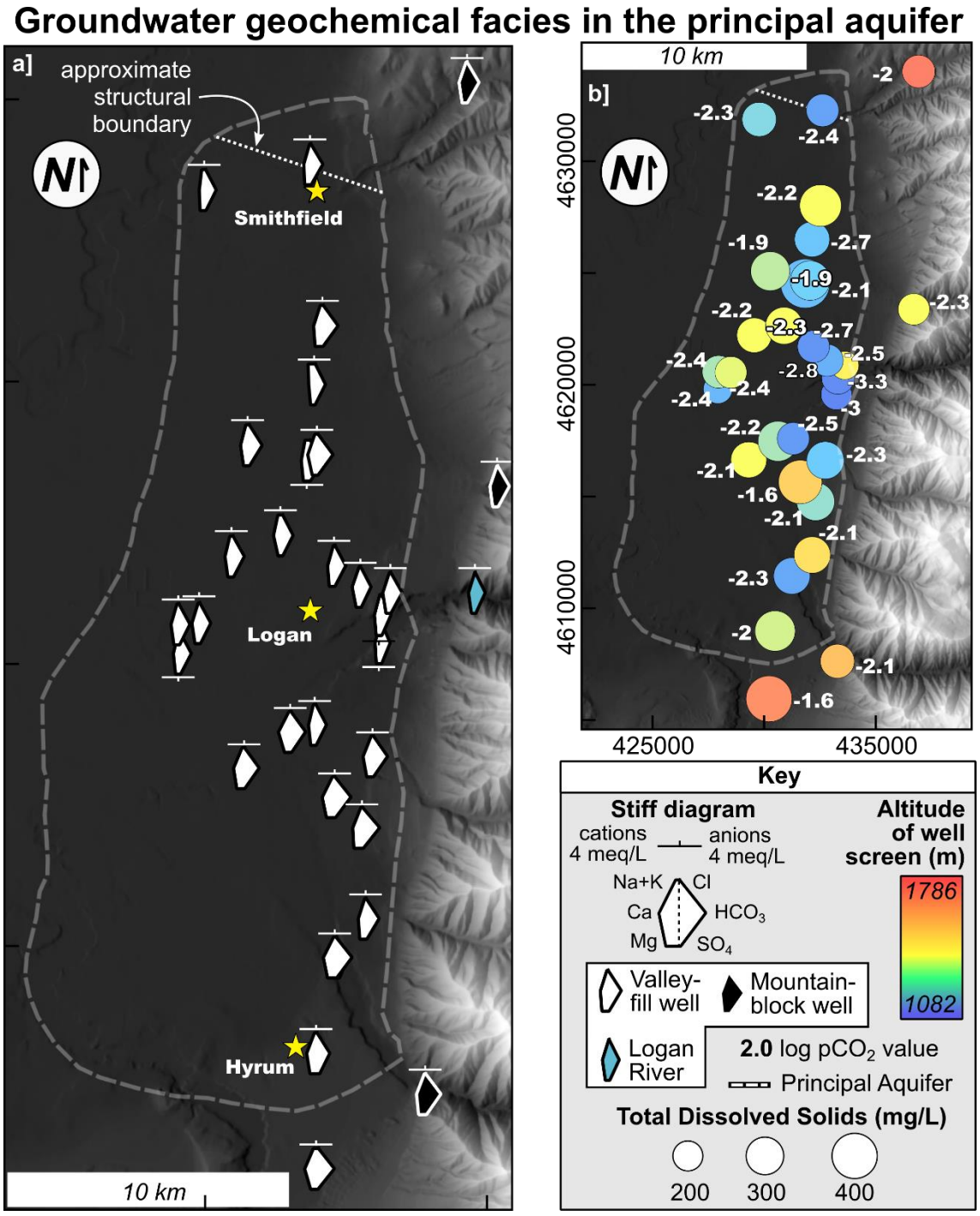

Figure 33. Groundwater facies in Cache Valley: Stiff (1951) diagrams (a), as well as TDS concentrations, altitude of the screened interval, and calculated pCO_2 (b). The northern structural boundary of the principal aquifer reflects the approximate edge of the College Ward subbasin (Oaks, written communication, 2018).

Narrower Stiff diagrams, lower pCO_2 values, and lower TDS concentrations are present in the vicinity of Smithfield, Utah than in wells to the south, and are similar to those measured in the proximal mountain-block well.These values may reflect subsurface recharge through secondary porosity in the quartzite block that separates the Bear River Range from Cache Valley. Different geochemical facies are also discernible in a Piper (1944) diagram that may support assessment of mountain-front recharge (Fig. 34).

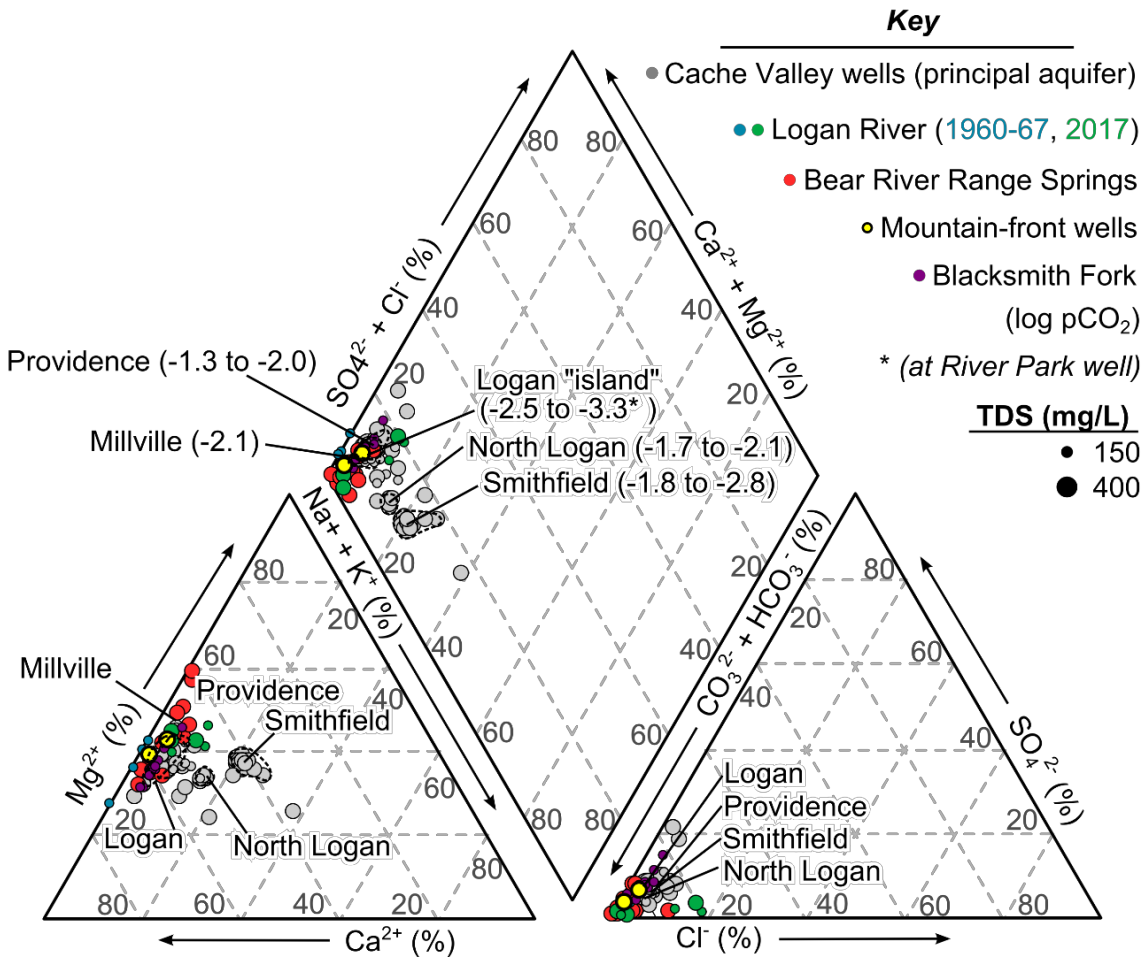

Figure 34. Piper (1944) diagram of Bear River Range surface water and groundwater, and Cache Valley groundwater. Groundwater chemistries of wells in Smithfield and North Logan are moderately dissimilar to those of mountain-block wells and springs.

The Logan River, alpine springs, and mountain-block wells all have low percentages of Na and K, similar to those observed in wells near Providence, Millville, and Logan. Wells in North Logan and Smithfield have higher percentages of Na and K, and cluster on the Piper diagram, separate from mountain-block wells and springs. High pCO_2 values near Providence and Hyrum are similar to those in mountain-block springs and wells, which may indicate subsurface recharge across the mountain front and into a zone with modern tritium values and possibly faster flow, as delineated by Robinson (1999).

Oxygen and hydrogen stable isotopes

Meteoric water lines

Oxygen and hydrogen stable isotopes for springs and surface water are similar to those observed in precipitation across the state of Utah (Bowen, 2017; Fig. 35). Snow samples lie along a significant linear trend (shown in blue), given by the formula:

$$\delta^2 H = 6.6 * \delta^{18} O + 13.3 \quad (34)$$

The standard error of regression (1.8‰) is slightly less than analytical precision (~2‰ for δ^2H and 0.06 for δ^{18}O). Due to a similarity between the 2017 snow line and the Utah meteoric water line (Eqn. 35; Fig. 35; Kendall and Coplen, 2001), it may reflect a seasonal shift of the general trend expected in Utah:

$$\delta^2 H = 6.7 * \delta^{18} O + 12.6 \quad (35)$$

Most spring stable-isotope samples collected during late winter appear to fall below the meteoric water line (lower δ^2H or higher δ^{18}O). Possibly, this may reflect the isotopic

value of late-fall recharge or a longer-term mean groundwater value, as they lie within the range of observed values in Utah.

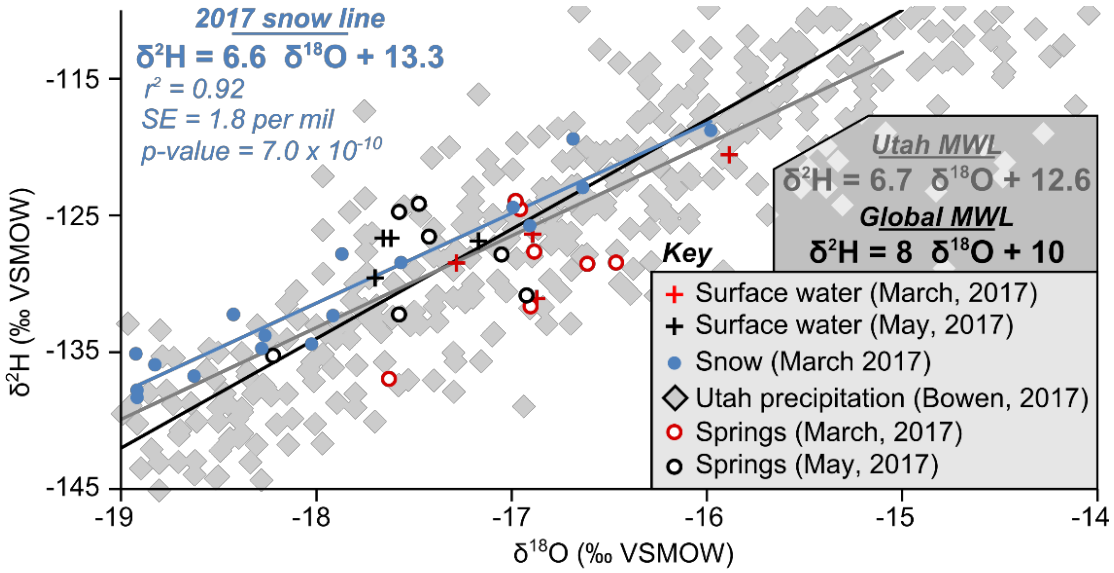

Figure 35. Oxygen and hydrogen isotopes for springs, streams, and snow in the Bear River Range in comparison to the global and Utah meteoric water lines.

Stable-isotope-altitude gradients

Isotopic values from Table 11 were assessed via analysis-of-variance (ANOVA) in order to statistically assess dominant topographic controls on fractionation in snowfall (Table 13). This effort tests the hypothesis proposed by Bright (2009) that progressive rainout of air masses traversing the Bear River Range produces a more significant impact on the stable isotope values of precipitation than the altitude at which the precipitation accumulates. ANOVA directly ranks the significance of possible controlling factors (e.g., longitude and altitude), and informs the choice of variables for subsequent linear regression (Berthoux and Brown, 2002).

Table 13. Significance of longitude and altitude to $\delta^{18}O$ in the analysis of variance.

Variable	Degrees of freedom	Sum of squares	F-statistic	Significance
		Two factors		
Longitude	1	3.8	10	>99%
Altitude	1	5.3	14	>99%
		One factor		
Altitude	1	9	26	>99.9%

The results support the notion that altitude is the primary influence on the fractionation of snowfall in the Bear River Range. While the F-statistic indicates a possible effect of longitude on $\delta^{18}O$ composition in the alpine snowpack, iterative adjustment of the model shows that it is not significant in conjunction with altitude and decreases in individual significance when assessed separately. Altitude, conversely, increases in significance to higher than 99.9% when used as the only predictor for $\delta^{18}O$, which is classical evidence for a better empirical link. Hence, altitude was chosen as the sole predictor variable for $\delta^{18}O$ in linear regression (Fig. 36):

$$\delta^{18}O = -0.0028 * Altitude - 12.2 \quad (36)$$

Goodness-of-fit statistics are critically important to determining the validity of regression-based altitude-gradient models and are listed below. The altitude gradient fits moderately well, with an r^2 value of 0.61 and a residual standard error (average difference) of 0.59‰. A p-value of 0.0001 and coefficients greater than 99.9% significant also indicate that the model is statistically sound. The altitude gradient (line slope) is -0.28 ‰ per 100 meters. The size of the 95% confidence interval (± 0.12 ‰) indicates that uncertainty is considerable. However, confidence intervals decrease with the volume of data included in the regression (Berthoux and Brown, 2002), and this value will decrease in future studies if a larger number of samples are collected.

Residuals (data normalized to the regression) show that error is uniformly distributed around the regression line. Adherence to a normal-score line on a quantile-quantile plot also shows that the errors are normally distributed, which is a baseline requirement for accepting a linear fit. Hence, although preliminary, this linear model may usefully describe altitude-related fractionation in Bear River Range snowfall.

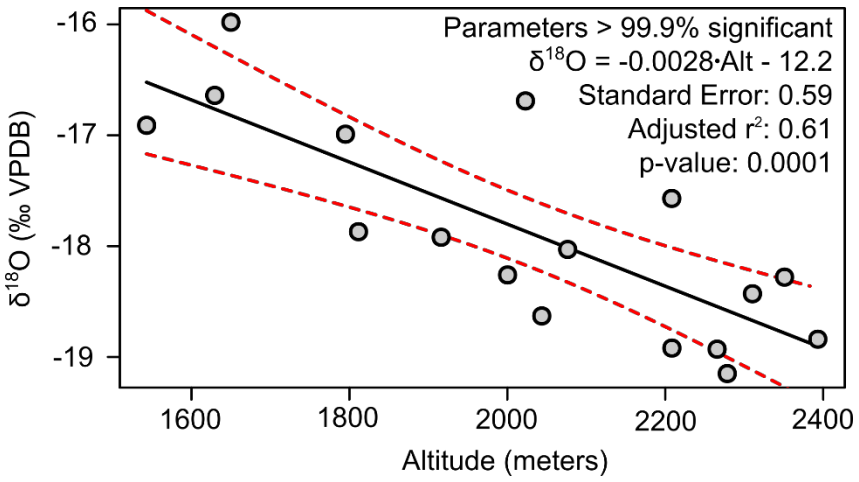

Figure 36. Best-fit line, goodness-of-fit statistics, and residuals for ordinary least-squares regression of snowpack $\delta^{18}O$ and altitude, with $\delta^{18}O$ as the dependent variable.

This altitude gradient is similar to others for rain or snow in the United States (Table 14). However, parameter goodness-of-fit statistics are rarely addressed or reported and usually consist of a simple r^2 value. It is readily apparent from parameter 95% confidence intervals reported above that the Bear River Range altitude gradient has loose bounds. However, whether or not altitude gradients in other physiographic settings also have high variance is unknown. According to good statistical practice, 95% confidence intervals should be reported in order to quantify error in future studies.

Table 14. Oxygen stable-isotope altitude gradients in North America. NR=not reported

Author	Location	Gradient (‰/100m)	n	r^2	Relief (m)	Standard error (‰)
Abbott et al. (2000)	Green Mountains, VT	-0.25 Rain/snow	5	0.96	1080	NR
Blasch and Bryson (2007)	Mogollon Escarpment, AZ	-0.26 Rain/snow	*High scatter, no reported r^2*		3050	NR
James et al. (2000)	Cascade Range, OR	-0.18 Snow			1500	NR
Brooks et al. (2012)	Willamette Valley, OR	-0.27 Rain/snow	615	0.85	1700	0.50
This study	Bear River Range, UT	-0.28 Snow	17	0.61	900	0.59

Although $\delta^{18}O$ is considered a dependent variable in most altitude-gradient models (e.g., James et al., 2000; Blasch and Bryson, 2007), the necessity of a Working-Hoteling confidence band for "reverse use" increases uncertainty when actually estimating mean recharge altitudes (Berthoux and Brown, 2002). Switching independent and dependent variables is uncommon in altitude-gradient studies, yet removes this complication. A second linear regression was performed with altitude as the dependent variable, with 95% confidence intervals applying to the mean altitude (Fig. 37):

$$Altitude = -226.3 * \delta^{18}O - 2017 \quad (37)$$

This more direct approach to relating $\delta^{18}O$ to altitude similarly has a moderate goodness-of-fit ($r^2 = 0.61$), but the residual standard error of 168 m indicates that its usefulness for prediction in small alpine catchments is limited. Parameter significance is high, with a low p-value of 0.0001 and a slope (-226 meters per 1 ‰) greater than 99.9% significant. The intercept is greater than 95% significant, still within acceptable levels. Residuals have uniform variance around a value of zero with no apparent trends or serial link, and adhere to a normal-score line on a quantile-quantile plot (Fig 37).

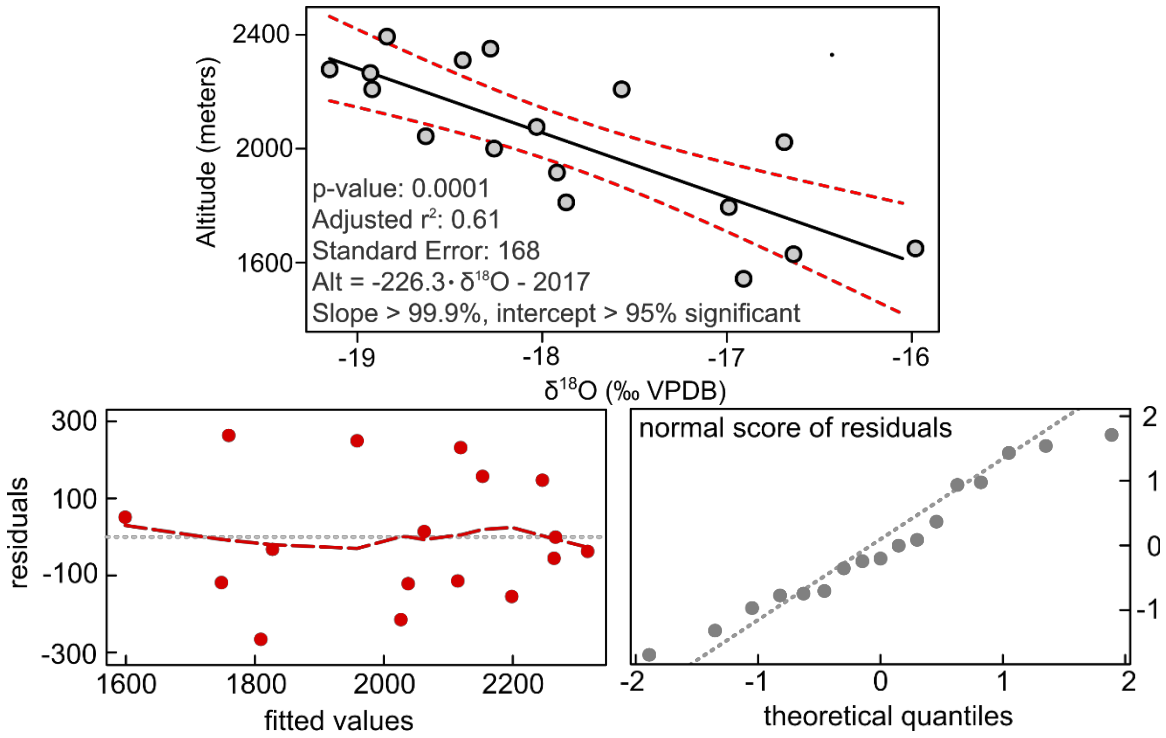

Figure 37. Best-fit line and 95% confidence intervals for ordinary least-squares regression of snowpack $\delta^{18}O$ and altitude, with altitude as the dependent variable.

Hydrogen isotopes were qualitatively shown by Bright (2009) to vary with longitude in the eastern Bear River Range and were thought subject to depletion via increased precipitation along longitudinal storm paths. However, iterative analysis-of-variance shows that longitude does not significantly affect δ^2H values and that variance is better explained by changes in altitude alone (Table 15). Accordingly, altitude was again chosen as the sole independent variable for a δ^2H altitude gradient.

Table 15. Significance of longitude and altitude to δ^2H in analysis of variance.

Variable	Degrees of freedom	Sum of squares	F-statistic	Significance
		Two factors		
Longitude	1	60.2	2.8	<90%
Altitude	1	303.6	14.2	>99%
		One factor		
Altitude	1	9.1	25.9	>99.9%

Linear modeling of hydrogen-isotopic variation with altitude results in a p-value of 0.001 and regression parameters greater than 99% significant (Fig. 38). However, an r^2 of 0.48 and a standard error of 4.6‰ suggests that δ^2H correlates less strongly to altitude. An inherent precision of ± 2 ‰ via analytical procedures contributes to this uncertainty.

$$\delta^2 H = -0.017 * Altitude - 96.3 \quad (38)$$

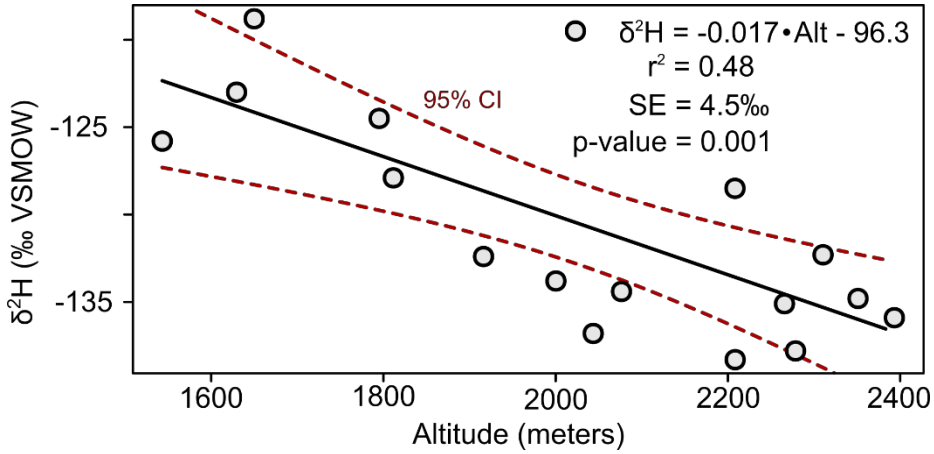

Figure 38. Best-fit line and 95% confidence intervals for ordinary least-squares regression of snowpack δ^2H and altitude, with δ^2H as the dependent variable.

Groundwater recharge altitudes are often estimated from $\delta^{18}O$ altitude-gradient regression of snow data (James et al., 2000; Poage and Chamberlain, 2001), yet runoff and infiltration are isotopically different from the original snowpack (Taylor and Greene, 2001). Melting also occurs earlier in the season at lower altitudes due to warmer temperatures and more rain-on-snow events (Holko et al., 2013). Hence, the alpine snowpack likely yields spatially and temporally variant isotopic signals to groundwater that do not align well with the initial altitude control. This, in turn, limits the utility of snow-core data for assessment of groundwater recharge unless stable isotopes in runoff

and at springs are also monitored over time (Unnikrishna et al., 2002). In this study, it was a first-order goal to test whether or not the isotopic signature of precipitation that contributes to recharge varies with altitude, which was demonstrated. As the snow sampling campaign took place during late winter in a mature alpine snowpack at peak snow-water equivalent (Fig. 39), comparison with the high-flow value of snowmelt in streams and springs may represent a mean meltwater composition (Taylor and Greene, 2002) and permit qualitative assessment of relative recharge altitudes.

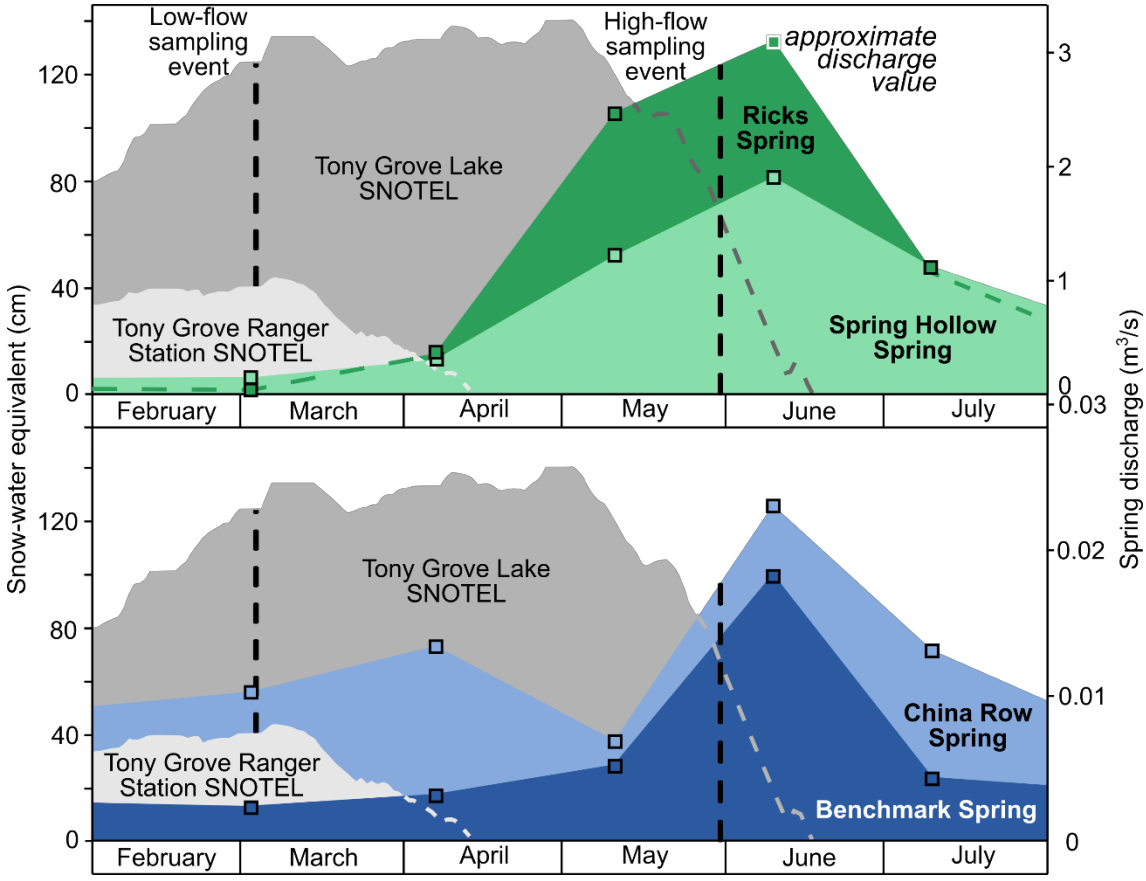

Figure 39. Timing of geochemical sampling events with respect to changes in the alpine snowpack (USDA, 2018) and hydrographs of major and minor springs.

Qualitative recharge altitudes were estimated from the linear relationship with $\delta^{18}O$ and are summarized in Table 16. As the actual link between the snowpack and the groundwater signatures was not rigorously determined in this study, and as the average residual difference (deviation of field data from the fitted line) was 168 m, stable isotopes are likely ill-suited for precise source-area identification in alpine karst. However, they may prove useful as screening tools to aid in targeting relative source elevations for many springs prior to a large-scale dye-trace campaign. Qualitative comparison of spring isotopic and dye-traced recharge altitudes may also yield inferences of source areas and are discussed in the following section.

Table 16. Mean altitudes and 95% confidence intervals for the snowpack contributing recharge to springs in Logan Canyon, estimated from the altitude gradient.

Spring	$\delta^{18}O$ (‰) (adjusted)	Mean recharge altitude above outlet (m)	95% confidence interval (m)	Dye-traced altitude range (m) (Spangler, 2001)
Ricks	-17.4	134	± 97	73-805
Benchmark	-18.3	371	± 97	98-122
Logan Cave	-17.7	293	± 88	37-390
Woodcamp	-18.0	422	± 87	335-963
China Row	-17.9	406	± 87	-
Dewitt	-17.7	445	± 89	390-878
Spring Hollow	-17.5	326	± 93	-

Recharge area interpretation

Generalized isotopic inferences of recharge altitudes for each spring are compared in this section to dye-trace, topographical, structural, and lithological data to further constrain spring source areas. Maps comparing each data type are shown in Figures 40-44 with topographic swath profiles (mean altitudes in black, maximum and minimum altitudes in gray) and $\delta^{18}O$-predicted recharge altitudes (blue horizontal line).

The $\delta^{18}O$-predicted mean recharge altitude for Ricks Spring is on the order of 100 m above the outlet, which is similar to the altitude of the lowest altitude source catchment (Bear Hollow; Table 16). However, Bear Hollow is small and unlikely to provide sufficient recharge to produce observed flow (Fig. 40). This suggests an isotopic under-prediction of recharge altitude with respect to the two far higher dye-traced sources, Tony Grove (640 m) and Bunchgrass Hollow (805 m). Likely, the Ricks Spring $\delta^{18}O$ value (-17.4‰; Table 10) represents mixing of high-altitude recharge with a significant amount of fault-diverted Logan River water ($\delta^{18}O$ = -17.6‰; Table 10; Spangler, 2001). USGS dye-trace data suggest that all other recharge occurs within the Garden City Limestone (Og; Spangler, 2001) as described in the PREVIOUS WORK chapter.

The $\delta^{18}O$-predicted mean recharge altitude for Benchmark Spring (300-400 m above the outlet) is higher than the dye-trace estimate (98-122 m; Table 16). If Benchmark Spring, like Logan Cave Spring, was to draw recharge from higher altitudes within Blind Hollow, both should have similar isotopic values from snowmelt runoff during high-flow conditions. Benchmark Spring's stable-isotope signature is clearly more negative across seasons (Table 10) and its hydrograph behaves in similar fashion to springs with high recharge altitudes. Hence, it is likely that a higher recharge zone within the Garden City Limestone (Og) supplies water to Benchmark Spring.

Logan Cave Spring dye traces to a small recharge area within Blind Hollow, which is underlain by the Garden City Limestone (Og; Spangler, 2001). The $\delta^{18}O$ prediction of recharge altitude (~300 m above the outlet; Table 16) is high enough to reflect the dye-traced source area (Fig. 41; 37-390 m).

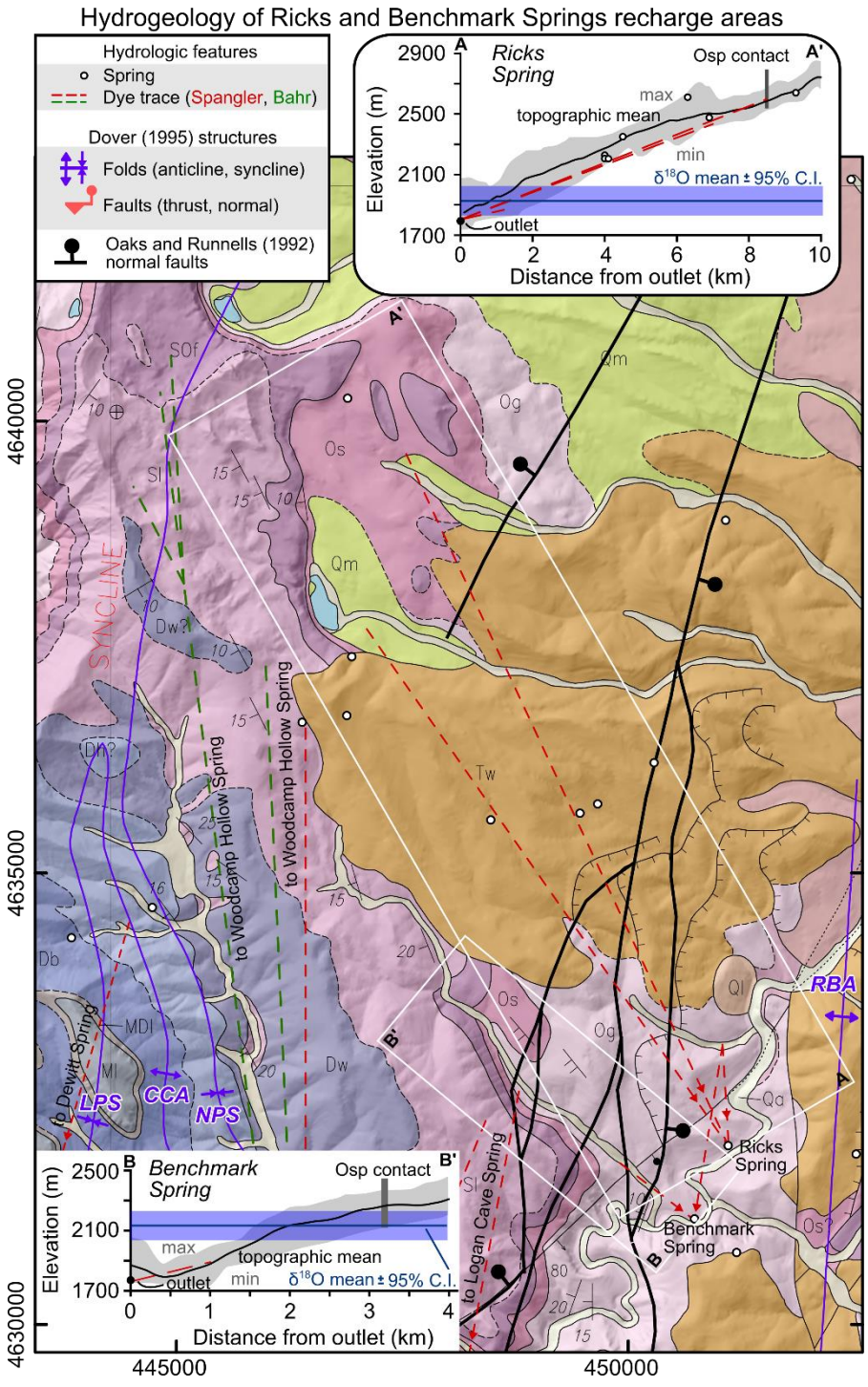

Figure 40. Stratigraphy, dye traces, $\delta^{18}O$-predicted recharge altitudes, and swath profiles for recharge areas contributing to Benchmark and Ricks Springs. LPS = Logan Peak syncline, CCA = Cottonwood Creek anticline, NPS = Naomi Peak syncline, RBA= Red Banks anticline.

Woodcamp Hollow Spring discharges from the Laketown Dolomite (Sl), and is dye-traced to recharge zones within the Laketown and Hyrum (Dh) Dolomites (Spangler, 2001). Accordingly, flow must also cross the Water Canyon Formation (Dw; Fig. 41), which is identified by Spangler (2004, 2012) as a primary aquifer unit and also comprises part of the flowpath to Dewitt Spring. Dye-trace estimates of source altitudes range from 335-963 m above the outlet, and align well with a $\delta^{18}O$ mean recharge altitude estimate of ~400 m (Table 16). Dye-trace data support the inference that the Cottonwood Creek anticline (Bahr, 2016) and the contact with the Swan Peak Formation (Os; Spangler, 2001) are effective structural and lower-contact flow barriers.

No dye-trace data exist for China Row Spring. However, the $\delta^{18}O$ value indicates that recharge sources from a low mean altitude, like those within several miles of the spring (Table 16; Fig. 42). China Row Spring emerges from the Laketown Dolomite (Sl), which is underlain by Swan Peak Formation (Os) that crops out approximately 3 km to the east. It is likely that the source area is stratigraphically controlled through the west-dipping, dolomite-bearing Laketown Dolomite.

Dye traces to Dewitt Spring place recharge at 390-878 m above the outlet, which align with the $\delta^{18}O$ prediction of mean recharge altitude (400-500 m; Table 16). Groundwater basin length is ~12 km, and is truncated by the axis of the Cottonwood Creek anticline (Bahr, 2016) and the contact with the Swan Peak Formation (Os; Spangler, 2001; Fig. 43). Dye traces link recharge in the Beirdneau Formation (Db) with the main spring outlets in the Water Canyon Formation (Dw), and flow necessarily passing through the Hyrum Dolomite (Dh; Spangler, 2001).

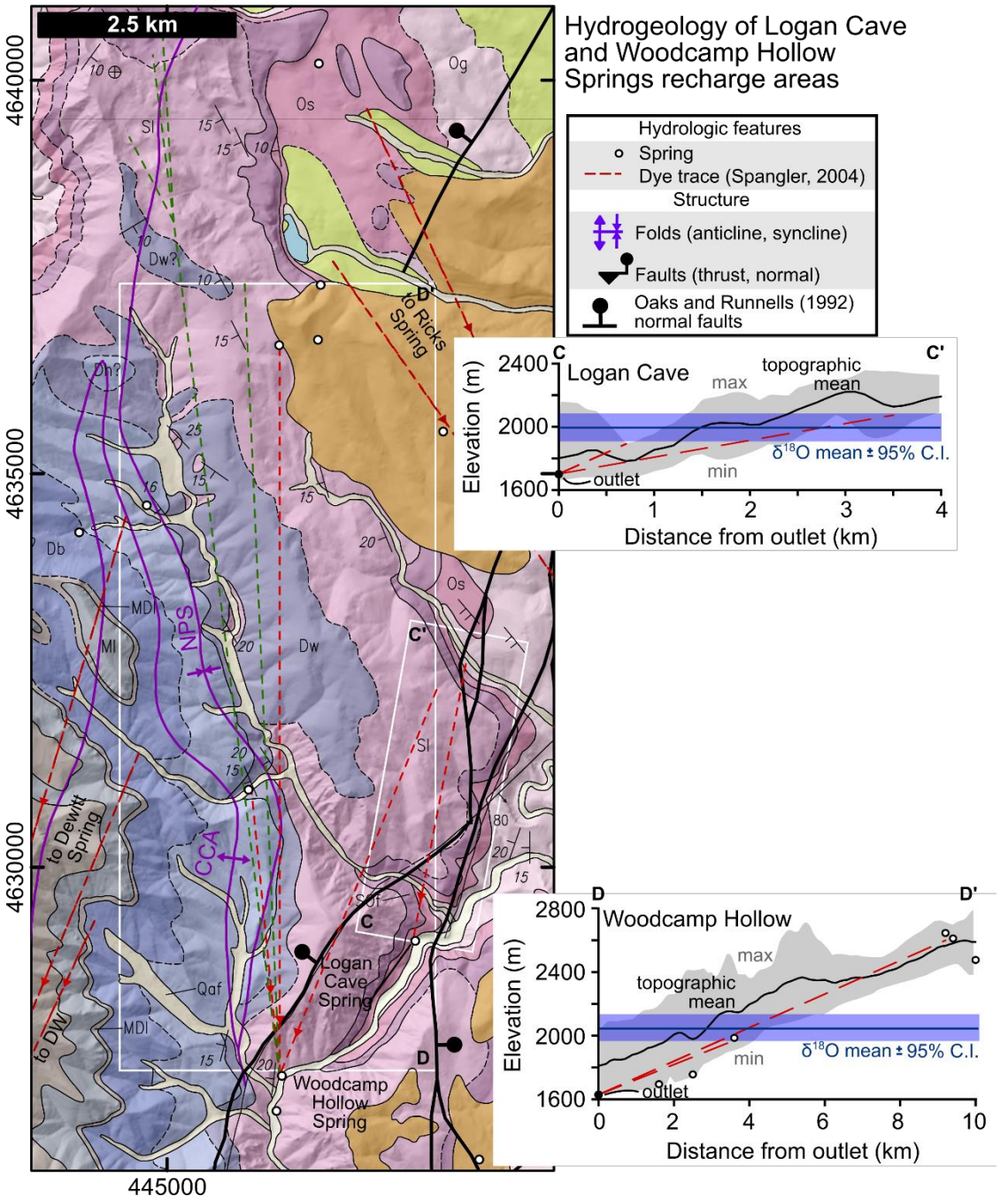

Figure 41. Stratigraphy, dye traces, hydrographic features, $\delta^{18}O$-predicted recharge altitudes, and swath profiles for recharge areas contributing to Woodcamp Hollow and Logan Cave Springs. NPS = Naomi Peak syncline, CCA = Cottonwood Creek anticline.

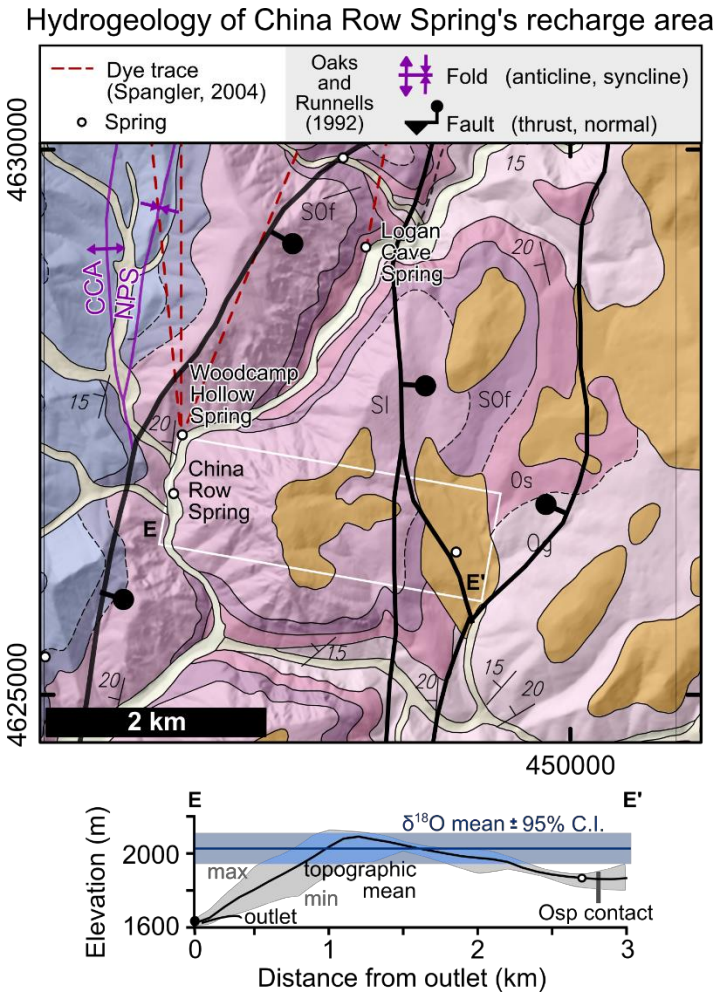

Figure 42. Stratigraphy, dye traces, hydrographic features, $\delta^{18}O$-predicted recharge altitudes, and swath profiles for recharge areas contributing to China Row Spring. CCA = Cottonwood Creek anticline, NPS = Naomi Peak syncline.

Spring Hollow Spring lacks dye-trace controls on recharge area dimensions (Fig. 44). A $\delta^{18}O$-predicted recharge altitude of 326 m above the outlet (Table 16) is similar to that of Dewitt Spring, whose outlet is 86 m lower. Recharge within the Spring Hollow surface catchment may be supplemented by lower-altitude infiltration and northward flow along faults (Dover, 1995) as the LPS locally flattens south of Logan Canyon (Oaks, verbal communication).

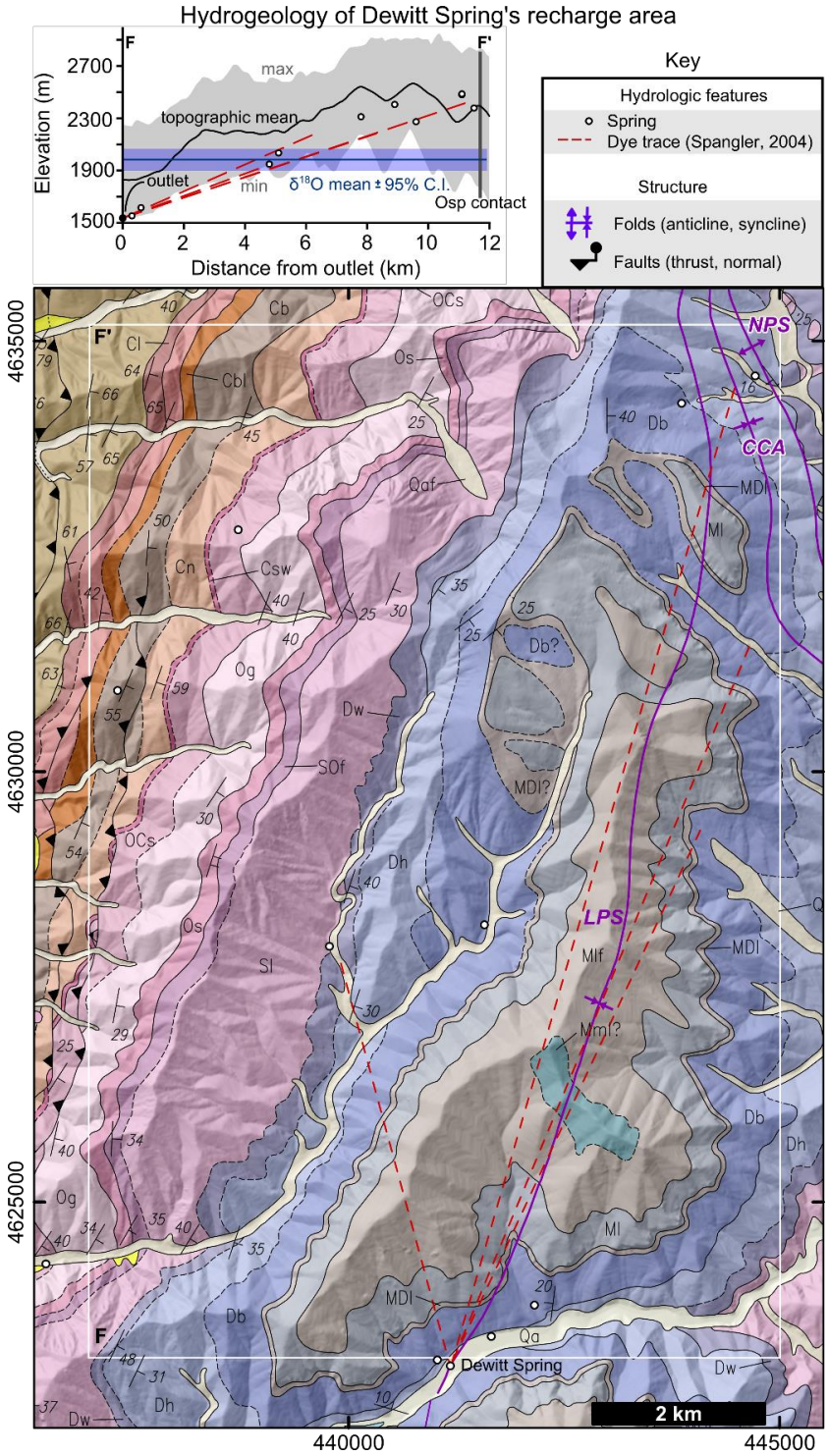

Figure 43. Stratigraphy, dye traces, hydrographic features, δ^{18}O-predicted recharge altitudes, and swath profiles for the Dewitt Spring recharge area. NPS = Naomi Peak syncline, CCA = Cottonwood Creek anticline, LPS = Logan Peak syncline.

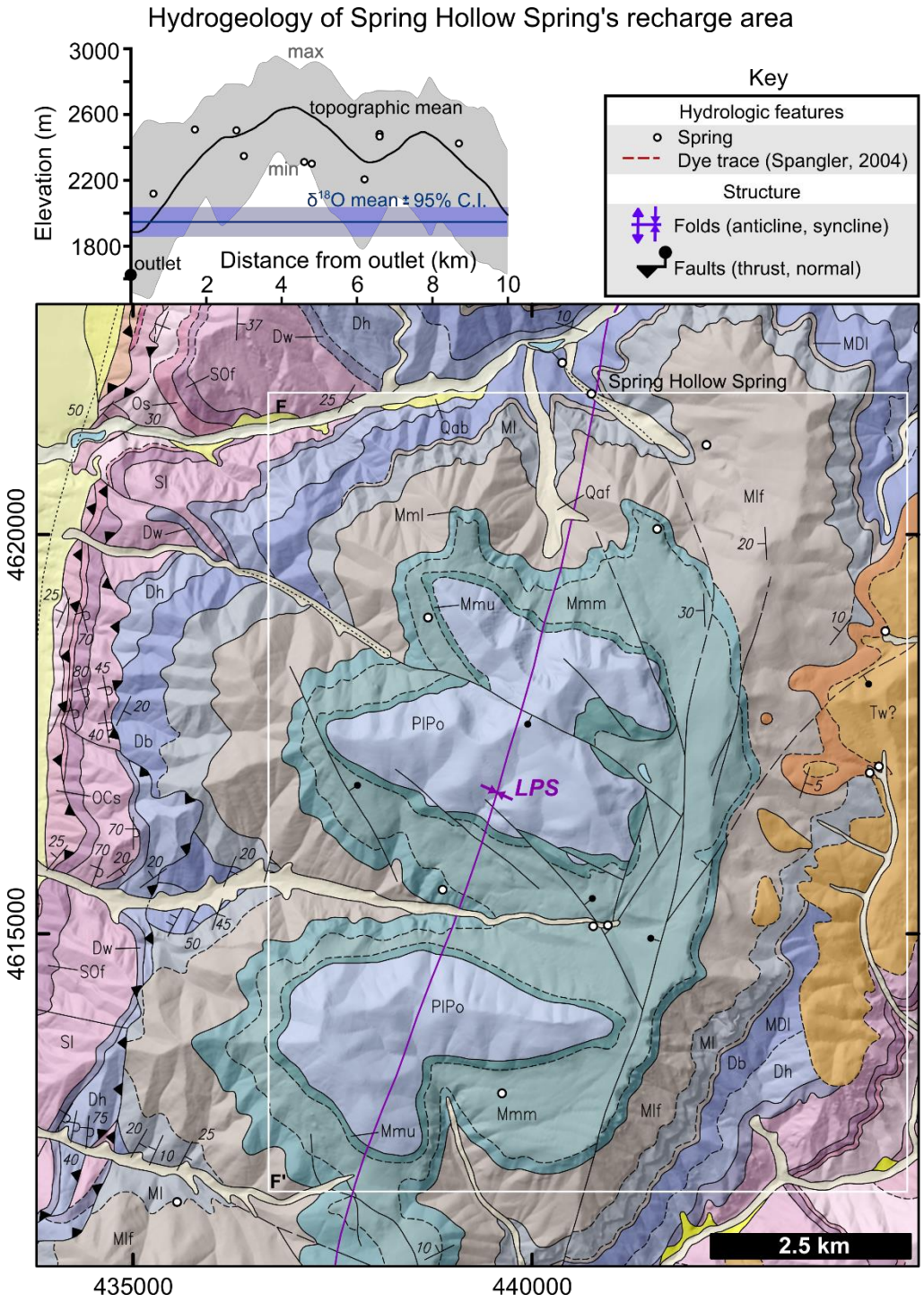

Figure 44. Stratigraphy, dye traces, hydrographic features, $\delta^{18}O$-predicted recharge altitudes, and swath profiles for recharge areas contributing to Spring Hollow Spring. LPS = Logan Peak syncline.

Water-rock interactions

PHREEQC reaction-path models

Total dissolved inorganic carbon (TDIC) and other geochemical data are presented in this section in an attempt to determine if open- or closed-system dissolution occurs along each spring's flowpath. Evolving TDIC concentrations were modeled in PHREEQC by simulating dissolution of stoichiometric dolomite or calcite along fixed-pCO_2 reaction paths ($10^{-3.4}$ to $10^{-1.5}$ atm; Fig. 45) proportional to the degree of interaction with soil CO_2 (Deines et al., 1974). Simulations were run in an open system (abundant gaseous CO_2) and a closed system (no gaseous CO_2), then were compared with field data from springs. Model constraints were checked against sample pCO_2 ($10^{-2.0}$ to $10^{-2.5}$ atm; Table 9), and saturation indices (calcite: -0.7 to 0.0, dolomite: -0.5 to 1.2; Table 9).

Interaction of initial recharge with soil CO_2 to an observed pCO_2 of $10^{-2.0}$ atm would produce less than 1 mmol/L of total dissolved inorganic carbon (TDIC) and lower pH to less than 5 (path *S*, Fig. 45). However, all springs drain groundwater with at least 3.4-3.7 mmol/L of TDIC and pH values greater than 7.3. Accordingly, concentrations in all springs require some level of interaction with aquifer materials. TDIC and pH data for springs lie near the reaction paths for high-pressure ($pCO_2 = 10^{-1.5}$ atm), closed-system (path *C*) and lower pressure ($pCO_2 = 10^{-2.5}$ to $10^{-2.0}$ atm), open-system (path *O*) dissolution of dolomite and calcite. Mass-balance calculations of carbon stable-isotope evolution in groundwater, presented in the following section, better distinguish geochemically closed-system from open-system flowpaths.

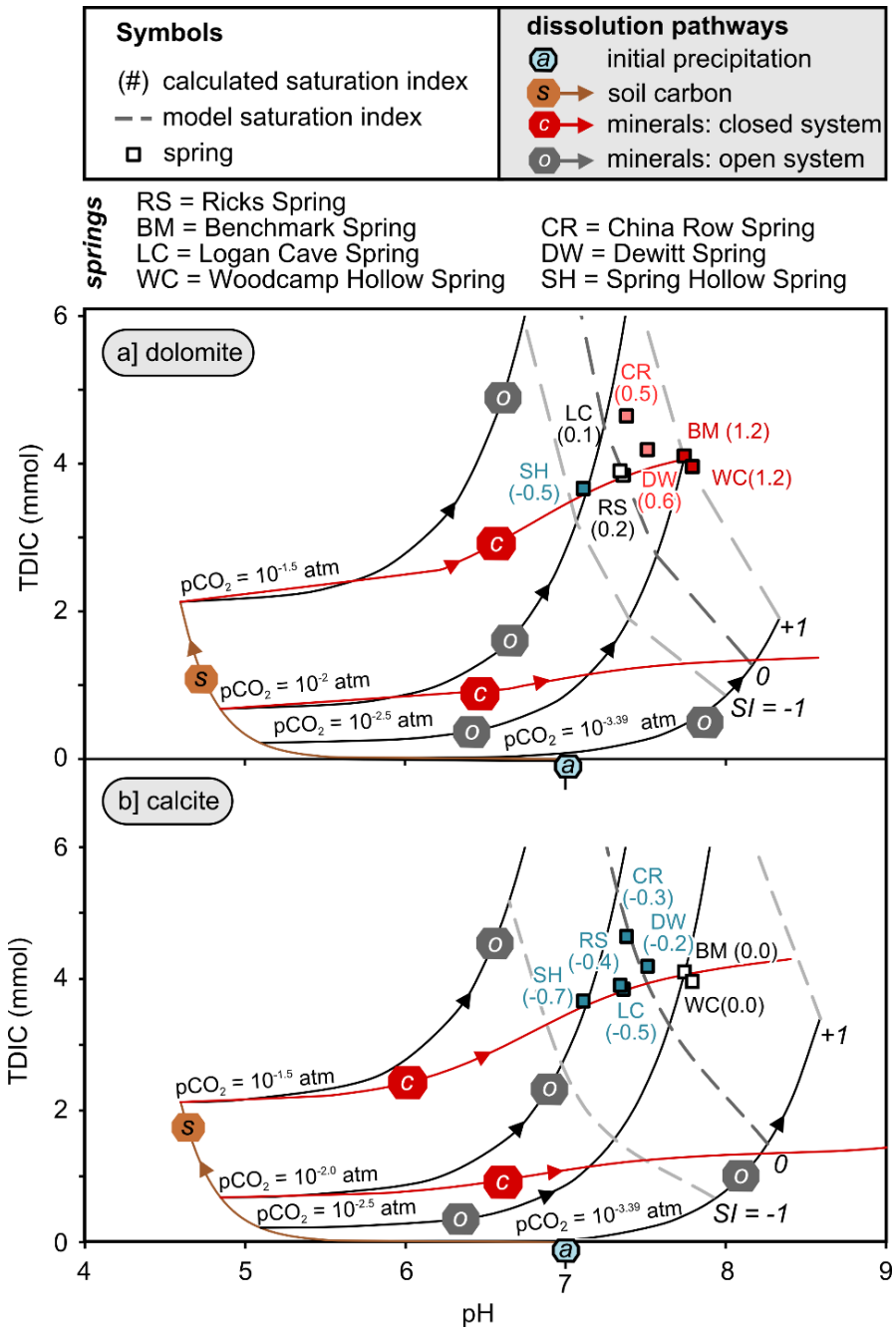

Figure 45. Reaction paths for groundwater interaction with stoichiometric dolomite or calcite along flowpaths with different fixed pCO_2 values.

Reaction paths for dissolution of stoichiometric dolomite at fixed pCO_2 between $10^{-2.0}$ and $10^{-2.5}$ atmospheres appear to bracket values for springs quite well (Fig. 45a),

and align closely with calculated dolomite-saturation indices for low-flow conditions (numbered in parentheses). Calcite reaction paths also align well with geochemical data (Fig. 45b), with saturation indices generally within the ± 0.3 uncertainty calculated in the RESULTS section.

Carbon stable-isotope evolution

Mass-balance calculations after Wigley (1972) were applied to isotopically constrain whether water-rock interactions occur in an open or closed system. Initial precipitation $\delta^{13}C$ of CO_2 was set to the current regional average for precipitation in equilibrium with atmosphere (-7.3 ‰) and soil-CO_2 $\delta^{13}C$ was set to the average value observed in the proximal Wasatch Mountains (-23.3 ‰; Cerling et al., 1991). Modeled pCO_2 reaction paths bracket measured values ($10^{-2.5}$ to $10^{-2.0}$ atm; Table 9). High $\delta^{13}C$ sample values (-9.9 to -11.8‰) and TDIC (4 to 5 mmol/L) clearly align with modeled groundwater-carbon evolution in an open system. This, in turn, implies that dissolution occurs mostly in conduit-dominated flowpaths (Fig. 46).

Calculated saturation indices match model predictions fairly well, with variance most likely explained by spatial differences in carbonate bedrock and soil $\delta^{13}C$. Spring Hollow is undersaturated with respect to stoichiometric dolomite, matches the expected TDIC and pH of the initial water-rock interaction model, and does not match the expected carbon stable isotope value (-15‰) from the mass-balance model. Possibly, this suggests mixing groundwater from two flowpaths that are saturated with respect to dolomite, which would produce apparent undersaturation with respect to dolomite.

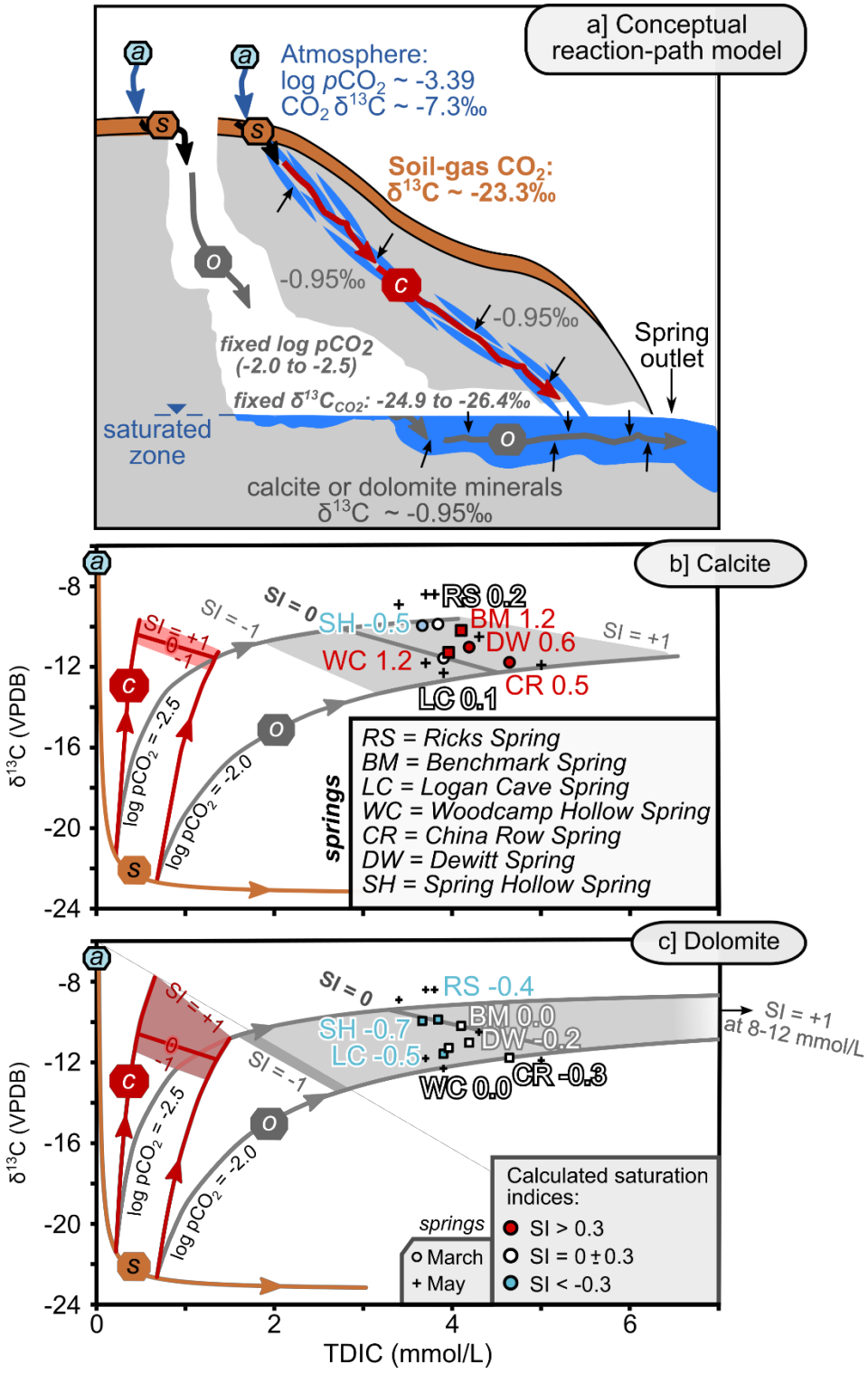

Figure 46. $\delta^{13}C$-evolution reaction-paths for groundwater dissolution of stoichiometric calcite or dolomite in open- (o) or closed-system (c) conditions.

Incongruent dissolution of flowpath minerals

Geochemical modeling up to this point in the analysis assumes that aquifer materials dissolve congruently, such that no coincident mineral precipitation occurs. If so, Ca/Mg molar ratios for stoichiometric dolomite (1.0), calcian dolomite (1.1-1.3) and calcite (44.0-89.0) in the Bear River Range (Kaliser, 1972) should be reflected in groundwater compositions from flowpaths with different geologic units. Ca/Mg ratios cluster around unity in all springs during low-flow conditions (Table 17) despite the fact that Benchmark and Logan Cave Springs are dye traced from recharge to discharge within the Garden City Limestone. The Ca/Mg ratio for Woodcamp Hollow Spring is also distinctly lower than unity in both March and May, which does not match the stoichiometry of any carbonate aquifer mineral. Finally, it is readily apparent that Ca/Mg ratios of all springs sampled in November 2018 are higher than unity (1.7-2.1).

Table 17. Ca/Mg molar ratios for springs in Logan Canyon

Spring	March		May		November	
	T (ºC)	Ca/Mg	T (ºC)	Ca/Mg	T (ºC)	Ca/Mg
Ricks	5.7	1.16	8.1	1.34	-	-
Benchmark	9.6	1.04	11.0	1.04	9.4	1.78
Logan Cave	7.3	0.93	9.1	0.99	-	-
Woodcamp Hollow	7.1	0.73	9.3	0.69	-	-
China Row	7.0	0.93	7.9	0.90	8.8	1.72
Dewitt	7.5	0.97	6.4	1.59	6.8	1.77
Spring Hollow	6.4	1.18	6.7	1.97	5.9	2.05

Taken together, the low values and seasonal variance of these ratios indicate that non-stoichiometric mineral dissolution processes control water-rock interactions. Langmuir (1971) and Wigley (1972) document the incongruent dissolution of dolomite in

low-temperature groundwater. Langmuir (1971) also defined expected equilibrium values over a range of environmental temperatures that match those observed in the Bear River Range during low-flow conditions (Fig. 47). Hence, winter groundwater conditions may approach thermodynamic equilibrium and drive water-rock interactions to achieve lower-than-unity Ca/Mg ratios. However, peak-flow Ca/Mg ratios for some springs rises above the expected temperature-dependent value.

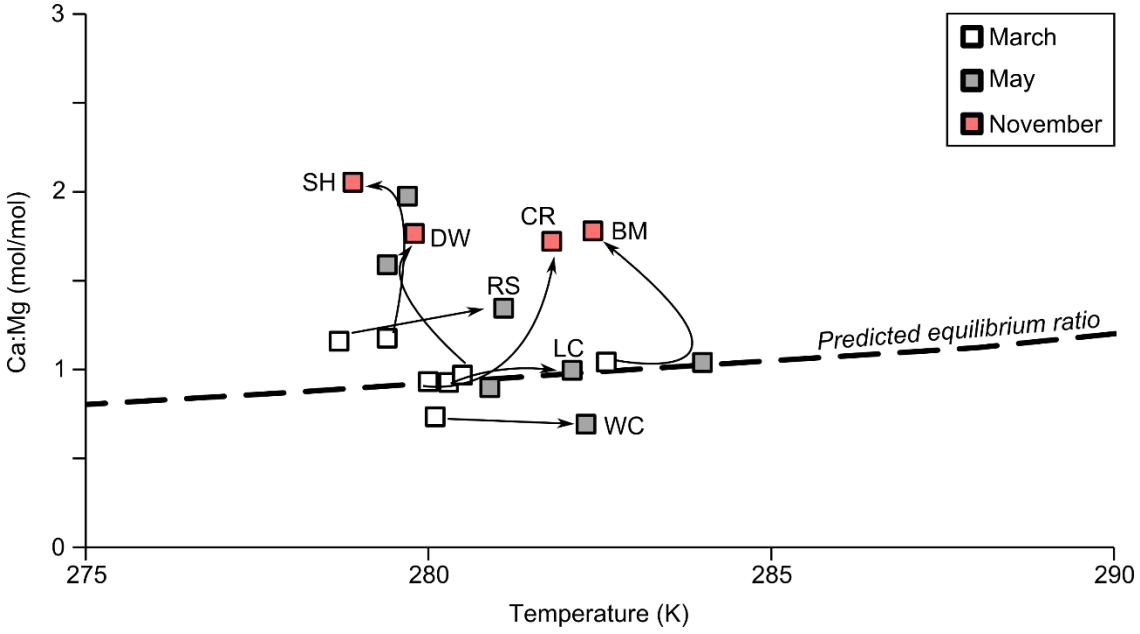

Figure 47. Equilibrium Ca/Mg ratios for calcite and dolomite at low temperatures (Langmuir, 1971) and field data from major springs in Logan Canyon.

Mixing of mature, Ca^{2+}-Mg^{2+}-HCO_3^- -type groundwater with surface water (as is the case during spring recharge) also is documented in other karst aquifers to drive incongruent dissolution of dolomite (Dominguez-Villar et al., 2017). This phenomenon is accompanied by lower Ca/Mg ratios during the mixing period and a return to higher values afterward. Ratios larger than unity may relate to such mixing effects or

progressive interaction with different lithological sequences specific to each flowpath (Hounslow, 1995).

Reaction paths for congruent dissolution of dolomite and varying additions of calcite form straight lines from the origin on a Ca/Mg cross-plot, with slopes controlled by the stoichiometry and amount of each dissolving mineral (Fig. 48). Comparison with field data indicates that Ca/Mg ratios equal to or greater than one are possibly due to congruent dissolution. However, samples collected at Logan Cave, Woodcamp Hollow, China Row, and Dewitt Springs in March 2017 plot below the reaction path for stoichiometric dolomite, the lowest-slope congruent reaction path.

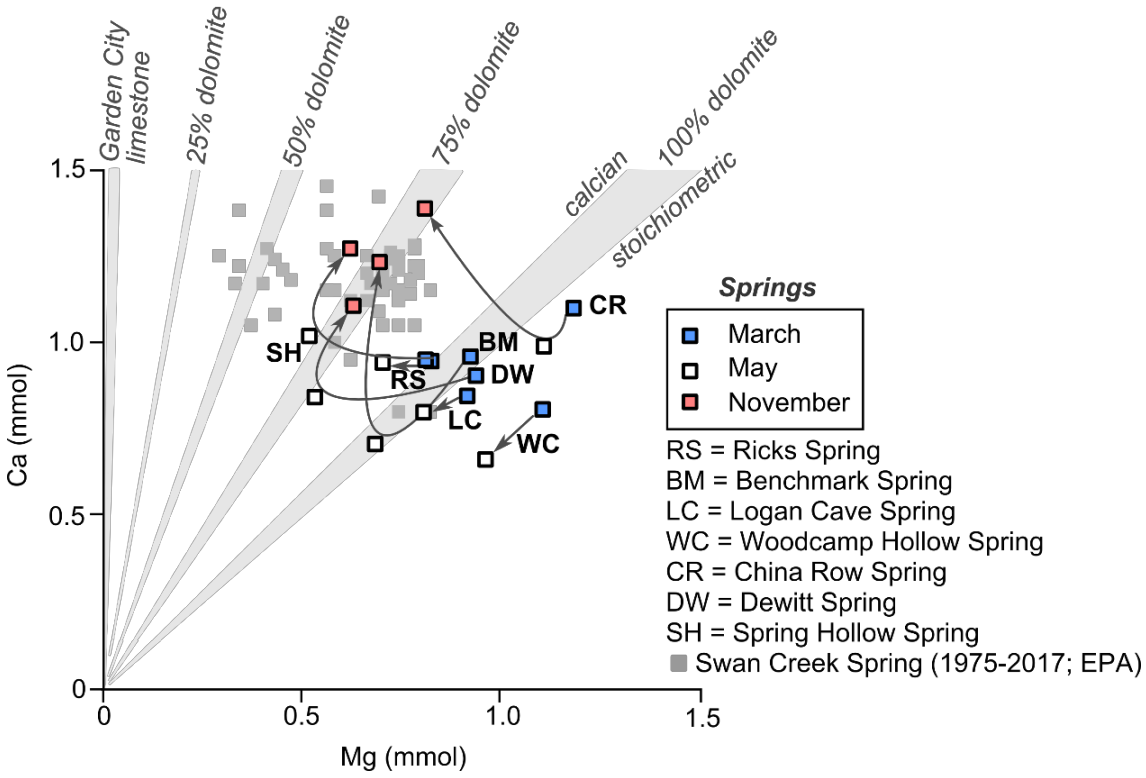

Figure 48. Calcium and magnesium mass evolution via dissolution of stoichiometric and calcian dolomite and values measured seasonally in Bear River Range springs.

As discussed above, cold groundwater temperatures during low-flow conditions (baseflow) indicate the possibility for incongruent dissolution, driven by increased solubility of dolomite over calcite in colder water (Williams et al., 2007). Ratios from long-term monitoring of Swan Creek Spring in the eastern Bear River Range (Fig. 48, gray squares; USEPA, 2017) also vary, supporting the inference that water-rock interactions likely adjust to reflect seasonal (temperature-driven) changes. To check the inference made from temperature data that Ca/Mg ratios less than one reflect incongruent dissolution of magnesium-bearing minerals, dissolution of stoichiometric dolomite, calcian dolomite, and magnesian calcite were simulated in PHREEQC (Figs. 49-50). Calcite saturation was fixed (once reached) as dolomite or magnesium-rich limestone dissolved, simulating incongruent dissolution.

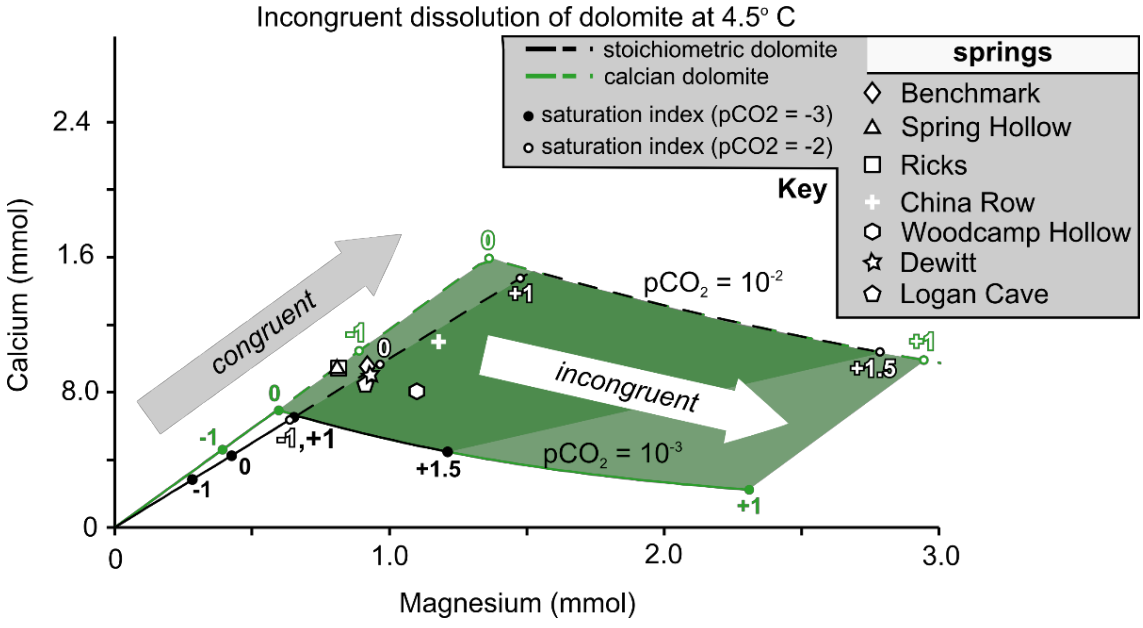

Figure 49. Calcium and magnesium mass evolution via incongruent dissolution of stoichiometric or calcian dolomite and measured values in Bear River Range springs.

The results show that dissolution of calcian and stoichiometric dolomite will proceed incongruently after groundwater reaches saturation or supersaturation, respectively (bold numbers). Reaction paths for incongruent dissolution of both stoichiometric and calcian dolomite, fixed at pCO_2 values of $10^{-2.0}$ and $10^{-3.0}$ atm, respectively, bracket observed groundwater concentrations and support the notion that at least some amount of incongruent dissolution occurs in the Bear River Range karst aquifer system.

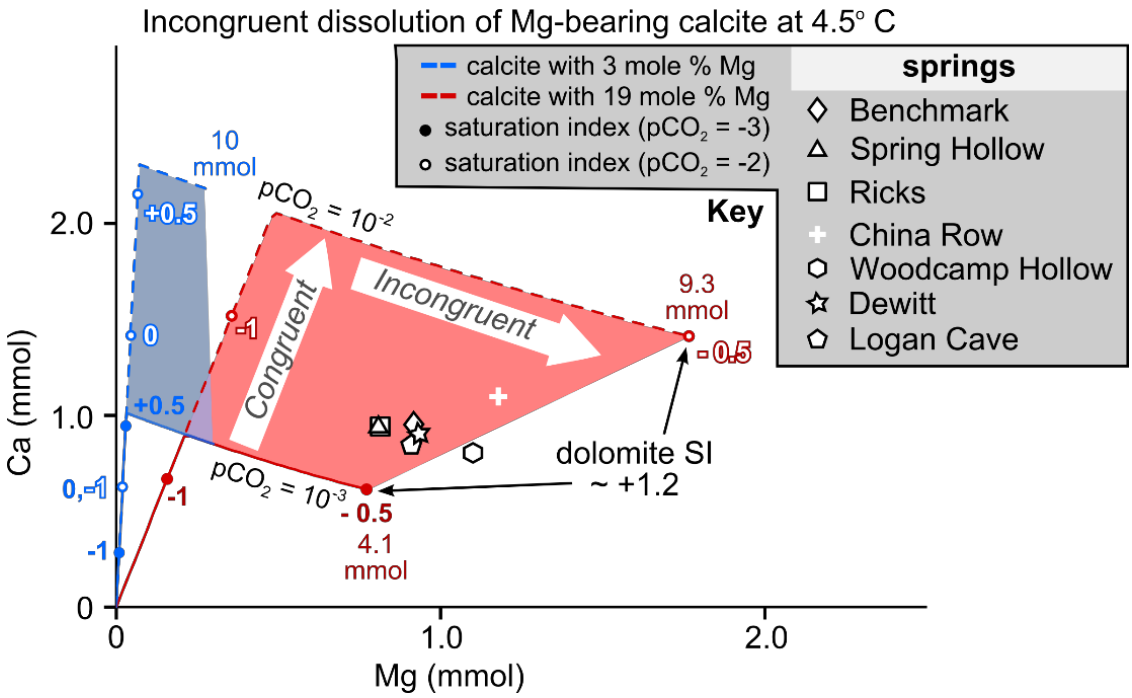

Figure 50. Calcium and magnesium mass evolution via incongruent dissolution of possible magnesian calcite end-member compositions and measured values in Bear River Range springs.

Groundwater interactions with magnesian calcite could possibly account for chemistries of the springs that drain the Garden City Limestone (Ricks, Benchmark, and

Logan Cave Springs) despite the fact that it may contain only a few mole-percent magnesium (Kaliser, 1972). It may also be possible that unmapped dolomite or clay-rich intervals could add to magnesium concentrations (Williams, 1948; Ross, 1951; Taylor et al., 1981). Hence, the observed calcium and magnesium concentrations could be produced by incongruent dissolution of 4-9 mmol of magnesium-rich calcite dissolved incongruently along a flowpath with a pCO_2 of less than $10^{-2.0}$ atm (Fig. 50). With an apparent dolomite and calcite saturation indices of 1.2 and -0.5, respectively, this model fits neither Logan Cave Spring (0.1, -0.5), nor Benchmark Spring (1.2, 0.0). This possibly indicates that flowpath heterogeneity or kinetic barriers cause a more complicated reaction path in the Garden City Limestone. Possibly, dolomite-saturated water discharging from springs in units above the Swan Peak Formation flows overland to re-infiltrate in the Garden City Limestone and contributes a Mg-rich groundwater chemistry to downgradient springs. Upwelling from the dolomite-rich St. Charles Formation or infiltration through de-dolomitizing zones observed on north-facing slopes (DeGraff, 1976; Oaks, verbal communication, 2018) could also contribute anomalous levels of Mg.

Saturation-index interpretation

Stoichiometric calcite- and dolomite-saturation indices of samples collected in March 2017 adhere to a linear trend (Fig. 51) possibly indicative of a single, dominant water-rock interaction. Indices from subsequent sampling excursions cluster near slight dolomite supersaturation and calcite undersaturation, strengthening the inference that fast-flowing groundwater is subjected to similar water-rock interactions across the aquifer

system. Groundwater never exceeds saturation with respect to calcite, despite the fact that dolomite saturation indices exceed a value of one. This, in turn, is a hallmark of incongruence that essentially fixes calcite saturation by permitting coincident precipitation as carbonate minerals dissolve (Langmuir, 1971).

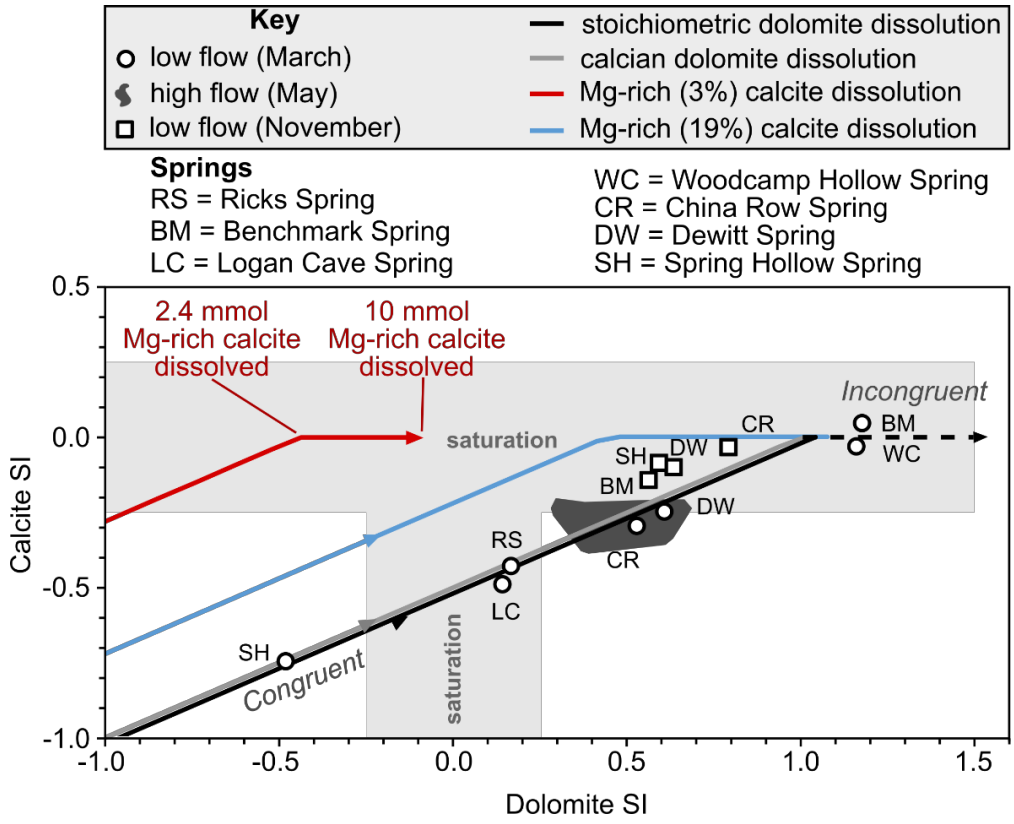

Figure 51. Modeled saturation indices for dissolution of calcian or stoichiometric dolomite and magnesian calcite end members, along with calculated values for Bear River Range springs, shown in terms of saturation with respect to calcite and dolomite.

Field data deviate from a reaction path of dissolving magnesian calcite, which may indicate the presence of a kinetic barrier in the Garden City Limestone that produces a dolomitic signature despite a primarily calcite mineralogy. However, adherence of saturation indices to a reaction path for dolomite dissolution may also imply that Mg-rich

surface water crosses the Swan Peak Formation and infiltrates within the Garden City Limestone. Finally, upwelling of geochemically mature groundwater from the dolomite-rich St. Charles Formation may add a significant component of magnesium to produce a more complicated reaction path than those modeled here.

Stoichiometric dolomite supersaturation is attainable via several mechanisms. As noted by Arvidson and Mackenzie (1999), calcite nucleation in an aquifer occurs rapidly and diminishes or essentially halts dolomite precipitation at low (environmental) temperatures. Morrow (1982) asserts that this kinetic impedance of dolomite precipitation from a supersaturated solution is likely due to the fact that magnesium surfaces become "contaminated" with calcium, which is less strongly hydrated. This leads to calcium occupation at, and subsequent isolation of, sites that would otherwise exchange with magnesium if allowed to equilibrate with groundwater over a longer period.

Other possible mechanisms for stoichiometric dolomite supersaturation are an abrupt decrease in flowpath pressure (White, 1997), dissolution of other evaporite minerals (Baldassare et al., 2010), or an increase in temperature (Langmuir, 1997). However, all springs except for Spring Hollow Spring discharge groundwater supersaturated with respect to stoichiometric dolomite. Unless aquifer hydraulics, lithology, and temperature are the same along each flowpath, they are unlikely to produce the ubiquitously observed stoichiometric dolomite supersaturation. However, groundwater also never exceeds saturation with respect to calcian dolomite (Fig. 52).

Dissolution of calcian dolomite inherently produces one degree of supersaturation with respect to stoichiometric dolomite, removing the need for additional mechanisms.

All springs adhere closely to the simulated reaction path of dissolving calcian dolomite, and never reach supersaturation with respect to it or calcite. Hence, it is likely that the local groundwater geochemical signatures for flowpaths outside of the Garden City Limestone primarily derive from dissolution of calcian dolomite.

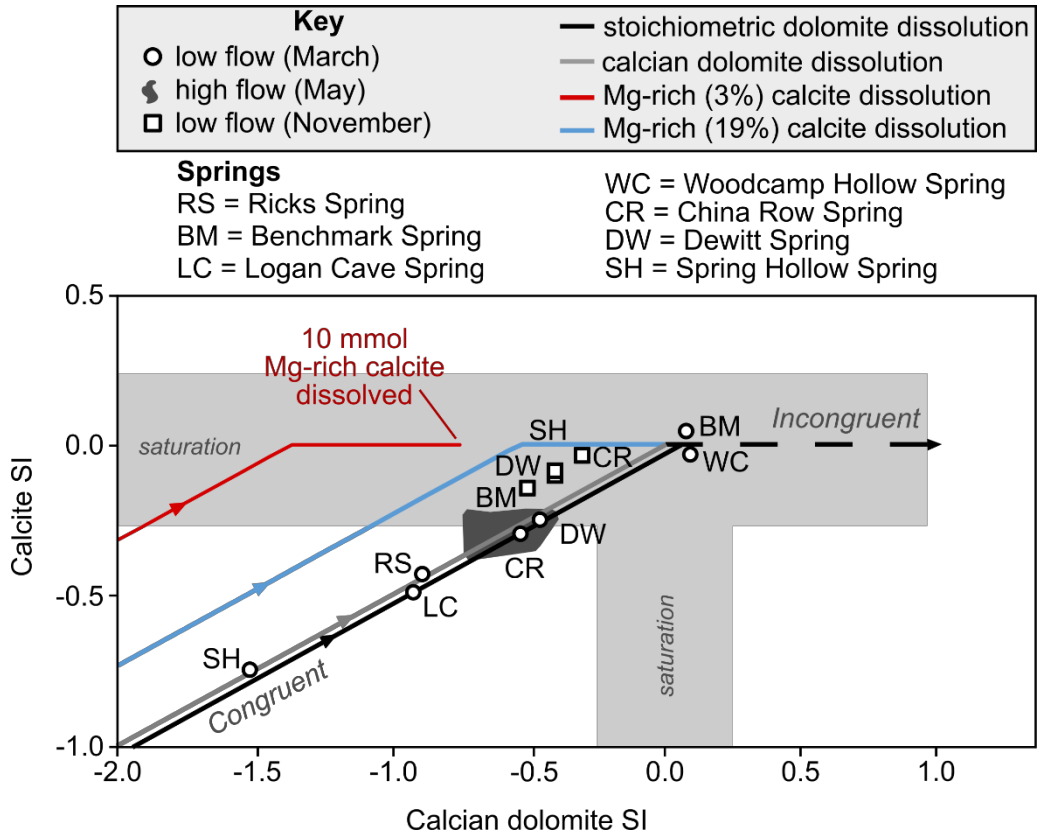

Figure 52. Modeled saturation indices for dissolution of calcian or stoichiometric dolomite and magnesian calcite, along with calculated values for Bear River Range springs, shown in terms of saturation with respect to calcite and calcian dolomite

Potential for groundwater mixing

Groundwater equilibrium with carbonate minerals demarcates a convex-up curve on a pCO_2-calcium cross-plot. Groundwater samples fall above the line when

supersaturated with respect to a given mineral and below the line when undersaturated. Those below the line may also reach undersaturation via mixing of two saturated or supersaturated water chemistries (Langmuir, 1997). All calcium concentrations fall below the equilibrium line for calcite and calcian dolomite (Fig. 53). However, these concentrations are also near equilibrium with stoichiometric dolomite and do not necessarily reflect mixing.

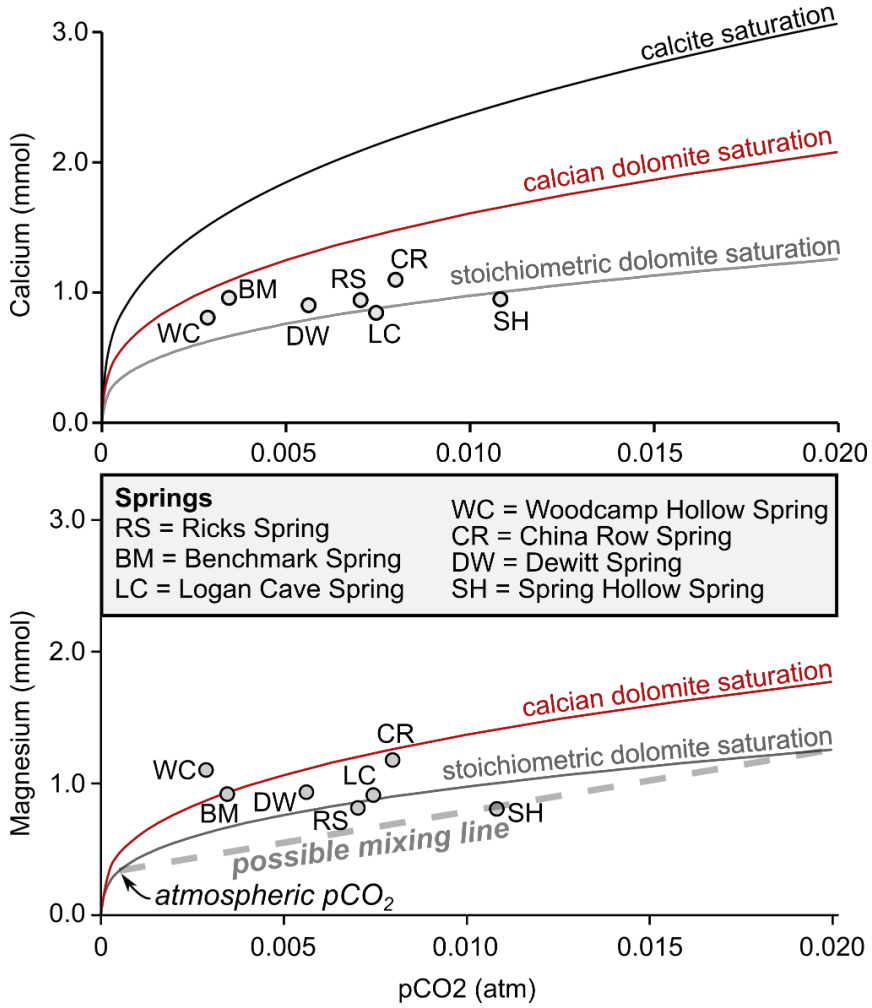

Figure 53. Calcium-pCO_2 and magnesium-pCO_2 plots to assess the possibility for groundwater mixing and equilibria with possible carbonate aquifer minerals.

Magnesium concentrations suggest saturation to supersaturation with respect to stoichiometric dolomite of all spring waters except Spring Hollow Spring (Table 9). As the latter falls below the equilibrium curve on a pCO_2 – Mg plot (Fig. 53), undersaturation may stem from mixing of groundwater from two different flowpaths. This is likely the case, as Spring Hollow Spring bears a $\delta^{13}C$ value and TDIC concentration of water supersaturated with respect to dolomite (Fig. 46).

Groundwater residence times

Estimates of groundwater age from lumped-parameter models (LPMs) of chlorlofluorocarbon and tritium data are presented in this section. As indicated earlier, MRC analysis indicates a saturated-zone residence time of at least several years, similar to the time required for geochemical reactions to produce dolomite equilibrium (Herman and White, 1985). Comparison of these inferences with LPM estimates is a first-order test for the possibility of slower moving groundwater, less permeable flowpaths, and greater aquifer storage.

Chlorofluorocarbon concentrations measured in pmoles/kg were corrected for temperature and recharge altitude (Table 16), then converted to atmospheric units of pptv after Busenberg et al. (2006). The corrected values are less than the contemporary atmospheric concentrations, with the exception of CFC-12 in China Row Spring that is likely contaminated (University of Utah Noble Gas Lab, written communication, 2018). Accordingly, China Row Spring was excluded from lumped-parameter models that involved CFC-12.

Piston-flow model (PFM)

Chlorofluorocarbons

Independent assessment of sample CFC-11, CFC-12, and CFC-113 concentrations with corresponding air curves (Fig. 54) to produce a residence time assumes that recharge enters and moves through an aquifer as a coherent packet (a piston-flow model).

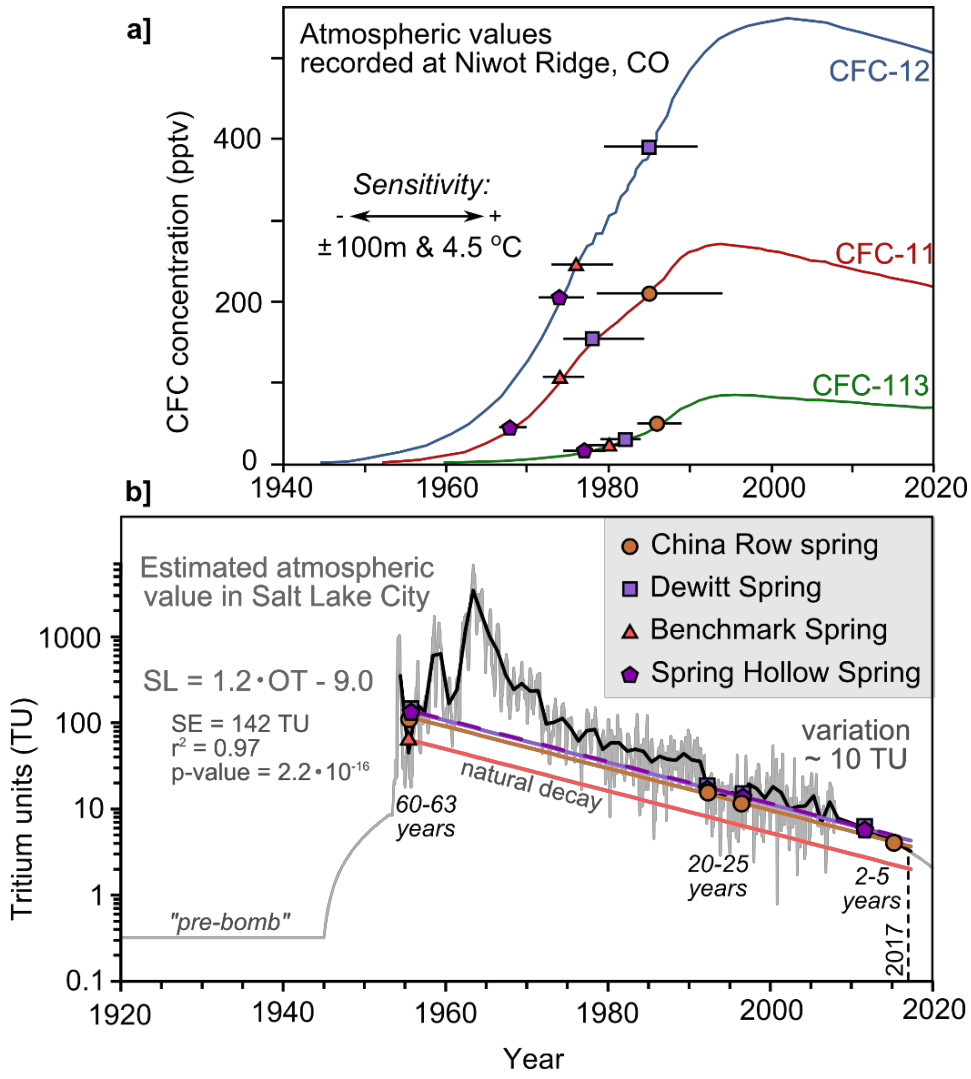

Figure 54. CFC and ^{3}H piston-flow models for recharge to the Bear River Range karst aquifer. Horizontal bars represent uncertainty quantified by the sensitivity analysis.

Piston-flow models of chlorofluorocarbon data (Fig. 54a) require all recharge to have entered the subsurface between the years of 1968-1985 (CFC-11), 1974-1985 (CFC-12), or 1977-1986 (CFC-113). Longest predicted groundwater residence times in the alpine karst aquifer accordingly range from 31 to 49 years. Propagation of variance of triplicate lab measurements through the model results in 95% confidence intervals of ± 1.4 and ± 2.1 years for CFC-11 in China Row and Dewitt Springs, respectively, and less than ± 0.5 years for other chlorofluorocarbons and other springs (Table 18).

Table 18. Groundwater age in the Bear River Range alpine karst aquifer system according to a piston-flow model of chloroflorocarbon concentrations. Sensitivity to parameter changes and variance of replicate measurements constrain uncertainty.

Spring	Tracer	Age (years)	Sensitivity (+/- years)	95% confidence intervals from analytical data (+/- years)
Dewitt	CFC-11	39	+3.5/-6.5	± 2.1
	CFC-12	32	+5.5/-6.0	± < 0.5
	CFC-13	35	+3.0/-2.0	± < 0.5
Spring Hollow	CFC-11	49	+1.5/-2.0	± < 0.5
	CFC-12	43	+2.5/-3.0	± < 0.5
	CFC-13	40	+2.5/-3.0	± < 0.5
China Row	CFC-11	32	+7.0/-9.0	± 1.4
	CFC-13	31	+2.5/-3.0	± < 0.5
Benchmark	CFC-11	43	+2.0/-3.0	± < 0.5
	CFC-12	41	+3.0/-4.5	± < 0.5
	CFC-13	37	+2.5/-2.5	± < 0.5

A sensitivity analysis was performed by varying recharge temperature by ± 4.5 ºC, as possible values range from snowmelt (0 ºC) to a warmer temperatures spring temperature (~9 ºC). Recharge altitude was also allowed to vary by ± 100 m, the approximate uncertainty in the estimates determined from linear regression of $\delta^{18}O$

values (Table 16). CFC-11 ages exhibit the highest sensitivity to parameter changes, with China Row Spring groundwater age ranging from +7.0/-9.0 (Table 18). However, model sensitivity for other springs and tracers are lower, near +2.5/-3.0, which is small in comparison with predicted ages (Table 18). CFC-113 had the lowest overall sensitivity to parameter variation, and was selected for lumped-parameter modeling, with a piston-flow residence time ranging from 31 to 40 years.

Tritium

Groundwater ages via piston-flow modeling of tritium data are more difficult to determine, as measured values are similar to multiple recent annual mean atmospheric concentrations estimated for northern Utah (Fig. 54b; Table 19). Radioactive decay paths for all samples except Benchmark Spring intersect the mean annual value (black solid line) between both 2 to 5 and 20 to 25 years ago. However, only the mean annual values between 1954-1957 intersect decay paths from all measured values. This result places a most likely piston-flow age within the range of 60-63 years ago.

Table 19. Groundwater age in the Bear River Range alpine-karst aquifer system according to a piston-flow model of tritium concentrations.

Spring	Tracer	Possible ages	Precision (TU)
Dewitt	^{3}H	2-5, 20-25, 60-63 years	± 0.5
Spring Hollow	^{3}H	2-5, 20-25, 60-63 years	± 0.5
China Row	^{3}H	2-5, 20-25, 60-63 years	± 0.5
Benchmark	^{3}H	60-63 years	± 0.5

Binary-mixing model (BMM)

Dye traces document the ability for some component of baseflow to move through Bear River Range karst with sub-annual transit times (Spangler, 2002). This suggests that a binary-mixing model (BMM) fixed at modern concentrations may be more accurate than a simple piston-flow model. The applicable age range for each binary mixing model is limited to the date that each tracer was first detected in the atmosphere.

The earliest detection at Niwot Ridge occurred in 1940 for CFC-11 and CFC-12 and in 1943 for CFC-113 (Jurgens et al., 2012). Earliest detection of atmospheric tritium above background levels occurred in 1945 at the Ottawa, Ontario, station from which the correlation with the Salt Lake City record was created. Hence, age estimates by this method are only possible if groundwater is younger than 72-77 years old, and also depend on the tracer used. Results of the binary mixing model for each chlorofluorocarbon pair are presented in Table 20.

Table 20. Groundwater age in the Bear River Range alpine karst aquifer system according to a binary-mixing model of chloroflorocarbon concentrations.

Spring	Tracers	% of discharge	Age (years)
Dewitt	CFC-11 & CFC-113	70%	42
	CFC-11 & CFC-12	40%	47
	CFC-12 & CFC-113	CFC-12 contaminated	-
Spring Hollow	CFC-11 & CFC-113	80%	70
	CFC-11 & CFC-12	CFC-12 contaminated	-
	CFC-12 & CFC-113	85%	46
Benchmark	CFC-11 & CFC-113	70%	47
	CFC-11 & CFC-12	70%	47
	CFC-12 & CFC-113	75%	46
China Row	CFC-11 & CFC-113	65%	33
	CFC-11 & CFC-12	CFC-12 contaminated	-
	CFC-12 & CFC-113	CFC-12 contaminated	-

Binary mixing models of groundwater age are graphically presented in Figures 55 and 56 as gray, dashed lines that connect two ages on a cross-plot of time-series atmospheric concentrations (black curves). The position of field data along the dashed lines indicates the percent contribution from either sub-annual or older flow to the groundwater sample. A binary-mixing model of CFC-11 and CFC-113 suggests that only 20-35% of each spring's low-flow discharge comprises sub-annual quick-flow (Fig. 55a).

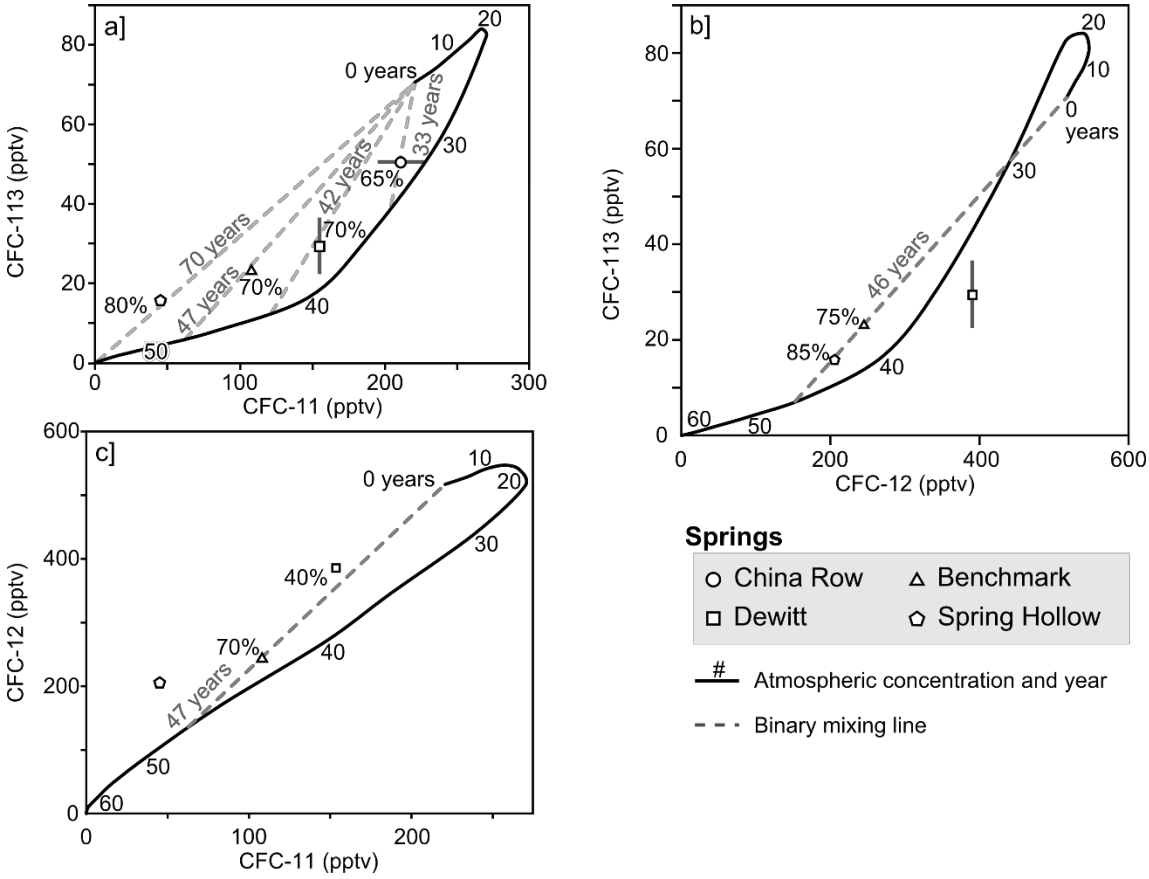

Figure 55. Chlorofluorocarbon binary-mixing models for recharge to the Bear River Range alpine karst system (the contaminated CFC-12 value from China Row Spring is excluded).

The oldest groundwater ages predicted via BMM range from 33 to 47 years for China Row, Dewitt, and Benchmark Springs, and closely match the original piston-flow interpretation. Spring Hollow Spring may drain the oldest water (~70 years), possibly beyond the scope of CFC dating. However, assessment of the Spring Hollow Spring's CFC-12 concentration indicates that the mixing end member may only be as old as 46 years (Fig. 55b). Assessment of CFC-12 in Benchmark (Fig. 55b) and Dewitt Springs (Fig. 55c) further supports an upper recharge age of approximately 46 to 47 years, respectively. Binary mixing models of tritium and each dissolved CFC likewise support the notion that groundwater is a mixture of sub-annual and decadal recharge, in this case 60 to 65 years old (Fig. 56; Table 21). The estimated percentages of decadal recharge, using tritium (0-80% decadal), vary more than those predicted using CFCs (40-85% decadal).

Taken together, it is likely that zones of lesser karstification exist in each spring's groundwater basin, yet only inhibit flow by several decades. Residence time of this magnitude was documented via tritium concentrations in dripwater recharge to a cave system in Israel (Even et al., 1986). A spread of ~35 years for the decadal-age component is similar to that of probability-density functions (PDFs) of age simulated for a karst aquifer in South Dakota (Long and Putnam, 2009).

A binary mixture of sub-annual and decadal residence times additionally supports the notion that the alpine-karst aquifer could accommodate more storage than predicted by extrapolation of the Mangin (1975) MRC model. This larger groundwater reservoir would respond less readily to droughts and could possibly explain the apparent minimum

flow limit of the Logan River (1.5 m^3/s). Even so, changes in recharge that extend beyond several decades (climatic shifts) would likely result in significant impacts to groundwater storage in alpine karst.

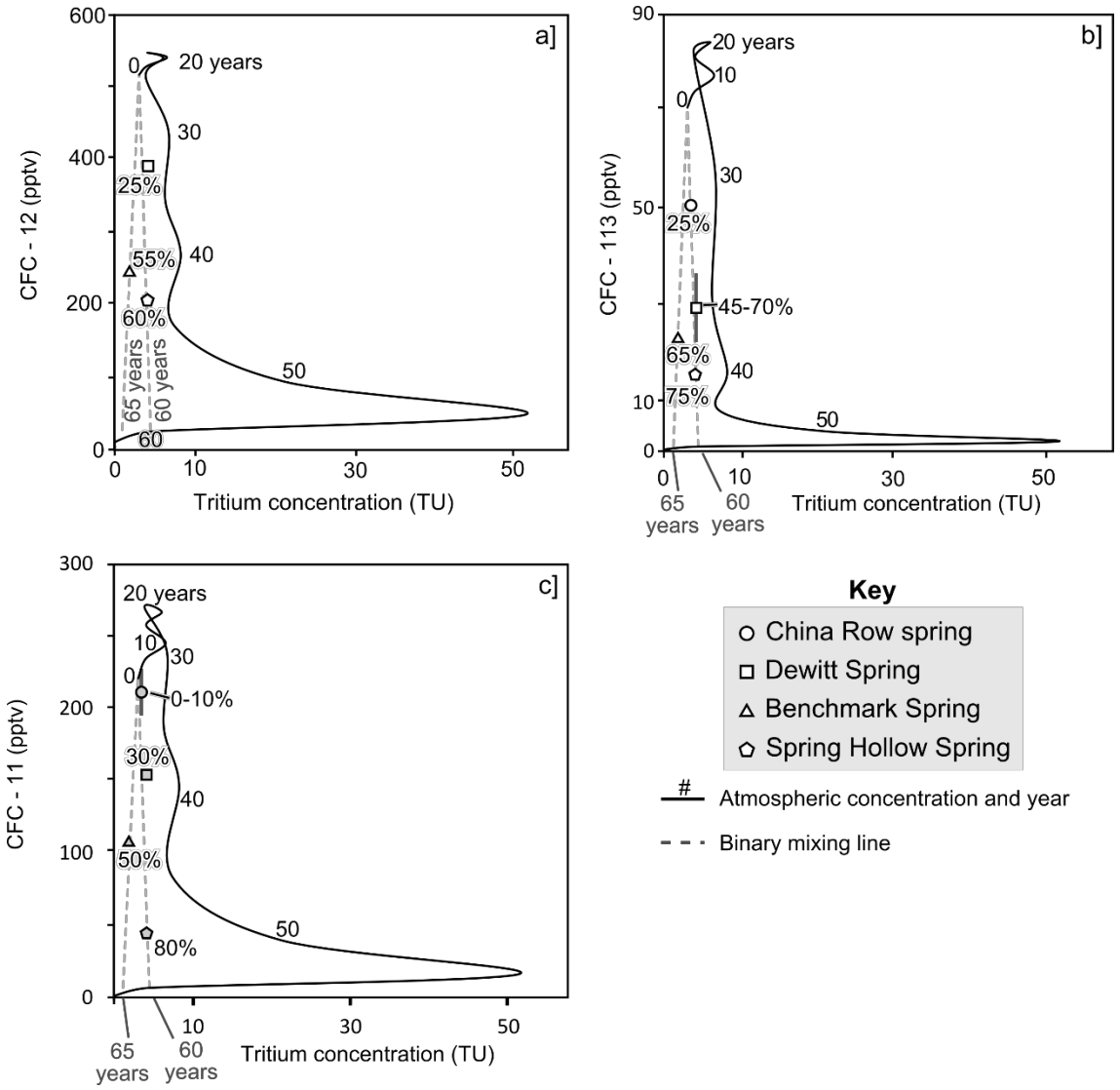

Figure 56. Tritium and chlorofluorocarbon binary-mixing models of groundwater age in the Bear River Range alpine-karst aquifer system. Dashed lines connect sub-annual recharge ages with decadal ages ranging from 60-65 years.

Table 21. Groundwater age in the Bear River Range alpine-karst-aquifer system according to a binary-mixing model of chloroflorocarbon and tritium concentrations.

Spring	Tracers	% of discharge	Age (years)
Dewitt	CFC-11 & ^{3}H	30%	60
	CFC-12 & ^{3}H	25%	60
	CFC-113 & ^{3}H	45-70%	60
Spring Hollow	CFC-11 & ^{3}H	80%	60
	CFC-12 & ^{3}H	60%	60
	CFC-113 & ^{3}H	75%	60
Benchmark	CFC-11 & ^{3}H	50%	65
	CFC-12 & ^{3}H	55%	65
	CFC-113 & ^{3}H	65%	65
China Row	CFC-11 & ^{3}H	0-10%	60
	CFC-113 & ^{3}H	25%	60

SUMMARY, CONCLUSIONS, AND RECOMMENDATIONS

Summary

The Bear River Range of northern Utah hosts at least one karst-aquifer system (Spangler, 2001). The possibility for mountain-block recharge (MBR) to Cache Valley bears implications for existing groundwater numerical models (Kariya et al., 1994; Myers, 2003) and for water-use and aquifer-storage-and-recovery (ASR) policies. The alpine-karst-aquifer system also supplies a municipal water resource (Dewitt Spring) and sustains the Logan River for much of the year.

Alpine-karst aquifers are thought to contain three types of groundwater flowpaths with different capabilities for velocity and storage: caverns, lower-permeability fractures and bedding planes, and enhanced interstitial space. Cavern-dominated flowpaths are represented as a single-porosity (conduit) model, whereby all flow is quick and storage is minimal. Adding lower-permeability fractures and bedding planes, then enhanced pore space, greatly increases storage and introduces significantly slower flow velocities. To date, dye traces confirm the existence of fast, conduit flow in the Bear River Range (Spangler, 2001, 2012). Other modes of flow have not been documented.

The primary goals of this study were twofold: a) to monitor the flow of the Logan River and all tributary springs and streams in the study area to constrain a possible magnitude of MBR and b) to geochemically parameterize the hydraulic behavior of alpine karst. I intended the estimate of MBR and inferences of alpine-karst hydraulics to inform a conceptual flow model useful for management of local surface and groundwater

resources. The conceptual model may also apply to and further understanding of alpine-karst aquifers in other parts of the world.

To accomplish the first goal, I measured the discharge of the Logan River and its tributary streams and springs monthly from August 2016 through November 2017. Monitoring ceased during months in which air temperatures dropped below the operable limit of field equipment (0 ºC) or in which stream velocity and stage proved unsafe. To accomplish the second goal, samples for stable-isotope and major-ion analyses were collected during high- and low-flow conditions at each surface-water and groundwater site. Subsequent sampling of two high-flow (Dewitt, Spring Hollow) and two low-flow (Benchmark, China Row) springs for chlorofluorocarbon and tritium analyses took place in November of 2017. Oxygen and hydrogen stable isotopes in snow cores from 1,812 m to 2,393 m in altitude were analyzed for a statistical relationship with topographic variables.

Due to cold winter temperatures and anomalously high runoff, it was not possible to collect a complete set of discharge measurements from December 2016 through February 2017 and from April 2017 through July 2017. Accordingly, losses to groundwater through the channel of the Logan River were not quantified during the high-flow months during which they were predicted to occur. Various techniques to estimate MBR were investigated, with a linear model producing the most reasonable results of 2.32×10^6 m^3/y (1.88×10^3 af/y), a value much lower than expected based on previous estimates of MBR (10^7-10^8 m^3/y, 10^4-10^5 af/y).

Hydrographs of all springs except Logan Cave and China Row Springs peaked during the month of June, possibly supporting a mean lag time of about one month. Hydrograph similarity of Benchmark Spring to those with known higher-altitude recharge areas supports the notion that some component of its flow has a distal source. Conversely, the Logan Cave Spring hydrograph behaves similarly to those of proximal streams, which suggests a hydraulic link, and rapid transit through a well-developed cavern system.

A master recession curve (MRC) of the Logan River was constructed from USGS gage records spanning 1922-2017, then used to assess possible hydraulic conceptual models of the alpine-karst aquifer. The Mangin (1975) model fits better both statistically and conceptually than other models, and thus supports the notion that groundwater in the unsaturated zone takes 64 days on average to drain into a much lower, saturated cavern network, that may hold up to 2.37×10^8 m^3 (1.92×10^5 af) of groundwater in dynamic storage. Flow from the saturated zone into the Logan River is rapid, with near-total drainage occurring in possibly as short as five years.

Year-to-year low-flow conditions likewise reflect high sensitivity to temporal changes in recharge, and provide a snapshot of the stored volume within the alpine-karst aquifer. It is likely that the alpine karst aquifer draining Logan Canyon loses at least 50% and up to 80% of groundwater recharge in a given year. The Logan River flows at a rate no lower than 1.5 m^3/s (54 cfs) at the end of baseflow, which may reflect the presence of a lower-permeability flowpath within the alpine-karst-aquifer system.

Chlorofluorocarbon and tritium concentrations in representative springs support this notion, and are likely best described by binary mixing of sub-annual recharge with 2-

to 65-year-old groundwater. The possible presence of older water may indicate that a lower permeability flowpath dominates during baseflow and that storage is greater than predicted by master recession-curve analysis. As a diffuse-flow component was not detected in any part of this analysis, it is likely that this predicted higher amount of storage is still sensitive to decadal-scale (or longer) changes in recharge.

Carbon stable-isotope values range from -9.9 ‰ to -11.8 ‰, which are intermediate between local soil-CO_2 (-23.3 ‰) and carbonate-bedrock (-0.95 ‰) values. Modeled reaction paths for dissolution of stoichiometric dolomite in an open system (abundant CO_2) align well with these data, and support the notion that most water-rock interactions occur in caverns. Saturation indices and low Ca/Mg ratios indicate that incongruent dissolution of calcian or stoichiometric dolomite also exerts a strong control on water-rock interactions. Geochemical facies analysis indicates that major-ion concentrations in the Cache Valley principal aquifer increase with distance from the mouth of Logan Canyon.

Stable isotopes of oxygen and hydrogen adhere to the Utah meteoric water line. Oxygen stable isotopes in the alpine snowpack display a significant statistical relationship with altitude (-0.28 ‰ per 100 meters), but not with increasing rainout distance as hypothesized by Bright (2009). Comparison of oxygen stable isotopes in springs and the snowpack aids in qualitatively constraining recharge areas, although low topographic relief of the samples and snowpack and runoff fractionation effects hinder utility. Benchmark and Ricks Springs have oxygen stable-isotope values that do not align well with dye-traced recharge altitudes, which may reflect an undocumented connection

with higher-altitude recharge and mixing with the Logan River, respectively. The linear relationship is statistically weaker for hydrogen stable isotopes, which are likely more susceptible to fractionation effects in the snowpack.

Conclusions

Several preliminary conclusions regarding MBR and karst-aquifer hydraulics in the Bear River Range are stated below. First, any contribution of the Logan River to MBR (possibly 2.32×10^6 m^3/y or 1.88×10^3 af/y) is very small when compared to the model-computed steady-state combined recharge rate of 1.78 m^3/s (63 cfs), or about 5.64×10^7 m^3/y (4.57×10^4 af/y) combined from the Wellsville Mountains and Bear River Range (Myers, 2003). If the 2015 data represent groundwater and surface-water interactions in a normal year, it is unlikely that losses from the Logan River contribute much subsurface recharge to Cache Valley.

Possibly, snowmelt infiltration in the mountain block contributes significantly to MBR, and has yet to be investigated. However, it may also be likely that most recharge occurs as seepage from the Logan River and canals along the mountain front in the vicinity of First Dam as mountain-front recharge (MFR). Groundwater TDS and pCO_2 values are low in this area of the principal aquifer, and increase radially away the mouth of Logan Canyon. This supports the notion that surface water enters the subsurface through locally unconfined sediments.

Master recession-curve (MRC) analysis reveals several hydraulic characteristics of the alpine-karst aquifer. It is most likely that the steep curvature of the fitted model

represents near-total drainage of high-altitude groundwater in the unsaturated zone and considerable lowering of the hydraulic gradient within two months. The smaller (baseflow) curvature indicates a possible mean residence time of several years. This interpretation aligns with the amount of time required for groundwater to equilibrate with calcian or stoichiometric dolomite. Lowest annual flows of the Logan River suggest that dynamic storage in the saturated zone fluctuates greatly from year to year, a result of rapid groundwater drainage and little long-term storage capability.

Despite this variability, no trend in dynamic storage is observable over the total number of gauged years, and historical Logan River discharge has never dropped below 1.5 m^3/s (54 cfs). This aligns well with a binary mixing model of chlorofluorocarbon and tritium concentrations that indicates that up to 80% of baseflow comprises groundwater that takes several decades to travel through the aquifer system. This would provide a stable, minimum amount of discharge to linked surface water systems on a year-to-year basis, but would not yield the much higher longevity associated with a true diffuse-flow component.

From $\delta^{13}C$ and major-ion data, it is likely that caverns are the primary flowpath to each spring and that open-system dissolution is the primary water-rock interaction. Groundwater dissolves either calcian or stoichiometric dolomite and a small net amount of calcite to produce the concentrations observed in springs. Along the flowpaths to several springs, dissolution may occur incongruently to form a Ca/Mg ratio less than one. All springs plot along a reaction path for dissolution of calcian dolomite, a primary aquifer material in the Bear River Range. Dissolution of high-magnesium calcite with

kinetic barriers to dolomite precipitation may explain the chemistries of Logan Cave, Benchmark, and Ricks Springs, which drain from the Garden City Limestone. Unmapped dolomite or clays within the Garden City Limestone, dolomite-rich underlying St. Charles Formation, de-dolomitization of north-facing slopes, and reinfiltration of dolomite-saturated groundwater may also add Mg to these springs.

Predicted recharge altitudes from the $\delta^{18}O$ gradient qualitatively align with dye-trace estimates, with the exception of Ricks and Benchmark Springs. However, it is likely that the misalignment of Ricks Spring is explained by mixing of alpine snowmelt with a diversion of the Logan River. Benchmark Spring may draw recharge from higher altitudes along an unidentified conduit, due to its lack of isotopic similarity with the nearby Logan Cave Spring. The similarity of the Benchmark Spring hydrograph to those of other springs further suggests that a hydraulic link with a higher altitude recharge area may exist. China Row Spring likely has a low-altitude recharge area, in keeping with areal exposure of the Swan Peak Formation.

Recommendations for future work

Acoustic Doppler Current Profiler (ADCP) technology (Muste et al., 2004) would permit measurement of Logan River discharge at high stages and flow velocities that are dangerous to measure with a flow meter and wading rod. If existing bridges partitioned monitored reaches, use of ADCP technology would most likely result in a complete set of discharge measurements during high-flow conditions. Long-term monitoring of the Logan River with an ADCP, and its tributary streams and springs with a wading rod and

flow meter, could verify conjectured temporal changes in surface-water and groundwater interactions. If monitored during multiple low- and high-water years, results could be used to determine an average amount of water lost to the subsurface in Logan Canyon and possibly strengthen the linear model proposed in this study.

Mountain-block recharge could be further constrained by hydrologic modeling of karst springs in Logan Canyon and range-front canyons that would estimate net losses to the subsurface. Several approaches are possible, including identification of groundwater abstractions via a large-scale snowmelt-runoff model (SRM) of the mountain block (Martinec, 1975; Martinec et al., 1994), or by direct distributed or lumped-simulation modeling of individual groundwater basins (Hartmann et al., 2012; Hartmann et al., 2014).

As $\propto$ from the fitted Mangin (1975) model relates to hydraulic parameters of the major groundwater flowpaths that contribute to the Logan River, estimation of some parameters would elucidate others. For example, an estimate of average saturated thickness could be produced by noble-gas analysis of selected springs after Manning and Solomon (2004), and surface investigation of springs and streams in Logan Canyon. A range of flowpath lengths could be constrained from existing hydrostratigraphic and geologic mapping. Storativities for different flowpath types (caverns, fractures, and porous media) could be estimated. These parameters together yield insight into the hydraulic conductivity of the dominant flowpath type. Knowledge of these parameters would further improve the groundwater conceptual flow model proposed in this thesis, and provide initial values for numerical flow modeling.

Mass-balance calculations of groundwater solutes (e.g., chloride) from the principal aquifer in easternmost southern Cache Valley would aid in establishing if recharge occurs as surface-water seepage at the mountain front (MFR) or through the subsurface from the mountain-block (MBR). If seepage at the mountain front is a major recharge mechanism as postulated in this study, it bears implications for the current hydrogeologic conceptual model and related numerical model. Further, this approach would directly support or undermine the notion of a physical link between the mountain-block karst-aquifer system and the adjacent valley-fill principal aquifer. Identification of discrete zones of mountain-block recharge would provide a target for future incremental-streamflow monitoring in adjacent surface catchments to spatially assess surface-water contributions to the subsurface. Investigations of this type would involve sampling valley-margin and mountain-block wells, as well as local streams and the Logan River above First Dam for chloride.

The presence of mountain-block recharge could also be assessed with noble-gas analysis of groundwater at valley-margin wells, after Manning and Solomon (2004). A predicted saturated-zone altitude that lies above major spring outlets in the mountain block would align with the notion that alpine groundwater migrates through the subsurface into Cache Valley. Conversely, a predicted-recharge altitude that is close to that of surface-water features along the valley margin would indicate dominance of MFR rather than MBR.

Karst aquifer hydraulics within the mountain block could be further elucidated by high-resolution flow and chemical monitoring of low- and high-discharge springs. This

could be accomplished by installing stage and electrical-conductivity meters at springs of interest (e.g., those sampled for CFCs and tritium in this study). High-resolution records would document whether or not the highest observed flow coincides with the lowest conductivity and how long after the onset of snowmelt it occurs. Creation of a rating curve to relate stage to discharge would also allow for high-resolution recession-curve analysis (and related hydraulic interpretation) of these springs.

Groundwater sources for Ricks Spring could be further clarified by sampling surface-water features in Tony Grove, Bunchgrass Hollow, and Bear Hollow, as well as the Logan River, for stable isotopes and conservative solutes, such as chloride. Sampling of seepage water from the cave system behind the Ricks Spring outlet could yield further insight to water-rock interactions within the Garden City Limestone. A detailed geochemical sampling campaign for springs that discharge immediately above and below the Swan Peak Formation could test its efficacy to partition the karst aquifer system and identify possible overland flowpaths.

Measurement of radioactive (^{36}Cl) and stable (^{35}Cl, ^{37}Cl) chloride in selected Bear River Range springs would constrain long groundwater residence times up to 1 Ma (Bentley et al., 1986). Unlike ^{14}C, radioactive and stable chlorine are not compromised by interaction with carbonate materials, and therefore would document the presence or lack of groundwater that could move interstitially through Paleozoic carbonate rocks in alpine settings.

Based on results of the MRC analysis and field observations that flow in ephemeral streams dwindles rapidly, it is likely that any lower-permeability flowpaths

exist near the water table. Hence, geochemical and physical investigation of inflows to caves that host perennial springs (i.e., intersect the water table) may elucidate the hydraulic nature of these flowpaths.

Finally, the physical process controlling the minimum discharge of the Logan River could possibly be elucidated by applying methods outlined in this thesis to other gaged fluvial systems in more arid alpine-karst environments. In such settings, it is likely that the hydraulic signal of possible fracture-dominated or even matrix-dominated flow could be more strongly expressed due to lower recharge, and hence better studied.

REFERENCES

Abbott, M.D., Lini, A., and Bierman, P.R., 2000, $\delta^{18}O$, δD, and ^{3}H measurements constrain groundwater recharge patterns in an upland fractured bedrock aquifer, Vermont, USA: Journal of Hydrology, v. 228, p. 101-112.

Aishlin, P., and McNamara, J.P., 2011, Bedrock infiltration and mountain block recharge accounting using chloride mass balance: Hydrological Processes, v. 25, p. 1934-1948.

Anderson, P.B., Susong, D.D., Wold, S.R., Heilweil, M., and Baskin, R.L., 1994, Hydrogeology of recharge areas and water quality of the principal aquifers along the Wasatch Front and adjacent areas, Utah: U.S. Geological Survey Water-Resources Investigations Report 93-4221, 74 p.

Arvidson, R.S., and Mackenzie, F.T., 1999, The dolomite problem: control of precipitation kinetics by temperature and saturation state: American Journal of Science, v. 299, p. 257-288.

Back, W., and Hanshaw, B.B., 1965, Chemical geohydrology: Advances in Hydroscience, v. 2, p. 49-109.

Bahr, K., 2016, Structural and lithological influences on the Tony Grove alpine karst system, Bear River Range, north-central Utah [M.S. thesis]: Logan, Utah State University, 212 p.

Baldassare, G., Pagliarulo, P., and Zuffiano, L.E., 2010, Water composition and minerals equilibria at the Syri I Kalter Spring and in the Bistrica River (South Albania): Water Resources, v. 38, no. 5, p. 662-669.

Beale, E.M., 1960, Confidence regions in non-linear estimations: Journal of the Royal Statistical Society, v. 22b, p. 41-88.

Becker, M.W., Georgian, T., Ambrose, H., Siniscalchi, J., and Fredrick, K., 2004, Estimating flow and flux of ground water discharge using water temperature and velocity: Journal of Hydrology, v. 296, p. 221-233.

Behar, S., Dates, G., and Byrne, J., 1996, Testing the waters: chemical and physical vital signs of a river: Montpelier, Vermont, River Watch Network, 211 p.

Bentley, H.W., Phillips, F.M., Davis, S.N., Habermehl, M.A., Airey, P.L., Calf, G.E., Elmore, D., Gove, H.E., and Torgersen, T., 1986, Chlorine 36 dating of very old

groundwater 1. The Great Artesian Basin, Australia: Water Resources Research, v. 22, no. 13, p. 1991-2001.

Berthoux, P.M., and Brown, L.C., 2002, Statistics for Environmental Engineers: Boca Raton, Florida, Lewis Publishers, CRC Press, 512 p.

Bischoff, W.D., 1998, Dissolution enthalpies of magnesian calcites: Aquatic Geochemistry, v. 4, p. 321-336.

Bjorklund, L.J., and McGreevy, L.J., 1971, Groundwater resources of Cache Valley, Utah and Idaho: Utah Department of Natural Resources Technical Publication 36, 72 p.

Blasch, K.W., and Bryson, J.R., 2007, Distinguishing sources of ground water recharge by using δ^2H and $\delta^{18}O$: Ground Water, v. 45, no. 3, p. 294-308.

Bowen, G., 2017, waterisotopes database: http://waterisotopes.org (accessed October 2018).

Bright, J., 2009, Isotope and major-ion chemistry of groundwater in Bear Lake Valley, Utah and Idaho, with emphasis on the Bear River Range, *in* Rosenbaum, J.G., and Kaufman, D.S., eds., Paleoenvironments of Bear Lake, Utah and Idaho, and its catchment: Geological Society of America Special Paper 450, p. 105–132.

Brooks, J.R., Wiginton, P.J., Phillips, D.L., Comeleo, R., and Coulombe, R., 2012, Willamette River Basin surface water isoscape ($\delta^{18}O$ and $\delta^{2}H$): temporal changes of source water within the river: Ecosphere, v. 3, no. 5, p. 1-39.

Busenberg, E., and Plummer, L.N., 1992, Use of Chlorofluorocarbons (CCl_3F and CCL_2F_2) as hydrologic tracers and age-dating tools: the alluvium and terrace system of central Oklahoma: Water Resources Research, v. 28, no. 9, p. 2257-2283.

Busenberg, E., Plummer, L.N., Cook, P.G., Solomon, D.K., Han, L.F., Groning, M., and Oster, H., 2006, Sampling and analytical methods, *in* Use of Chlorofluorocarbons in Hydrology: a Guidebook: Vienna, International Atomic Energy Agency, p 199-220.

Cerling, T.E., Solomon, D.K., Quade, J.A., and Bowman, J.R., 1991, On the isotopic composition of carbon in soil carbon dioxide: Geochimica et Cosmochimica Acta, v. 55, p. 3403-3405.

Chang, T.L., and Li, W.J., 1990, A calibrated measurement of the atomic weight of carbon: Chinese Science Bulletin, v. 35, no. 4, p. 290-296.

Chappelle, J.C., 1975. Mineralization in the Bear River Range, Utah-Idaho [M.S. thesis]: Logan, Utah State University, 63 p.

Chiodini, G., Frondini, F., Cardellini, C., Parello, F., and Peruzzi, L., 2000, Rate of diffuse carbon dioxide Earth degassing estimated from carbon balance of regional aquifers: The case of central Apennine, Italy: Journal of Geophysical Research, v. 105, no. B4, p. 8423-8434.

Choi, J., Hulseapple, S.M., Conklin, M.H., and Harvey, J.W., 1998, Modeling CO_2 degassing and pH in a stream-aquifer system: Journal of Hydrology, v. 209, p. 297-310.

Clark, I.D., and Fritz, P., 1997, Environmental Isotopes in Hydrogeology: Boca Raton, Florida, Lewis Publishers, CRC Press, 550 p.

Clyde, C.G., Jeppson, R.W., and Liu, W.K., 1994, A groundwater model of Cache Valley, Utah: Utah Water Resarch Laboratory Paper 532, 113 p.

Coplen, T.B., Herczeg, A.L., and Barnes, C., 2000, Isotope engineering—using stable isotopes of the water molecule to solve practical problems, *in* Cook, P., and Herczeg, A., eds., Environmental Tracers in Subsurface Hydrology: New York, Springer Science+Business Media, 529 p.

Cotagne, A., 1968, Les variations de debit en periode non influence par les precipitations: la Houille Blanch, p. 416-436.

Craig, H., 1961, Isotopic variation in meteoric water: Science, v. 133, no. 3465, p. 1702-1703.

Crowe, C.T., Elger, D.F., and Roberson, J.A., 2001, Engineering fluid mechanics: New York, John Wiley and Sons, 705 p.

Darling, W.G., Gooddy, D.C., MacDonald, A.M., and Morris, B.L., 2012, The practicalities of using CFCs and SF6 for groundwater dating and tracing: Applied Geochemistry, v. 27, no. 9, p. 1688-1697.

Davis, C.R., 2017, Sequence stratigraphy, chemostratigraphy, and biostratigraphy of lower Ordovician units in northeastern and western central Utah: regional implications [M.S. thesis]: Logan, Utah State University, 244 p.

DeGraff, J.V., 1976, Quaternary geomorphic features of the Bear River Range, north-central Utah [M.S. thesis]: Logan, Utah State University, 199 p.

Deines, P., 1980, The isotopic composition of reduced organic carbon, *in* Fritz, P., and Fontes, J.C., eds., Handbook of Environmental Isotope Geochemistry: Amsterdam, Elsevier, v. 1, p. 329-406.

Deines, P., Langmuir, D., and Harmon, R.S., 1974, Stable carbon isotope ratios and the existence of a gas phase in the evolution of carbonate waters: Geochimica et Cosmochimica Acta, v. 38, p. 1147-1164.

Delbart, C., Barbecot, F., Valdes, D., Tognelli, A., Fourre, E., Purtschert, R., Couchoux, L., and Jean-Baptiste, P., 2014, Investigation of young water inflow in karst aquifers using SF_6-CFC-^{3}H/He-^{85}Kr-^{39}Ar and stable isotope components: Applied Geochemistry, v. 50, p. 164-176.

Doctor, D.H., and Alexander, E.C., 2005, Interpretation of water chemistry and stable isotope data from a karst aquifer according to flow regimes identified through hydrograph recession analysis, *in* Proceedings, U.S. Geological Survey Karst Interest Group, Rapid City, South Dakota: U.S. Geological Survey Water-Resources Investigations Report 2005-5160, p. 82-92.

Doctor, D.H., Kendall, C., Sebestyen, S.D., Shanley, J.B., Ohte, N., and Boyer, E.W., 2008, Carbon isotope fractionation of dissolved inorganic carbon (DIC) due to outgassing of carbon dioxide from a headwater stream: Hydrological Processes, v. 22, p. 2410-2423.

Dominguez-Villar, D., Vazquiz-Navarro, J.A., and Krklec, K., 2017, The role of gypsum and/or dolomite dissolution in tufa precipitation: lessons from the hydrochemistry of a carbonate-sulphate karst system: Earth Surface Processes and Landforms, v. 42, p. 245-258.

Dover, J.H., 1995, Geologic map of the Logan 30' x 60' quadrangle, Cache and Rich Counties, Utah, and Lincoln and Uinta Counties, Wyoming: Utah Geological Survey Miscellaneous Publication MP06-8 DM, scale 1:100,000, 1 sheet.

Eisenlohr, L., Kiraly, L., Bouzelboudjen, M., and Rossier, Y., 1997, Numerical simulation as a tool for checking the interpretation of karst spring hydrographs: Journal of Hydrology, v. 193, no. 1-4, p. 306-315.

Evans, J.P., McCalpin, J.P., and Holmes, D.C., 1996, Geologic map of the Logan quadrangle, Cache County, Utah: Utah Geological Survey Map 96-1, scale 1:24,000, 2 sheets, 16 p. text.

Evans, J.P., and Oaks, R.Q., Jr, 1996, Three-dimensional variations in extensional fault shape and basin form: the Cache Valley basin, eastern Basin and Range province, United States: Geological Society of America Bulletin, v. 108, p. 1580-1593.

Even, H., Carmi, I., Magaritz, M., and Gerson, R., 1986, Timing the transport of water through the upper vadose zone in a karstic system above a cave in Israel: Earth Surface Processes and Landforms, v. 11, no. 2, p. 181–191.

Fetter, C.W., 2001, Applied Hydrogeology: Upper Saddle River, New Jersey, Prentice-Hall, 598 p.

Filippini, M., Squarzoni, G., De Waele, J., Fiorucci, A., Vigna, B., Grillo, B., Riva, A., Rossetti, S., Zini, L., Casagrande, G., Stumpp, C., and Gargini, A., 2018, Differentiated spring behavior under changing hydrological conditions in an alpine karst aquifer: Journal of Hydrology, v. 556, p. 572-584.

Ford, D., and Williams, P.D., 2007, Karst Hydrogeology and Geomorphology: Chichester, West Sussex, John Wiley and Sons, 576 p.

Francis, G.G., 1972, Stratigraphy and environmental analysis of the Swan Peak Formation and Eureka Quartzite, northern Utah [M.S. thesis]: Logan, Utah State University, 125 p.

Frondini, F., Zucchini, A., and Comodi, P., 2014, Water-rock interactions and trace element distribution in dolomite aquifers: the Sassolungo and Sella systems (northern Italy): Geochemical Journal, v. 48, p. 231-246.

Gat, J.R., and Gonfiantini, R., eds., 1981, Stable isotope hydrology of deuterium and oxygen-18 in the water cycle: Vienna, International Atomic Energy Agency, 339 p.

Gat, J.R., Mook, W., and Meijer, H., 2001, Environmental isotopes in the hydrologic cycle: atmospheric water: Paris, UNESCO, Technical Documents in Hydrology, v. II, no. 39, 113 p.

Gathro, J., Lachmar, T.E., and DeLima, C., 2016, Secrets of the subsurface: surface water recharge from the upper Logan River to ground water in Cache Valley, Utah: Geological Society of America Abstracts with Programs, v. 48, no. 7, paper no. 331-1.

Goessel, K.M., Oaks, Jr., R.Q., Perkins, M.E., and Janecke, S.U., 1999, Tertiary stratigraphy and structural geology, Wellsville Mountains to Junction Hills, north-

central Utah, *in* Spangler, L.E., and Allen, C.J., eds., Geology of Northern Utah and Vicinity: Utah Geological Association Publication 27, p. 45-69.

Gooseff, M.N., Evans, J.P., Kolesar, P., Lachmar, T.E., and Payn, R., 2005, Hydrologic contributions of springs to the Logan River, Utah: Abstract H51C-02 presented at 2005 Spring Meeting, AGU, New Orleans, Louisiana, 23-27 May.

Gregor, M., and Malik, P., 2012, Construction of master recession curve using genetic algorithms: Journal of Hydrology and Hydromechanics, v. 60, no. 1, p. 3-15.

Groning, M., Van Duren, M., and Andreescu, L., 2007, Metrological characteristics of the conventional measurement scales for hydrogen and oxygen stable isotope amount ratios: the δ-scales, *in* Proceedings, International Workshop on Combining and Reporting Analytical Results: the Role of Traceability and Uncertainty for Comparing Analytical Results: Rome, Royal Society of Chemistry, p. 62-72.

Hartmann, A., Goldscheider, N., Wagener, T., Lange, J., and Weiler, M., 2014, Karst water resources in a changing world: review of hydrological modeling approaches: Reviews of Geophysics, v. 52, p. 218-242.

Hartmann, A., Kralik, M., Humer, F., Lange, J., and Weiler, M., 2012, Identification of a karst system's intrinsic hydrodynamic parameters: upscaling from single springs to the whole aquifer: Environmental Earth Sciences, v. 65, p. 2377-2389.

Herman, J.S., and Lorah, M.M., 1987, CO_2 outgassing and calcite precipitation in Falling Spring Creek, Virginia: Chemical Geology, v. 2, no. 3-4, p. 251-262.

Herman, J.S., and White, W.B., 1985, Dissolution kinetics of dolomite: effects of lithology and fluid flow velocity: Geochimica et Cosmochimica Acta, v. 49, p. 2017-2026.

Holko, L., Danko, M., Dosa, M., Kostka, Z., Sanda, M., Pfister, L., and Iffly, J.F., 2013, Spatial and temporal variability of stable water isotopes in snow related hydrological processes: Die Bodenkultur, v. 64, no. 3-4, p. 39-45.

Hounslow, A., 1995, Water Quality Data: Analysis and Interpretation: Boca Raton, Florida, Lewis Publishers, CRC Press, p. 1-416.

Hynek, S.A., Steenburgh, W.J., and Poulos, G.S., 2004, Oxygen isotope ratios of recently fallen snow over the Wasatch Mountains of northern Utah: Abstract C51B-1038 presented at 2004 Fall Meeting, AGU, San Francisco, California, 13-17 December.

International Atomic Energy Agency (IAEA), 2014, global network of isotopes in precipitation, the GNIP database: http://www.iaea.org/water (accessed August 2017).

Inkenbrandt, P.C., 2010, Estimates of the hydraulic parameters of aquifers in Cache Valley, Utah and Idaho [M.S. thesis]: Logan, Utah State University, 157 p.

Jacobson, R.L., and Langmuir, D., 1974, Controls on the quality of some carbonate spring waters: Journal of Hydrology, v. 106, p. 1023-1045.

James, E.R., Manga, M., Rose, T.P., and Hudston, G.B., 2000, The use of temperature and the isotopes of O, H, C, and noble gases to determine the pattern and spatial extent of groundwater flow: Journal of Hydrology, v. 237, p. 100-112.

Jurgens, B.C., Bohlke, J.K., and Eberts, S.M., 2012, TracerLPM (Version 1): an Excel® workbook for interpreting groundwater age distributions from environmental tracer data: U.S. Geological Survey Techniques and Methods Report 4-F3, 60 p.

Kalbus, E., Reinstorf, F., and Schirmer, M., 2006, Measuring methods for groundwater-surface water interactions: a review: Hydrology and Earth System Sciences, v. 10, p. 873-887.

Kaliser, B.N., 1972, Environmental geology of Bear Lake area, Rich County, Utah: Utah Geological and Mineralogical Survey Bulletin 96, 32 p.

Kariya, K.A., Roark, D.M., and Hanson, K.M., 1994, Hydrogeology of Cache Valley, Cache County, Utah, and adjacent part of Idaho, with emphasis on simulation of groundwater flow: Utah Department of Natural Resources Technical Publication 108, 120 p.

Katz, B.G., Sepulveda, A.A., and Verdi, R.J., 2009, Estimating nitrogen loading to ground water and assessing vulnerability to nitrate contamination in a large karstic springs basin, Florida: Journal of the American Water Resources Association, v. 45, no. 3, p. 607-627.

Kendall, C., and Coplen, T.B., 2001, Distribution of oxygen-18 and deuterium in river waters across the United States: Hydrological Processes, v. 15, p. 1363-1393.

Kendall, C., and Doctor, D.H., 2003, Stable Isotope Applications in Hydrologic Studies, *in* Drever, J., ed., Treatise on Geochemistry: Amsterdam, Elsevier, v. 5, p. 319-364.

King, V.F., 2004, Water budget estimates for the Powder Mountain region, Cache and Weber Counties, Utah: methods and proper use of ground-water recharge estimations, *in* Spangler, L.E., ed., Groundwater in Utah: Resource, Protection, and Remediation: Salt Lake City, Utah Geological Association Publication 31, p. 219-234.

Kolesar, P.T., Evans, J.P., Gooseff, M.N., Lachmar, T.E., and Payn, R., 2005, A tale of two (or more) karsts, Bear River Range, Cache National Forest, Utah: Geological Society of America Abstracts with Programs, v. 37, no. 7, p. 177.

Kovacs, A., and Perrochet, P., 2008, A quantitative approach to spring hydrograph decomposition: Journal of Hydrology, v. 352, p. 16-29.

Lachmar, T.E., Myers, B., and Robinson, J.M., 2004, Updated conceptual and MODFLOW ground-water models of Cache Valley, Utah and Idaho, *in* Spangler, L.E., ed., Ground Water in Utah: Resource, Protection, and Remediation: Salt Lake City, Utah Geological Association Publication 31, p. 43-58.

Land, L., and Huff, G.F., 2010, Multi-tracer investigation of groundwater residence time in a karstic aquifer: Bitter Lake National Wildlife Refuge, New Mexico, USA: New Mexico Bureau of Geology and Mineral Resources Open-File Report 521, p. 455-472.

Langmuir, D., 1971, Geochemistry of some carbonate ground waters in central Pennsylvania: Geochimica et Cosmochimica Acta, v. 35, no. 10, p. 1023-1045.

Langmuir, D., 1997, Aqueous Environmental Geochemistry: Upper Saddle River, New Jersey, Prentice-Hall, 600 p.

Lin, Y., Clayton, R.N., and Groning, M., 2010, Calibration of delta(17)O and delta(18)O of international measurement standards – VSMOW, VSMOW2, SLAP, and SLAP2: Rapid Communications in Mass Spectrometry, v. 24, no. 6, p. 773-776.

Long, A.J., and Putnam, L.D., 2009, Age-distribution estimation for karst groundwater: issues of parameterization and complexity in inverse modeling by convolution: Journal of Hydrology, v. 376, p. 579-588.

Lowe, M., and Galloway, C.L., 1993, Provisional geologic map of the Smithfield quadrangle, Cache County, Utah: Utah Geological Survey Map 143, scale 1:24,000, 2 sheets, 18 p. text.

Maillet, E., 1905, Essais d'hydraulique souterraine et fluviale: Paris, Hermann, 218 p.

Małoszewski, P., and Zuber, A., 1985, On the theory of tracer experiments in fissured rocks with a porous matrix: Journal of Hydrology, v. 79, p. 333-358.

Maloszewski, P., and Zuber, A., 1993, Principles and practice of calibration and validation of mathematical models for the interpretation of environmental tracer data in aquifers: Advances in Water Resources, v. 16, p. 173-190.

Mangin, A., 1975, Contribution a l'etude hydrodynamique des aquifers karstiques: Annales de Speleologie, v. 26, p. 283-339.

Manning, A.H., and Solomon, D.K., 2004, Constraining mountain-block recharge to the eastern Salt Lake Valley, Utah with dissolved noble gas and tritium data: Water Science and Application, v. 9, p. 139-158.

Martinec, J., 1975, Snowmelt runoff model for river flow forecasts: Nordic Hydrology, v. 6, p. 145-154.

Martinec, J., Rango, A., and Roberts, R., 1994, The snowmelt runoff model (SRM) user's manual: Berne, Switzerland, University of Berne.

McCalpin, J.P, 1989, Surficial geologic map of the East Cache fault zone, Cache County, Utah: U.S. Geological Survey Miscellaneous Field Studies Map MF-2107, scale 1:50,000, 1 sheet.

McCalpin, J.P., 1994, Neotectonic deformation along the East Cache fault zone, Cache County, Utah: Utah Geological Survey Special Study 83, 37 p.

Michel, R.L., 1989, Tritium deposition in the continental United States, 1953-83: U.S. Geological Survey Water-Resources Investigations Report 89-4072, 46 p.

Mook, W., 2001, Environmental isotopes in the hydrological: introduction – theory, methods, review: Paris, UNESCO/International Atomic Energy Agency, Technical Documents in Hydrology, v. 1, no. 39, 164 p.

Moral, F., Cruz-Sanjulian, J.J., and Olias, M., 2008, Geochemical evolution of groundwater in the carbonate aquifers of Sierra de Segura (Betic Cordillera, southern Spain): Journal of Hydrology, v. 360, p. 281-296.

Morrow, D.W., 1982, Diagenesis 1. Dolomite – Part 1: The chemistry of dolomitization and dolomite precipitation: Geoscience Canada, v. 9, no. 1, p. 5-13.

Mundorff, J.C., 1971, Nonthermal springs of Utah: Utah Geological and Mineralogical Survey Water-Resources Bulletin 16, 70 p.

Muste, M., Yu, K., and Spasojevic, M., 2004, Practical aspects of ADCP data use for quantification of mean river flow characteristics: moving-vessel measurements: Flow Measurement and Instrumentation, v. 15, no. 1, p. 1-16.

Myers, B., 2003, Simulation of groundwater flow in Cache Valley, Utah and Idaho [M.S. thesis]: Logan, Utah State University, 81 p.

Neilson, B.T., Tennant, H., Stout, T.L., Miller, M.P., Gabor, R.S., Jameel, Y., Millington, M. Gelderloos, A., Bowen, G.J., and Brooks, P.D., 2018, Stream centric methods for determining groundwater contributions in karst mountain watersheds: Water Resources Research, v. 54, no. 9, p. 6708-6724.

Niwot Ridge LTER: long-term ecological research dataset: http://niwot.colorado.edu/data (accessed January 2018).

NOAA Earth System Research Laboratory, global monitoring division: https://www.esrl.noaa.gov (accessed January 2018).

NOAA National Weather Service, Salt Lake City office online weather data: http://w2.weather.gov/climate/xmacis.php?wfo=slc (accessed April 2018).

Oaks, R.Q., Jr, 2004, Geologic evaluation of drillers' logs of water wells and associated hydrogeological evidence in the Nibley City - College Ward area, Cache Valley, north-central Utah: Report for Cache-Landmark Engineering, 9 p.

Oaks, R.Q., Jr., Janecke, S.U., Rittenour, T.M., Nelson, M.S., and Erickson, T.L., 2014, Up to four deep-water pluvial lakes in Cache Valley, Utah-Idaho, including the Cutler Dam lake cycle at ~1445 m and possible Little Valley lake cycle at ~1485 m: Evidence for possible excavation on Cutler Narrows prior to 420 ka, *in* Herschler, R., and Link, P.K., eds., Abstracts of the Workshop on Late Cenozoic to Recent Geologic and Biotic History of the Snake River, p. 34-35.

Oaks, R.Q., Jr., Janecke, S.U., Rittenour, T.M., Erickson, T.L., and Nelson. M.S., 2018, OSL age dating of two, perhaps three, pre-Bonneville deep-water pluvial lakes in Cache Valley, Utah-Idaho: implications of their unexpected high altitudes for excavation of Cutler Narrows from a level above 1494 m (4901'), down to the present 1314 m (4310') mainly during the Bonneville lake cycle: Utah Geological Survey Symposium on Lake Bonneville, Salt Lake City, 3-4 October, 2018.

Oaks, R.Q., Jr., and Runnells, T.R., 1992, The Wasatch Formation in the central Bear River Range, northern Utah: Utah Geological Survey Contract Report 92-8, 79 p., 7 plates.

Oaks, R.Q., Jr., Smith, K.A., Janecke, S.U., Perkins, M.E., and Nash, W.P., 1999, Stratigraphy and tectonics of Tertiary strata of southern Cache Valley, north-central Utah, *in* Spangler, L.E., and Allen, C.J., eds., Geology of Northern Utah and Vicinity: Utah Geological Association Publication 27, p. 71-110.

Olsen, A.A., 2007, Discharge monitoring, chemical characterization, and source identification of springs along the east side of southern Cache Valley, Utah [M.S. thesis]: Logan, Utah State University, 186 p.

Oriel, S.S., and Platt, L.B., 1979, Younger-over-older thrust plates in southeastern Idaho: Geological Society of America Abstracts with Programs, v. 11, p. 278.

Oriel, S.S., and Platt, L.B., 1980, Geologic map of the Preston 1º x 2º quadrangle, southeastern Idaho and western Wyoming: U.S. Geological Survey Miscellaneous Investigations Series Map I-1127, scale 1:250,000, 1 sheet.

Ozyurt, N.N., 2008, Residence time distribution in the Kirkgoz karst springs (Anntalya-Turkey) as a tool for contamination vulnerability assessment: Environmental Geology, v. 53, p. 1571-1583.

Padilla, A., Bulido-Bosch, A., and Mangin, A., 1994, Relative importance of baseflow and quickflow from hydrographs of karst springs: Ground Water, v. 32, no. 2, p. 267-277.

Parkhurst, D.L., and Appelo, C.A., 2013, Description of input and examples for PHREEQC version 3—A computer program for speciation, batch-reaction, one-dimensional transport, and inverse geochemical calculations: U.S. Geological Survey Techniques and Methods, book 6, chapter A43, 497 p.

Piper, A.M., 1944, A graphic procedure in the geochemical interpretation of water-analyses: American Geophysical Union Transactions, v. 6, p. 914-923.

Plummer, L.N., Busenberg, E., and Cook, P.G., 2006, Principles of chlorofluorocarbon dating, *in* Groning, M., Han, L.F., and Aggarwal, P., eds., Use of Chlorofluorocarbons in Hydrology: a Guidebook: Vienna, International Atomic Energy Agency, p. 17-29.

Plummer, L.N., and Glynn, P.D., 2013, Radiocarbon dating in groundwater systems, *in* Suckow, A., Aggarwal, P.K., and Araguas-Araguas, L., eds., Isotope Methods for Dating Old Groundwater: Vienna, International Atomic Energy Agency, p. 33-89.

Plummer, L.N., and Mackenzie, F.T., 1974, Predicting mineral solubility from rate data: application to the dissolution of magnesian calcites: American Journal of Science, v. 274, p. 61-83.

Plummer, L.N., Wigley, T.M., and Parkhurst, D.L., 1978, The kinetics of calcite dissolution in CO_2-water systems at 5ºC to 60ºC and 0.0 to 1.0 atm CO_2: American Journal of Science, v. 278, p. 179-216.

Poage, M.A., and Chamberlain, C.P., 2001, Empirical relationships between elevation and the stable isotope composition of precipitation and surface waters: considerations for studies of paleoelevation change: American Journal of Science, v. 301, p. 1-15.

Pope, D.W., and Brough, R.C., 1996, Utah's Weather and Climate: Salt Lake City, Publisher's Press, 245p.

Revesz, K., and Coplen, T.B., 2008a, Determination of the d[$^{2}H/^{1}H$] of water: RSIL lab code 1574, *in* Revesz, K., and Coplen, T.B., eds., Methods of the Reston Stable Isotope Laboratory: U.S. Geological Survey Techniques and Methods 10-C1, 27 p.

Revesz, K., and Coplen, T.B., 2008b, Determination of the d[$^{18}O/^{16}O$] of water: RSIL lab code 489, *in* Revesz, K., and Coplen, T.B., eds., Methods of the Reston Stable Isotope Laboratory: U.S. Geological Survey Techniques and Methods, 10-C2, 28 p.

Rice, K.C., 1987, Hydrogeology and hydrochemistry of springs in Mantua Valley and vicinity, north-central Utah [M.S. thesis]: Logan, Utah State University, 124 p.

Rice, K.C., and Spangler, L.E., 1999, Hydrology and geochemistry of carbonate springs in Mantua Valley, northern Utah, *in* Spangler, L.E., and Allen C.J., eds., Geology of Northern Utah and Vicinity: Salt Lake City, Utah Geological Association Publication 27, p. 337–352.

Roark, D.M., and Hansen, K.M., 1992, Selected hydrologic data for Cache Valley, Utah and Idaho, 1969-91: U.S. Geological Survey Open-File Report 92-173, also Utah Hydrologic-Data Report 48, 65 p.

Robinson, J.M., 1999, Chemical and hydrostratigraphic characterization of ground water and surface water interaction in Cache Valley, Utah [M.S. thesis]: Logan, Utah State University, 184 p.

Rorabaugh, M.I., 1964, Changes in Bank Storage: Gentbrugge, Belgium, International Association of Scientific Hydrology, no. 63, p. 432-441.

Ross, R.J., Jr., 1951, Stratigraphy of the Garden City Formation in northeastern Utah, and its trilobite fauna: New Haven, Connecticut, Yale Peabody Museum Bulletin 5, 161 p.

Rozenski, K., Froehlich, K., and Mook, W., 2001, Environmental isotopes in the hydrological cycle: surface water: Paris, UNESCO, Technical Documents in Hydrology, v. III, no. 39, 117 p.

Scripps Institute of Oceanography, Mauna Loa observatory CO2 database: http://scrippsco2.ucsd.edu/data/atmospheric_co2/ (accessed July 2018).

Solder, J.E., Stolp, B.J., Heilweil, V.M., and Susong, D.D., 2016, Characterization of mean transit time at large springs in the upper Colorado River Basin, USA: a tool for assessing groundwater discharge variability: Hydrogeology Journal, v. 24, no. 8, p. 2017-2033.

Solomon, D.K., 2017, University of Utah dissolved and noble gas lab tritium collection guide: http://www.noblegaslab.utah.edu/pdfs/tritium_collection.pdf (accessed May 2017).

Solomon, D.K., Plummer, L.N., Busenberg, E., and Cook P., 2006, Practical applications of CFCs in hydrological investigations, *in* Groning, M., Han, L.F., and Aggarwal, P., eds., Use of Chlorofluorocarbons in Hydrology: a Guidebook: Vienna, International Atomic Energy Agency, p. 89-103.

Spangler, L.E., 2001, Delineation of recharge areas for karst springs in Logan Canyon, Bear River Range, northern Utah, *in* Proceedings, Karst Interest Group: U.S. Geological Survey Water-Resources Investigations Report 01-4011, p. 186-193.

Spangler, L.E., 2002, Use of dye tracing to determine conduit flow paths within source-protection areas of a karst spring and wells in the Bear River Range, northern Utah: U.S. Geological Survey Water-Resources Investigation Report 2-4174, 6 p.

Spangler, L.E., 2004, Delineation of recharge areas for karst springs in Logan Canyon, Bear River Range, northern Utah *in* Proceedings, Karst Interest Group: U.S. Geological Survey Water-Resources Investigations Report 01-4011, p. 186-193.

Spangler, L.E., 2012, Karst hydrogeology of the Bear River Range in the vicinity of Logan Canyon, northern Utah: Beneath the Forest, Uinta-Wasatch-Cache National Forest, v. 5, no. 1, p. 12-20.

Sperber, C.M., Wilkinson, B.H., and Peacor, D.R., 1984, Rock composition, dolomite stoichiometry, and rock/water reactions in dolomitic carbonate rocks: Journal of Geology, v. 92, p. 609–622.

Stiff, H.A., 1951, The interpretation of chemical water analysis by means of patterns: Journal of Petroleum Technology, v. 3, no. 10, p. 15-17.

Szramek, K., McIntosh, J.C., Williams, E.L., Kanduc, T., Ogrinc, N., and Walter, L.M., 2007, Relative weathering intensity of calcite versus dolomite in carbonate-bearing temperate zone watersheds: carbonate geochemistry and fluxes from catchments within the St. Lawrence and Danube river basins: Geochemistry, Geophysics, Geosystems, v. 8, no. 4, 26 p.

Taylor, C.J., and Greene, E.A., 2001, Hydrogeologic characterization and methods used in the investigation of karst hydrology, *in* Rosenberry, D.O., and LaBaugh, J.W., eds., Field Techniques for Estimating Water Fluxes between Surface Water and Groundwater: U.S. Geological Survey Techniques and Methods 4-D2, p. 75-114.

Taylor, M.E., Landing, E., and Gillet, S.L., 1981, The Cambrian-Ordovician transition in the Bear River Range, Utah-Idaho: a preliminary evaluation, *in* Proceedings, Second International Symposium on the Cambrian System: U.S. Geological Survey Open-File Report 81-743, p. 222-227.

Templin, W.E., Herbert, R.A., Stainaker, C.B., Horn, M., and Solley, W.B., 1980, National handbook of recommended methods for water data acquisition: Reston, Virginia, U.S. Geological Survey Office of Water Data Acquisiton.

Teutsch, G., and Sauter, M., 1991, Groundwater modeling in karst terranes: scale effects, data acquisition, and field validation: Ground Water Management, v. 10, p. 17-35.

Thomas, K., Oaks, R.Q., Jr., Inkenbrandt, P., Sabbah, W., and Lowe, M., 2011, Cache Valley principal aquifer storage and recovery site assessment: phase I: Utah Department of Natural Resources Open-File Report 579, 57 p.

Unnikrishna, P.V., McDonnell, J.J., and Kendall, C., 2002, Isotopic variations in a Sierra Nevada snowpack and their relation to meltwater: Journal of Hydrology, v. 260, p. 38-57.

U.S. Department of Agriculture (USDA), Natural Resources Conservation Service snow telemetry database, https://www.wcc.nrcs.usda.gov/snow/ (accessed January 2018).

U.S. Environmental Protection Agency (USEPA) water quality database (WQX): https://www.epa.gov/waterdata/water-quality-data-wqx (accessed January 2017).

U.S. Geological Survey (USGS) groundwater dating laboratory, Reston, Virginia: http://water.usgs.gov/lab/software/air_curve/ (accessed November 2017).

U.S. Geological Survey (USGS) national elevation dataset, https://catalog.data.gov/dataset/usgs-national-elevation-dataset-ned (accessed September 2016).

U.S. Geological Survey (USGS) national water information system, https://waterdata.usgs.gov/nwis/qw (accessed March 2018).

Utah Division of Water Rights (UDWR) water distribution and regulation database, https://www.waterrights.utah.gov/ (accessed January 2018).

Van der Land, C., Wood, R., Van Dijke, M., Jiang, Z., Corbett, P., and Couples, G., 2013, Modelling the permeability evolution of carbonate rocks: Marine and Petroleum Geology, v. 48, p. 1-7.

Vogel, J.C., Grootes, P.M., and Mook, W.G., 1970, Isotopic fractionation between gaseous and dissolved carbon dioxide: Zeitschrift fur Physik, v. 230, no. 3, p. 225-238.

White, W.B., 1993, Analysis of karst aquifers, *in* Alley, W.M., ed., Regional Ground Water Quality: New York, Van Nostrand Reinhold, p. 471–489.

White, W.B., 1997, Thermodynamic equilibrium, kinetics, activation barriers, and reaction mechanisms for chemical reactions in karst terrains: Environmental Geology, v. 30, p. 46-58.

White, W.B., 2002, Karst hydrology: recent developments and open questions: Engineering Geology, v. 65, p. 85-105.

White, W.B., 2003, Conceptual models for karstic aquifers: Speleogenesis and Evolution of Karst Aquifers, v. 1, no. 1, p 11-16.

Wigley, T.M., 1972, The incongruent solution of dolomite: Geochimica et Cosmochimica Acta, v. 37, p. 1397-1402.

Wigley, T.M., Plummer, L.N., and Pearson, F., 1978, Mass transfer and carbon isotope evolution in natural water systems: Geochimica et Cosmochimica Acta, v. 42, p. 1117-1139.

Wilde, F.D., 2008, Guidelines for field-measured water-quality properties (ver. 2.0): U.S. Geological Survey Techniques of Water-Resources Investigations, book 9, chapter A6, section 6.0, p. 3-29.

Williams, J.S., 1948, Geology of the Paleozoic rocks, Logan quadrangle, Utah: Geological Society of America Bulletin, v. 59, p. 1121-1184.

Williams, J.S., 1958. Geologic atlas of Utah, Cache County: Utah Geological and Mineral Survey Bulletin, v. 64, 98 p.

Williams, J.S., 1962, Geology of southern Cache Valley, Utah: Geological Survey Professional Paper 257-C, p. 131-150.

Williams, E.L., Szramek, K.J., Jin, L, Ku, T.C., and Walter, L.M., 2007, The carbonate system geochemistry of shallow groundwater-surface water systems in temperate glaciated watersheds (Michigan, USA): Significance of open-system dolomite weathering: Geological Society of America Bulletin, v. 119, no. 516, p. 515-528.

Wilson, J.R., 1976, Glaciated dolomite karst in the Bear River Range, Utah [Ph.D. dissertation]: Salt Lake City, University of Utah, 123 p.

Wilson, J.L., and Guan, H., 2004, Mountain-block hydrology and mountain-front recharge: Water Science and Application, v. 9, p. 113-137.

Winter, T.C., Harvey, J.W., Franke, O.L., and Alley, W.M., 1998, Ground water and surface water: a single resource: U.S. Geological Survey Circular 1139, 79 p.

Yager, R.M., Plummer, L.N., Kauffman, L.J., Doctor, D.L., Nelms, D.L., and Schlosser P., 2013, Comparison of age distributions estimated from environmental tracers by using binary-dilution and numerical models of fractured and folded karst: Shenandoah Valley of Virginia and West Virginia, USA: Hydrology Journal, v. 21, p. 1193-1217.

APPENDICES

Appendix A: Raw discharge data

Discharge measurements on 8/27/2016

The upper Logan River was measured on 8/27/2016 using a wading rod and flow meter.

Distance from bank (ft)	Depth (ft)	Velocity (ft/s)	Average velocity (ft/s)	Area (ft^2)	Discharge (cfs)
0.0	0.72	0.03	0.02	0.04	0.00
2.0	0.79	0.01	0.02	1.51	0.03
4.0	1.31	0.00	0.01	2.10	0.01
6.0	0.92	1.49	0.75	2.23	1.66
8.2	0.72	0.86	1.18	1.80	2.12
10.3	0.72	2.36	1.61	1.52	2.44
12.0	0.79	1.57	1.97	1.28	2.52
14.2	0.85	1.41	1.49	1.80	2.69
16.3	0.79	0.23	0.82	1.72	1.41
18.3	1.31	1.35	0.79	2.10	1.66
20.3	1.44	1.30	1.33	2.76	3.65
21.8	1.25	2.90	2.10	2.02	4.24
24.0	0.98	2.95	2.93	2.45	7.18
25.2	1.18	2.73	2.84	1.30	3.69
27.0	0.72	2.58	2.66	1.71	4.55
29.0	0.66	2.41	2.50	1.38	3.44
31.0	0.59	1.99	2.20	1.25	2.74
33.0	0.66	2.24	2.12	1.25	2.64
35.0	0.72	1.89	2.07	1.38	2.85
38.1	0.52	0.00	0.95	1.93	1.83
				Total (cfs):	51.3
				(m3/s):	1.45

Ricks Spring was measured on 8/27/2016 using a wading rod and flow meter.

Distance from bank (ft)	Depth (ft)	Velocity (ft/s)	Average velocity (ft/s)	Area (ft^2)	Discharge (cfs)
0.0	0.00	0.00	0.00	0.00	0.00
1.0	0.07	0.00	0.00	0.00	0.00
Rock	0	0	0.00	0.00	0.00
5.0	0.07	0.96	0.96	0.00	0.00
6.0	0.46	2.74	1.85	0.26	0.49
7.0	0.59	0.98	0.98	0.52	0.51
7.9	0.46	0.23	0.61	0.47	0.29
Rock	0.00	0.00	0.00	0.00	0.00
10.4	0.33	0.23	0.23	0.26	0.06
Rock	0.00	0.00	0.12	0.00	0.00
12.1	0.26	0.05	0.03	0.00	0.00
13.0	0.59	1.73	1.73	0.38	0.66
14.0	0.39	0.26	1.00	0.49	0.49
15.0	0.33	0.09	0.09	0.36	0.03

16.0	0.20	0.25	0.17	0.26	0.04
17.4	0.39	2.88	2.88	0.41	1.19
19.0	0.26	0.15	1.52	0.52	0.80
20.0	0.07	0.00	0.00	0.16	0.00
21.0	0.33	1.12	0.56	0.20	0.11
22.0	0.20	0.16	0.16	0.26	0.04
23.1	0.46	0.07	0.12	0.36	0.04
24.0	0.59	0.67	0.67	0.47	0.32
25.0	0.52	0.05	0.36	0.56	0.20
Rock (effective bank)	0.00	0.00	0.00	0.13	0.00
27.0	0.46	0.00	0.00	0.00	0.00
27.9	0.00	0.00	0.00	0.00	0.00
				Total (cfs):	5.28
				(m3/s):	0.149

Temple Fork was measured on 8/27/2016 using a wading rod and flow meter.

Distance from bank (ft)	Depth (ft)	Velocity (ft/s)	Average velocity (ft/s)	Area (ft^2)	Discharge (cfs)
0.0	0.33	1.04	0.52	0.02	0.01
1.0	0.52	2.09	1.57	0.43	0.67
2.0	0.59	1.95	2.02	0.56	1.13
3.0	0.72	1.74	1.85	0.66	1.21
4.0	0.66	2.05	1.90	0.69	1.31
5.0	0.59	1.48	1.77	0.62	1.10
6.0	0.85	2.02	1.75	0.72	1.26
7.0	0.72	2.01	2.02	0.79	1.59
8.0	0.85	1.68	1.85	0.79	1.45
9.0	0.72	2.01	1.85	0.79	1.45
10.0	0.79	1.57	1.79	0.75	1.35
11.0	0.72	1.94	1.76	0.75	1.32
12.0	0.72	1.03	1.49	0.72	1.07
13.4	0.72	0.73	0.88	1.01	0.89
13.8	0.00	0.00	0.37	0.14	0.05
				Total (cfs):	15.9
				(m3/s):	0.449

Benchmark Spring was measured on 8/27/2016 using a wading rod and flow meter.

Distance from bank (ft)	Depth (ft)	Velocity (ft/s)	Average velocity (ft/s)	Area (ft^2)	Discharge (cfs)
0.0	0.00	0.00	0.00	0.00	0.00
0.1	0.33	0.69	0.35	0.02	0.01
0.5	0.26	0.38	0.54	0.12	0.07
1.0	0.20	0.11	0.25	0.10	0.02
1.1	0.00	0.00	0.06	0.01	0.00

Total (cfs):	0.10
(m3/s):	0.00275

Logan Cave Spring was measured on 8/27/2016 using a wading rod and flow meter.

Distance from bank (ft)	Depth (ft)	Velocity (ft/s)	Average velocity (ft/s)	Area (ft^2)	Discharge (cfs)
0.0	0.00	0.00	0.00	0.00	0.00
1.0	0.33	0.13	0.07	0.16	0.01
2.0	0.39	2.09	1.11	0.36	0.40
2.9	0.33	0.29	1.19	0.32	0.39
3.6	0.20	0.00	0.15	0.18	0.03
				Total (cfs):	0.82
				(m3/s):	0.0233

Woodcamp Hollow Spring was measured on 8/27/2016 using a wading rod and flow meter.

Distance from bank (ft)	Depth (ft)	Velocity (ft/s)	Average velocity (ft/s)	Area (ft^2)	Discharge (cfs)
0.0	0.00	0.00	0.00	0.00	0.00
0.9	0.33	0.36	0.18	0.15	0.03
2.0	0.39	1.22	0.79	0.40	0.31
3.0	0.33	0.03	0.63	0.36	0.23
4.3	0.52	0.22	0.13	0.55	0.07
5.5	0.98	1.07	0.65	0.91	0.58
6.5	0.79	2.21	1.64	0.89	1.45
7.5	0.79	4.50	3.36	0.79	2.64
8.5	0.46	5.05	4.78	0.62	2.98
9.5	0.72	3.93	4.49	0.59	2.65
10.5	0.39	1.08	2.51	0.56	1.40
11.5	0.52	0.76	0.92	0.46	0.42
12.6	0.00	0.00	0.38	0.29	0.11
13.8	0.00	0.00	0.00	0.00	0.00
14.0	0.33	0.88	0.44	0.03	0.01
14.2	0.00	0.00	0.44	0.03	0.01
				Total (cfs):	12.9
				(m3/s):	0.365

China Row Spring was measured on 8/27/2016 using the Crowe et al. (2001) method for pipe flow.

Pipe diameter (ft)	2.00
Sediment + Water depth (ft)	0.75
Sediment depth (ft)	0.33
Water depth (ft)	0.42
Velocity (ft/s)	0.30
Total (cfs):	0.22
Total (m3/s):	0.00626

The middle Logan River was measured on 8/27/2016 using a wading rod and flow meter.

Distance from bank (ft)	Depth (ft)	Velocity (ft/s)	Average velocity (ft/s)	Area (ft^2)	Discharge (cfs)
0.0	0.00	0.00	0.00	0.00	0.00
3.0	0.66	0.67	0.34	0.98	0.33
6.0	0.92	0.62	0.65	2.36	1.52
9.0	1.12	1.95	1.29	3.05	3.92
12.0	1.38	1.75	1.85	3.74	6.92
15.0	1.25	2.60	2.18	3.94	8.56
18.0	1.18	1.50	2.05	3.64	7.47
21.0	1.31	1.83	1.67	3.74	6.23
24.1	1.57	2.29	2.06	4.48	9.22
27.0	1.64	2.55	2.42	4.66	11.28
30.0	1.51	2.02	2.29	4.72	10.80
33.1	1.77	1.69	1.86	5.09	9.43
36.0	1.38	2.39	2.04	4.57	9.32
39.0	1.38	2.19	2.29	4.13	9.47
42.0	1.64	1.75	1.97	4.53	8.92
45.0	1.44	1.88	1.82	4.63	8.40
48.0	1.31	1.60	1.74	4.13	7.19
51.0	0.66	2.02	1.81	2.95	5.34
54.0	0.26	0.00	1.01	1.38	1.39
54.0	0.00	0.00	0.00	0.00	0.00
				Total (cfs):	126
				(m3/s):	3.56

Right Hand Fork was measured on 8/27/2016 using a wading rod and flow meter.

Distance from bank (ft)	Depth (ft)	Velocity (ft/s)	Average velocity (ft/s)	Area (ft^2)	Discharge (cfs)
0.0	0.20	0.07	0.04	0.00	0.00
1.0	0.46	2.10	1.09	0.33	0.36
2.0	0.72	2.13	2.12	0.59	1.25
2.9	0.92	2.18	2.16	0.74	1.59
4.0	0.72	1.95	2.07	0.90	1.86
5.5	0.46	2.20	2.08	0.89	1.84
6.5	1.05	1.56	1.88	0.75	1.42
7.5	0.46	0.00	0.78	0.75	0.59
8.9	0.26	0.00	0.00	0.51	0.00
9.0	0.00	0.00	0.00	0.01	0.00
				Total (cfs):	8.90
				(m^3/s):	0.252

Dewitt Spring was measured on 8/27/2016 using a wading rod and flow meter.

Distance from bank (ft)	Depth (ft)	Velocity (ft/s)	Average velocity (ft/s)	Area (ft^2)	Discharge (cfs)
0.0	0.00	0.00	0.00	0.00	0.00
0.3	0.52	1.32	0.66	0.07	0.05
3.6	0.52	1.75	1.54	1.76	2.70
7.0	0.52	1.48	1.62	1.76	2.84
7.3	0.00	0.00	0.74	0.07	0.06
				Total (cfs):	5.64
				(m3/s):	0.160

The lower Logan River side channel was measured on 8/27/2016 using a wading rod and flow meter.

Distance from bank (ft)	Depth (ft)	Velocity (ft/s)	Average velocity (ft/s)	Area (ft^2)	Discharge (cfs)
0.0	0.00	0.00	0.00	0.00	0.00
1.0	0.59	0.05	0.03	0.30	0.01
2.0	0.66	0.04	0.05	0.62	0.03
3.0	0.92	0.01	0.03	0.79	0.02
4.0	0.98	0.03	0.02	0.95	0.02
5.0	0.72	0.03	0.03	0.85	0.03
6.0	0.39	0.01	0.02	0.56	0.01
7.1	0.00	0.00	0.01	0.22	0.00
				Total (cfs):	0.11
				(m3/s):	0.00317

The lower Logan River was measured on 8/27/2016 using a wading rod and flow meter.

Distance from bank (ft)	Depth (ft)	Velocity (ft/s)	Average velocity (ft/s)	Area (ft^2)	Discharge (cfs)
0.0	0.13	0.00	0.00	0.01	0.00
3.1	0.79	0.85	0.43	1.42	0.61
6.1	1.64	0.61	0.73	3.64	2.66
9.1	1.44	1.85	1.23	4.63	5.69
12.1	1.44	2.10	1.98	4.33	8.55
15.1	1.77	2.22	2.16	4.82	10.42
18.1	1.84	2.33	2.28	5.41	12.32
21.1	1.71	2.15	2.24	5.32	11.91
24.1	1.71	2.31	2.23	5.12	11.41
27.1	1.71	2.14	2.23	5.12	11.39
30.1	1.71	2.30	2.22	5.12	11.36
33.1	1.71	2.23	2.27	5.12	11.59
36.1	1.57	2.11	2.17	4.92	10.68
39.1	1.77	2.13	2.12	5.02	10.64
42.1	1.44	1.49	1.81	4.82	8.73
45.1	1.12	1.41	1.45	3.84	5.57
48.1	0.85	0.93	1.17	2.95	3.45
49.6	0.00	0.00	0.47	0.64	0.30

Total (cfs):	137
(m3/s):	3.88

The west branch of Spring Hollow Spring was measured on 8/27/2016 using a wading rod and flow meter.

Distance from bank (ft)	Depth (ft)	Velocity (ft/s)	Average velocity (ft/s)	Area (ft^2)	Discharge (cfs)
0.0	0.00	0.00	0.00	0.00	0.00
0.9	0.13	0.00	0.00	0.06	0.00
1.9	0.20	0.00	0.00	0.16	0.00
2.9	0.26	0.02	0.01	0.23	0.00
3.9	0.46	0.48	0.25	0.36	0.09
4.9	0.72	0.63	0.56	0.59	0.33
5.9	0.85	1.38	1.01	0.79	0.79
6.3	0.85	0.74	1.06	0.34	0.36
7.6	0.79	0.57	0.66	1.07	0.70
8.9	0.72	0.69	0.63	0.98	0.62
9.9	0.46	0.43	0.56	0.59	0.33
10.9	0.13	0.00	0.22	0.30	0.06
11.6	0.00	0.00	0.00	0.05	0.00
				Total (cfs):	3.28
				(m3/s):	0.0930

The east branch of Spring Hollow Spring was measured on 8/27/2016 using a wading rod and flow meter.

Distance from bank (ft)	Depth (ft)	Velocity (ft/s)	Average velocity (ft/s)	Area (ft^2)	Discharge (cfs)
0.0	0.00	0.00	0.00	0.00	0.00
1.0	0.39	0.32	0.16	0.20	0.03
2.0	0.33	0.36	0.34	0.36	0.12
3.0	0.52	1.38	0.87	0.43	0.37
4.0	0.52	3.32	2.35	0.52	1.23
5.0	0.59	0.99	2.16	0.56	1.20
6.0	0.39	1.71	1.35	0.49	0.66
7.0	0.33	2.00	1.86	0.36	0.67
7.7	0.33	0.00	1.00	0.23	0.23
8.7	0.00	0.00	0.00	0.16	0.00
				Total (cfs):	4.52
				(m3/s):	0.128

Discharge measurements on 10/4/2016

The upper Logan River was measured on 10/4/2016 using a wading rod and flow meter.

Distance from bank (ft)	Depth (ft)	Velocity (ft/s)	Average velocity (ft/s)	Area (ft^2)	Discharge (cfs)
0.0	0.00	0.00	0.00	0.00	0.00
2.1	0.46	0.00	0.00	0.48	0.00
4.2	0.66	0.00	0.00	1.17	0.00

6.2	1.05	0.54	0.27	1.71	0.46
8.2	1.12	1.97	1.26	2.17	2.72
10.2	1.12	2.12	2.05	2.23	4.56
12.2	0.92	2.11	2.12	2.03	4.30
14.2	0.79	1.70	1.91	1.71	3.25
16.2	0.79	1.10	1.40	1.57	2.20
18.2	0.79	0.68	0.89	1.57	1.40
Rock	0.00	0.00	0.34	0.00	0.00
20.6	0.72	0.00	0.00	0.00	0.00
21.2	0.79	0.07	0.04	0.45	0.02
23.2	0.66	0.12	0.10	1.44	0.14
25.2	0.72	0.87	0.50	1.38	0.68
27.2	0.33	0.56	0.72	1.05	0.75
28.6	0.00	0.00	0.28	0.23	0.06
				Total (cfs):	20.5
				(m3/s):	0.582

Ricks Spring was measured on 10/4/2016 using a wading rod and flow meter.

Distance from bank (ft)	Depth (ft)	Velocity (ft/s)	Average velocity (ft/s)	Area (ft^2)	Discharge (cfs)
0.0	0.26	0.13	0.13	0.00	0.00
1.0	0.26	0.68	0.41	0.26	0.11
2.0	0.33	2.52	1.60	0.30	0.47
2.8	0.26	0.24	1.38	0.24	0.33
Rock	0.00	0.00	0.12	0.00	0.00
7.1	0.13	0.00	0.00	0.00	0.00
7.9	0.26	1.22	0.61	0.16	0.10
8.8	0.20	0.93	1.08	0.21	0.22
Rock	0.00	0.00	0.47	0.00	0.00
10.7	0.13	0.18	0.09	0.00	0.00
11.5	0.13	0.57	0.38	0.10	0.04
Rock	0.00	0.00	0.29	0.00	0.00
12.2	0.26	1.68	0.84	0.00	0.00
13.2	0.20	1.77	1.73	0.23	0.40
14.2	0.13	0.40	1.09	0.16	0.18
Rock	0.00	0.00	0.20	0.00	0.00
15.3	0.13	0.67	0.34	0.00	0.00
16.3	0.13	0.07	0.37	0.13	0.05
17.3	0.13	0.24	0.16	0.13	0.02
18.3	0.39	0.38	0.31	0.26	0.08
19.3	0.33	0.33	0.36	0.36	0.13
20.3	0.33	0.26	0.30	0.33	0.10
20.5	0.33	0.00	0.13	0.07	0.01
				Total (cfs):	2.22

				(m3/s):	0.0629

Temple Fork was measured on 10/4/2016 using a wading rod and flow meter.

Distance from bank (ft)	Depth (ft)	Velocity (ft/s)	Average velocity (ft/s)	Area (ft^2)	Discharge (cfs)
0.0	0.20	0.04	0.04	0.00	0.00
1.0	0.33	1.79	0.92	0.26	0.24
2.0	0.46	1.31	1.55	0.39	0.61
3.0	0.52	1.69	1.50	0.49	0.74
4.0	0.46	2.20	1.95	0.49	0.96
5.0	0.46	1.96	2.08	0.46	0.96
6.0	0.52	1.67	1.82	0.49	0.89
7.0	0.52	1.95	1.81	0.52	0.95
8.0	0.46	1.77	1.86	0.49	0.92
9.0	0.52	1.83	1.80	0.49	0.89
10.0	0.52	1.55	1.69	0.52	0.89
11.0	0.46	1.41	1.48	0.49	0.73
12.0	0.46	1.35	1.38	0.46	0.63
13.0	0.39	0.11	0.73	0.43	0.31
14.0	0.20	0.00	0.06	0.30	0.02
14.6	0.00	0.00	0.00	0.06	0.00
				Total (cfs):	9.72
				(m3/s):	0.275

Benchmark Spring was measured on 10/4/2016 using a wading rod and flow meter.

Distance from bank (ft)	Depth (ft)	Velocity (ft/s)	Average velocity (ft/s)	Area (ft^2)	Discharge (cfs)
0.0	0.29	0.97	0.97	0.00	0.00
0.6	0.29	0.62	0.80	0.18	0.14
1.3	0.21	0.00	0.31	0.16	0.05
				Total (cfs):	0.19
				(m3/s):	0.00548

Logan Cave Spring was measured on 10/4/2016 using a wading rod and flow meter.

Distance from bank (ft)	Depth (ft)	Velocity (ft/s)	Average velocity (ft/s)	Area (ft^2)	Discharge (cfs)
0.0	0.07	0.00	0.00	0.00	0.00
1.0	0.26	0.15	0.08	0.16	0.01
2.0	0.33	1.56	0.86	0.30	0.25
3.0	0.33	0.32	0.94	0.33	0.31
3.6	0.33	0.08	0.20	0.20	0.04
				Total (cfs):	0.61
				(m3/s):	0.0173

Woodcamp Hollow Spring was measured on 10/4/2016 using a wading rod and flow meter.

Distance from bank (ft)	Depth (ft)	Velocity (ft/s)	Average velocity (ft/s)	Area (ft^2)	Discharge (cfs)
0.0	0.00	0.00	0.00	0.00	0.00

0.6	0.26	0.65	0.33	0.08	0.03
1.6	0.20	0.02	0.34	0.23	0.08
2.6	0.26	0.29	0.16	0.23	0.04
3.6	0.13	1.55	0.92	0.20	0.18
4.6	0.39	3.35	2.45	0.26	0.64
5.6	0.39	4.18	3.77	0.39	1.48
6.6	0.33	3.12	3.65	0.36	1.32
7.6	0.39	3.73	3.43	0.36	1.24
8.6	0.46	3.41	3.57	0.43	1.52
9.6	0.39	1.15	2.28	0.43	0.97
10.7	0.20	0.08	0.62	0.32	0.20
11.6	0.20	0.07	0.08	0.18	0.01
13.0	0.13	0.43	0.25	0.23	0.06
				Total (cfs):	7.76
				(m3/s):	0.220

China Row Spring was measured on 10/4/2016 using the Crowe et al. (2001) method for pipe flow.

Pipe diameter (ft)	2.00
Sediment + Water depth (ft)	0.83
Sediment depth (ft)	0.17
Water depth (ft)	0.67
Velocity (ft/s)	0.27
Total (cfs):	0.30
(m3/s):	0.00852

The middle Logan River was measured on 10/4/2016 using a wading rod and flow meter.

Distance from bank (ft)	Depth (ft)	Velocity (ft/s)	Average velocity (ft/s)	Area (ft^2)	Discharge (cfs)
0.0	0.00	0.00	0.00	0.00	0.00
0.4	0.00	0.00	0.00	0.00	0.00
3.4	0.46	1.52	0.76	0.69	0.52
6.4	0.52	0.32	0.92	1.48	1.36
9.4	0.66	1.68	1.00	1.77	1.77
12.4	0.79	1.97	1.83	2.17	3.95
15.4	0.79	1.97	1.97	2.36	4.65
18.2	0.92	1.92	1.95	2.39	4.65
21.2	0.72	1.84	1.88	2.46	4.63
24.2	0.98	1.40	1.62	2.56	4.15
27.2	1.18	1.89	1.65	3.25	5.34
30.2	0.85	2.21	2.05	3.05	6.26
33.2	1.05	1.62	1.92	2.85	5.47
36.2	1.18	1.82	1.72	3.35	5.76
39.2	1.05	2.02	1.92	3.35	6.43
42.2	0.92	1.12	1.57	2.95	4.64

44.9	0.79	1.59	1.36	2.30	3.12
47.9	0.52	1.40	1.50	1.97	2.94
48.4	0.52	1.00	1.20	0.26	0.31
				Total (cfs):	65.9
				(m3/s):	1.87

Right Hand Fork was measured on 10/4/2016 using a wading rod and flow meter.

Distance from bank (ft)	Depth (ft)	Velocity (ft/s)	Average velocity (ft/s)	Area (ft^2)	Discharge (cfs)
0.0	0.00	0.00	0.00	0.00	0.00
1.0	0.59	2.14	1.07	0.30	0.32
2.0	0.26	2.52	2.33	0.43	0.99
3.4	0.52	1.40	1.96	0.55	1.08
4.3	0.46	2.88	2.14	0.44	0.95
5.3	0.46	1.42	2.15	0.46	0.99
6.3	0.33	2.18	1.80	0.39	0.71
7.3	0.13	0.00	1.09	0.23	0.25
7.9	0.00	0.00	0.00	0.04	0.00
				Total (cfs):	5.28
				(m3/s):	0.150

Dewitt Spring was measured on 10/4/2016 using a wading rod and flow meter.

Distance from bank (ft)	Depth (ft)	Velocity (ft/s)	Average velocity (ft/s)	Area (ft^2)	Discharge (cfs)
0.0	0.00	0.00	0.00	0.00	0.00
0.3	1.51	0.66	0.33	0.21	0.07
3.6	1.51	1.11	0.89	5.06	4.47
7.0	1.51	0.99	1.05	5.06	5.31
7.3	0.00	0.00	0.50	0.21	0.11
				Total (cfs):	10.0
				(m3/s):	0.282

The lower Logan River was measured on 10/4/2016 using a wading rod and flow meter.

Distance from bank (ft)	Depth (ft)	Velocity (ft/s)	Average velocity (ft/s)	Area (ft^2)	Discharge (cfs)
0.0	0.00	0.00	0.00	0.00	0.00
2.0	0.46	0.01	0.01	0.46	0.00
4.0	0.72	0.37	0.19	1.18	0.22
6.0	0.79	0.11	0.24	1.51	0.36
8.0	1.05	0.46	0.29	1.84	0.52
10.0	0.92	1.55	1.01	1.97	1.98
12.0	0.98	1.75	1.65	1.90	3.14
14.0	1.12	1.91	1.83	2.10	3.84
16.1	1.25	1.84	1.88	2.48	4.65
18.0	1.31	1.78	1.81	2.43	4.40
20.0	1.18	1.88	1.83	2.49	4.56

22.0	1.18	1.56	1.72	2.36	4.06
24.0	1.18	1.82	1.69	2.36	3.99
26.0	1.12	1.84	1.83	2.30	4.20
28.0	1.12	1.86	1.85	2.23	4.13
30.0	1.12	1.66	1.76	2.23	3.93
32.0	1.12	1.83	1.75	2.23	3.89
34.0	1.05	1.90	1.87	2.17	4.04
36.0	0.98	1.70	1.80	2.03	3.66
38.0	0.98	1.65	1.68	1.97	3.30
40.0	0.98	1.67	1.66	1.97	3.27
42.0	0.92	1.45	1.56	1.90	2.97
44.0	0.85	1.34	1.40	1.77	2.47
46.0	0.85	1.07	1.21	1.71	2.06
48.0	0.72	0.52	0.80	1.57	1.25
50.2	0.00	0.00	0.26	0.79	0.21
				Total (cfs):	71.1
				(m3/s):	2.01

The west branch of Spring Hollow Spring was measured on 10/4/2016 using a wading rod and flow meter.

Distance from bank (ft)	Depth (ft)	Velocity (ft/s)	Average velocity (ft/s)	Area (ft^2)	Discharge (cfs)
0.0	0.13	0.00	0.00	0.00	0.00
1.0	0.26	0.16	0.08	0.20	0.02
2.0	0.39	1.30	0.73	0.33	0.24
2.9	0.33	2.12	1.71	0.32	0.56
Rock	0.00	0.00	1.06	0.00	0.00
4.1	0.33	0.18	0.09	0.00	0.00
5.2	0.33	0.17	0.18	0.36	0.06
6.1	0.33	0.03	0.10	0.30	0.03
7.3	0.07	0.06	0.05	0.24	0.01
8.3	0.00	0.00	0.03	0.03	0.00
				Total (cfs):	0.91
				(m3/s):	0.0259

The east branch of Spring Hollow Spring was measured on 10/4/2016 using a wading rod and flow meter.

Distance from bank (ft)	Depth (ft)	Velocity (ft/s)	Average velocity (ft/s)	Area (ft^2)	Discharge (cfs)
0.0	0.00	0.00	0.00	0.00	0.00
1.0	0.20	0.64	0.32	0.10	0.03
2.0	0.20	0.20	0.42	0.20	0.08
3.0	0.26	0.73	0.47	0.23	0.11
4.0	0.39	2.96	1.85	0.33	0.61
5.0	0.39	0.79	1.88	0.39	0.74
6.0	0.33	2.82	1.81	0.36	0.65
7.0	0.26	1.04	1.93	0.30	0.57

8.0	0.20	0.00	0.52	0.23	0.12
				Total (cfs):	2.9
				(m3/s):	0.0823

Discharge measurements on 11/5/2016

The upper Logan River was measured on 11/5/2016 using a wading rod and flow meter.

Distance from bank (ft)	Depth (ft)	Velocity (ft/s)	Average velocity (ft/s)	Area (ft^2)	Discharge (cfs)
0.0	0.00	0.00	0.00		0.00
0.4	0.13	0.00	0.00	0.03	0.00
3.3	0.66	0.68	0.34	1.14	0.39
5.3	0.46	1.29	0.99	1.12	1.10
7.3	0.33	0.64	0.97	0.79	0.76
9.3	0.85	0.27	0.46	1.18	0.54
11.3	0.46	2.25	1.26	1.31	1.65
13.3	0.46	1.49	1.87	0.92	1.72
15.3	0.79	0.40	0.95	1.25	1.18
17.3	0.72	0.93	0.67	1.51	1.00
19.3	0.52	1.87	1.40	1.25	1.75
21.3	0.46	1.70	1.79	0.98	1.76
23.8	0.66	1.45	1.58	1.39	2.20
25.3	0.46	3.25	2.35	0.84	1.97
27.3	0.46	2.99	3.12	0.92	2.87
29.3	0.33	1.02	2.01	0.79	1.58
31.3	0.33	1.82	1.42	0.66	0.93
33.3	0.39	2.37	2.10	0.72	1.51
35.3	0.26	1.80	2.09	0.82	1.71
37.3	0.39	1.65	1.73	0.49	0.85
39.3	0.39	0.80	1.23	0.79	0.96
40.0	0.00	0.00	0.40	0.39	0.16
				Total (cfs):	26.6
				(m3/s):	0.753

Ricks Spring was measured on 11/5/2016 using a wading rod and flow meter.

Distance from bank (ft)	Depth (ft)	Velocity (ft/s)	Average velocity (ft/s)	Area (ft^2)	Discharge (cfs)
0.0	0.07	0.79	0.79	0.00	0.00
1.2	0.33	1.21	1.00	0.24	0.24
2.6	0.26	0.30	0.76	0.41	0.31
Rock	0.00	0.00	0.15	0.00	0.00
6.9	0.13	0.00	0.00	0.00	0.00
7.9	0.13	1.26	0.63	0.13	0.08
8.8	0.20	0.00	0.63	0.15	0.09
Rock	0.00	0.00	0.00	0.00	0.00

10.5	0.07	0.06	0.03	0.00	0.00
11.9	0.20	2.51	1.29	0.18	0.24
12.8	0.13	1.89	2.20	0.15	0.32
13.7	0.13	0.48	1.19	0.12	0.14
14.5	0.07	0.09	0.29	0.08	0.02
15.7	0.13	0.81	0.45	0.12	0.05
16.7	0.07	0.01	0.41	0.10	0.04
17.7	0.33	0.02	0.02	0.20	0.00
18.7	0.33	0.42	0.22	0.33	0.07
19.7	0.26	0.15	0.29	0.30	0.08
20.7	0.00	0.00	0.08	0.13	0.01
				Total (cfs):	1.71
				(m3/s):	0.0484

Temple Fork was measured on 11/5/2016 using a wading rod and flow meter.

Distance from bank (ft)	Depth (ft)	Velocity (ft/s)	Average velocity (ft/s)	Area (ft^2)	Discharge (cfs)
0.0	0.07	0.00	0.00	0.00	0.00
1.2	0.39	2.00	1.00	0.28	0.28
2.2	0.46	1.02	1.51	0.43	0.64
3.2	0.52	1.77	1.40	0.49	0.69
4.2	0.52	2.46	2.12	0.52	1.11
5.2	0.52	1.93	2.20	0.52	1.15
6.2	0.46	2.00	1.97	0.49	0.97
7.2	0.52	2.23	2.12	0.49	1.04
8.2	0.46	2.16	2.20	0.49	1.08
9.2	0.52	2.18	2.17	0.49	1.07
10.2	0.52	1.67	1.93	0.52	1.01
11.2	0.52	1.34	1.51	0.52	0.79
12.2	0.46	1.38	1.36	0.49	0.67
13.2	0.39	0.62	1.00	0.43	0.43
14.2	0.20	0.00	0.31	0.30	0.09
14.8	0.00	0.00	0.00	0.06	0.00
				Total (cfs):	11.0
				(m3/s):	0.312

Benchmark Spring was measured on 11/5/2016 using a wading rod and flow meter.

Distance from bank (ft)	Depth (ft)	Velocity (ft/s)	Average velocity (ft/s)	Area (ft^2)	Discharge (cfs)
0.0	0.00	0.00	0.00	0.00	0.00
0.2	0.20	0.95	0.48	0.02	0.01
0.6	0.13	1.27	1.11	0.05	0.05
1.2	0.07	0.00	0.64	0.06	0.04
				Total (cfs):	0.10
				(m3/s):	0.00277

Logan Cave Spring was measured on 11/5/2016 using a wading rod and flow meter.

Distance from bank (ft)	Depth (ft)	Velocity (ft/s)	Average velocity (ft/s)	Area (ft^2)	Discharge (cfs)
0.0	0.13	0.00	0.00	0.00	0.00
1.1	0.26	1.34	0.67	0.22	0.15
2.1	0.20	3.44	2.39	0.23	0.55
3.1	0.26	0.85	2.15	0.23	0.49
3.3	0.00	0.00	0.43	0.03	0.01
				Total (cfs):	1.20
				(m3/s):	0.0339

Woodcamp Hollow Spring was measured on 11/5/2016 using a wading rod and flow meter.

Distance from bank (ft)	Depth (ft)	Velocity (ft/s)	Average velocity (ft/s)	Area (ft^2)	Discharge (cfs)
0.0	0.00	0.00	0.00	0.00	0.00
1.1	0.20	1.81	0.91	0.11	0.10
2.3	0.26	0.40	1.11	0.28	0.30
3.4	0.33	2.73	1.57	0.32	0.51
4.5	0.39	1.78	2.26	0.40	0.90
5.5	0.33	3.82	2.80	0.36	1.01
6.4	0.26	5.80	4.81	0.27	1.28
7.4	0.39	3.96	4.88	0.33	1.60
8.4	0.46	2.72	3.34	0.43	1.42
9.4	0.52	1.13	1.93	0.49	0.95
10.4	0.39	0.27	0.70	0.46	0.32
11.4	0.26	1.02	0.65	0.33	0.21
12.4	0.20	0.00	0.51	0.23	0.12
13.4	0.13	0.00	0.00	0.16	0.00
14.4	0.20	0.31	0.16	0.16	0.03
15.4	0.20	0.00	0.16	0.20	0.03
16.3	0.00	0.00	0.00	0.09	0.00
				Total (cfs):	8.77
				(m3/s):	0.248

China Row Spring was measured on 11/5/2016 using the Crowe et al. (2001) method for pipe flow.

Pipe diameter (ft)	2.00
Sediment + Water depth (ft)	0.83
Sediment depth (ft)	0.17
Water depth (ft)	0.67
Velocity (ft/s)	0.20
Total (cfs):	0.22
(m3/s):	0.00631

The middle Logan River was measured on 11/5/2016 using a wading rod and flow meter.

Distance from bank (ft)	Depth (ft)	Velocity (ft/s)	Average velocity (ft/s)	Area (ft^2)	Discharge (cfs)
0.0	0.52	1.20	1.20	0.00	0.00
3.1	0.66	1.76	1.48	1.83	2.71
6.1	0.98	1.49	1.63	2.46	4.00
8.8	1.12	1.94	1.72	2.83	4.86
12.1	1.25	1.89	1.92	3.90	7.46
15.1	1.12	1.55	1.72	3.54	6.09
18.0	1.05	2.17	1.86	3.14	5.84
21.1	1.25	1.91	2.04	3.56	7.26
23.1	1.05	1.37	1.64	2.30	3.77
25.9	1.05	1.44	1.41	2.94	4.13
29.1	0.98	2.01	1.73	3.25	5.61
32.1	0.92	1.80	1.91	2.85	5.44
35.1	0.79	1.94	1.87	2.56	4.79
38.1	0.72	1.91	1.93	2.26	4.36
41.1	0.59	1.58	1.75	1.97	3.44
44.1	0.39	1.03	1.31	1.48	1.93
47.1	0.26	0.38	0.71	0.98	0.69
48.6	0.00	0.00	0.19	0.20	0.04
				Total (cfs):	72.4
				(m3/s):	2.05

Right Hand Fork was measured on 11/5/2016 using a wading rod and flow meter.

Distance from bank (ft)	Depth (ft)	Velocity (ft/s)	Average velocity (ft/s)	Area (ft^2)	Discharge (cfs)
0.0	0.00	0.00	0.00	0.00	0.00
1.0	0.20	0.49	0.25	0.10	0.02
2.0	0.39	2.23	1.36	0.30	0.40
3.0	0.46	2.55	2.39	0.43	1.02
4.0	0.39	1.34	1.95	0.43	0.83
5.0	0.33	1.21	1.28	0.36	0.46
6.0	0.59	1.78	1.50	0.46	0.69
7.0	0.39	2.51	2.15	0.49	1.06
8.0	0.26	0.84	1.68	0.33	0.55
9.0	0.07	0.00	0.42	0.16	0.07
9.3	0.00	0.00	0.00	0.06	0.00
				Total (cfs):	5.10
				(m3/s):	0.144

Dewitt Spring was measured on 11/5/2016 using a wading rod and flow meter.

Distance from bank (ft)	Depth (ft)	Velocity (ft/s)	Average velocity (ft/s)	Area (ft^2)	Discharge (cfs)
0.0	0.00	0.00	0.00	0.00	0.00
0.3	1.51	0.30	0.15	0.21	0.03

3.6	1.51	0.35	0.33	5.06	1.64
7.0	1.51	0.35	0.35	5.06	1.77
7.3	0.00	0.00	0.18	0.21	0.04
				Total (cfs):	3.48
				(m3/s):	0.0986

The lower Logan River was measured on 11/5/2016 using a wading rod and flow meter.

Distance from bank (ft)	Depth (ft)	Velocity (ft/s)	Average velocity (ft/s)	Area (ft^2)	Discharge (cfs)
0.0	0.07	0.00	0.00	0.00	0.00
1.9	0.13	0.33	0.17	0.19	0.03
3.9	0.59	0.23	0.28	0.72	0.20
5.9	1.18	0.24	0.24	1.77	0.42
7.9	1.05	1.29	0.77	2.23	1.71
9.9	0.98	1.80	1.55	2.03	3.14
11.9	1.05	1.95	1.88	2.03	3.81
13.9	1.12	2.21	2.08	2.17	4.50
15.9	1.25	2.11	2.16	2.36	5.10
17.9	1.31	1.88	2.00	2.56	5.11
19.9	1.25	2.01	1.95	2.56	4.98
21.9	1.18	2.03	2.02	2.43	4.90
23.9	1.18	2.09	2.06	2.36	4.87
25.9	1.12	2.12	2.11	2.30	4.83
27.9	1.18	1.82	1.97	2.30	4.52
29.9	1.18	1.77	1.80	2.36	4.24
31.9	1.18	2.06	1.92	2.36	4.52
33.9	1.18	1.95	2.01	2.36	4.74
35.9	1.12	1.93	1.94	2.30	4.46
37.9	1.05	1.89	1.91	2.17	4.14
39.9	0.98	1.64	1.77	2.03	3.59
41.9	0.98	1.80	1.72	1.97	3.39
43.9	0.85	1.43	1.62	1.84	2.97
45.9	0.85	1.29	1.36	1.71	2.32
47.9	0.72	0.95	1.12	1.57	1.76
49.5	0.00	0.00	0.48	0.58	0.27
				Total (cfs):	84.5
				(m3/s):	2.39

The west branch of Spring Hollow Spring was measured on 11/5/2016 using a wading rod and flow meter.

Distance from bank (ft)	Depth (ft)	Velocity (ft/s)	Average velocity (ft/s)	Area (ft^2)	Discharge (cfs)
0.0	0.07	0.00	0.00	0.00	0.00
1.0	0.20	0.00	0.00	0.13	0.00
2.0	0.26	0.16	0.08	0.23	0.02
3.0	0.33	1.76	0.96	0.30	0.28

4.0	0.46	0.89	1.33	0.39	0.52
5.0	0.26	0.00	0.45	0.36	0.16
6.0	0.33	0.47	0.24	0.30	0.07
7.0	0.26	0.40	0.44	0.30	0.13
8.0	0.07	0.47	0.44	0.16	0.07
9.0	0.07	0.00	0.24	0.07	0.02
9.5	0.00	0.00	0.00	0.02	0.00
				Total (cfs):	1.27
				(m3/s):	0.0359

The east branch of Spring Hollow Spring was measured on 11/5/2016 using a wading rod and flow meter.

Distance from bank (ft)	Depth (ft)	Velocity (ft/s)	Average velocity (ft/s)	Area (ft^2)	Discharge (cfs)
0.0	0.00	0.00	0.00	0.00	0.00
0.1	0.07	0.00	0.00	0.00	0.00
1.1	0.26	0.13	0.07	0.16	0.01
2.1	0.26	0.25	0.19	0.26	0.05
3.1	0.26	0.19	0.22	0.26	0.06
4.1	0.52	4.44	2.32	0.39	0.91
5.1	0.39	1.19	2.82	0.46	1.29
6.1	0.26	1.13	1.16	0.33	0.38
7.1	0.20	0.44	0.79	0.23	0.18
8.1	0.00	0.00	0.22	0.10	0.02
				Total (cfs):	2.91
				(m3/s):	0.0823

Discharge measurements on 3/3/2017

The upper Logan River was measured on 3/3/2017 using a wading rod and flow meter.

Distance from bank (ft)	Depth (ft)	Velocity (ft/s)	Average velocity (ft/s)	Area (ft^2)	Discharge (cfs)
0.0	0.49	0.18	0.18	0.00	0.00
2.1	0.59	3.73	1.96	1.14	2.22
4.1	0.98	4.04	3.89	1.57	6.12
6.1	0.89	3.40	3.72	1.87	6.96
8.1	0.89	2.18	2.79	1.77	4.94
10.1	0.69	3.30	2.74	1.57	4.32
12.1	0.89	2.83	3.07	1.57	4.83
14.1	0.59	2.52	2.68	1.48	3.95
16.1	0.89	1.19	1.86	1.48	2.74
18.1	0.89	1.58	1.39	1.77	2.45
20.0	0.89	1.41	1.50	1.68	2.52
22.1	1.08	1.21	1.31	2.07	2.71
24.1	1.08	2.02	1.62	2.17	3.50
26.1	1.28	2.50	2.26	2.36	5.34

28.1	0.69	0.32	1.41	1.97	2.78
29.6	0.00	0.00	0.16	0.52	0.08
				Total (cfs):	55.4
				(m3/s):	1.57

Ricks Spring was measured on 3/3/2017 using a wading rod and flow meter.

Distance from bank (ft)	Depth (ft)	Velocity (ft/s)	Average velocity (ft/s)	Area (ft^2)	Discharge (cfs)
0.0	0.00	0.00	0.00	0.00	0.00
1.1	0.25	0.25	0.13	0.14	0.02
2.1	0.49	1.90	1.08	0.37	0.40
2.7	0.39	0.37	1.14	0.27	0.30
4.7	0.20	0.70	0.54	0.59	0.32
5.6	0.10	0.15	0.43	0.13	0.06
6.9	0.20	0.00	0.08	0.19	0.01
7.7	0.39	0.66	0.33	0.24	0.08
8.6	0.20	0.48	0.57	0.27	0.15
9.0	rock start	0.00	0.24	0.04	0.01
9.8	rock end	0.00	0.00	0.00	0.00
9.9	0.15	0.34	0.17	0.01	0.00
10.1	rock start	0.00	0.17	0.01	0.00
10.4	rock end	0.00	0.00	0.00	0.00
10.6	0.10	0.36	0.18	0.01	0.00
11.6	0.10	0.21	0.29	0.10	0.03
12.6	0.30	0.95	0.58	0.20	0.11
13.6	0.20	0.62	0.79	0.25	0.19
14.5	0.00	0.00	0.31	0.09	0.03
15.0	0.00	0.00	0.00	0.00	0.00
15.4	0.15	0.37	0.19	0.03	0.01
16.6	0.20	0.11	0.24	0.21	0.05
17.8	0.30	0.15	0.13	0.30	0.04
18.6	0.44	0.48	0.32	0.30	0.09
19.6	0.39	0.12	0.30	0.42	0.13
20.4	0.39	0.49	0.31	0.31	0.10
20.6	rock start	0.00	0.25	0.04	0.01
20.9	rock end	0.00	0.00	0.00	0.00
21.3	0.30	0.26	0.13	0.06	0.01
22.4	0.00	0.00	0.13	0.16	0.02
				Total (cfs):	2.16
				(m3/s):	0.0611

Temple Fork was measured on 3/3/2017 using a wading rod and flow meter.

Distance from bank (ft)	Depth (ft)	Velocity (ft/s)	Average velocity (ft/s)	Area (ft^2)	Discharge (cfs)
0.0	0.00	0.00	0.00	0.00	0.00

0.5	0.34	0.44	0.22	0.09	0.02
1.5	0.30	1.04	0.74	0.32	0.24
2.5	0.69	1.67	1.36	0.49	0.67
3.5	0.59	0.47	1.07	0.64	0.68
4.5	0.69	1.81	1.14	0.64	0.73
5.5	0.59	2.20	2.01	0.64	1.28
6.5	0.59	0.38	1.29	0.59	0.76
7.5	0.69	0.65	0.52	0.64	0.33
8.5	0.79	2.28	1.47	0.74	1.08
9.5	0.79	1.81	2.05	0.79	1.61
10.5	0.79	2.16	1.99	0.79	1.56
11.5	0.79	2.15	2.16	0.79	1.70
12.5	0.79	1.94	2.05	0.79	1.61
13.5	0.69	1.91	1.93	0.74	1.42
14.5	0.69	1.81	1.86	0.69	1.28
15.5	0.00	0.00	0.91	0.34	0.31
				Total (cfs):	15.3
				(m3/s):	0.433

Benchmark Spring was measured on 3/3/2017 using a wading rod and flow meter.

Distance from bank (ft)	Depth (ft)	Velocity (ft/s)	Average velocity (ft/s)	Area (ft^2)	Discharge (cfs)
0.2	0.15	0.00	0.00	0.00	0.00
0.8	0.30	0.46	0.23	0.13	0.03
1.3	0.20	0.27	0.37	0.13	0.05
				Total (cfs):	0.08
				(m3/s):	0.00218

The west branch of Logan Cave Spring was measured on 3/3/2017 using a wading rod and flow meter.

Distance from bank (ft)	Depth (ft)	Velocity (ft/s)	Average velocity (ft/s)	Area (ft^2)	Discharge (cfs)
0.0	0.00	0.00	0.00	0.00	0.00
1.0	0.30	0.03	0.02	0.15	0.00
2.0	0.39	0.00	0.02	0.34	0.01
3.0	0.79	1.19	0.60	0.59	0.35
4.0	0.89	1.07	1.13	0.84	0.95
5.0	0.89	0.34	0.71	0.89	0.62
5.6	0.00	0.00	0.17	0.27	0.05
				Total (cfs):	1.97
				(m3/s):	0.0559

The east branch of Logan Cave Spring was measured on 3/3/2017 using a wading rod and flow meter.

Distance from bank (ft)	Depth (ft)	Velocity (ft/s)	Average velocity (ft/s)	Area (ft^2)	Discharge (cfs)
0.0	0.00	0.00	0.00	0.62	0.00
0.6	0.25	0.84	0.42	0.05	0.02

2.1	0.25	0.32	0.58	0.37	0.21
2.2	0.25	0.11	0.22	0.02	0.00
				Total (cfs):	0.24
				(m3/s):	0.00673

Woodcamp Hollow Spring was measured on 3/3/2017 using a wading rod and flow meter.

Distance from bank (ft)	Depth (ft)	Velocity (ft/s)	Average velocity (ft/s)	Area (ft^2)	Discharge (cfs)
0.0	0.00	0.00	0.00	0.00	0.00
1.0	0.30	0.79	0.40	0.15	0.06
2.0	0.20	0.20	0.50	0.25	0.12
3.0	0.39	0.97	0.59	0.30	0.17
4.0	0.59	0.00	0.49	0.49	0.24
5.1	0.69	2.01	1.01	0.70	0.71
6.0	0.64	2.53	2.27	0.60	1.36
7.0	0.49	4.03	3.28	0.57	1.86
8.0	0.79	2.79	3.41	0.64	2.18
9.0	0.64	4.11	3.45	0.71	2.46
10.0	0.64	1.04	2.58	0.64	1.65
11.0	0.49	0.90	0.97	0.57	0.55
12.0	0.30	0.04	0.47	0.39	0.19
13.0	0.30	0.07	0.06	0.30	0.02
14.1	0.00	0.00	0.04	0.16	0.01
				Total (cfs):	11.6
				(m3/s):	0.327

China Row Spring was measured on 3/3/2017 using the Crowe et al. (2001) method for pipe flow.

Pipe diameter (ft)	2.00
Sediment + Water depth (ft)	0.66
Sediment depth (ft)	0.17
Water depth (ft)	0.49
Velocity (ft/s)	0.46
Total (cfs):	0.36
(m3/s):	0.0102

The middle Logan River was measured on 3/3/2017 using a wading rod and flow meter.

Distance from bank (ft)	Depth (ft)	Velocity (ft/s)	Average velocity (ft/s)	Area (ft^2)	Discharge (cfs)
0.0	0.00	0.00	0.00	0.00	0.00
1.0	0.59	0.62	0.31	0.30	0.09
4.4	1.38	1.64	1.13	3.35	3.79
7.0	2.07	1.80	1.72	4.48	7.71
10.0	2.26	1.97	1.89	6.50	12.26
13.0	2.07	1.84	1.90	6.50	12.36
16.0	1.48	1.41	1.62	5.32	8.63

19.0	1.87	1.31	1.36	5.02	6.84
22.0	1.87	0.89	1.10	5.61	6.17
24.5	1.67	2.13	1.51	4.43	6.68
27.5	1.48	2.20	2.17	4.72	10.23
30.5	1.57	1.77	1.99	4.58	9.09
33.5	1.57	1.61	1.69	4.72	7.98
35.9	1.48	1.31	1.46	3.66	5.35
39.0	1.18	1.15	1.23	4.12	5.07
42.0	0.98	0.92	1.03	3.25	3.36
45.0	0.20	0.30	0.61	1.77	1.08
48.3	0.00	0.00	0.15	0.32	0.05
				Total (cfs):	107
				(m3/s):	3.02

Right Hand Fork was measured on 3/3/2017 using a wading rod and flow meter.

Distance from bank (ft)	Depth (ft)	Velocity (ft/s)	Average velocity (ft/s)	Area (ft^2)	Discharge (cfs)
0.0	0.00	0.00	0.00	0.00	0.00
1.0	0.54	1.52	0.76	0.27	0.21
2.0	0.79	2.73	2.13	0.66	1.41
3.0	1.03	1.95	2.34	0.91	2.13
4.0	1.13	1.82	1.89	1.08	2.04
5.0	0.79	2.64	2.23	0.96	2.14
6.0	1.18	1.93	2.29	0.98	2.25
7.0	0.84	4.18	3.06	1.01	3.08
8.0	1.03	2.67	3.43	0.94	3.20
9.0	0.39	0.00	1.34	0.71	0.95
9.8	0.00	0.00	0.00	0.41	0.00
				Total (cfs):	17.4
				(m3/s):	0.493

Dewitt Spring was measured on 3/3/2017 using a wading rod and flow meter.

Distance from bank (ft)	Depth (ft)	Velocity (ft/s)	Average velocity (ft/s)	Area (ft^2)	Discharge (cfs)
0.0	0.00	0.00	0.00	0.00	0.00
0.3	0.98	0.93	0.47	0.14	0.06
3.6	0.98	0.86	0.90	3.30	2.95
7.0	0.98	0.88	0.87	3.30	2.87
7.3	0.00	0.00	0.44	0.14	0.06
				Total (cfs):	5.95
				(m3/s):	0.168

The lower Logan River was measured on 3/3/2017 using a wading rod and flow meter.

Distance from bank (ft)	Depth (ft)	Velocity (ft/s)	Average velocity (ft/s)	Area (ft^2)	Discharge (cfs)
0.0	0.30	0.38	0.38	0.00	0.00

3.0	0.79	0.40	0.39	1.62	0.63
6.0	1.97	0.40	0.40	4.13	1.65
9.0	1.67	1.77	1.09	5.46	5.93
12.0	1.67	2.33	2.05	5.02	10.29
15.0	1.87	2.37	2.35	5.32	12.49
18.0	2.07	2.41	2.39	5.91	14.11
21.0	1.97	2.27	2.34	6.05	14.16
24.0	1.87	2.10	2.19	5.76	12.58
27.0	1.87	1.94	2.02	5.61	11.33
30.0	1.87	2.39	2.17	5.61	12.15
33.0	1.87	2.05	2.22	5.61	12.46
36.0	1.77	2.09	2.07	5.46	11.31
39.0	1.57	1.94	2.02	5.02	10.11
42.0	1.57	1.72	1.83	4.72	8.65
45.0	1.28	1.49	1.61	4.28	6.87
48.0	1.08	0.65	1.07	3.54	3.79
49.9	0.00	0.00	0.33	1.03	0.33
				Total (cfs):	149
				(m3/s):	4.22

The lower Logan River side channel was measured on 3/3/2017 using a wading rod and flow meter.

Distance from bank (ft)	Depth (ft)	Velocity (ft/s)	Average velocity (ft/s)	Area (ft^2)	Discharge (cfs)
0.0	0.00	0.00	0.00	0.00	0.00
1.0	0.30	0.00	0.00	0.15	0.00
2.0	0.69	0.00	0.00	0.49	0.00
3.0	0.98	0.18	0.09	0.84	0.08
4.0	1.18	0.25	0.22	1.08	0.23
5.0	1.03	0.00	0.13	1.11	0.14
6.0	0.79	0.00	0.00	0.91	0.00
8.6	0.00	0.00	0.00	1.02	0.00
				Total (cfs):	0.45
				(m3/s):	0.0126

The west branch of Spring Hollow Spring was measured on 3/3/2017 using a wading rod and flow meter.

Distance from bank (ft)	Depth (ft)	Velocity (ft/s)	Average velocity (ft/s)	Area (ft^2)	Discharge (cfs)
0.0	0.00	0.00	0.00	0.00	0.00
1.5	0.30	0.00	0.00	0.22	0.00
2.0	0.30	0.21	0.11	0.15	0.02
3.3	0.44	0.70	0.46	0.48	0.22
4.0	0.49	0.07	0.39	0.33	0.13
5.2	0.39	0.22	0.15	0.53	0.08
6.1	0.30	0.39	0.31	0.31	0.09
7.0	0.30	0.84	0.62	0.27	0.16

8.4	0.25	0.05	0.45	0.38	0.17
9.3	0.00	0.00	0.03	0.11	0.00
				Total (cfs):	0.87
				(m3/s):	0.0245

The east branch of Spring Hollow Spring was measured on 3/3/2017 using a wading rod and flow meter.

Distance from bank (ft)	Depth (ft)	Velocity (ft/s)	Average velocity (ft/s)	Area (ft^2)	Discharge (cfs)
0.0	0.00	0.00	0.00	0.00	0.00
0.9	0.39	0.73	0.37	0.18	0.06
2.0	0.39	0.18	0.46	0.43	0.20
3.0	0.49	1.78	0.98	0.44	0.43
4.0	0.69	2.23	2.01	0.59	1.18
4.9	0.59	0.88	1.56	0.58	0.90
6.0	0.39	1.86	1.37	0.54	0.74
7.0	0.30	1.25	1.56	0.34	0.54
7.9	0.00	0.00	0.63	0.13	0.08
				Total (cfs):	4.14
				(m3/s):	0.117

Discharge measurements on 4/7/2017

The upper Logan River was measured on 4/7/2017 using a wading rod and flow meter.

Distance from bank (ft)	Depth (ft)	Velocity (ft/s)	Average velocity (ft/s)	Area (ft^2)	Discharge (cfs)
0.0	0.00	0.00	0.00	0.00	0.00
2.0	0.89	0.00	0.00	0.89	0.00
5.0	1.48	0.70	0.35	3.54	1.24
8.0	1.48	0.72	0.71	4.43	3.14
11.0	1.77	1.83	1.28	4.87	6.21
14.0	1.77	2.75	2.29	5.32	12.17
17.0	1.67	2.68	2.72	5.17	14.03
20.0	1.48	2.47	2.58	4.72	12.17
23.0	1.87	3.12	2.80	5.02	14.03
26.0	1.97	0.65	1.89	5.76	10.85
29.0	1.87	1.55	1.10	5.76	6.33
32.0	1.67	0.62	1.09	5.32	5.77
35.0	1.67	2.14	1.38	5.02	6.93
38.0	1.57	2.46	2.30	4.87	11.21
41.0	2.17	2.39	2.43	5.61	13.61
44.0	1.87	2.28	2.34	6.05	14.13
47.0	1.38	1.69	1.99	4.87	9.67
50.0	0.69	0.00	0.85	3.10	2.62
53.7	0.00	0.00	0.00	0.00	0.00
				Total (cfs):	144

(m3/s):	4.08

Ricks Spring was measured on 4/7/2017 using a wading rod and flow meter.

Distance from bank (ft)	Depth (ft)	Velocity (ft/s)	Average velocity (ft/s)	Area (ft^2)	Discharge (cfs)
0.0	0.00	0.00	0.00	0.00	0.00
0.6	0.20	0.66	0.33	0.06	0.02
1.6	0.30	0.14	0.40	0.25	0.10
2.4	rock start	0.00	0.07	0.12	0.01
5.2	rock end	0.00	0.00	0.00	0.00
5.6	0.39	2.40	1.20	0.08	0.09
6.6	0.59	2.28	2.34	0.49	1.15
7.6	0.79	3.26	2.77	0.69	1.91
8.1	rock start	0.00	1.63	0.20	0.32
9.6	rock end	0.00	0.00	0.00	0.00
10.1	0.39	1.77	0.89	0.10	0.09
11.1	0.39	1.16	1.47	0.39	0.58
11.3	rock start	0.00	0.58	0.04	0.02
12.3	rock end	0.00	0.00	0.00	0.00
12.6	0.59	1.40	0.70	0.09	0.06
13.6	0.69	2.38	1.89	0.64	1.21
14.6	0.30	1.38	1.88	0.49	0.93
15.6	0.39	1.58	1.48	0.34	0.51
16.6	0.20	0.58	1.08	0.30	0.32
17.6	0.49	2.82	1.70	0.34	0.59
18.6	0.49	2.40	2.61	0.49	1.28
19.6	0.39	1.20	1.80	0.44	0.80
20.6	0.30	1.77	1.49	0.34	0.51
21.6	0.39	1.16	1.47	0.34	0.50
22.6	0.39	1.95	1.56	0.39	0.61
23.6	0.79	0.95	1.45	0.59	0.86
24.6	0.69	1.34	1.15	0.74	0.85
25.6	0.69	0.45	0.90	0.69	0.62
26.6	0.49	0.00	0.23	0.59	0.13
27.6	0.30	0.53	0.27	0.39	0.10
28.4	0.00	0.00	0.27	0.12	0.03
				Total (cfs):	14.20
				(m3/s):	0.402

Temple Fork was measured on 4/7/2017 using a wading rod and flow meter.

Distance from bank (ft)	Depth (ft)	Velocity (ft/s)	Average velocity (ft/s)	Area (ft^2)	Discharge (cfs)
0.0	0.00	0.00	0.00	0.00	0.00
0.2	0.39	1.16	0.58	0.04	0.02
1.2	0.39	1.28	1.22	0.39	0.48

2.2	0.49	5.84	3.56	0.44	1.58
3.2	0.79	2.56	4.20	0.64	2.69
4.2	1.18	5.30	3.93	0.98	3.87
5.2	1.18	5.09	5.20	1.18	6.14
6.2	0.98	3.41	4.25	1.08	4.60
7.2	1.08	3.15	3.28	1.03	3.39
8.2	0.89	3.74	3.45	0.98	3.39
9.2	0.79	2.32	3.03	0.84	2.54
10.2	0.69	1.14	1.73	0.74	1.28
11.2	0.79	3.72	2.43	0.74	1.79
12.2	0.89	3.54	3.63	0.84	3.04
13.2	0.89	3.02	3.28	0.89	2.91
14.2	0.69	3.61	3.32	0.79	2.61
15.2	0.59	2.59	3.10	0.64	1.98
16.2	0.49	1.71	2.15	0.54	1.16
17.2	0.10	0.00	0.86	0.30	0.25
17.8	0.00	0.00	0.00	0.03	0.00
				Total (cfs):	43.71
				(m3/s):	1.24

Benchmark Spring was measured on 4/7/2017 using a wading rod and flow meter.

Distance from bank (ft)	Depth (ft)	Velocity (ft/s)	Average velocity (ft/s)	Area (ft^2)	Discharge (cfs)
0.0	0.00	0.00	0.00	0.00	0.00
0.1	0.15	0.24	0.12	0.01	0.00
1.0	0.15	0.91	0.58	0.06	0.04
1.5	0.20	0.44	0.68	0.10	0.07
1.7	0.00	0.00	0.22	0.02	0.00
				Total (cfs):	0.11
				(m3/s):	0.00306

Cottonwood Creek was measured on 4/7/2017 using a wading rod and flow meter.

Distance from bank (ft)	Depth (ft)	Velocity (ft/s)	Average velocity (ft/s)	Area (ft^2)	Discharge (cfs)
0.0	0.00	0.00	0.00	0.00	0.00
0.7	0.39	0.84	0.42	0.14	0.06
1.7	0.59	0.81	0.83	0.49	0.41
2.7	0.59	2.09	1.45	0.59	0.86
3.7	0.49	1.22	1.66	0.54	0.90
4.7	0.69	1.24	1.23	0.59	0.73
5.7	0.79	1.98	1.61	0.74	1.19
6.7	0.59	0.41	1.20	0.69	0.82
7.9	0.00	0.00	0.21	0.35	0.07
				Total (cfs):	5.03
				(m3/s):	0.142

The west branch of Logan Cave Spring was measured on 4/7/2017 using a wading rod and flow meter.

Distance from bank (ft)	Depth (ft)	Velocity (ft/s)	Average velocity (ft/s)	Area (ft^2)	Discharge (cfs)
0.0	0.00	0.00	0.00	0.00	0.00
1.0	0.30	0.75	0.38	0.15	0.06
2.0	0.49	2.43	1.59	0.39	0.63
3.0	0.69	3.23	2.83	0.59	1.67
3.8	0.69	0.95	2.09	0.55	1.15
3.9	0.00	0.00	0.48	0.03	0.02
				Total (cfs):	3.52
				(m3/s):	0.0997

The east branch of Logan Cave Spring was measured on 4/7/2017 using a wading rod and flow meter.

Distance from bank (ft)	Depth (ft)	Velocity (ft/s)	Average velocity (ft/s)	Area (ft^2)	Discharge (cfs)
0.0	0.00	0.00	0.00	0.00	0.00
0.5	0.30	0.74	0.37	0.07	0.03
1.5	0.49	2.53	1.64	0.39	0.64
2.5	0.59	1.75	2.14	0.54	1.16
3.5	0.39	5.97	3.86	0.49	1.90
4.4	0.49	1.41	3.69	0.40	1.47
4.7	0.00	0.00	0.71	1.24	0.87
				Total (cfs):	6.07
				(m3/s):	0.172

Woodcamp Hollow Spring was measured on 4/7/2017 using a wading rod and flow meter.

Distance from bank (ft)	Depth (ft)	Velocity (ft/s)	Average velocity (ft/s)	Area (ft^2)	Discharge (cfs)
0.0	0.00	0.00	0.00	0.00	0.00
0.8	0.30	0.49	0.25	0.12	0.03
1.8	0.59	0.00	0.25	0.44	0.11
2.8	0.49	0.00	0.00	0.54	0.00
3.8	0.39	1.34	0.67	0.44	0.30
4.8	0.49	1.52	1.43	0.44	0.63
5.8	0.79	3.29	2.41	0.64	1.54
6.8	0.69	3.23	3.26	0.74	2.41
7.8	0.69	4.44	3.84	0.69	2.64
8.8	0.79	2.50	3.47	0.74	2.56
9.8	0.79	6.34	4.42	0.79	3.48
10.8	0.69	1.96	4.15	0.74	3.06
11.8	0.49	0.46	1.21	0.59	0.71
12.8	0.30	0.01	0.24	0.39	0.09
13.8	0.30	0.91	0.46	0.30	0.14
14.4	0.00	0.00	0.46	0.09	0.04
				Total (cfs):	17.74

(m3/s):	0.503

Woodcamp Hollow Creek was measured on 4/7/2017 using a wading rod and flow meter.

Distance from bank (ft)	Depth (ft)	Velocity (ft/s)	Average velocity (ft/s)	Area (ft^2)	Discharge (cfs)
0.0	0.00	0.00	0.00	0.00	0.00
0.5	0.20	0.00	0.00	0.05	0.00
1.5	0.34	0.34	0.17	0.27	0.05
2.5	0.39	0.12	0.23	0.37	0.08
3.5	0.20	0.01	0.07	0.30	0.02
4.5	0.39	0.60	0.31	0.30	0.09
5.5	0.39	2.65	1.63	0.39	0.64
6.5	0.39	1.94	2.30	0.39	0.90
7.5	0.34	0.78	1.36	0.37	0.50
8.5	0.20	1.14	0.96	0.27	0.26
9.5	0.20	0.16	0.65	0.20	0.13
10.5	0.30	0.65	0.41	0.25	0.10
11.5	0.59	1.55	1.10	0.44	0.49
12.5	0.39	0.00	0.78	0.49	0.38
13.5	0.30	1.66	0.83	0.34	0.29
14.0	0.00	0.00	0.83	0.07	0.06
				Total (cfs):	3.99
				(m3/s):	0.113

China Row Spring was measured on 4/7/2017 using the Crowe et al. (2001) method for pipe flow.

Pipe diameter (ft)	2.00
Sediment + Water depth (ft)	0.66
Sediment depth (ft)	0.17
Water depth (ft)	0.49
Velocity (ft/s)	0.60
Total (cfs):	0.47
(m3/s):	0.0133

Right Hand Fork was measured on 4/7/2017 using a wading rod and flow meter.

Distance from bank (ft)	Depth (ft)	Velocity (ft/s)	Average velocity (ft/s)	Area (ft^2)	Discharge (cfs)
0.0	0.00	0.00	0.00	0.00	0.00
1.2	0.89	1.44	0.72	0.53	0.38
2.3	0.98	3.12	2.28	1.03	2.35
3.3	0.98	5.60	4.36	0.98	4.29
4.3	1.48	5.70	5.65	1.23	6.95
5.3	0.98	3.98	4.84	1.23	5.95
6.3	0.98	5.05	4.52	0.98	4.44
7.3	1.48	5.20	5.13	1.23	6.31
8.3	1.38	5.24	5.22	1.43	7.45

9.3	0.89	5.98	5.61	1.13	6.35
10.3	0.79	5.46	5.72	1.13	6.47
12.3	0.00	0.00	2.73	0.79	2.15
				Total (cfs):	53.10
				(m3/s):	1.50

Dewitt Spring was measured on 4/7/2017 using a wading rod and flow meter.

Distance from bank (ft)	Depth (ft)	Velocity (ft/s)	Average velocity (ft/s)	Area (ft^2)	Discharge (cfs)
0.0	0.00	0.00	0.00	0.00	0.00
0.3	2.02	0.77	0.39	0.29	0.11
3.6	2.02	0.99	0.88	6.76	5.95
7.0	2.02	0.94	0.97	6.76	6.52
7.3	0.00	0.00	0.47	0.29	0.13
				Total (cfs):	12.72
				(m3/s):	0.360

The west branch of Spring Hollow Spring was measured on 4/7/2017 using a wading rod and flow meter.

Distance from bank (ft)	Depth (ft)	Velocity (ft/s)	Average velocity (ft/s)	Area (ft^2)	Discharge (cfs)
0.0	0.00	0.00	0.00	0.00	0.00
1.0	0.15	0.00	0.00	0.07	0.00
2.0	0.20	0.00	0.00	0.17	0.00
3.0	0.20	0.76	0.38	0.20	0.07
4.0	0.39	1.12	0.94	0.30	0.28
5.0	0.49	0.85	0.99	0.44	0.44
6.0	0.69	0.91	0.88	0.59	0.52
7.0	0.79	0.34	0.63	0.74	0.46
8.0	0.49	0.48	0.41	0.64	0.26
9.0	0.49	0.24	0.36	0.49	0.18
10.0	0.39	1.75	1.00	0.44	0.44
11.0	0.30	1.44	1.60	0.34	0.55
12.0	0.20	0.13	0.79	0.25	0.19
12.7	0.00	0.00	0.07	0.07	0.00
				Total (cfs):	3.40
				(m3/s):	0.0962

The east branch of Spring Hollow Spring was measured on 4/7/2017 using a wading rod and flow meter.

Distance from bank (ft)	Depth (ft)	Velocity (ft/s)	Average velocity (ft/s)	Area (ft^2)	Discharge (cfs)
0.0	0.00	0.00	0.00	0.00	0.00
1.0	0.44	1.70	0.85	0.40	0.34
2.2	0.39	0.78	1.24	0.42	0.52
3.2	0.44	1.48	1.13	0.50	0.57
4.2	0.69	2.86	2.17	0.57	1.24
5.2	1.03	2.04	2.45	0.86	2.11

6.2	0.98	1.11	1.58	1.01	1.59
7.2	0.89	0.04	0.58	0.94	0.54
8.2	0.79	0.00	0.02	0.84	0.02
9.2	0.69	0.00	0.00	0.74	0.00
9.7	0.00	0.00	0.00	0.34	0.00
				Total (cfs):	6.91
				(m3/s):	0.196

Discharge measurements on 5/11/2017

Ricks Spring was measured on 5/11/2017 using a wading rod and flow meter.

Distance from bank (ft)	Depth (ft)	Velocity (ft/s)	Average velocity (ft/s)	Area (ft^2)	Discharge (cfs)
0.0	0.00	0.00	0.00	0.00	0.00
1.0	0.39	0.73	0.37	0.20	0.07
2.0	0.49	1.00	0.87	0.44	0.38
3.0	0.49	0.08	0.54	0.49	0.27
3.1	rock start	0.00	0.04	0.02	0.00
5.4	rock end	0.00	0.00	0.00	0.00
6.1	0.79	3.00	1.50	0.28	0.41
7.1	0.98	4.70	3.85	0.89	3.41
8.1	1.08	4.48	4.59	1.03	4.74
9.0	1.08	1.52	3.00	0.97	2.92
10.2	0.39	2.34	1.93	0.89	1.71
11.1	0.79	2.90	2.62	0.53	1.39
11.9	0.69	1.01	1.96	0.59	1.15
13.2	0.98	3.08	2.05	1.09	2.22
14.2	1.08	5.11	4.10	1.03	4.23
15.2	0.79	5.86	5.49	0.94	5.13
16.2	0.79	6.00	5.93	0.79	4.67
17.2	0.59	5.38	5.69	0.69	3.92
18.2	0.89	4.45	4.92	0.74	3.63
19.2	0.98	5.32	4.89	0.94	4.57
21.2	0.89	5.47	5.40	1.87	10.09
22.2	0.98	4.71	5.09	0.94	4.76
23.2	0.98	5.33	5.02	0.98	4.94
24.2	1.28	5.55	5.44	1.13	6.16
25.2	1.28	3.85	4.70	1.28	6.01
26.2	1.18	1.28	2.57	1.23	3.16
27.2	1.28	1.99	1.64	1.23	2.01
28.2	1.08	2.94	2.47	1.18	2.91
29.2	0.69	0.00	1.47	0.89	1.30
30.2	0.69	1.50	0.75	0.69	0.52
30.6	0.00	0.00	0.75	0.14	0.10

Total (cfs):	86.8
(m3/s):	2.46

Temple Fork was measured on 5/11/2017 using a wading rod and flow meter.

Distance from bank (ft)	Depth (ft)	Velocity (ft/s)	Average velocity (ft/s)	Area (ft^2)	Discharge (cfs)
0.0	0.00	0.00	0.00	0.00	0.00
1.0	0.79	0.40	0.20	0.39	0.08
2.0	0.89	3.17	1.79	0.84	1.49
3.0	1.28	3.85	3.51	1.08	3.80
4.0	1.38	3.16	3.51	1.33	4.66
5.0	1.28	3.63	3.40	1.33	4.51
6.0	1.28	4.91	4.27	1.28	5.46
7.0	1.57	4.39	4.65	1.43	6.64
8.0	1.57	2.74	3.57	1.57	5.61
9.0	1.57	2.81	2.78	1.57	4.37
10.0	1.57	3.01	2.91	1.57	4.58
11.0	1.67	4.52	3.77	1.62	6.11
12.0	1.48	4.72	4.62	1.57	7.28
13.0	1.38	4.85	4.79	1.43	6.83
14.0	1.38	3.32	4.09	1.38	5.63
15.0	1.38	3.54	3.43	1.38	4.73
16.0	1.18	3.06	3.30	1.28	4.22
16.5	0.00	0.00	1.53	0.30	0.45
				Total (cfs):	76.5
				(m3/s):	2.17

Benchmark Spring was measured on 5/11/2017 using a wading rod and flow meter.

Distance from bank (ft)	Depth (ft)	Velocity (ft/s)	Average velocity (ft/s)	Area (ft^2)	Discharge (cfs)
0.0	0.00	0.00	0.00	0.00	0.00
0.4	0.20	0.77	0.39	0.08	0.03
0.8	0.20	0.50	0.64	0.08	0.05
1.3	0.20	0.68	0.59	0.05	0.03
				Total (cfs):	0.11
				(m3/s):	0.00319

An overflow channel of Benchmark Spring was measured on 5/11/201 using a wading rod and flow meter.

Distance from bank (ft)	Depth (ft)	Velocity (ft/s)	Average velocity (ft/s)	Area (ft^2)	Discharge (cfs)
0.0	0.00	0.00	0.00	0.00	0.00
0.6	0.49	0.39	0.20	0.15	0.03
1.3	0.00	0.00	0.20	0.15	0.03
				Total (cfs):	0.06
				(m3/s):	0.00170

An unknown tributary draining Blind Hollow was measured on 5/11/2017 using the Crowe et al. (2001) method for pipe flow.

Pipe diameter (ft)	3.00
Sediment + Water depth (ft)	0.59
Sediment depth (ft)	0.00
Water depth (ft)	0.59
Velocity (ft/s)	3.38
Total (cfs):	3.33
(m3/s):	0.943

Cottonwood Creek was measured on 5/11/2017 using a wading rod and flow meter.

Distance from bank (ft)	Depth (ft)	Velocity (ft/s)	Average velocity (ft/s)	Area (ft^2)	Discharge (cfs)
0.0	0.69	2.98	2.98	0.00	0.00
1.0	0.89	4.08	3.53	0.79	2.78
2.0	0.69	4.61	4.35	0.79	3.42
3.0	0.98	5.04	4.83	0.84	4.04
4.0	1.08	4.92	4.98	1.03	5.15
5.0	1.18	5.13	5.03	1.13	5.69
6.0	0.89	5.11	5.12	1.03	5.29
7.0	0.98	4.08	4.60	0.94	4.30
8.0	0.69	2.22	3.15	0.84	2.64
9.0	0.49	1.25	1.74	0.59	1.02
10.7	0.00	0.00	0.63	0.42	0.26
				Total (cfs):	34.6
				(m3/s):	0.979

The channelized portion of Logan Cave Spring was measured on 5/11/201 using a wading rod and flow meter.

Distance from bank (ft)	Depth (ft)	Velocity (ft/s)	Average velocity (ft/s)	Area (ft^2)	Discharge (cfs)
0.0	0.00	0.00	0.00	0.00	0.00
1.0	0.39	0.69	0.35	0.20	0.07
2.0	0.49	2.77	1.73	0.44	0.77
3.0	0.59	2.45	2.61	0.00	0.00
3.7	0.59	1.04	1.75	0.00	0.00
3.8	0.59	0.00	0.52	0.00	0.00
				Total (cfs):	0.8
				(m3/s):	0.0236

The portion of Logan Cave Spring flowing through culverts was measured on 5/11/2017 using the Crowe et al. (2001) method for pipe flow.

Pipe diameter (ft)	2.00
Sediment + Water depth (ft)	1.08
Sediment depth (ft)	0.00
Water depth (ft)	1.08
Velocity (ft/s)	7.11

Total (cfs):	12.34
(m3/s):	0.349
Pipe diameter (ft)	2.00
Sediment + Water depth (ft)	1.18
Sediment depth (ft)	0.00
Water depth (ft)	1.18
Velocity (ft/s)	0.94
Total (cfs):	1.82
(m3/s):	0.0515

Woodcamp Hollow Spring was measured on 5/11/2017 using a wading rod and flow meter.

Distance from bank (ft)	Depth (ft)	Velocity (ft/s)	Average velocity (ft/s)	Area (ft^2)	Discharge (cfs)
0.0	0.00	0.00	0.00	0.00	0.00
1.0	0.69	0.00	0.00	0.34	0.00
1.7	0.00	0.00	0.00	0.00	0.00
2.5	1.28	1.38	0.69	0.51	0.35
3.5	1.57	1.62	1.50	1.43	2.14
4.5	1.57	3.04	2.33	1.57	3.67
5.5	1.38	5.05	4.05	1.48	5.97
6.5	1.87	5.27	5.16	1.62	8.38
7.5	1.67	5.49	5.38	1.77	9.53
8.5	1.77	5.71	5.60	1.72	9.65
9.5	1.77	5.41	5.56	1.77	9.85
10.5	1.48	5.11	5.26	1.62	8.54
11.5	0.89	4.81	4.96	1.18	5.86
12.5	0.59	5.21	5.01	0.74	3.70
13.5	0.98	4.60	4.91	0.79	3.86
14.5	0.59	0.08	2.34	0.79	1.84
15.9	0.00	0.00	0.04	1.00	0.04
				Total (cfs):	73.4
				(m3/s):	2.08

Woodcamp Hollow Creek was measured on 5/11/2017 using a wading rod and flow meter.

Distance from bank (ft)	Depth (ft)	Velocity (ft/s)	Average velocity (ft/s)	Area (ft^2)	Discharge (cfs)
0.0	0.00	0.00	0.00	0.00	0.00
1.0	0.49	1.75	0.88	0.25	0.22
2.0	0.89	2.88	2.32	0.69	1.60
3.0	0.98	4.54	3.71	0.94	3.47
4.0	1.08	3.45	4.00	1.03	4.13
5.0	1.38	3.17	3.31	1.23	4.07
6.0	1.28	2.40	2.79	1.33	3.70
7.0	1.38	4.83	3.62	1.33	4.80

8.0	1.57	3.35	4.09	1.48	6.04
9.0	1.48	7.43	5.39	1.53	8.22
10.0	1.38	1.17	4.30	1.43	6.14
10.5	0.00	0.00	0.59	0.34	0.20
13.5	0.00	0.00	0.00	0.00	0.00
14.0	0.30	1.91	0.96	0.07	0.07
15.0	0.49	2.69	2.30	0.39	0.91
16.7	0.00	0.00	1.35	0.42	0.56
				Total (cfs):	44.1
				(m3/s):	1.25

China Row Spring was measured on 5/11/2017 using the Crowe et al. (2001) method for pipe flow.

Pipe diameter (ft)	2.00
Sediment + Water depth (ft)	0.74
Sediment depth (ft)	0.25
Water depth (ft)	0.49
Velocity (ft/s)	0.29
Total (cfs):	0.24
(m3/s):	0.00685

Right Hand Fork was measured on 5/11/2017 using a wading rod and flow meter.

Distance from bank (ft)	Depth (ft)	Velocity (ft/s)	Average velocity (ft/s)	Area (ft^2)	Discharge (cfs)
0.0	0.00	0.00	0.00	0.00	0.00
0.5	0.30	0.04	0.02	0.07	0.00
1.5	0.69	1.27	0.66	0.49	0.32
2.5	1.08	5.35	3.31	0.89	2.93
3.5	0.98	6.27	5.81	1.03	6.00
4.5	1.28	3.60	4.94	1.13	5.59
5.5	0.98	5.09	4.35	1.13	4.92
6.5	1.38	4.48	4.79	1.18	5.65
7.5	1.18	4.98	4.73	1.28	6.05
8.5	0.98	5.09	5.04	1.08	5.45
9.5	0.79	4.61	4.85	1.08	5.25
10.5	0.98	3.70	4.16	0.89	3.68
11.1	0.00	0.00	1.85	0.30	0.55
				Total (cfs):	46.4
				(m3/s):	1.31

Dewitt Spring was measured on 5/11/2017 using a wading rod and flow meter.

Distance from bank (ft)	Depth (ft)	Velocity (ft/s)	Average velocity (ft/s)	Area (ft^2)	Discharge (cfs)
0.0	0.00	0.00	0.00	0.00	0.00
0.3	2.85	0.87	0.44	0.41	0.18
3.6	2.85	0.94	0.91	9.56	8.65

7.0	2.85	0.79	0.87	9.56	8.27
7.3	0.00	0.00	0.40	0.41	0.16
				Total (cfs):	17.3
				(m3/s):	0.489

Ann upslope tributary near Dewitt Spring was measured on 5/11/2017 using a wading rod and flow meter.

Distance from bank (ft)	Depth (ft)	Velocity (ft/s)	Average velocity (ft/s)	Area (ft^2)	Discharge (cfs)
0.0	0.00	0.00	0.00	0.00	0.00
1.0	0.39	0.94	0.47	0.20	0.09
2.0	0.79	1.25	1.10	0.59	0.65
3.0	0.39	1.63	1.44	0.59	0.85
4.0	0.69	2.02	1.83	0.54	0.99
5.0	0.69	0.20	1.11	0.69	0.76
6.0	0.39	0.30	0.25	0.54	0.14
7.2	0.00	0.00	0.15	0.24	0.04
				Total (cfs):	3.5
				(m3/s):	0.0995

The west branch of Spring Hollow Spring was measured on 5/11/2017 using a wading rod and flow meter.

Distance from bank (ft)	Depth (ft)	Velocity (ft/s)	Average velocity (ft/s)	Area (ft^2)	Discharge (cfs)
0.0	0.00	0.00	0.00	0.00	0.00
1.0	0.39	0.00	0.00	0.20	0.00
2.0	0.39	0.24	0.12	0.39	0.05
3.0	0.49	0.00	0.12	0.44	0.05
4.0	0.69	0.46	0.23	0.59	0.14
5.0	0.98	0.31	0.39	0.84	0.32
6.0	0.98	0.46	0.39	0.98	0.38
7.0	1.08	3.36	1.91	1.03	1.97
8.0	0.98	3.42	3.39	1.03	3.50
9.0	0.89	4.59	4.01	0.94	3.74
10.0	0.98	5.54	5.07	0.94	4.74
11.0	0.59	6.49	6.02	0.79	4.74
12.0	0.89	2.63	4.56	0.74	3.37
13.5	0.00	0.00	1.32	0.66	0.87
				Total (cfs):	23.9
				(m3/s):	0.676

The east branch of Spring Hollow Spring was measured on 5/11/2017 using a wading rod and flow meter.

Distance from bank (ft)	Depth (ft)	Velocity (ft/s)	Average velocity (ft/s)	Area (ft^2)	Discharge (cfs)
0.0	0.00	0.00	0.00	0.00	0.00
1.0	0.20	0.00	0.00	0.21	0.00
2.0	0.39	2.04	1.02	0.30	0.30
3.0	0.49	1.97	2.01	0.44	0.89

4.0	0.59	2.72	2.35	0.54	1.27
5.0	0.89	1.98	2.35	0.74	1.73
6.0	0.98	4.47	3.23	0.94	3.02
7.0	1.18	5.37	4.92	1.08	5.33
8.0	0.98	2.80	4.09	1.08	4.42
9.0	0.98	0.52	1.66	0.98	1.63
10.0	1.08	0.00	0.26	1.03	0.27
11.4	0.00	0.00	0.00	0.54	0.00
				Total (cfs):	18.9
				(m3/s):	0.534

Discharge measurements on 6/10/2017

Temple Fork was measured on 6/10/2017 using a wading rod and flow meter.

Distance from bank (ft)	Depth (ft)	Velocity (ft/s)	Average velocity (ft/s)	Area (ft^2)	Discharge (cfs)
0.0	0.00	0.00	0.00	0.00	0.00
1.1	1.28	2.18	1.09	0.70	0.77
2.1	1.28	3.57	2.88	1.28	3.68
3.1	1.08	4.11	3.84	1.18	4.54
4.1	1.28	2.90	3.51	1.18	4.14
5.1	1.38	3.27	3.09	1.33	4.10
6.1	1.38	3.17	3.22	1.38	4.44
7.1	1.38	3.84	3.51	1.38	4.83
8.1	1.38	3.88	3.86	1.38	5.32
9.1	1.57	4.34	4.11	1.48	6.07
10.1	1.48	3.62	3.98	1.53	6.07
11.1	1.48	3.25	3.44	1.48	5.07
12.1	1.48	2.99	3.12	1.48	4.61
13.1	1.38	3.17	3.08	1.43	4.40
14.1	1.28	3.37	3.27	1.33	4.35
15.2	0.00	0.00	1.69	0.70	1.19
				Total (cfs):	63.6
				(m3/s):	1.80

Benchmark Spring was measured on 6/10/2017 using a wading rod and flow meter.

Distance from bank (ft)	Depth (ft)	Velocity (ft/s)	Average velocity (ft/s)	Area (ft^2)	Discharge (cfs)
0.0	0.20	1.01	1.01	0.00	0.00
1.4	0.20	1.01	1.01	0.28	0.28
Overflow					
0.0	0.39	0.84	0.84	0.00	0.00
1.1	0.39	0.84	0.84	0.43	0.36
				Total (cfs):	0.64
				(m3/s):	0.0181

Cottonwood Creek was measured on 6/10/2017 using a wading rod and flow meter.

Distance from bank (ft)	Depth (ft)	Velocity (ft/s)	Average velocity (ft/s)	Area (ft^2)	Discharge (cfs)
0.0	0.59	0.92	0.92	0.00	0.00
1.1	0.79	3.46	2.19	0.76	1.66
2.1	0.98	4.40	3.93	0.89	3.48
3.1	1.08	5.36	4.88	1.03	5.04
4.1	1.18	4.67	5.02	1.13	5.68
5.1	1.08	5.21	4.94	1.13	5.59
6.1	0.79	4.99	5.10	0.94	4.77
7.1	0.79	4.10	4.55	0.79	3.58
8.1	0.49	2.76	3.43	0.64	2.19
9.1	0.59	1.43	2.10	0.54	1.13
10.1	0.20	0.35	0.89	0.39	0.35
11.0	0.00	0.00	0.18	0.09	0.02
				Total (cfs):	33.5
				(m3/s):	0.949

The channelized portion of Logan Cave Spring was measured on 6/10/2017 using a wading rod and flow meter.

Distance from bank (ft)	Depth (ft)	Velocity (ft/s)	Average velocity (ft/s)	Area (ft^2)	Discharge (cfs)
0.0	0.00	0.00	0.00	0.00	0.00
1.5	0.30	0.00	0.00	0.22	0.00
2.0	0.59	0.36	0.18	0.22	0.04
3.0	0.59	3.22	1.79	0.59	1.06
4.0	0.49	2.07	2.65	0.54	1.43
4.7	0.69	0.50	1.29	0.41	0.53
4.9	0.00	0.00	0.25	0.07	0.02
				Total (cfs):	3.08
				(m3/s):	0.0872

The portion of Logan Cave Spring flowing through culverts was measured on 6/10/2017 using the Crowe et al. (2001) method for pipe flow.

Pipe diameter (ft)	2.00
Sediment + Water depth (ft)	1.08
Sediment depth (ft)	0.00
Water depth (ft)	1.08
Velocity (ft/s)	0.35
Pipe diameter (ft)	2.00
Sediment + Water depth (ft)	1.28
Sediment depth (ft)	0.00
Water depth (ft)	1.28
Velocity (ft/s)	2.73

Total (cfs):	6.40
(m3/s):	0.181

Woodcamp Hollow Creek was measured on 6/10/2017 using a wading rod and flow meter.

Distance from bank (ft)	Depth (ft)	Velocity (ft/s)	Average velocity (ft/s)	Area (ft^2)	Discharge (cfs)
0.0	0.00	0.00	0.00	0.00	0.00
1.0	0.59	1.80	0.90	0.30	0.27
2.0	0.49	4.35	3.08	0.54	1.66
3.0	0.98	0.42	2.39	0.74	1.76
4.0	1.48	3.80	2.11	1.23	2.60
5.0	1.57	3.23	3.52	1.53	5.36
6.0	1.38	3.41	3.32	1.48	4.90
7.0	1.48	5.64	4.53	1.43	6.46
8.0	1.48	5.09	5.37	1.48	7.92
9.0	1.08	0.00	2.55	1.28	3.26
10.0	0.89	0.03	0.02	0.98	0.01
11.0	0.49	0.00	0.02	0.69	0.01
12.0	0.39	0.00	0.00	0.44	0.00
14.0	0.49	2.39	1.20	0.89	1.06
15.0	0.39	0.16	1.28	0.44	0.56
16.7	0.00	0.00	0.08	0.33	0.03
				Total (cfs):	35.9
				(m3/s):	1.02

China Row Spring was measured on 6/10/2017 using the Crowe et al. (2001) method for pipe flow.

Pipe diameter (ft)	2.00
Sediment + Water depth (ft)	0.66
Sediment depth (ft)	0.17
Water depth (ft)	0.49
Velocity (ft/s)	0.45
Total (cfs):	0.35
(m3/s):	0.00988

Right Hand Fork was measured on 6/10/2017 using a wading rod and flow meter.

Distance from bank (ft)	Depth (ft)	Velocity (ft/s)	Average velocity (ft/s)	Area (ft^2)	Discharge (cfs)
0.0	0.00	0.00	0.00	0.00	0.00
1.0	0.59	1.66	0.83	0.30	0.25
2.0	0.69	1.26	1.46	0.64	0.93
3.0	0.79	3.36	2.31	0.74	1.71
4.0	0.49	2.67	3.02	0.64	1.93
5.0	0.98	2.92	2.80	0.74	2.06
6.0	0.98	3.28	3.10	0.98	3.05
7.0	0.89	2.13	2.71	0.94	2.53

8.0	0.30	3.08	2.61	0.59	1.54
9.0	0.30	2.42	2.75	0.30	0.81
9.6	0.00	0.00	1.21	0.27	0.32
				Total (cfs):	15.1
				(m3/s):	0.428

Dewitt Spring was measured on 6/10/2017 using a wading rod and flow meter.

Distance from bank (ft)	Depth (ft)	Velocity (ft/s)	Average velocity (ft/s)	Area (ft^2)	Discharge (cfs)
0.0	0.00	0.00	0.00	0.00	0.00
0.3	4.23	0.76	0.38	0.60	0.23
3.6	4.23	2.62	1.69	14.18	23.96
7.0	4.23	2.64	2.63	14.18	37.29
7.3	0.00	0.00	1.32	0.60	0.79
				Total (cfs):	62.3
				(m3/s):	1.76

The west branch of Spring Hollow Spring was measured on 6/10/2017 using a wading rod and flow meter.

Distance from bank (ft)	Depth (ft)	Velocity (ft/s)	Average velocity (ft/s)	Area (ft^2)	Discharge (cfs)
0.0	0.00	0.00	0.00	0.00	0.00
3.0	0.59	0.64	0.32	0.89	0.28
4.0	0.59	4.81	2.73	0.59	1.61
5.0	0.79	3.99	4.40	0.69	3.03
6.0	0.79	4.98	4.49	0.79	3.53
7.0	1.18	3.97	4.48	0.98	4.40
8.0	1.28	0.01	1.99	1.23	2.45
9.0	1.18	4.14	2.08	1.23	2.55
10.0	1.28	5.79	4.97	1.23	6.11
11.0	1.48	7.25	6.52	1.38	8.98
12.0	0.98	6.83	7.04	1.23	8.66
13.0	1.28	3.09	4.96	1.13	5.61
14.0	1.08	3.46	3.28	1.18	3.87
15.0	0.00	0.00	1.73	0.54	0.94
				Total (cfs):	52.0
				(m3/s):	1.47

The east branch of Spring Hollow Spring was measured on 6/10/2017 using a wading rod and flow meter.

Distance from bank (ft)	Depth (ft)	Velocity (ft/s)	Average velocity (ft/s)	Area (ft^2)	Discharge (cfs)
0.0	0.00	0.00	0.00	0.00	0.00
1.0	0.69	1.96	0.98	0.17	0.17
2.0	0.69	0.99	1.48	0.69	1.02
3.0	0.49	0.73	0.86	0.59	0.51
4.0	0.69	3.47	2.10	0.59	1.24
5.0	1.08	4.76	4.12	0.89	3.65

6.0	0.89	1.26	3.01	0.98	2.96
7.0	0.89	2.99	2.13	0.89	1.88
8.0	0.69	3.18	3.09	0.79	2.43
9.0	0.39	0.06	1.62	0.54	0.88
9.5	0.00	0.00	0.03	0.20	0.01
				Total (cfs):	14.7
				(m3/s):	0.417

Discharge measurements on 7/8/2017

Ricks Spring was measured on 7/8/2017 using a wading rod and flow meter.

Distance from bank (ft)	Depth (ft)	Velocity (ft/s)	Average velocity (ft/s)	Area (ft^2)	Discharge (cfs)
0.0	0.00	0.00	0.00	0.00	0.00
1.0	0.39	0.64	0.32	0.20	0.06
2.0	0.39	0.81	0.73	0.39	0.29
3.0	0.30	0.00	0.41	0.34	0.14
Rock	0.00	0.00	0.00	0.00	0.00
6.6	1.08	3.48	1.74	1.95	3.39
7.6	0.98	3.66	1.83	1.03	3.69
8.6	1.08	2.36	3.01	1.03	3.11
9.7	0.30	0.81	1.59	0.76	1.20
10.8	0.89	0.98	0.90	0.65	0.58
11.8	0.30	0.54	0.76	0.59	0.45
12.8	0.30	2.87	1.71	0.30	0.50
13.8	0.89	3.69	3.28	0.59	1.94
14.8	0.89	4.23	3.96	0.89	3.51
15.8	0.89	0.40	2.32	0.89	2.05
16.8	0.69	3.99	2.20	0.79	1.73
17.8	0.98	2.91	3.45	0.84	2.89
18.8	0.89	2.27	2.59	0.94	2.42
19.8	0.59	2.34	2.31	0.74	1.70
20.8	0.49	3.59	2.97	0.54	1.61
21.8	0.69	4.04	3.82	0.59	2.25
22.8	0.69	3.03	3.54	0.69	2.44
23.8	0.59	2.40	2.72	0.64	1.74
24.8	0.49	2.09	2.25	0.54	1.22
25.8	0.49	0.53	1.31	0.49	0.64
26.9	0.39	1.54	1.04	0.44	0.46
27.9	0.79	0.99	1.27	0.65	0.82
28.9	0.30	0.00	0.50	0.54	0.27
29.9	0.20	0.14	0.07	0.25	0.02
30.9	0.00	0.00	0.07	0.10	0.01
				Total (cfs):	41.1

				(m3/s):	1.16

Temple Fork was measured on 7/8/2017 using a wading rod and flow meter.

Distance from bank (ft)	Depth (ft)	Velocity (ft/s)	Average velocity (ft/s)	Area (ft^2)	Discharge (cfs)
0.0	0.00	0.00	0.00	0.00	0.00
1.0	1.08	2.73	1.37	0.54	0.74
2.0	1.08	3.23	2.98	1.08	3.23
3.0	0.98	2.61	2.92	1.03	3.02
4.0	1.28	2.97	2.79	1.13	3.16
5.0	1.18	3.22	3.10	1.23	3.81
6.0	1.18	2.44	2.83	1.18	3.34
7.0	1.28	2.83	2.64	1.23	3.24
8.0	1.28	3.00	2.92	1.28	3.73
9.0	1.28	3.63	3.32	1.28	4.24
10.0	1.28	3.04	3.34	1.28	4.27
11.0	1.18	3.54	3.29	1.23	4.05
12.0	1.18	2.36	2.95	1.18	3.48
13.0	1.18	2.48	2.42	1.18	2.86
14.0	1.18	2.39	2.44	1.18	2.88
14.8	0.00	0.00	1.20	0.47	0.56
				Total (cfs):	46.6
				(m3/s):	1.32

Benchmark Spring was measured on 7/8/2017 using a wading rod and flow meter.

Distance from bank (ft)	Depth (ft)	Velocity (ft/s)	Average velocity (ft/s)	Area (ft^2)	Discharge (cfs)
0.0	0.10	0.00	0.00	0.00	0.00
0.8	0.20	1.31	0.66	0.11	0.07
1.5	0.10	0.00	0.66	0.11	0.07
				Total (cfs):	0.15
				(m3/s):	0.00411

Cottonwood Creek was measured on 7/8/2017 using a wading rod and flow meter.

Distance from bank (ft)	Depth (ft)	Velocity (ft/s)	Average velocity (ft/s)	Area (ft^2)	Discharge (cfs)
0.0	0.00	0.00	0.00	0.00	0.00
1.0	0.30	2.68	1.34	0.15	0.20
1.8	0.20	0.03	1.36	0.20	0.27
3.1	0.39	2.46	1.25	0.38	0.48
4.1	0.49	2.37	2.42	0.44	1.07
5.1	0.49	2.79	2.58	0.49	1.27
6.1	0.30	1.26	2.03	0.39	0.80
7.4	0.00	0.00	0.63	0.19	0.12
				Total (cfs):	4.20
				(m3/s):	0.119

The channelized portion of Logan Cave Spring was measured on 7/8/2017 using a wading rod and flow meter.

Distance from bank (ft)	Depth (ft)	Velocity (ft/s)	Average velocity (ft/s)	Area (ft^2)	Discharge (cfs)
0.0	0.00	0.00	0.00	0.00	0.00
1.0	0.39	1.03	0.52	0.20	0.10
2.0	0.69	2.13	1.58	0.54	0.86
3.0	0.59	1.55	1.84	0.64	1.18
3.3	0.69	0.00	0.78	0.19	0.15
				Total (cfs):	2.28
				(m3/s):	0.0646

The portion of Logan Cave Spring flowing through culverts was measured on 7/8/2017 using the Crowe et al. (2001) method for pipe flow.

Pipe diameter (ft)	2.00
Sediment + Water depth (ft)	0.20
Sediment depth (ft)	0.00
Water depth (ft)	0.20
Velocity (ft/s)	0.83
Total (cfs):	0.13
(m3/s):	0.00375

Woodcamp Hollow Spring was measured on 7/8/2017 using a wading rod and flow meter.

Distance from bank (ft)	Depth (ft)	Velocity (ft/s)	Average velocity (ft/s)	Area (ft^2)	Discharge (cfs)
0.0	0.00	0.00	0.00	0.00	0.00
0.5	1.18	0.09	0.05	0.30	0.01
1.5	1.28	7.05	3.57	1.23	4.39
2.5	1.38	3.89	5.47	1.33	7.27
3.5	1.38	3.48	3.69	1.38	5.08
4.5	1.67	4.33	3.91	1.53	5.96
5.5	1.77	1.37	2.85	1.72	4.91
6.5	1.67	1.32	1.35	1.72	2.32
7.5	1.87	1.92	1.62	1.77	2.87
8.5	1.18	1.15	1.54	1.53	2.34
9.5	1.48	0.04	0.60	1.33	0.79
10.5	0.69	4.69	2.37	1.08	2.56
11.5	0.79	3.75	4.22	0.74	3.12
12.5	0.69	0.22	1.99	0.74	1.47
12.8	0.00	0.00	0.11	0.10	0.01
				Total (cfs):	43.1
				(m3/s):	1.22

Woodcamp Hollow Creek was measured on 7/8/2017 using a wading rod and flow meter.

Distance from bank (ft)	Depth (ft)	Velocity (ft/s)	Average velocity (ft/s)	Area (ft^2)	Discharge (cfs)
0.0	0.00	0.00	0.00	0.00	0.00
1.8	0.20	0.00	0.00	0.18	0.00

3.0	0.49	2.13	1.07	0.41	0.44
4.0	0.69	1.22	1.68	0.59	0.99
5.0	0.69	1.07	1.15	0.69	0.79
6.0	0.79	2.01	1.54	0.74	1.14
7.0	0.79	1.25	1.63	0.79	1.28
7.6	0.00	0.00	0.63	0.24	0.15
9.2	0.00	0.00	0.00	0.00	0.00
9.9	0.20	0.30	0.15	0.07	0.01
10.7	0.00	0.00	0.15	0.08	0.01
				Total (cfs):	4.81
				(m3/s):	0.136

China Row Spring was measured on 7/8/2017 using the Crowe et al. (2001) method for pipe flow.

Pipe diameter (ft)	2.00
Sediment + Water depth (ft)	0.84
Sediment depth (ft)	0.25
Water depth (ft)	0.59
Velocity (ft/s)	0.45
Total (cfs):	0.46
(m3/s):	0.0131

Right Hand Fork was measured on 7/8/2017 using a wading rod and flow meter.

Distance from bank (ft)	Depth (ft)	Velocity (ft/s)	Average velocity (ft/s)	Area (ft^2)	Discharge (cfs)
0.0	0.00	0.00	0.00	0.00	0.00
1.0	0.39	0.51	0.26	0.20	0.05
2.0	0.59	1.99	1.25	0.49	0.62
3.0	0.79	1.12	1.56	0.69	1.07
4.0	0.59	2.09	1.61	0.69	1.11
5.0	0.39	4.41	3.25	0.49	1.60
6.0	0.79	4.03	4.22	0.59	2.49
7.0	0.98	0.68	2.36	0.89	2.09
8.0	0.49	1.95	1.32	0.74	0.97
8.6	0.30	1.19	1.57	0.24	0.37
9.7	0.20	0.00	0.60	0.27	0.16
10.3	0.00	0.00	0.00	0.06	0.00
				Total (cfs):	10.5
				(m3/s):	0.298

Dewitt Spring was measured on 7/8/2017 using a wading rod and flow meter.

Distance from bank (ft)	Depth (ft)	Velocity (ft/s)	Average velocity (ft/s)	Area (ft^2)	Discharge (cfs)
0.0	0.00	0.00	0.00	0.00	0.00
0.3	5.12	1.15	0.58	0.73	0.42
3.6	5.12	0.84	1.00	17.15	17.06

7.0	5.12	0.73	0.79	17.15	13.46
7.3	0.00	0.00	0.37	0.73	0.27
				Total (cfs):	31.2
				(m3/s):	0.884

The west branch of Spring Hollow Spring was measured on 7/8/2017 using a wading rod and flow meter.

Distance from bank (ft)	Depth (ft)	Velocity (ft/s)	Average velocity (ft/s)	Area (ft^2)	Discharge (cfs)
0.0	0.00	0.00	0.00	0.00	0.00
1.0	0.30	0.00	0.00	0.15	0.00
2.0	0.30	1.51	0.76	0.30	0.22
3.0	0.20	3.22	2.37	0.25	0.58
4.0	0.79	2.86	3.04	0.49	1.50
5.0	0.79	4.25	3.56	0.79	2.80
6.0	1.08	2.34	3.30	0.94	3.08
7.0	1.18	4.47	3.41	1.13	3.85
8.0	0.98	5.60	5.04	1.08	5.45
9.0	1.28	5.48	5.54	1.13	6.27
10.0	1.38	3.44	4.46	1.33	5.93
11.0	1.48	3.16	3.30	1.43	4.71
12.0	0.59	0.00	1.58	1.03	1.63
12.5	0.89	0.00	0.00	0.37	0.00
13.0	0.59	0.54	0.27	0.37	0.10
13.6	0.00	0.00	0.27	0.18	0.05
				Total (cfs):	36.2
				(m3/s):	1.02

The east branch if Spring Hollow Spring was measured on 7/8/2017 using a wading rod and flow meter.

Distance from bank (ft)	Depth (ft)	Velocity (ft/s)	Average velocity (ft/s)	Area (ft^2)	Discharge (cfs)
0.0	0.00	0.00	0.00	0.00	0.00
1.0	0.20	0.68	0.34	0.03	0.01
2.0	0.20	0.00	0.34	0.20	0.07
3.2	0.20	0.00	0.00	0.20	0.00
4.1	0.59	4.03	2.02	0.47	0.95
5.1	0.59	1.24	2.64	0.53	1.40
6.1	0.30	0.38	0.81	0.44	0.36
7.5	0.20	1.37	0.88	0.25	0.22
7.9	0.00	0.00	0.69	0.14	0.09
				Total (cfs):	3.10
				(m3/s):	0.0877

Discharge measurements on 8/13/2017

The upper Logan River was measured on 8/13/2017 using a wading rod and flow meter.

Distance from bank (ft)	Depth (ft)	Velocity (ft/s)	Average velocity (ft/s)	Area (ft^2)	Discharge (cfs)

0.0	0.00	0.00	0.00	0.00	0.00
2.0	0.98	0.39	0.20	0.98	0.19
4.0	0.79	0.41	0.40	1.77	0.71
6.0	1.08	0.70	0.56	1.87	1.04
8.0	1.18	2.69	1.70	2.26	3.84
10.0	1.28	1.47	2.08	2.46	5.12
12.0	1.28	2.89	2.18	2.56	5.58
14.0	0.98	2.80	2.85	2.26	6.44
16.0	0.89	2.52	2.66	1.87	4.97
18.0	1.38	2.14	2.33	2.26	5.27
20.0	1.48	1.87	2.01	2.85	5.72
22.0	1.08	2.50	2.19	2.56	5.59
24.0	1.08	3.19	2.85	2.17	6.16
26.0	0.89	2.41	2.80	1.97	5.51
28.0	1.08	1.09	1.75	1.97	3.44
30.0	1.18	1.30	1.20	2.26	2.71
32.0	1.28	2.34	1.82	2.46	4.48
34.0	1.48	2.86	2.60	2.76	7.17
36.0	1.57	1.97	2.42	3.05	7.37
38.0	1.67	4.36	3.17	3.25	10.28
40.0	1.18	3.65	4.01	2.85	11.43
42.0	0.59	0.42	2.04	1.77	3.61
43.5	0.00	0.00	0.21	0.59	0.12
				Total (cfs):	107
				(m3/s):	3.02

Ricks Spring was measured on 8/13/2017 using a wading rod and flow meter.

Distance from bank (ft)	Depth (ft)	Velocity (ft/s)	Average velocity (ft/s)	Area (ft^2)	Discharge (cfs)
0.0	0.00	0.00	0.00	0.00	0.00
1.0	0.20	0.36	0.18	0.10	0.02
2.0	0.20	0.00	0.18	0.20	0.04
2.1	rock start	0.00	0.00	0.01	0.00
4.9	rock end	0.00	0.00	0.00	0.00
5.9	0.89	3.61	1.81	0.44	0.80
7.0	0.89	3.72	3.67	0.97	3.57
7.8	rock start	0.00	1.86	0.35	0.66
9.3	rock end	0.00	0.00	0.00	0.00
10.1	0.69	0.88	0.44	0.28	0.12
11.2	rock start	0.00	0.44	0.38	0.17
12.1	rock end	0.00	0.00	0.00	0.00
13.1	0.69	2.72	1.36	0.34	0.47
14.1	0.59	1.66	2.19	0.64	1.40
15.1	0.39	0.09	0.88	0.49	0.43

16.1	0.39	2.98	1.54	0.39	0.60
17.1	0.69	2.21	2.60	0.54	1.40
18.1	0.59	2.17	2.19	0.64	1.40
19.1	0.49	0.34	1.26	0.54	0.68
20.1	0.20	1.30	0.82	0.34	0.28
21.1	0.49	1.40	1.35	0.34	0.47
22.1	0.39	2.02	1.71	0.44	0.76
23.1	0.49	1.44	1.73	0.44	0.77
24.1	0.30	0.50	0.97	0.39	0.38
25.1	0.49	0.42	0.46	0.39	0.18
26.3	0.49	0.01	0.22	0.59	0.13
27.3	0.39	0.60	0.31	0.44	0.14
28.5	0.00	0.00	0.30	0.24	0.07
				Total (cfs):	14.9
				(m3/s):	0.423

Temple Fork was measured on 8/13/2017 using a wading rod and flow meter.

Distance from bank (ft)	Depth (ft)	Velocity (ft/s)	Average velocity (ft/s)	Area (ft^2)	Discharge (cfs)
0.0	0.00	0.00	0.00	0.00	0.00
1.0	0.79	0.00	0.00	0.39	0.00
2.0	0.89	1.12	0.56	0.84	0.47
3.0	0.98	1.76	1.44	0.94	1.35
4.0	0.89	1.78	1.77	0.94	1.66
5.0	0.89	3.40	2.59	0.89	2.29
6.0	0.89	3.07	3.24	0.89	2.87
7.0	1.08	2.76	2.92	0.98	2.87
8.0	0.98	1.16	1.96	1.03	2.03
9.0	1.08	2.43	1.80	1.03	1.86
10.0	1.18	2.73	2.58	1.13	2.92
11.0	1.18	2.79	2.76	1.18	3.26
12.0	1.08	2.34	2.57	1.13	2.90
13.0	0.98	2.99	2.67	1.03	2.75
14.0	0.89	1.61	2.30	0.94	2.15
15.0	0.79	2.06	1.84	0.84	1.54
16.0	0.79	1.98	2.02	0.79	1.59
16.6	0.00	0.00	0.99	0.20	0.19
				Total (cfs):	32.7
				(m3/s):	0.926

Benchmark Spring was measured on 8/13/2017 using a wading rod and flow meter.

Distance from bank (ft)	Depth (ft)	Velocity (ft/s)	Average velocity (ft/s)	Area (ft^2)	Discharge (cfs)
0.0	0.10	0.09	0.09	0.00	0.00
0.8	0.20	0.85	0.47	0.11	0.05

1.5	0.15	0.25	0.55	0.13	0.07
				Total (cfs):	0.12
				(m3/s):	0.00349

The channelized portion of Logan Cave Spring was measured on 8/13/2017 using a wading rod and flow meter.

Distance from bank (ft)	Depth (ft)	Velocity (ft/s)	Average velocity (ft/s)	Area (ft^2)	Discharge (cfs)
0.0	0.00	0.00	0.00	0.00	0.00
1.0	0.39	0.87	0.44	0.20	0.09
2.2	0.49	2.47	1.67	0.53	0.89
3.2	0.49	1.30	1.89	0.49	0.93
3.6	0.39	0.09	0.70	0.18	0.12
				Total (cfs):	2.02
				(m3/s):	0.0573

The portion of Logan Cave Spring flowing through culverts was measured on 8/13/2017 using the Crowe et al. (2001) method for pipe flow.

Pipe diameter (ft)	2.00
Sediment + Water depth (ft)	0.20
Sediment depth (ft)	0.00
Water depth (ft)	0.20
Velocity (ft/s)	0.85
Total (cfs):	0.14
(m3/s):	0.00385

Woodcamp Hollow Spring was measured on 8/13/2017 using a wading rod and flow meter.

Distance from bank (ft)	Depth (ft)	Velocity (ft/s)	Average velocity (ft/s)	Area (ft^2)	Discharge (cfs)
0.0	0.00	0.00	0.00	0.00	0.00
0.2	0.20	2.25	1.13	0.02	0.02
0.5	0.00	0.00	1.13	0.03	0.03
2.6	0.00	0.00	0.00	0.00	0.00
2.7	0.30	4.22	2.11	0.01	0.03
2.8	0.00	0.00	2.11	0.01	0.03
3.8	0.00	0.00	0.00	0.00	0.00
4.8	0.49	0.49	0.25	0.25	0.06
5.8	0.98	1.30	0.90	0.74	0.66
6.7	0.79	2.93	2.12	0.80	1.69
7.7	0.79	3.94	3.44	0.79	2.70
8.7	1.08	5.07	4.51	0.94	4.21
10.7	0.98	6.73	5.90	2.07	12.20
11.7	0.69	3.94	5.34	0.84	4.46
12.7	0.59	0.91	2.43	0.64	1.55
13.7	0.30	1.15	1.03	0.44	0.46
14.7	0.20	2.73	1.94	0.25	0.48

15.2	0.00	0.00	1.37	0.05	0.07
				Total (cfs):	28.7
				(m3/s):	0.811

Woodcamp Hollow Creek was measured on 8/13/2017 using a wading rod and flow meter.

Distance from bank (ft)	Depth (ft)	Velocity (ft/s)	Average velocity (ft/s)	Area (ft^2)	Discharge (cfs)
0.0	0.10	0.00	0.00	0.00	0.00
1.0	0.10	0.85	0.43	0.10	0.04
2.0	0.30	0.00	0.43	0.20	0.08
3.0	0.49	4.50	2.25	0.39	0.89
4.0	0.59	1.57	3.04	0.54	1.64
5.0	0.39	0.37	0.97	0.49	0.48
5.1	0.00	0.00	0.19	0.02	0.00
				Total (cfs):	3.14
				(m3/s):	0.0888

China Row Spring was measured on 8/13/2017 using a wading rod and flow meter.

Pipe Diameter (ft)		2.00
Sediment + water depth (ft)		0.84
Sediment depth (ft)		0.25
Water depth (ft)		0.59
Velocity (ft/s)		0.26
	Total (cfs):	0.27
	(m3/s):	0.00756

The middle Logan River was measured on 8/13/2017 using a wading rod and flow meter.

Distance from bank (ft)	Depth (ft)	Velocity (ft/s)	Average velocity (ft/s)	Area (ft^2)	Discharge (cfs)
0.0	0.00	0.00	0.00	0.00	0.00
3.0	0.69	1.37	0.69	1.03	0.71
6.0	1.18	1.61	1.49	2.81	4.18
9.0	1.38	2.08	1.85	3.84	7.08
12.0	1.57	2.24	2.16	4.43	9.57
15.0	1.67	1.89	2.07	4.87	10.06
18.0	1.67	3.10	2.50	5.02	12.52
21.0	1.97	3.02	3.06	5.46	16.72
24.0	1.97	2.67	2.85	5.91	16.80
27.0	1.97	2.27	2.47	5.91	14.59
30.0	2.17	2.21	2.24	6.20	13.89
33.0	1.87	2.36	2.29	6.05	13.83
36.0	2.26	2.42	2.39	6.20	14.82
39.0	2.46	3.41	2.92	7.09	20.66
42.0	2.46	2.66	3.04	7.38	22.40
45.0	1.77	2.03	2.35	6.35	14.89

48.0	0.79	1.55	1.79	3.84	6.87
50.0	0.00	0.00	0.78	0.79	0.61
				Total (cfs):	200
				(m3/s):	5.67

Right Hand Fork was measured on 8/13/2017 using a wading rod and flow meter.

Distance from bank (ft)	Depth (ft)	Velocity (ft/s)	Average velocity (ft/s)	Area (ft^2)	Discharge (cfs)
0.0	0.00	0.00	0.00	0.00	0.00
1.0	0.59	1.01	0.51	0.30	0.15
2.0	0.79	2.80	1.91	0.69	1.31
3.0	0.98	2.92	2.86	0.89	2.53
4.0	0.89	0.35	1.64	0.94	1.53
5.0	0.69	2.98	1.67	0.79	1.31
6.0	0.98	3.15	3.07	0.84	2.56
7.0	0.69	2.80	2.98	0.84	2.49
8.0	0.69	0.50	1.65	0.69	1.14
9.0	0.39	0.01	0.26	0.54	0.14
10.7	0.00	0.00	0.01	0.59	0.00
				Total (cfs):	13.2
				(m3/s):	0.373

Dewitt Spring was measured on 8/13/2017 using a wading rod and flow meter.

Distance from bank (ft)	Depth (ft)	Velocity (ft/s)	Average velocity (ft/s)	Area (ft^2)	Discharge (cfs)
0.0	0.00	0.00	0.00	0.00	0.00
0.3	0.69	2.85	1.43	0.10	0.14
3.6	0.69	1.86	2.36	2.31	5.44
7.0	0.69	1.90	1.88	2.31	4.34
7.3	0.00	0.00	0.95	0.10	0.09
				Total (cfs):	10.0
				(m3/s):	0.283

The lower Logan River was measured on 8/13/2017 using a wading rod and flow meter.

Distance from bank (ft)	Depth (ft)	Velocity (ft/s)	Average velocity (ft/s)	Area (ft^2)	Discharge (cfs)
0.0	0.00	0.00	0.00	0.00	0.00
3.0	2.26	0.82	0.41	3.40	1.39
6.0	2.85	1.66	1.24	7.68	9.52
9.0	2.76	2.53	2.10	8.42	17.63
12.0	2.66	2.97	2.75	8.12	22.33
15.0	2.76	3.18	3.08	8.12	24.97
18.0	2.76	2.92	3.05	8.27	25.22
21.0	2.76	2.91	2.92	8.27	24.10
24.0	2.66	2.60	2.76	8.12	22.37
27.0	2.66	3.08	2.84	7.97	22.64

30.0	2.56	2.77	2.93	7.83	22.89
33.0	2.26	2.65	2.71	7.23	19.61
36.0	2.17	2.58	2.62	6.65	17.39
39.0	1.87	2.14	2.36	6.06	14.30
42.0	1.57	1.73	1.94	5.17	10.00
45.0	0.98	0.40	1.07	3.84	4.09
46.3	0.00	0.00	0.20	0.64	0.13
				Total (cfs):	259
				(m3/s):	7.32

The lower Logan River side channel was measured on 8/13/2017 using a wading rod and flow meter.

Distance from bank (ft)	Depth (ft)	Velocity (ft/s)	Average velocity (ft/s)	Area (ft^2)	Discharge (cfs)
0.0	0.00	0.00	0.00	0.00	0.00
1.0	0.20	0.00	0.00	0.10	0.05
2.0	0.30	0.00	0.00	0.25	0.00
3.0	0.49	0.00	0.00	0.39	0.00
4.0	0.69	0.00	0.00	0.59	0.00
5.0	0.79	0.00	0.00	0.74	0.00
6.0	0.79	0.00	0.00	0.79	0.00
7.0	0.69	0.08	0.04	0.74	0.03
8.0	0.79	0.44	0.26	0.74	0.19
9.0	0.79	0.31	0.38	0.79	0.30
10.0	0.79	0.26	0.29	0.79	0.22
11.0	0.59	0.12	0.19	0.69	0.13
12.0	0.39	0.00	0.06	0.49	0.03
13.0	0.20	0.00	0.00	0.30	0.00
14.0	0.00	0.00	0.00	0.10	0.00
				Total (cfs):	0.95
				(m3/s):	0.0269

The west branch of Spring Hollow Spring was measured on 8/13/2017 using a wading rod and flow meter.

Distance from bank (ft)	Depth (ft)	Velocity (ft/s)	Average velocity (ft/s)	Area (ft^2)	Discharge (cfs)
0.0	0.00	0.00	0.00	0.00	0.00
1.0	0.20	0.32	0.16	0.10	0.02
2.0	0.30	0.59	0.46	0.25	0.11
2.7	0.30	1.09	0.84	0.21	0.17
3.8	0.39	0.13	0.61	0.38	0.23
5.0	0.69	3.12	1.63	0.65	1.06
6.0	0.59	4.11	3.62	0.64	2.31
7.1	0.79	4.48	4.30	0.76	3.26
8.1	0.89	1.81	3.15	0.84	2.63
9.1	0.98	3.81	2.81	0.94	2.63
10.8	0.39	0.97	2.39	1.17	2.80

12.0	0.00	0.00	0.49	0.24	0.11
				Total (cfs):	15.3
				(m3/s):	0.434

The east branch of Spring Hollow Spring was measured on 8/13/2017 using a wading rod and flow meter.

Distance from bank (ft)	Depth (ft)	Velocity (ft/s)	Average velocity (ft/s)	Area (ft^2)	Discharge (cfs)
0.0	0.00	0.00	0.00	0.00	0.00
1.0	0.30	1.11	0.56	0.06	0.03
2.0	0.39	0.14	0.63	0.34	0.22
3.1	0.30	0.17	0.16	0.34	0.05
4.1	0.79	3.57	1.87	0.60	1.11
5.1	0.79	2.06	2.82	0.79	2.22
6.1	0.39	0.14	1.10	0.59	0.65
7.1	0.39	2.40	1.27	0.39	0.50
8.1	0.30	0.19	1.30	0.34	0.45
8.4	0.00	0.00	0.10	0.15	0.01
				Total (cfs):	5.24
				(m3/s):	0.148

Discharge measurements on 9/9/2017

The upper Logan River was measured on 9/9/2017 using a wading rod and flow meter.

Distance from bank (ft)	Depth (ft)	Velocity (ft/s)	Average velocity (ft/s)	Area (ft^2)	Discharge (cfs)
0.0	0.00	0.00	0.00	0.00	0.00
2.0	0.89	0.70	0.35	0.89	0.31
4.0	0.79	0.79	0.75	1.67	1.25
6.0	0.79	1.43	1.11	1.57	1.75
8.0	0.98	1.99	1.71	1.77	3.03
10.0	1.08	1.24	1.62	2.07	3.34
12.0	0.89	1.43	1.34	1.97	2.63
14.0	1.08	1.17	1.30	1.97	2.56
16.0	1.18	1.82	1.50	2.26	3.38
18.0	1.18	1.00	1.41	2.36	3.33
20.0	0.79	1.43	1.22	1.97	2.39
22.0	1.18	2.48	1.96	1.97	3.85
24.0	1.18	1.70	2.09	2.36	4.94
26.0	1.28	1.68	1.69	2.46	4.16
28.0	1.18	2.08	1.88	2.46	4.63
30.0	0.79	2.44	2.26	1.97	4.45
32.0	1.18	2.29	2.37	1.97	4.66
34.0	1.18	3.64	2.97	2.36	7.00
36.0	0.59	1.57	2.61	1.77	4.62
38.0	0.30	0.02	0.80	0.89	0.70

39.2	0.00	0.00	0.01	0.18	0.00
				Total (cfs):	63.0
				(m3/s):	1.78

Ricks Spring was measured on 9/9/2017 using a wading rod and flow meter.

Distance from bank (ft)	Depth (ft)	Velocity (ft/s)	Average velocity (ft/s)	Area (ft^2)	Discharge (cfs)
0.0	0.00	0.00	0.00	0.00	0.00
1.1	0.49	0.48	0.24	0.27	0.06
2.1	0.69	3.13	1.81	0.59	1.07
2.7	0.49	1.54	2.34	0.35	0.83
2.8	rock start	0.00	0.77	0.02	0.02
4.7	rock end	0.00	0.00	0.00	0.00
4.8	0.39	1.66	0.83	0.02	0.02
5.9	0.30	0.47	1.07	0.38	0.40
6.1	rock start	0.00	0.24	0.03	0.01
6.9	rock end	0.00	0.00	0.00	0.00
7.1	0.49	0.89	0.45	0.05	0.02
8.1	0.59	2.28	1.59	0.54	0.86
9.1	0.30	2.12	2.20	0.44	0.97
10.1	0.10	1.78	1.95	0.20	0.38
11.1	0.30	1.30	1.54	0.20	0.30
12.1	0.59	2.31	1.81	0.44	0.80
13.1	0.30	1.58	1.95	0.44	0.86
14.1	0.20	2.06	1.82	0.25	0.45
15.4	0.39	0.92	1.49	0.38	0.57
16.4	0.49	0.56	0.74	0.44	0.33
17.4	0.39	1.28	0.92	0.44	0.41
18.4	0.49	1.07	1.18	0.44	0.52
19.4	0.39	0.25	0.66	0.44	0.29
20.4	0.30	0.19	0.22	0.34	0.08
22.1	0.39	0.29	0.24	0.59	0.14
23.2	0.00	0.00	0.15	0.22	0.03
				Total (cfs):	9.42
				(m3/s):	0.267

Temple Fork was measured on 9/9/2017 using a wading rod and flow meter.

Distance from bank (ft)	Depth (ft)	Velocity (ft/s)	Average velocity (ft/s)	Area (ft^2)	Discharge (cfs)
0.0	0.20	0.00	0.00	0.00	0.00
1.0	0.69	0.12	0.06	0.44	0.03
2.0	0.89	1.09	0.61	0.79	0.48
3.0	0.79	0.95	1.02	0.84	0.85
4.0	0.79	1.73	1.34	0.79	1.06
5.0	0.79	3.03	2.38	0.79	1.87

6.0	0.69	2.18	2.61	0.74	1.92
7.0	0.89	2.72	2.45	0.79	1.93
8.0	0.79	1.01	1.87	0.84	1.56
9.0	0.89	2.28	1.65	0.84	1.38
10.0	0.98	2.68	2.48	0.94	2.32
11.0	1.08	2.30	2.49	1.03	2.57
12.0	0.98	2.00	2.15	1.03	2.22
13.0	0.89	2.99	2.50	0.94	2.33
14.0	0.79	1.13	2.06	0.84	1.72
15.0	0.79	2.44	1.79	0.79	1.41
16.0	0.69	1.15	1.80	0.74	1.33
18.0	0.00	0.00	0.58	0.69	0.40
				Total (cfs):	25.4
				(m3/s):	0.719

Benchmark Spring was measured on 9/9/2017 using the Crowe et al. (2001) method for pipe flow.

Pipe diameter (ft)	1.50
Sediment + Water depth (ft)	0.20
Sediment depth (ft)	0.00
Water depth (ft)	0.20
Velocity (ft/s)	0.53
Total (cfs):	0.07
(m3/s):	0.00198

The channelized portion of Logan Cave Spring was measured on 9/9/2017 using a wading rod and flow meter.

Distance from bank (ft)	Depth (ft)	Velocity (ft/s)	Average velocity (ft/s)	Area (ft^2)	Discharge (cfs)
0.0	0.00	0.00	0.00	0.00	0.00
1.0	0.30	0.84	0.42	0.15	0.06
2.0	0.39	2.88	1.86	0.34	0.64
3.0	0.20	1.01	1.95	0.30	0.57
3.3	0.30	0.11	0.56	0.07	0.04
3.4	0.30	0.00	0.06	0.03	0.00
				Total (cfs):	1.32
				(m3/s):	0.0374

The portion of Logan Cave Spring flowing through culverts was measured on 9/9/2017 using the Crowe et al. (2001) method for pipe flow.

Pipe diameter (ft)	2.00
Sediment + Water depth (ft)	0.17
Sediment depth (ft)	0.00
Water depth (ft)	0.17
Velocity (ft/s)	0.62
Total (cfs):	0.08
(m3/s):	0.00227

Woodcamp Hollow Spring was measured on 9/9/2017 using a wading rod and flow meter.

Distance from bank (ft)	Depth (ft)	Velocity (ft/s)	Average velocity (ft/s)	Area (ft^2)	Discharge (cfs)
0.0	0.00	0.00	0.00	0.00	0.00
1.8	0.30	0.27	0.14	0.27	0.04
2.8	0.98	1.02	0.65	0.64	0.41
3.8	1.28	0.24	0.63	1.13	0.71
4.8	1.18	1.87	1.06	1.23	1.30
5.8	1.18	0.00	0.94	1.18	1.10
6.8	1.18	4.19	2.10	1.18	2.47
7.8	0.39	4.15	4.17	0.79	3.28
8.8	0.69	3.56	3.86	0.54	2.09
9.8	0.69	3.24	3.40	0.69	2.34
10.8	0.79	0.89	2.07	0.74	1.52
11.8	0.49	0.62	0.76	0.64	0.48
12.8	0.49	0.61	0.62	0.49	0.30
13.8	0.39	0.00	0.31	0.44	0.14
15.7	0.00	0.00	0.00	0.37	0.00
				Total (cfs):	16.2
				(m3/s):	0.459

Woodcamp Hollow Creek was measured on 9/9/2017 using a wading rod and flow meter.

Distance from bank (ft)	Depth (ft)	Velocity (ft/s)	Average velocity (ft/s)	Area (ft^2)	Discharge (cfs)
0.0	0.00	0.00	0.00	0.00	0.00
1.2	0.08	0.42	0.21	0.05	0.01
1.4	0.00	0.00	0.21	0.01	0.00
2.7	0.00	0.00	0.00	0.00	0.00
3.0	0.49	0.00	0.00	0.07	0.00
3.8	0.49	0.03	0.02	0.39	0.01
4.8	0.49	0.92	0.48	0.49	0.23
6.7	0.00	0.00	0.46	0.47	0.22
				Total (cfs):	0.47
				(m3/s):	0.0132

China Row Spring was measured on 9/9/2017 using the Crowe et al. (2001) method for pipe flow.

Pipe diameter (ft)	2.00
Sediment + Water depth (ft)	0.75
Sediment depth (ft)	0.17
Water depth (ft)	0.58
Velocity (ft/s)	0.22
Total (cfs):	0.21
(m3/s):	0.00593

The middle Logan River was measured on 9/9/2017 using a wading rod and flow meter.

Distance from bank (ft)	Depth (ft)	Velocity (ft/s)	Average velocity (ft/s)	Area (ft^2)	Discharge (cfs)
0.0	0.00	0.00	0.00	0.00	0.00
3.0	0.98	1.95	0.98	1.48	1.44
6.0	2.17	2.30	2.13	4.72	10.04
9.0	2.46	2.53	2.42	6.94	16.76
12.0	2.07	2.35	2.44	6.79	16.57
15.0	1.77	2.43	2.39	5.76	13.76
18.0	1.77	2.24	2.34	5.32	12.41
21.0	1.97	1.69	1.97	5.61	11.02
24.0	1.48	2.78	2.24	5.17	11.55
27.0	1.67	2.53	2.66	4.72	12.54
30.0	1.48	2.70	2.62	4.72	12.35
33.0	1.48	2.35	2.53	4.43	11.18
36.0	1.48	1.94	2.15	4.43	9.50
39.0	1.08	1.97	1.96	3.84	7.50
42.0	0.98	1.27	1.62	3.10	5.02
45.0	0.59	0.90	1.09	2.36	2.56
48.0	0.00	0.00	0.45	0.89	0.40
				Total (cfs):	155
				(m3/s):	4.38

Right Hand Fork was measured on 9/9/2017 using a wading rod and flow meter.

Distance from bank (ft)	Depth (ft)	Velocity (ft/s)	Average velocity (ft/s)	Area (ft^2)	Discharge (cfs)
0.0	0.00	0.00	0.00	0.00	0.00
0.4	0.00	0.00	0.00	0.00	0.00
1.2	0.30	0.84	0.42	0.12	0.05
2.2	0.79	1.45	1.15	0.54	0.62
3.4	0.89	3.06	2.26	1.00	2.26
4.7	0.39	2.34	2.70	0.83	2.25
5.6	0.69	2.41	2.38	0.49	1.16
6.5	0.98	2.49	2.45	0.75	1.84
7.5	0.69	2.33	2.41	0.84	2.02
8.3	0.59	0.22	1.28	0.51	0.65
9.5	0.00	0.00	0.11	0.59	0.06
11.1	0.00	0.00	0.00	0.55	0.00
				Total (cfs):	10.9
				(m3/s):	0.309

Dewitt Spring was measured on 9/9/2017 using a wading rod and flow meter.

Distance from bank (ft)	Depth (ft)	Velocity (ft/s)	Average velocity (ft/s)	Area (ft^2)	Discharge (cfs)
0.0	0.00	0.00	0.00	0.00	0.00
0.3	0.79	1.76	0.88	0.11	0.10

3.6	0.79	2.27	2.02	2.64	5.32
7.0	0.79	1.74	2.01	2.64	5.29
7.3	0.00	0.00	0.87	0.11	0.10
				Total (cfs):	10.8
				(m3/s):	0.306

The lower Logan River was measured on 9/9/2017 using a wading rod and flow meter.

Distance from bank (ft)	Depth (ft)	Velocity (ft/s)	Average velocity (ft/s)	Area (ft^2)	Discharge (cfs)
0.0	0.00	0.00	0.00	0.00	0.00
3.0	1.77	0.59	0.30	2.66	0.78
6.0	2.56	1.45	1.02	6.50	6.63
9.0	2.36	2.35	1.90	7.38	14.03
12.0	2.26	2.32	2.34	6.94	16.20
15.0	2.46	2.40	2.36	7.09	16.72
18.0	2.46	2.62	2.51	7.38	18.53
21.0	2.36	2.29	2.46	7.23	17.76
24.0	2.36	2.35	2.32	7.09	16.44
27.0	2.36	2.48	2.42	7.09	17.11
30.0	2.17	2.29	2.39	6.79	16.20
33.0	1.97	2.35	2.32	6.20	14.39
36.0	1.77	1.90	2.13	5.61	11.92
39.0	1.57	2.03	1.97	5.02	9.86
42.0	1.38	1.48	1.76	4.43	7.77
45.0	0.69	0.49	0.99	3.10	3.05
45.8	0.00	0.00	0.25	0.28	0.07
				Total (cfs):	187
				(m3/s):	5.31

The lower Logan River side channel was measured on 9/9/2017 using a wading rod and flow meter.

Distance from bank (ft)	Depth (ft)	Velocity (ft/s)	Average velocity (ft/s)	Area (ft^2)	Discharge (cfs)
0.0	0.00	0.00	0.00	0.00	0.00
3.8	0.59	0.18	0.09	1.12	0.10
4.8	0.59	0.72	0.45	0.59	0.27
5.8	0.59	0.05	0.39	0.59	0.23
				Total (cfs):	0.59
				(m3/s):	0.0168

The west branch of Spring Hollow Spring was measured on 9/9/2017 using a wading rod and flow meter.

Distance from bank (ft)	Depth (ft)	Velocity (ft/s)	Average velocity (ft/s)	Area (ft^2)	Discharge (cfs)
0.0	0.00	0.00	0.00	0.00	0.00
1.1	0.30	0.00	0.00	0.16	0.00
2.1	0.49	0.35	0.18	0.39	0.07
3.1	0.69	0.13	0.24	0.59	0.14

4.1	0.79	0.29	0.21	0.74	0.16
5.1	0.69	1.08	0.69	0.74	0.51
6.1	0.79	1.82	1.45	0.74	1.07
7.1	1.28	1.23	1.53	1.03	1.58
8.1	1.18	1.83	1.53	1.23	1.88
8.8	0.89	1.81	1.82	0.72	1.32
10.1	0.49	1.60	1.71	0.90	1.53
11.2	0.00	0.00	0.80	0.27	0.22
				Total (cfs):	8.46
				(m3/s):	0.240

The east branch of Spring Hollow Spring was measured on 9/9/2017 using a wading rod and flow meter.

Distance from bank (ft)	Depth (ft)	Velocity (ft/s)	Average velocity (ft/s)	Area (ft^2)	Discharge (cfs)
0.0	0.00	0.00	0.00	0.00	0.00
1.1	0.30	0.65	0.33	0.06	0.02
1.9	0.30	0.35	0.50	0.32	0.16
3.4	0.30	0.16	0.26	0.24	0.06
4.1	0.69	1.85	1.01	0.74	0.74
5.1	0.59	1.21	1.53	0.45	0.69
6.1	0.20	0.00	0.61	0.39	0.24
6.9	0.39	1.20	0.60	0.30	0.18
7.9	0.30	1.46	1.33	0.28	0.37
9.5	0.00	0.00	0.73	0.15	0.11
				Total (cfs):	2.56
				(m3/s):	0.0725

Discharge measurements on 10/7/2017

The upper Logan River was measured on 10/7/2017 using a wading rod and flow meter.

Distance from bank (ft)	Depth (ft)	Velocity (ft/s)	Average velocity (ft/s)	Area (ft^2)	Discharge (cfs)
0.0	0.00	0.00	0.00	0.00	0.00
2.1	0.69	0.52	0.26	0.72	0.19
3.7	0.79	1.72	1.12	1.18	1.32
5.4	0.69	2.34	2.03	1.25	2.55
7.1	0.79	3.46	2.90	1.25	3.64
9.1	0.49	2.13	2.80	1.28	3.58
11.1	0.49	3.90	3.02	0.98	2.97
13.1	1.38	1.94	2.92	1.87	5.46
15.1	1.18	1.39	1.67	2.56	4.26
17.1	0.49	3.37	2.38	1.67	3.98
19.1	0.49	3.02	3.20	0.98	3.14
21.1	0.49	2.69	2.86	0.98	2.81
23.1	0.89	1.41	2.05	1.38	2.82
25.1	0.98	1.33	1.37	1.87	2.56
27.1	0.98	0.40	0.87	1.97	1.70
29.1	0.69	1.35	0.88	1.67	1.46

31.1	1.18	1.76	1.56	1.87	2.91
33.1	1.18	2.60	2.18	2.36	5.15
35.1	1.28	2.84	2.72	2.46	6.69
36.9	0.00	0.00	1.42	1.15	1.64
				Total (cfs):	58.8
				(m3/s):	1.67

Ricks Spring was measured on 10/7/2017 using a wading rod and flow meter.

Distance from bank (ft)	Depth (ft)	Velocity (ft/s)	Average velocity (ft/s)	Area (ft^2)	Discharge (cfs)
0.0	0.00	0.00	0.00	0.00	0.00
0.4	0.59	2.42	1.21	0.12	0.14
1.4	0.39	3.77	3.10	0.49	1.52
2.4	0.49	2.50	3.14	0.44	1.39
2.8	rock start	0.00	1.25	0.10	0.12
4.6	rock end	0.00	0.00	0.00	0.00
4.8	0.30	2.01	1.01	0.03	0.03
5.3	0.30	1.06	1.54	0.15	0.23
5.8	0.20	0.32	0.69	0.12	0.08
5.9	0.00	0.00	0.16	0.01	0.00
6.9	0.00	0.00	0.00	0.00	0.00
7.1	0.39	0.49	0.25	0.04	0.01
8.0	0.39	2.17	1.33	0.35	0.47
8.8	0.20	1.90	2.04	0.24	0.48
9.3	rock start	0.00	0.95	0.05	0.05
9.8	rock end	0.00	0.00	0.00	0.00
10.5	0.30	1.45	0.73	0.10	0.07
11.8	0.39	1.57	1.51	0.45	0.68
12.8	0.20	0.20	0.89	0.30	0.26
13.7	0.10	1.65	0.93	0.13	0.12
14.3	0.30	0.60	1.13	0.12	0.13
14.5	rock start	0.00	0.30	0.03	0.01
15.0	rock end	0.00	0.00	0.00	0.00
15.2	0.30	0.71	0.36	0.03	0.01
16.3	0.39	0.65	0.68	0.38	0.26
17.3	0.30	0.73	0.69	0.34	0.24
18.3	0.39	0.92	0.83	0.34	0.28
19.3	0.30	0.31	0.62	0.34	0.21
20.3	0.49	0.02	0.17	0.39	0.06
21.8	0.39	0.25	0.14	0.66	0.09
22.9	0.00	0.00	0.13	0.22	0.03
				Total (cfs):	6.99
				(m3/s):	0.198

Temple Fork was measured on 10/7/2017 using a wading rod and flow meter.

Distance from bank (ft)	Depth (ft)	Velocity (ft/s)	Average velocity (ft/s)	Area (ft^2)	Discharge (cfs)
0.0	0.00	0.00	0.00	0.00	0.00
1.3	0.69	0.63	0.32	0.45	0.14
2.4	0.79	1.42	1.03	0.81	0.83
3.3	0.69	1.58	1.50	0.66	1.00
4.2	0.79	1.92	1.75	0.66	1.16

5.1	0.79	1.73	1.83	0.71	1.29
6.1	0.89	1.36	1.55	0.84	1.29
7.1	0.79	2.06	1.71	0.84	1.43
8.1	0.89	2.09	2.08	0.84	1.74
9.1	0.98	1.85	1.97	0.94	1.84
10.1	1.08	2.70	2.28	1.03	2.35
11.1	0.98	2.41	2.56	1.03	2.64
12.1	0.98	2.78	2.60	0.98	2.55
13.1	0.69	2.47	2.63	0.84	2.20
14.1	0.79	1.55	2.01	0.74	1.48
15.1	0.79	1.30	1.43	0.79	1.12
16.1	0.69	0.10	0.70	0.74	0.52
17.9	0.00	0.00	0.05	0.62	0.03
				Total (cfs):	23.6
				(m3/s):	0.669

Benchmark Spring was measured on 10/7/2017 using a wading rod and flow meter.

Distance from bank (ft)	Depth (ft)	Velocity (ft/s)	Average velocity (ft/s)	Area (ft^2)	Discharge (cfs)
0.0	0.00	0.00	0.00	0.00	0.00
0.1	0.20	0.72	0.36	0.01	0.00
0.8	0.20	0.37	0.55	0.13	0.07
1.3	0.20	0.34	0.36	0.10	0.03
1.5	0.20	0.00	0.17	0.07	0.01
				Total (cfs):	0.12
				(m3/s):	0.00341

The channelized portion of Logan Cave Spring was measured on 10/7/2017 using a wading rod and flow meter.

Distance from bank (ft)	Depth (ft)	Velocity (ft/s)	Average velocity (ft/s)	Area (ft^2)	Discharge (cfs)
0.0	0.00	0.00	0.00	0.00	0.00
0.9	0.20	0.88	0.44	0.09	0.04
1.9	0.30	1.11	1.00	0.25	0.24
2.8	0.30	1.76	1.44	0.27	0.38
3.5	0.00	0.00	0.88	0.10	0.09
				Total (cfs):	0.76
				(m3/s):	0.0214

The portion of Logan Cave Spring flowing through culverts was measured on 10/7/2017 using the Crowe et al. (2001) method for pipe flow.

Pipe diameter (ft)	2.00
Sediment + Water depth (ft)	0.10
Sediment depth (ft)	0.00
Water depth (ft)	0.10
Velocity (ft/s)	1.23
Total (cfs):	0.07
(m3/s):	0.00198

Woodcamp Hollow Spring was measured on 10/7/2017 using a wading rod and flow meter.

Distance from bank (ft)	Depth (ft)	Velocity (ft/s)	Average velocity (ft/s)	Area (ft^2)	Discharge (cfs)
0.0	0.00	0.00	0.00		0.00

1.0	0.30	0.00	0.00	0.15	0.00
1.4	0.39	0.00	0.00	0.14	0.00
1.9	0.59	0.92	0.46	0.25	0.11
2.9	0.20	0.15	0.54	0.39	0.21
3.9	0.20	1.82	0.99	0.20	0.19
4.9	0.20	2.21	2.02	0.20	0.40
5.9	0.69	3.17	2.69	0.44	1.19
6.9	0.79	4.10	3.64	0.74	2.68
7.8	0.69	5.20	4.65	0.66	3.09
8.9	0.49	5.50	5.35	0.65	3.48
9.9	0.49	5.26	5.38	0.49	2.65
10.9	0.39	2.66	3.96	0.44	1.75
11.9	0.30	0.88	1.77	0.34	0.61
13.4	0.20	2.66	1.77	0.37	0.65
14.1	0.00	0.00	1.33	0.07	0.09
				Total (cfs):	17.1
				(m3/s):	0.485

Woodcamp Hollow Creek was measured on 10/7/2017 using a wading rod and flow meter.

Distance from bank (ft)	Depth (ft)	Velocity (ft/s)	Average velocity (ft/s)	Area (ft^2)	Discharge (cfs)
0.6	0.20	0.33	0.33	0.11	0.04

China Row Spring was measured on 10/7/2017 using the Crowe et al. (2001) method for pipe flow.

Pipe diameter (ft)	2.00
Sediment + Water depth (ft)	0.67
Sediment depth (ft)	0.08
Water depth (ft)	0.58
Velocity (ft/s)	0.31
Total (cfs):	0.27
(m3/s):	0.00765

The middle Logan River was measured on 10/7/2017 using a wading rod and flow meter.

Distance from bank (ft)	Depth (ft)	Velocity (ft/s)	Average velocity (ft/s)	Area (ft^2)	Discharge (cfs)
0.0	0.00	0.00	0.00	0.00	0.00
3.0	1.38	1.14	0.57	2.07	1.18
6.1	2.07	1.49	1.32	5.34	7.02
9.1	2.07	2.41	1.95	6.20	12.09
12.1	2.26	1.91	2.16	6.50	14.03
15.1	1.77	1.59	1.75	6.05	10.59
18.1	1.77	2.09	1.84	5.32	9.78
21.1	1.77	0.58	1.34	5.32	7.10
24.1	1.28	2.15	1.37	4.58	6.25
27.1	1.48	2.32	2.24	4.13	9.24
30.1	1.38	2.48	2.40	4.28	10.28
33.1	1.08	2.46	2.47	3.69	9.12
36.1	1.28	1.89	2.18	3.54	7.71
39.1	1.08	1.48	1.69	3.54	5.97
42.1	0.89	1.42	1.45	2.95	4.28
45.1	0.59	0.65	1.04	2.21	2.29
46.2	0.00	0.00	0.33	0.32	0.11

Total (cfs):	117
(m3/s):	3.31

Right Hand Fork was measured on 10/7/2017 using a wading rod and flow meter.

Distance from bank (ft)	Depth (ft)	Velocity (ft/s)	Average velocity (ft/s)	Area (ft^2)	Discharge (cfs)
0.0	0.00	0.00	0.00	0.00	0.00
1.0	0.59	0.44	0.22	0.30	0.06
2.0	0.79	1.43	0.94	0.69	0.64
3.0	0.98	1.82	1.63	0.89	1.44
4.0	0.79	0.52	1.17	0.89	1.04
5.3	0.89	1.37	0.95	1.09	1.03
6.0	0.98	1.89	1.63	0.65	1.07
7.0	0.89	0.53	1.21	0.94	1.13
7.8	0.79	0.71	0.62	0.67	0.41
9.0	0.49	0.30	0.51	0.77	0.39
10.0	0.30	0.00	0.15	0.59	0.09
10.2	0.00	0.00	0.00	0.08	0.00
				Total (cfs):	7.30
				(m3/s):	0.207

Dewitt Spring was measured on 10/7/2017 using a wading rod and flow meter.

Distance from bank (ft)	Depth (ft)	Velocity (ft/s)	Average velocity (ft/s)	Area (ft^2)	Discharge (cfs)
0.0	0.00	0.00	0.00	0.00	0.00
0.3	0.79	1.53	0.77	0.11	0.09
3.6	0.79	1.13	1.33	2.64	3.51
7.0	0.79	1.10	1.12	2.64	2.94
7.3	0.00	0.00	0.55	0.11	0.06
				Total (cfs):	6.60
				(m3/s):	0.187

The lower Logan River was measured on 10/7/2017 using a wading rod and flow meter.

Distance from bank (ft)	Depth (ft)	Velocity (ft/s)	Average velocity (ft/s)	Area (ft^2)	Discharge (cfs)
0.0	0.00	0.00	0.00	0.00	0.00
3.0	1.08	0.15	0.08	1.62	0.12
6.3	1.97	1.03	0.59	5.03	2.97
9.1	1.87	1.98	1.51	5.37	8.09
12.1	1.77	2.18	2.08	5.46	11.36
15.1	2.07	2.30	2.24	5.76	12.90
18.1	1.97	2.45	2.38	6.05	14.38
21.1	2.07	2.55	2.50	6.05	15.13
24.1	1.97	2.27	2.41	6.05	14.59
27.1	1.97	2.54	2.41	5.91	14.20
30.1	1.97	2.32	2.43	5.91	14.35
33.1	1.97	2.20	2.26	5.91	13.35
36.1	1.77	2.27	2.24	5.61	12.54
39.1	1.57	1.83	2.05	5.02	10.29
42.1	1.48	1.76	1.80	4.58	8.22
45.1	1.28	1.38	1.57	4.13	6.49
48.1	0.69	0.09	0.74	6.50	4.77
49.0	0.00	0.00	0.05	0.31	0.01

Total (cfs):	164
(m3/s):	4.64

The west branch of Spring Hollow Spring was measured on 10/7/2017 using a wading rod and flow meter.

Distance from bank (ft)	Depth (ft)	Velocity (ft/s)	Average velocity (ft/s)	Area (ft^2)	Discharge (cfs)
0.0	0.00	0.00	0.00	0.00	0.00
1.1	0.59	0.44	0.22	0.32	0.07
2.1	0.59	0.03	0.24	0.59	0.14
3.1	0.39	0.40	0.22	0.49	0.11
4.1	0.49	1.99	1.20	0.44	0.53
5.1	0.98	1.16	1.58	0.74	1.16
6.1	0.89	1.36	1.26	0.94	1.18
7.1	0.69	1.40	1.38	0.79	1.09
8.1	0.49	0.45	0.93	0.59	0.55
9.1	0.49	0.96	0.71	0.49	0.35
9.5	0.00	0.00	0.48	0.10	0.05
				Total (cfs):	5.21
				(m3/s):	0.148

The east branch of Spring Hollow Spring was measured on 10/7/2017 using a wading rod and flow meter.

Distance from bank (ft)	Depth (ft)	Velocity (ft/s)	Average velocity (ft/s)	Area (ft^2)	Discharge (cfs)
0.0	0.00	0.00	0.00	0.00	0.00
0.7	0.39	0.17	0.09	0.06	0.01
1.7	0.30	0.88	0.53	0.24	0.13
2.7	0.39	0.35	0.62	0.34	0.21
3.7	0.49	1.19	0.77	0.44	0.34
4.7	0.39	0.70	0.95	0.44	0.42
5.7	0.20	0.77	0.74	0.30	0.22
6.7	0.20	0.60	0.69	0.20	0.13
7.6	0.00	0.00	0.30	0.10	0.03
				Total (cfs):	1.48
				(m3/s):	0.0420

Discharge measurements on 11/18/2017

The upper Logan River was measured on 11/18/2017 using a wading rod and flow meter.

Distance from bank (ft)	Depth (ft)	Velocity (ft/s)	Average velocity (ft/s)	Area (ft^2)	Discharge (cfs)
0.0	0.00	0.00	0.00	0.00	0.00
3.0	0.69	1.12	0.56	1.03	0.58
6.0	0.98	0.96	1.04	2.51	2.61
9.0	0.79	1.22	1.09	2.66	2.90
12.0	0.59	2.59	1.91	2.07	3.94
15.5	0.89	1.79	2.19	2.58	5.66
18.0	0.59	2.07	1.93	1.85	3.56
21.0	0.79	2.04	2.06	2.07	4.25
24.0	0.69	2.04	2.04	2.21	4.52
27.0	0.98	1.93	1.99	2.51	4.98

30.0	0.49	1.63	1.78	2.21	3.94
33.0	0.89	1.90	1.77	2.07	3.65
36.0	1.08	3.26	2.58	2.95	7.62
39.5	0.00	0.00	1.63	1.89	3.09
				Total (cfs):	51.3
				(m3/s):	1.45

Ricks Spring was measured on 11/18/2017 using a wading rod and flow meter.

Distance from bank (ft)	Depth (ft)	Velocity (ft/s)	Average velocity (ft/s)	Area (ft^2)	Discharge (cfs)
0.0	0.00	0.00	0.00	0.00	0.00
1.0	0.30	2.13	1.07	0.15	0.16
2.0	0.59	2.01	2.07	0.44	0.92
2.7	0.00	0.00	1.01	0.21	0.21
4.6	0.00	0.00	0.00	0.00	0.00
5.2	0.20	1.85	0.93	0.06	0.05
5.7	0.20	1.20	1.53	0.10	0.15
5.9	0.00	0.00	0.60	0.02	0.01
6.9	0.00	0.00	0.00	0.00	0.00
7.2	0.39	1.08	0.54	0.06	0.03
8.2	0.39	2.22	1.65	0.39	0.65
9.2	0.00	0.00	1.11	0.20	0.22
10.2	0.00	0.00	0.00	0.00	0.00
10.7	0.30	1.11	0.56	0.07	0.04
11.7	0.20	0.60	0.86	0.25	0.21
12.7	0.20	0.66	0.63	0.20	0.12
13.7	0.20	1.50	1.08	0.20	0.21
14.5	0.20	0.54	1.02	0.16	0.16
15.7	0.30	0.57	0.56	0.30	0.16
16.7	0.20	0.52	0.55	0.25	0.13
17.9	0.20	0.43	0.48	0.24	0.11
18.7	0.30	0.40	0.42	0.20	0.08
20.0	0.30	0.32	0.36	0.38	0.14
20.6	0.00	0.00	0.16	0.09	0.01
21.0	0.00	0.00	0.00	0.00	0.00
21.7	0.30	0.09	0.05	0.10	0.00
23.0	0.00	0.00	0.05	0.19	0.01
				Total (cfs):	3.80
				(m3/s):	0.108

Temple Fork was measured on 11/18/2017 using a wading rod and flow meter.

Distance from bank (ft)	Depth (ft)	Velocity (ft/s)	Average velocity (ft/s)	Area (ft^2)	Discharge (cfs)
0.0	0.00	0.00	0.00	0.00	0.00
0.9	0.89	1.63	0.82	0.40	0.32
1.9	0.69	1.75	1.69	0.79	1.33
2.9	0.69	2.19	1.97	0.69	1.36
3.9	0.79	0.97	1.58	0.74	1.17
4.9	0.79	1.93	1.45	0.79	1.14
5.9	0.89	1.12	1.53	0.84	1.28
6.9	0.89	1.48	1.30	0.89	1.15
7.9	0.89	2.53	2.01	0.89	1.78
8.9	0.89	2.05	2.29	0.89	2.03
9.9	0.79	2.42	2.24	0.84	1.87
10.9	0.89	2.44	2.43	0.84	2.03
11.9	0.89	1.27	1.86	0.89	1.64
12.9	0.89	1.82	1.55	0.89	1.37
13.9	0.89	1.38	1.60	0.89	1.42
14.5	0.00	0.00	0.69	0.27	0.18
				Total (cfs):	20.1
				(m3/s):	0.568

Benchmark Spring was measured on 11/18/2017 using a wading rod and flow meter.

Distance from bank (ft)	Depth (ft)	Velocity (ft/s)	Average velocity (ft/s)	Area (ft^2)	Discharge (cfs)
0.0	0.20	0.45	0.45	0.00	0.00
0.5	0.15	0.66	0.56	0.09	0.05
1.1	0.10	0.24	0.45	0.11	0.05
1.2	0.10	0.00	0.12	0.01	0.00
				Total (cfs):	0.10
				(m3/s):	0.00286

The channelized portion of Logan Cave Spring was measured on 11/18/2017 using a wading rod and flow meter.

Distance from bank (ft)	Depth (ft)	Velocity (ft/s)	Average velocity (ft/s)	Area (ft^2)	Discharge (cfs)
0.0	0.00	0.00	0.00	0.00	0.00
1.0	0.25	0.68	0.34	0.12	0.04
2.0	0.30	3.40	2.04	0.27	0.55
3.0	0.44	1.29	2.35	0.37	0.87
3.1	0.44	0.00	0.65	0.04	0.03
				Total (cfs):	1.49
				(m3/s):	0.0421

The portion of Logan Cave Spring flowing through culverts was measured on 11/18/2017 using the Crowe et al. (2001) method for pipe flow.

Pipe diameter (ft)	2.00
Sediment + Water depth (ft)	0.13

Sediment depth (ft)	0.00
Water depth (ft)	0.13
Velocity (ft/s)	0.90
Total (cfs):	0.07
(m3/s):	0.00208

Woodcamp Hollow Spring was measured on 11/18/2017 using a wading rod and flow meter.

Distance from bank (ft)	Depth (ft)	Velocity (ft/s)	Average velocity (ft/s)	Area (ft^2)	Discharge (cfs)
0.0	0.00	0.00	0.00	0.00	0.00
0.9	0.30	0.12	0.06	0.13	0.01
1.9	0.59	0.86	0.49	0.44	0.22
2.9	0.59	0.03	0.45	0.59	0.26
3.9	0.49	1.38	0.71	0.54	0.38
4.9	0.59	0.77	1.08	0.54	0.58
5.6	0.59	2.82	1.80	0.41	0.74
6.6	0.30	4.69	3.76	0.44	1.66
7.6	0.30	5.27	4.98	0.30	1.47
8.6	0.89	3.52	4.40	0.59	2.60
9.6	0.79	2.42	2.97	0.84	2.48
10.6	0.30	4.42	3.42	0.54	1.85
11.6	0.39	2.01	3.22	0.34	1.11
12.6	0.10	0.53	1.27	0.25	0.31
13.2	0.00	0.00	0.27	0.03	0.01
13.8	0.00	0.00	0.00	0.00	0.00
14.2	0.00	0.00	0.00	0.00	0.00
14.4	0.20	0.00	0.00	0.02	0.00
14.9	0.00	0.00	0.00	0.05	0.00
15.2	0.00	0.00	0.00	0.00	0.00
15.4	0.20	0.34	0.17	0.02	0.00
16.4	0.20	0.00	0.17	0.20	0.03
17.4	0.00	0.00	0.00	0.10	0.00
				Total (cfs):	13.7
				(m3/s):	0.389

China Row Spring was measured on 11/18/2017 using the Crowe et al. (2001) method for pipe flow.

Pipe diameter (ft)	2.00
Sediment + Water depth (ft)	0.75
Sediment depth (ft)	0.04
Water depth (ft)	0.71
Velocity (ft/s)	0.31
Total (cfs):	0.33

(m3/s):	0.00931

The middle Logan River was measured on 11/18/2017 using a wading rod and flow meter.

Distance from bank (ft)	Depth (ft)	Velocity (ft/s)	Average velocity (ft/s)	Area (ft^2)	Discharge (cfs)
0.0	0.00	0.00	0.00	0.00	0.00
4.2	1.77	1.04	0.52	3.72	1.93
7.2	2.26	1.29	1.17	6.05	7.05
10.2	2.36	2.21	1.75	6.94	12.14
13.2	2.26	1.70	1.96	6.94	13.57
16.2	1.67	1.40	1.55	5.91	9.15
19.2	1.77	1.86	1.63	5.17	8.42
22.2	1.67	1.94	1.90	5.17	9.82
25.2	1.57	2.31	2.13	4.87	10.35
28.2	1.48	1.93	2.12	4.58	9.70
31.2	1.48	2.20	2.07	4.43	9.15
34.2	1.28	2.11	2.16	4.13	8.91
37.2	0.98	1.72	1.92	3.40	6.50
40.2	0.98	1.20	1.46	2.95	4.31
43.2	0.89	1.11	1.16	2.81	3.24
46.2	0.30	0.00	0.56	1.77	0.98
47.9	0.00	0.00	0.00	0.25	0.00
				Total (cfs):	115
				(m3/s):	3.26

Right Hand Fork was measured on 11/18/2017 using a wading rod and flow meter.

Distance from bank (ft)	Depth (ft)	Velocity (ft/s)	Average velocity (ft/s)	Area (ft^2)	Discharge (cfs)
0.0	0.00	0.00	0.00	0.00	0.00
1.0	0.59	0.69	0.35	0.30	0.10
2.0	0.79	1.45	1.07	0.69	0.74
3.0	0.89	1.74	1.60	0.84	1.33
4.0	0.98	1.88	1.81	0.94	1.69
5.0	0.39	2.33	2.11	0.69	1.45
6.0	0.59	1.95	2.14	0.49	1.05
7.0	0.69	1.30	1.63	0.64	1.04
8.0	0.49	1.04	1.17	0.59	0.69
9.0	0.39	0.30	0.67	0.44	0.30
10.0	0.39	0.25	0.28	0.54	0.15
10.6	0.00	0.00	0.13	0.15	0.02
				Total (cfs):	8.56
				(m3/s):	0.243

Dewitt Spring was measured on 11/18/2017 using a wading rod and flow meter.

Distance from bank (ft)	Depth (ft)	Velocity (ft/s)	Average velocity (ft/s)	Area (ft^2)	Discharge (cfs)
0.0	0.00	0.00	0.00	0.00	0.00
0.3	2.26	0.52	0.26	0.32	0.08
3.6	2.36	0.63	0.58	7.75	4.46
7.0	2.36	0.45	0.54	7.91	4.27
7.3	0.00	0.00	0.23	0.34	0.08
				Total (cfs):	8.89
				(m3/s):	0.252

The lower Logan River was measured on 11/18/2017 using a wading rod and flow meter.

Distance from bank (ft)	Depth (ft)	Velocity (ft/s)	Average velocity (ft/s)	Area (ft^2)	Discharge (cfs)
0.0	0.00	0.00	0.00	0.00	0.00
2.5	0.79	0.13	0.07	1.02	0.07
5.5	1.18	0.35	0.24	2.95	0.71
8.5	1.77	1.45	0.90	4.43	3.99
11.5	1.48	1.83	1.64	4.87	7.99
14.5	1.57	2.09	1.96	4.58	8.97
17.5	1.77	2.16	2.13	5.02	10.67
20.5	1.77	2.19	2.18	5.32	11.56
23.5	1.87	1.90	2.05	5.46	11.17
26.5	1.77	2.29	2.10	5.46	11.44
29.5	1.87	2.06	2.18	5.46	11.88
32.5	1.77	2.12	2.09	5.46	11.42
35.5	1.77	2.25	2.19	5.32	11.61
38.5	1.57	1.99	2.12	5.02	10.64
41.5	1.48	1.77	1.88	4.58	8.60
44.5	1.28	1.67	1.72	4.13	7.11
47.5	0.98	1.13	1.40	7.38	10.33
50.8	0.00	0.00	0.57	1.62	0.92
				Total (cfs):	139
				(m3/s):	3.94

The lower Logan River side channel was measured on 11/18/2017 using a wading rod and flow meter.

Distance from bank (ft)	Depth (ft)	Velocity (ft/s)	Average velocity (ft/s)	Area (ft^2)	Discharge (cfs)
0.0	0.00	0.00	0.00	0.00	0.00
1.0	0.20	0.00	0.00	0.10	0.00
2.0	0.20	0.04	0.02	0.20	0.00
3.0	0.10	0.00	0.02	0.15	0.00
3.6	0.00	0.00	0.00	0.03	0.00
5.0	0.00	0.00	0.00	0.00	0.00

6.0	0.20	0.00	0.00	0.10	0.00
7.0	0.20	0.10	0.05	0.20	0.01
8.0	0.20	0.00	0.05	0.20	0.01
9.0	0.00	0.00	0.00	0.10	0.00
				Total (cfs):	0.03
				(m3/s):	0.000753

The west branch of Spring Hollow Spring was measured on 11/18/2017 using a wading rod and flow meter.

Distance from bank (ft)	Depth (ft)	Velocity (ft/s)	Average velocity (ft/s)	Area (ft^2)	Discharge (cfs)
0.0	0.00	0.00	0.00	0.00	0.00
1.1	0.20	0.00	0.00	0.11	0.00
2.1	0.59	0.01	0.01	0.39	0.00
3.1	0.59	0.00	0.01	0.59	0.00
4.1	0.69	0.06	0.03	0.64	0.02
5.1	0.59	0.31	0.19	0.64	0.12
6.1	0.89	0.59	0.45	0.74	0.33
7.1	0.79	0.67	0.63	0.84	0.53
8.1	1.08	0.86	0.77	0.94	0.72
9.1	0.98	0.93	0.90	1.03	0.92
10.1	0.30	0.56	0.75	0.64	0.48
11.1	0.59	0.35	0.46	0.44	0.20
12.2	0.00	0.00	0.18	0.32	0.06
				Total (cfs):	3.38
				(m3/s):	0.0956

The east branch of Spring Hollow Spring was measured on 11/18/2017 using a wading rod and flow meter.

Distance from bank (ft)	Depth (ft)	Velocity (ft/s)	Average velocity (ft/s)	Area (ft^2)	Discharge (cfs)
0.0	0.00	0.00	0.00	0.00	0.00
1.0	0.20	0.34	0.17	0.00	0.00
2.0	0.20	0.18	0.26	0.20	0.05
3.0	0.30	0.51	0.35	0.25	0.08
4.0	0.39	1.57	1.04	0.34	0.36
5.0	0.30	1.16	1.37	0.34	0.47
6.0	0.30	0.38	0.77	0.30	0.23
7.0	0.10	0.06	0.22	0.20	0.04
7.7	0.00	0.00	0.03	0.05	0.00
				Total (cfs):	1.24
				(m3/s):	0.0350

Appendix B: Wells used in Cache Valley groundwater facies analysis

Table B. Wells and groundwater samples selected for Cache Valley geochemical facies analysis.

Name	Altitude (ft)	pH	Depth (ft)	Date	T °C	Ca mg/L	Mg mg/L	K mg/L	Na mg/L	Cl mg/L	HCO3 mg/L	SO4 mg/L	TDS mg/L	log pCO2
(A-10-1)27dab-1	5162	7.3	-	2013-2016	12.2	64.6	23.2	0.67	9.8	12	312.9	9.1	254	-1.9
(A-10-1)28dba-1	4870	7.4	140	1968	12	56	23	5.9	9	12	272.0	25	294	-2.1
(A-10-1)4daa-1	4790	7.1	-	1990	-	84	26	13	16	26	386.7	20	409	-1.6
(A-10-1)4daa-1	4790	7.4	472	1968	12	68	28	1.4	12	12	294.0	56	334	-2.0
(A-11-1)10dad-1	4638	7.7	366	1966	-	66	25	3	6	15	329.4	14	296	-2.3
(A-11-1)15bdb-1	4565	7.2	145	1998-2011	12	83	32.9	2.7	8.7	14.3	368.8	24.5	377	-1.6
(A-11-1)15ddb-1	4680	7.6	385	1989	13.5	66	36	0	7.9	7.1	381.9	19	304	-2.1
(A-11-1)27adb-1	4650	7.5	290	1998	10	53.5	26.7	1.6	5.4	4.8	289.0	15.8	285	-2.1
(A-11-1)27cdc-1	4620	7.6	496	1968	11	72	19	0.7	5.1	5.3	252.0	55	284	-2.3
(A-11-1)6aab-1	4430	7.7	230	1989	16	47	20	0	12	9.3	244.0	7	187	-2.4
(A-11-1)8ddc-1	4477	7.5	138	1989	11	68	28	0	7	20	347.7	24	276	-2.1
(A-11-1)9aad-1	4495	7.8	385	1989	11.5	47	20	0	13	11	244.0	13	229	-2.5
(A-11-1)9acb-2	4483	7.6	182	1960	-	83	25	1	7.6	12	333.0	22	331	-2.2
(A-12-1)10ccc-1	4460	8	210	1963	-	38	16	5.3	44	17	245.0	13	268	-2.7
(A-12-1)15ccb-1	4484	7.5	210	1965	-	68	23	6	16	11	338.0	7	325	-2.1
(A-12-1)16ddd-1	4477	7.4	243	1968	22	56	26	0	32	12	327.0	16	469	-1.9
(A-12-1)17daa-1	4449	7.3	144	1990-2017	20.2	57.8	22.9	6.7	17.7	9.5	290.8	11.2	318	-1.9
(A-12-1)24ada-1	5060	7.6	721	2015	10.9	53.9	21.7	0.5	2.7	2.0	255.0	7.0	219	-2.3
(A-12-1)27cab-1	4550	8	800	1964	-	48	23	1.8	5.3	10	245.0	6.2	227	-2.7
(A-12-1)27dcd-1	4625	8.1	470	1962	-	56.5	18	1.2	4.9	6.5	236.0	15.5	228	-2.8
(A-12-1)28baa-5	4486	7.6	147	1960	-	56	15	6.7	23	18	252.0	19	291	-2.3
(A-12-1)29acc-1	4450	7.6	108	1989	23	52	20	0	18	11	259.9	18	261	-2.2
(A-12-1)31dab-1	4433	7.7	132	1960-1962	17.2	52.3	20.3	1.6	8.8	8.2	248.7	17.7	234	-2.4
(A-12-1)32cbb-1	4437	7.7	107	1961-1962	15	53	20	1.2	7	6.3	245.5	14.5	224	-2.4
(A-12-1)34cca-1	4550	8.2	1000	1963	-	42	21	1.5	7	8	197.0	9	210	-3.0

Name	Altitude (ft)	pH	Depth (ft)	Date	T °C	Ca mg/L	Mg mg/L	K mg/L	Na mg/L	Cl mg/L	HCO3 mg/L	SO4 mg/L	TDS mg/L	log pCO2
(A-12-1)35bba-1	4783	7.8	434	1989	10	53	19	0	4.9	7.6	257.4	9	174	-2.5
(A-12-1)35bcc-1	4600	8.5	978	1963	-	46	21	0.2	6.5	10	218.0	14	234	-3.3
(A-12-1)3cbd-2	4478	7.6	136	1966	-	62	32	6	12	15	339.0	8	352	-2.2
(A-13-1)13dcb-1	5100	7.3	213	1998	9.5	55.2	20.8	0.6	3.9	4.8	262.0	4.8	237	-2.0
(A-13-1)28aaa-1	4595	7.7	477	1968	11	48	26	0.5	5.2	5.1	266.0	7.5	233	-2.4
(A-13-1)29bcd-1	4450	7.6	173	1970-2017	13.4	41	22.5	1.6	25.1	9	240.7	11.4	255	-2.3
UT4900223 Well #4	4780	7.5	269	2015	14.5	62	29.6	0.8	5.6	6.2	337.9	18.7	252	-2.1